Summer 8-15-2019

Individual Differences in Human Brain Functional Network Organization

Benjamin A. Seitzman
Washington University in St. Louis

WASHINGTON UNIVERSITY IN ST. LOUIS

Division of Biology and Biomedical Sciences
Neurosciences

Dissertation Examination Committee:
Steven E. Petersen, Chair
Deanna M. Barch
Christina N. Lessov-Schlaggar
Bradley L. Schlaggar
Joshua S. Shimony

Individual Differences in Human Brain Functional Network Organization

by
Benjamin A. Seitzman

A dissertation presented to
The Graduate School
of Washington University in
partial fulfillment of the
requirements for the degree
of Doctor of Philosophy

August 2019
St. Louis, Missouri

Table of Contents

List of Figures

List of Tables

Acknowledgments

There are many people I need to thank for helping me navigate the PhD journey successfully. I'll thank my sources of funding first, since I often forget to do so during talks (unless I do so first). The National Institutes of Health, the James S. McDonnell Foundation, and the McDonnell Center for Systems Neuroscience provided financial support for my dissertation research, and for that I am extremely grateful. Next, I'd like to thank my dissertation committee, who provided ample feedback and support throughout my time studying network variants.

Thank you, Josh, for lending me your knowledge and time. I learned just how evanescent the latter can be, depending on the week. I look forward to our future collaborations. Thank you, Hristina, for your rigor and love of the nitty-gritty. I think some of the most fun I had doing science was looking at (bizarre) distributions of data and talking about statistics with you. The wine didn't hurt, either. Thank you, Brad, for your relentless optimism. You were a much-needed light illuminating the dark skeptical sea that is the Petersen lab. Thank you, Deanna, for your expertise and punctuality. Your insightful questions and deep knowledge of the behavioral side of my work led to many interesting discoveries and resulted in a much stronger research product. And, even though you may be the busiest one out of all of us, you still managed to ensure we never missed a deadline. I couldn't have asked for a better dissertation committee chair. Finally, thank you, Steve. You have provided tremendous insight, intuition, skepticism, and guidance during our pursuit of good science. And, more importantly, you have mentored (and some might say managed) me deftly. Your skills as a scientist and critical thinker are world renowned. However, your talent as a leader of people (a.k.a. minions a.k.a. puds) is criminally

underrated. I've grown in so many ways over the past five years, and I believe that you deserve the lion's share of credit for that. Thank you all so very much.

I would not have succeeded without support from the rest of the folks in the Petersen, Schlaggar, Dosenbach, and Greene labs. Thank you all for dealing with my "Benisms" and general weirdness, and a special thank you to Melissa, Sarah, Carmen, Laura, and anyone else who made one of our several BBQ runs over the years. Thank you to my PhD cohort and the rest of my friends who are also on a PhD journey at WashU. I've sincerely enjoyed spending time with all of you. You are some of the best drinking/softball/concert/study/D&D/workout/etc. buddies a guy could hope for. A special thank you to Chad Donahue for indulging me in many a kvetch session at Kaldi's. And, a special shout out to my former roommate and cohortmate Alex Cammack. I'm really glad we hit it off while sitting on that couch in the lobby of the Parkway Hotel during revisit, and I'm even more glad we were able to share a living space for a few years. I still think our greatest achievement is moving my desk twice. Thank you to the greatest trivia team in St. Louis for many fun-filled and beer-filled Thursday evenings. Dw/oB for life. Thank you to the Pub Crawl Committee for allowing me to serve for a few years. I look forward to your future endeavors.

Thank you to my YSP cohort. I don't know if any of us realized the commitment we were making when we signed up, but it was a tremendous four years, and I'm so happy I got to share it with all of you and our mentees. I look forward to seeing the amazing things they achieve in the future. Thank you to my Camp Rainbow family. I am most proud of the things we've accomplished together, and I can't wait for our next opportunity to bring joy to our campers.

Thank you to the Neuroscience Retreat committee for letting me organize a couple of parties and coordinate a couple of Thach awards. More importantly, thank you, Anneliese, for trusting us to make two retreat videos. Let the record show that Ben and Brian did all of the hard work and brought all of the talent to our movie-making business. I am a humble professor/actor wrangler and “ideas” guy.

Finally, thank you to my family for your enduring love and support throughout this process. There were a few dark times when I was unsure if I could go on. You guided me through and never once questioned my capabilities. Thank you so much for that, and for, you know, bringing me into the world, raising me, providing a stable home life, etc. I wouldn’t be the person or scientist that I am today without you.

Benjamin A. Seitzman

Washington University in St. Louis

August 2019

ABSTRACT OF THE DISSERTATION

Individual Differences in Human Brain Functional Network Organization

by

Benjamin A. Seitzman

Doctor of Philosophy in Biology and Biomedical Sciences

Neurosciences

Washington University in St. Louis, 2019

Professor Steven E. Petersen, Chair

The human brain is organized at many spatial scales, including the level of areas and systems. Resting-state functional magnetic resonance imaging is a non-invasive technique that allows for the study of areal- and systems-level brain organization *in vivo*. Over two decades of research has sought to identify and characterize the functional communities that comprise the brain's network architecture. Consequently, a convergent description of group-average functional network organization in healthy adults has emerged. Recent advances have allowed for the study of such organization in single individuals. Investigation of functional network organization in highly sampled individuals has revealed brain regions that deviate from the group-level description, i.e. individual differences in human brain functional network organization. This dissertation work characterizes individual differences in functional network organization, referred to as *network variants*, across a large sample of healthy adults. Network variants appear to be stable over time within an individual and organized systematically across individuals. They occur in characteristic cortical locations and associate with characteristic functional networks. Further, their task-evoked activity is consistent with their idiosyncratic functional network association. Finally, individuals may be sub-typed into one of two groups, where individuals in the same sub-group have a similar distribution of network variants. The sub-group phenomenon

is heritable and relates to differences in neuropsychological measures of behavior. Network variants appear to be trait-like, functionally-relevant components of individual human brain functional network organization.

Chapter 1: Introduction

A crucial step towards understanding how the human brain processes information and controls behavior is to understand its organization, in terms of both structure and function. Historically, investigators performed lesion-symptom mapping studies, extending from the early observations of Paul Broca (Broca, 1861), to localize certain behaviors and functions to specific regions of the brain. Later, Charles Sherrington and Wilder Penfield employed focal stimulation of brain regions in order to map the functional organization of motor cortex in great apes and humans (Penfield and Jasper, 1954). Recent technological advances have allowed for the study of brain organization non-invasively (Posner et al., 1988). An important innovation was the discovery of resting-state functional magnetic resonance imaging (rsfMRI), a powerful non-invasive technique that allows investigators to study human brain organization *in vivo* (Snyder and Raichle, 2012). There are many spatial scales at which brain organization may be investigated, including the level of areas and systems (Churchland and Sejnowski, 1988). rsfMRI is particularly useful for the study of areal and systems-level brain organization.

In the mid 90s, Barat Biswal and colleagues reported the first observation that ongoing (spontaneous) blood oxygen level dependent (BOLD) signal fluctuations are correlated between spatially distinct but functionally related regions of the brain at rest, i.e. when subjects are awake and alert, but not engaged in a task (Biswal et al., 1995). The BOLD signal is an indirect measure of neural activity (Logothetis et al., 2001), although the causal mechanisms relating changes in neural activity to changes in the BOLD signal remain unknown (Logothetis and Wandell, 2004). Over two decades of research since Biswal's discovery have revealed that there are well correlated spontaneous fluctuations in the BOLD signal between regions of the brain that are

constitutive components of known anatomical systems, such as the motor system (Biswal et al., 1995) and the visual system (Nir et al., 2006; Vincent et al., 2007), as well as more recently identified and less obviously anatomically constrained systems, such as two distinct systems for executive control (Dosenbach et al., 2007, 2006; Seeley et al., 2007) and two attention systems (Corbetta and Shulman, 2002; Petersen and Posner, 2012).

Investigators have exploited the powerful rsfMRI technique and this phenomenon of synchronous, spontaneous BOLD signal fluctuations to develop increasingly comprehensive descriptions of the functional sub-systems that comprise the brain's network architecture (Power et al., 2011; Yeo et al., 2011). Functional network organization is often identified via graph-theoretic network science techniques in which regions of the brain are assigned to distinct communities in an abstract network space (Bullmore and Sporns, 2009; Rosvall and Bergstrom, 2008; Rubinov and Sporns, 2010). Consequently, a converging picture of human brain functional network organization has emerged, and subsequent studies have led to informative distinctions between healthy adult control groups and a variety of patient populations (Greene et al., 2016; He et al., 2007; Seeley et al., 2009; Siegel et al., 2018; van den Heuvel et al., 2010) and healthy individuals at different stages of development (Chan et al., 2014; Greene et al., 2014; Nielsen et al., 2018). For a recent review of group-average functional network organization, see (Seitzman et al., 2019).

Many of these studies have focused on the cerebral cortex isolated from the rest of the brain (e.g., Yeo et al., 2011). Separately, some investigations have focused on non-cortical structures, such as the amygdala (Roy et al., 2009), hippocampus (Kahn et al., 2008), basal ganglia (Di

Martino et al., 2008), and cerebellum (Marek et al., 2018). However, relatively few research efforts have performed an in-depth exploration of the whole brain from a network perspective. One reason for this deficiency is a lack of well-defined network nodes, or regions of interest (ROIs), that extensively sample both the cortex and non-cortical structures (e.g., Power et al., 2011). Interactions between the cortex and non-cortical structures have been observed to be critical in numerous studies, e.g. many forms of psychopathology appear to relate to cortico-striatal relationships (Greene et al., 2013; Lynall et al., 2010; Sheffield et al., 2015; Vonsattel et al., 1985). Thus, there is a need for a set of whole-brain ROIs that are well-constrained and sample all of these brain regions. One aim of this dissertation is to develop such a set of ROIs.

While the aforementioned findings have begun to shape our understanding of normal and pathological brain function, much of this work has focused on a group-level description, similar to describing the central tendency or mean. The mean is a useful and often edifying statistic to know; however, the variance is as or frequently more revealing than the mean (Patten et al., 2018). Thus, there is a clear need for a systematic characterization of variance, i.e. individual differences in functional brain organization. Individual differences promise to yield a potent mechanism by which we may further our understanding of normal and pathological brain function. Towards this end, recent work has demonstrated that there are elements of group-level functional brain organization that are noticeably variable across individuals, including regions of frontal and temporo-parietal cortex (Bijsterbosch et al., 2018; Braga and Buckner, 2017; Finn et al., 2015; Evan M Gordon et al., 2017; Evan M. Gordon et al., 2017a, 2017b; Kong et al., 2018; Laumann et al., 2015; Mueller et al., 2013; Wang et al., 2015). That is, there seem to be regions

of cortex with distinctive patterns of BOLD signal correlations that may reflect functional divergence in individuals.

For instance, Laumann and colleagues performed an in-depth study of a single highly sampled individual (Poldrack et al., 2015), which was an important step towards resolving the methodological challenges of studying individual differences via rsfMRI. Their work directly led to the discovery of punctate regions of cortex in the individual's brain with a pattern of BOLD signal correlations that is remarkably different from the group-average pattern (derived from typical healthy controls). Upon further inspection, they demonstrated that these regions overlap with unique features in the individual's functional network organization (Laumann et al., 2015). The remaining aims of this dissertation directly build upon these findings in order to characterize fully these distinctive features of functional network organization in individuals. We call such features *network variants*.

The group-level account of healthy brain network organization has yielded valuable perspective on both regional differences in task-evoked BOLD activity and differences in functional organization in patient populations. Similarly, a robust account of individual differences in functional network organization is poised to provide a fresh perspective on the nature of brain organization and may provide compelling insight into behavioral variability. Moreover, descriptions of functional network organization that incorporate network variants may reveal critical deviations in atypical (pathological) brain organization that have been obscured thus far by the smearing that occurs when averaging across individuals. Such a result may lead to more

effective treatments for individuals with diseases that affect functional brain organization, such as anxiety (Sylvester et al., 2013).

One intriguing open question is to what extent are individual differences in functional network organization trait-like. Network variants may represent traits unique to a person that diverge across individuals as a consequence of a combination of factors, including genetics, environment, and individual experience. Alternatively, they may reflect less interesting differences in an individual's state during data acquisition, such as level of arousal or differences in head motion (Laumann et al., 2017; Siegel et al., 2017). If network variants are trait-like, then they will likely demonstrate stability over time within an individual (e.g., eye color does not change across an individual's lifespan), as well as some kind of systematic patterning across individuals (e.g., some dogs have pointy ears while other dogs have floppy ears). Finally, if network variants are bonafide traits, then they will demonstrate some degree of heritability, i.e. some amount of variance in network variants will be explained by genetics (Chabris et al., 2015; Turkheimer, 2000).

To investigate these possibilities, several datasets of highly sampled individuals were used. Analyses were performed on rsfMRI data and were extended to a variety of well-established behavioral measures and task domains in order to characterize network variants across a large number of individuals. Potential links between specific patterns of network variants and individual differences in behavior and task-evoked activity were investigated. Finally, the heritability of network variants was explored.

1.1 Chapter 1 References

Bijsterbosch, J.D., Woolrich, M.W., Glasser, M.F., Robinson, E.C., Beckmann, C.F., Van Essen, D.C., Harrison, S.J., Smith, S.M., 2018. The relationship between spatial configuration and functional connectivity of brain regions. Elife 7. doi:10.7554/eLife.32992

Biswal, B., Yetkin, F.Z., Haughton, V.M., Hyde, J.S., 1995. Functional connectivity in the motor cortex of resting human brain using echo-planar MRI. Magn. Reson. Med. 34, 537–541. doi:10.1002/mrm.1910340409

Braga, R.M., Buckner, R.L., 2017. Parallel Interdigitated Distributed Networks within the Individual Estimated by Intrinsic Functional Connectivity. Neuron 95, 457–471.e5. doi:10.1016/j.neuron.2017.06.038

Broca, P., 1861. Remarques sur le siège de la faculté du langage articulé, suivies d'une observation d'aphémie (perte de la parole). Bull. la Société Anat. 6, 330–357.

Bullmore, E., Sporns, O., 2009. Complex brain networks: graph theoretical analysis of structural and functional systems. Nat. Rev. Neurosci. 10, 186–98. doi:10.1038/nrn2575

Chabris, C.F., Lee, J.J., Cesarini, D., Benjamin, D.J., Laibson, D.I., 2015. The Fourth Law of Behavior Genetics. Curr. Dir. Psychol. Sci. 24, 304–312. doi:10.1177/0963721415580430

Chan, M.Y., Park, D.C., Savalia, N.K., Petersen, S.E., Wig, G.S., 2014. Decreased segregation of brain systems across the healthy adult lifespan. Proc. Natl. Acad. Sci. 111, E4997–E5006. doi:10.1073/pnas.1415122111

Churchland, P.S., Sejnowski, T.J., 1988. Perspectives on Cognitive Neuroscience. Science (80-.). 242, 741–745. doi:10.1126/science.3055294

Corbetta, M., Shulman, G.L., 2002. Control of goal-directed and stimulus-driven attention in the brain. Nat. Rev. Neurosci. 3, 201–15. doi:10.1038/nrn755

Di Martino, A., Scheres, A., Margulies, D.S., Kelly, A.M.C., Uddin, L.Q., Shehzad, Z., Biswal, B., Walters, J.R., Castellanos, F.X., Milham, M.P., 2008. Functional Connectivity of Human Striatum: A Resting State fMRI Study. Cereb. Cortex 18, 2735–2747. doi:10.1093/cercor/bhn041

Dosenbach, N.U.F., Fair, D.A., Miezin, F.M., Cohen, A.L., Wenger, K.K., Dosenbach, R. a T., Fox, M.D., Snyder, A.Z., Vincent, J.L., Raichle, M.E., Schlaggar, B.L., Petersen, S.E., 2007. Distinct brain networks for adaptive and stable task control in humans. Proc. Natl. Acad. Sci. U. S. A. 104, 11073–8. doi:10.1073/pnas.0704320104

Dosenbach, N.U.F., Visscher, K.M., Palmer, E.D., Miezin, F.M., Wenger, K.K., Kang, H.C., Burgund, E.D., Grimes, A.L., Schlaggar, B.L., Petersen, S.E., 2006. A Core System for the Implementation of Task Sets. Neuron 50, 799–812. doi:10.1016/j.neuron.2006.04.031

Finn, E.S., Shen, X., Scheinost, D., Rosenberg, M.D., Huang, J., Chun, M.M., Papademetris, X., Constable, R.T., 2015. Functional connectome fingerprinting: Identifying individuals using patterns of brain connectivity. Nat. Neurosci. 18, 1664–1671. doi:10.1038/nn.4135

Gordon, E.M., Laumann, T.O., Adeyemo, B., Gilmore, A.W., Nelson, S.M., Dosenbach, N.U.F., Petersen, S.E., 2017a. Individual-specific features of brain systems identified with resting state functional correlations. Neuroimage 146, 918–939. doi:10.1016/j.neuroimage.2016.08.032

Gordon, E.M., Laumann, T.O., Adeyemo, B., Petersen, S.E., 2017b. Individual Variability of the System-Level Organization of the Human Brain. Cereb. Cortex 27, 386–399. doi:10.1093/cercor/bhv239

Gordon, E.M., Laumann, T.O., Gilmore, A.W., Petersen, S.E., Nelson, S.M., Dosenbach, N.U.F., Gordon, E.M., Laumann, T.O., Gilmore, A.W., Newbold, D.J., Greene, D.J., 2017. Precision Functional Mapping of Individual Human NeuroResource Precision Functional Mapping of Individual Human Brains. Neuron 95, 1–17. doi:10.1016/j.neuron.2017.07.011

Greene, D.J., Black, K.J., Schlaggar, B.L., 2013. Neurobiology and functional anatomy of tic disorders. Tourette Syndr. doi:http://dx.doi.org/10.1093/med/9780199796267.003.0012

Greene, D.J., Church, J.A., Dosenbach, N.U.F., Nielsen, A.N., Adeyemo, B., Nardos, B., Petersen, S.E., Black, K.J., Schlaggar, B.L., 2016. Multivariate pattern classification of pediatric Tourette syndrome using functional connectivity MRI. Dev. Sci. 19, 581–598. doi:10.1111/desc.12407

Greene, D.J., Laumann, T.O., Dubis, J.W., Ihnen, S.K., Neta, M., Power, J.D., Pruett, J.R., Black, K.J., Schlaggar, B.L., 2014. Developmental changes in the organization of functional connections between the basal ganglia and cerebral cortex. J. Neurosci. 34, 5842–54. doi:10.1523/JNEUROSCI.3069-13.2014

He, B.J., Snyder, A.Z., Vincent, J.L., Epstein, A., Shulman, G.L., Corbetta, M., 2007. Breakdown of Functional Connectivity in Frontoparietal Networks Underlies Behavioral Deficits in Spatial Neglect. Neuron 53, 905–918. doi:10.1016/j.neuron.2007.02.013

Kahn, I., Andrews-Hanna, J.R., Vincent, J.L., Snyder, A.Z., Buckner, R.L., 2008. Distinct Cortical Anatomy Linked to Subregions of the Medial Temporal Lobe Revealed by Intrinsic Functional Connectivity. J. Neurophysiol. 100, 129–139. doi:10.1152/jn.00077.2008

Kong, R., Li, J., Orban, C., Sabuncu, M.R., Liu, H., Schaefer, A., Sun, N., Zuo, X.-N., Holmes, A.J., Eickhoff, S.B., Yeo, B.T.T., 2018. Spatial Topography of Individual-Specific Cortical

Networks Predicts Human Cognition, Personality, and Emotion. Cereb. Cortex. doi:10.1093/cercor/bhy123

Laumann, T.O., Gordon, E.M., Adeyemo, B., Snyder, A.Z., Joo, S.J., Chen, M.-Y., Gilmore, A.W., McDermott, K.B., Nelson, S.M., Dosenbach, N.U.F., Schlaggar, B.L., Mumford, J.A., Poldrack, R.A., Petersen, S.E., 2015. Functional System and Areal Organization of a Highly Sampled Individual Human Brain. Neuron 1–14. doi:10.1016/j.neuron.2015.06.037

Laumann, T.O., Snyder, A.Z., Mitra, A., Gordon, E.M., Gratton, C., Adeyemo, B., Gilmore, A.W., Nelson, S.M., Berg, J.J., Greene, D.J., McCarthy, J.E., Tagliazucchi, E., Laufs, H., Schlaggar, B.L., Dosenbach, N.U.F., Petersen, S.E., 2017. On the Stability of BOLD fMRI Correlations. Cereb. Cortex 27, 4719–4732. doi:10.1093/cercor/bhw265

Logothetis, N.K., Pauls, J., Augath, M., Trinath, T., Oeltermann, A., 2001. Neurophysiological investigation of the basis of the fMRI signal. Nature 412, 150–7. doi:10.1038/35084005

Logothetis, N.K., Wandell, B.A., 2004. Interpreting the BOLD Signal. Annu. Rev. Physiol. 66, 735–769. doi:10.1146/annurev.physiol.66.082602.092845

Lynall, M.-E., Bassett, D.S., Kerwin, R., McKenna, P.J., Kitzbichler, M., Muller, U., Bullmore, E., 2010. Functional connectivity and brain networks in schizophrenia. J. Neurosci. 30, 9477–9487. doi:10.1523/JNEUROSCI.0333-10.2010

Marek, S., Siegel, J.S., Gordon, E.M., Raut, R. V., Gratton, C., Newbold, D.J., Ortega, M., Laumann, T.O., Adeyemo, B., Miller, D.B., Zheng, A., Lopez, K.C., Berg, J.J., Coalson, R.S., Nguyen, A.L., Dierker, D., Van, A.N., Hoyt, C.R., McDermott, K.B., Norris, S.A., Shimony, J.S., Snyder, A.Z., Nelson, S.M., Barch, D.M., Schlaggar, B.L., Raichle, M.E., Petersen, S.E., Greene, D.J., Dosenbach, N.U.F., 2018. Spatial and Temporal Organization of the Individual Human Cerebellum. Neuron.

Mueller, S., Wang, D., Fox, M.D., Yeo, B.T.T., Sepulcre, J., Sabuncu, M.R., Shafee, R., Lu, J., Liu, H., 2013. Individual Variability in Functional Connectivity Architecture of the Human Brain. Neuron 77, 586–595. doi:10.1016/j.neuron.2012.12.028

Nielsen, A.N., Greene, D.J., Gratton, C., Dosenbach, N.U.F., Petersen, S.E., Schlaggar, B.L., 2018. Evaluating the Prediction of Brain Maturity From Functional Connectivity After Motion Artifact Denoising. Cereb. Cortex 1–15. doi:10.1093/cercor/bhy117

Nir, Y., Hasson, U., Levy, I., Yeshurun, Y., Malach, R., 2006. Widespread functional connectivity and fMRI fluctuations in human visual cortex in the absence of visual stimulation. Neuroimage 30, 1313–1324. doi:10.1016/j.neuroimage.2005.11.018

Patten, M.L., Newhart, M., Patten, M.L., Newhart, M., 2018. The Mean and Standard Deviation, in: Understanding Research Methods. pp. 219–221. doi:10.4324/9781315213033-71

Penfield, W., Jasper, H., 1954. Epilepsy and the Functional Anatomy of the Human Brain. Little, Brown, and Company, Boston, MA.

Petersen, S.E., Posner, M.I., 2012. The attention system of the human brain: 20 years after. Annu. Rev. Neurosci. 35, 73–89. doi:10.1146/annurev-neuro-062111-150525

Poldrack, R.A., Laumann, T.O., Koyejo, O., Gregory, B., Hover, A., Chen, M.Y., Gorgolewski, K.J., Luci, J., Joo, S.J., Boyd, R.L., Hunicke-Smith, S., Simpson, Z.B., Caven, T., Sochat, V., Shine, J.M., Gordon, E., Snyder, A.Z., Adeyemo, B., Petersen, S.E., Glahn, D.C., Mckay, D.R., Curran, J.E., Göring, H.H.H., Carless, M.A., Blangero, J., Dougherty, R., Leemans, A., Handwerker, D.A., Frick, L., Marcotte, E.M., Mumford, J.A., 2015. Long-term neural and physiological phenotyping of a single human. Nat. Commun. 6. doi:10.1038/ncomms9885

Posner, M.I., Petersen, S.E., Fox, P.T., Raichle, M.E., 1988. Localization of cognitive operations in the human brain. Science 240, 1627–1631. doi:10.1126/science.3289116

Power, J.D., Cohen, A.L., Nelson, S.M., Wig, G.S., Barnes, K.A., Church, J.A., Vogel, A.C., Laumann, T.O., Miezin, F.M., Schlaggar, B.L., Petersen, S.E., 2011. Functional Network Organization of the Human Brain. Neuron 72, 665–678. doi:10.1016/j.neuron.2011.09.006

Rosvall, M., Bergstrom, C.T., 2008. Maps of random walks on complex networks reveal community structure. Proc. Natl. Acad. Sci. U. S. A. 105, 1118–1123. doi:10.1073/pnas.0706851105

Roy, A.K., Shehzad, Z., Margulies, D.S., Kelly, a. M.C., Uddin, L.Q., Gotimer, K., Biswal, B.B., Castellanos, F.X., Milham, M.P., 2009. Functional connectivity of the human amygdala using resting state fMRI. Neuroimage 45, 614–626. doi:10.1016/j.neuroimage.2008.11.030

Rubinov, M., Sporns, O., 2010. Complex network measures of brain connectivity: Uses and interpretations. Neuroimage 52, 1059–1069. doi:10.1016/j.neuroimage.2009.10.003

Seeley, W.W., Crawford, R.K., Zhou, J., Miller, B.L., Greicius, M.D., 2009. Neurodegenerative Diseases Target Large-Scale Human Brain Networks. Neuron 62, 42–52. doi:10.1016/j.neuron.2009.03.024

Seeley, W.W., Menon, V., Schatzberg, A.F., Keller, J., Glover, G.H., Kenna, H., Reiss, A.L., Greicius, M.D., 2007. Dissociable intrinsic connectivity networks for salience processing and executive control. J. Neurosci. 27, 2349–2356. doi:10.1523/JNEUROSCI.5587-06.2007

Seitzman, B.A., Snyder, A.Z., Leuthardt, E.C., Shimony, J.S., 2019. The state of resting state networks. Top. Magn. Reson. Imaging 28, 189–196. doi:10.1097/RMR.0000000000000214

Sheffield, J.M., Repovs, G., Harms, M.P., Carter, C.S., Gold, J.M., MacDonald, A.W., Daniel Ragland, J., Silverstein, S.M., Godwin, D., Barch, D.M., 2015. Fronto-parietal and cingulo-

opercular network integrity and cognition in health and schizophrenia. Neuropsychologia 73, 82–93. doi:10.1016/j.neuropsychologia.2015.05.006

Siegel, J.S., Mitra, A., Laumann, T.O., Seitzman, B.A., Raichle, M., Corbetta, M., Snyder, A.Z., 2017. Data quality influences observed links between functional connectivity and behavior. Cereb. Cortex 27, 4492–4502. doi:10.1093/cercor/bhw253

Siegel, J.S., Seitzman, B.A., Ramsey, L.E., Ortega, M., Gordon, E.M., Dosenbach, N.U.F., Petersen, S.E., Shulman, G.L., Corbetta, M., 2018. Re-emergence of modular brain networks in stroke recovery. Cortex 101, 44–59. doi:10.1016/j.cortex.2017.12.019

Snyder, A.Z., Raichle, M.E., 2012. A brief history of the resting state: The Washington University perspective. Neuroimage. doi:10.1016/j.neuroimage.2012.01.044

Sylvester, C.M., Barch, D.M., Corbetta, M., Power, J.D., Schlaggar, B.L., Luby, J.L., 2013. Resting state functional connectivity of the ventral attention network in children with a history of depression or anxiety. J. Am. Acad. Child Adolesc. Psychiatry 52. doi:10.1016/j.jaac.2013.10.001

Turkheimer, E., 2000. Three laws of behavior genetics and what they mean. Curr. Dir. Psychol. Sci. 9, 160–164. doi:10.1111/1467-8721.00084

Van den Heuvel, M.P., Mandl, R.C.W., Stam, C.J., Kahn, R.S., Hulshoff Pol, H.E., 2010. Aberrant frontal and temporal complex network structure in schizophrenia: a graph theoretical analysis. J. Neurosci. 30, 15915–15926. doi:10.1523/JNEUROSCI.2874-10.2010

Vincent, J.L., Patel, G.H., Fox, M.D., Snyder, A.Z., Baker, J.T., Van Essen, D.C., Zempel, J.M., Snyder, L.H., Corbetta, M., Raichle, M.E., 2007. Intrinsic functional architecture in the anaesthetized monkey brain. Nature 447, 83–6. doi:10.1038/nature05758

Vonsattel, J.-P., Myers, R.H., Stevens, T.J., Ferrante, R.J., Bird, E.D., Richardson, E.P., 1985. Neuropathological Classification of Huntington's Disease. J. Neuropathol. Exp. Neurol. 44, 559–577. doi:10.1097/00005072-198511000-00003

Wang, D., Buckner, R.L., Fox, M.D., Holt, D.J., Holmes, A.J., Stoecklein, S., Langs, G., Pan, R., Qian, T., Li, K., Baker, J.T., Stufflebeam, S.M., Wang, K., Wang, X., Hong, B., Liu, H., 2015. Parcellating cortical functional networks in individuals. Nat. Neurosci. 18, 1853–1860. doi:10.1038/nn.4164

Yeo, B.T.T., Krienen, F.M., Sepulcre, J., Sabuncu, M.R., Lashkari, D., Hollinshead, M., Roffman, Joshua L. Smoller, J.W., Zöllei, L., Polimeni, J.R., Fischl, B., Liu, H., Buckner, R.L., 2011. The organization of the human cerebral cortex estimated by intrinsic functional connectivity. J. Neurophysiol. 106, 1125–1165.

Chapter 2: A set of functionally-defined brain regions with improved representation of the subcortex and cerebellum

An important aspect of network-based analysis is robust node definition. This issue is critical for functional brain network analyses, as poor node choice can lead to spurious findings and misleading inferences about functional brain organization. Two sets of functional brain nodes from our group are well represented in the literature: (1) 264 volumetric regions of interest (ROIs) reported in Power et al., 2011 and (2) 333 cortical surface parcels reported in Gordon et al., 2016. However, subcortical and cerebellar structures are either incompletely captured or missing from these ROI sets. Therefore, properties of functional network organization involving the subcortex and cerebellum may be underappreciated thus far. Here, we apply a winner-take-all partitioning method to resting-state fMRI data to generate novel functionally-constrained ROIs in the thalamus, basal ganglia, amygdala, hippocampus, and cerebellum. We validate these ROIs in three datasets using several criteria, including agreement with existing literature and anatomical atlases. Further, we demonstrate that combining these ROIs with established cortical ROIs recapitulates and extends previously described functional network organization. This new set of ROIs is made publicly available for general use, including a full list of MNI coordinates and functional network labels.

2.1 Introduction

The brain is organized into areas that interact with one another to form distributed large-scale networks (Allman and Kaas, 1971; Felleman and Van Essen, 1991; Petersen and Sporns, 2015). Researchers studying the brain at the network level have revealed both basic principles of brain organization (Bassett and Bullmore, 2006; Honey et al., 2007; Power et al., 2011; Sporns et al.,

2004; van den Heuvel and Sporns, 2011; Yeo et al., 2011) and insights into neurologic and psychiatric diseases (Corbetta and Shulman, 2011; Kim et al., 2014; Seeley et al., 2009; Sorg et al., 2007). Much of this work has borrowed concepts and tools from the field of graph theory in order to model the brain as a network (Bullmore and Sporns, 2009; Sporns, 2011). A graph is a mathematical description of a network, which comprises a set of elements (nodes) and their pairwise relationships (edges (Bondy and Murty, 1976)). Therefore, network approaches require the definition of a set of nodes, such as regions of interest (ROIs) in the case of brain networks.

Ideally, nodes should be internally coherent (e.g., functionally homogeneous) and independent, separable units (Bullmore and Bassett, 2011; Butts, 2009, 2008; Wig et al., 2011). Brain areas and their constituent components—local circuits, columns, and domains (Kaas, 2012)—display many of these properties, and thus, are suitable nodes for brain network analysis. Research efforts focused on node definition often employ data-driven techniques to parcellate the cerebral cortex into a set of ROIs meant to represent putative functionally homogeneous brain areas (Cohen et al., 2008; Craddock et al., 2012; Glasser et al., 2016; Gordon et al., 2016; Nelson et al., 2010; Power et al., 2011; Schaefer et al., 2017; Wig et al., 2013). Most such studies have used resting-state functional connectivity MRI, which measures correlations in low-frequency blood-oxygen-level-dependent (BOLD) signals across the whole brain while subjects remain awake and alert without engaging in an explicit task (Biswal et al., 1995; Gusnard and Raichle, 2001; Snyder and Raichle, 2012). While many of these existing sets of ROIs sample the cortex quite well, most approaches have under-sampled or completely omitted the subcortex and cerebellum (but see Ji et al., 2019).

The poorer representation of these structures is a limitation of previous work, as closed loop anatomical circuits connect the subcortex and cerebellum to the cortex (Woolsey et al., 2008). In addition, these structures are known to be integral for many behavioral, cognitive, and affective functions. For example, regions of the cerebellum are involved in adaptive behaviors (Thach et al., 1992), including fast adaptations, like eye-blink conditioning (Steinmetz et al., 1992; Perrett et al., 1993), as well as those that occur over longer timescales, like prism adaptation (Martin et al., 1996; Baizer et al., 1999; Morton and Bastian, 2004), and higher order cognitive functions, such as semantic processing (Fiez, 2016; Guell et al., 2018). Likewise, regions of the basal ganglia and thalamus are important for both lower level sensory and higher order cognitive functions (Alexander et al., 1986; Jones, 1985). Furthermore, subcortical structures and the cerebellum have been implicated in a variety of neurologic and psychiatric diseases. For instance, the basal ganglia are affected in several movement disorders (Greene et al., 2017, 2013; Rajput, 1993; Vonsattel et al., 1985), the hippocampus is disrupted in Alzheimer Disease (Hardy and Selkoe, 2002), the amygdala is implicated in Major Depressive Disorder (Frodl et al., 2002) and Urbach-Wiethe Disease (Siebert et al., 2003), and the cerebellum is disturbed in Schizophrenia (Andreasen et al., 1996; Bigelow et al., 2006; Brown et al., 2005; Kim et al., 2014) and Autism Spectrum Disorder (Fatemi et al., 2002), to name a few. Moreover, interactions between the cortex and both subcortical and cerebellar regions are crucial for carrying out functions in health (Bostan and Strick, 2018; Greene et al., 2014; Hwang et al., 2017; Kiritani et al., 2012) and disease (Andreasen et al., 1999; Gratton et al., 2018a; Schmahmann, 2004). Because of these interactions between multiple structures, it has been postulated that subcortical regions may have important hub-like properties for integrating brain systems (Hwang et al., 2017) and may constrain network-level topology (Bell and Shine, 2016;

Garrett et al., 2018). Thus, brain network analyses should include these important regions in order to have a more complete picture of brain organization and function.

An issue potentially impeding the inclusion of these regions is that subcortical and deep cerebellar nuclei are small relative to the spatial resolution of fMRI, often occupying just a few voxels, whereas brain areas in the cerebral cortex (e.g. Area V1) are typically larger. Furthermore, depending on the acquisition sequence, these regions may have lower signal quality (Ojemann et al., 1997) or, especially for the cerebellum, may be captured incompletely. Finally, most existing techniques for parcellating the brain into areas, such as gradient-based techniques (Cohen et al., 2008; Gordon et al., 2016; Nelson et al., 2010; Wig et al., 2013), were designed for the cortical surface, making them less easily applied to structures where surface-based mapping is less appropriate (basal ganglia, thalamus), prone to error (medial temporal lobe) (Wisse et al., 2014), or less well-established (cerebellum). Despite these difficulties, inclusion of the subcortex and cerebellum is crucial to properly represent the brain as a network. While there are existing anatomical atlases of the subcortex (Morel, 2013) and cerebellum (Diedrichsen et al., 2009), functionally defined regions may complement anatomical ones and provide a better correspondence to functionally defined cortical areas and task-based measures from fMRI.

Our lab previously published two (now widely used) sets of ROIs: (1) 264 volumetric ROIs (Power et al., 2011) and (2) 333 surface-based cortical parcels (Gordon et al., 2016). The first was created via combined task fMRI meta-analysis and resting-state functional correlation mapping, and the second was created via a gradient-based parcellation of resting-state fMRI data. These two ROI sets sample the cortex well, representing a diverse set of brain areas that

can be organized into functional networks. Many investigators have used them to describe functional brain organization in a variety of healthy samples (Power et al., 2013; Zanto and Gazzaley, 2013), lifespan cohorts (Baniqued et al., 2018; Gallen et al., 2016; Gu et al., 2015; Nielsen et al., 2018; Rudolph et al., 2017), as well as populations with neurologic and psychiatric diseases (Gratton et al., 2018a; Greene et al., 2016; Sheffield et al., 2015; Siegel et al., 2018). However, the first set (264 volumetric ROIs) under-samples subcortical and cerebellar structures, as only 17 ROIs are non-cortical, and the second set (333 parcels) is restricted to the cortex only, similar to other popular ROI sets, e.g. (Glasser et al., 2016; Yeo et al., 2011).

The goal of the current study was to expand these ROI sets to better represent subcortical and cerebellar structures. Novel ROIs were created in the thalamus, basal ganglia, and cerebellum by use of a data-driven, winner-take-all partitioning technique that operates on resting-state fMRI data (Choi et al., 2012; Greene et al., 2014; Zhang et al., 2010). Additional ROIs were generated in the amygdala and hippocampus, and all ROIs were validated via several criteria. Finally, we characterized whole-brain functional network organization using these refined subcortical and cerebellar ROIs combined with previously established cortical ROIs. The fully updated set of ROIs is made publicly available for general use, including a list of coordinates and consensus functional network labels, at https://greenelab.wustl.edu/data_software.

2.2 Material and Methods

2.2.1 Primary dataset- WashU 120

Dataset characteristics

The primary dataset used in this study has been described previously (Power et al., 2011). Eyes-open resting-state fMRI data were acquired from 120 healthy, right-handed, native English speaking, young adults (60 F, age range 18-32, mean age 24.7). Subjects were recruited from the Washington University community and screened with a self-report questionnaire. Exclusion criteria included no current or previous history of neurologic or psychiatric diagnosis as well as no head injuries resulting in a loss of consciousness for more than 5 minutes. Informed consent was obtained from all participants, and the Washington University Internal Review Board approved the study. The data are available at https://legacy.openfmri.org/dataset/ds000243/.

Data acquisition

A Siemens MAGNETOM Tim TRIO 3.0T MRI scanner and a 12 channel Head Matrix Coil were used to obtain T1-weighted (MP-RAGE, 2.4s TR, 1x1x1mm voxels) and BOLD contrast sensitive (gradient echo EPI, 2.5s TR, 4x4x4mm voxels) images from each subject. The mean amount of BOLD data acquired per subject was 14 minutes (336 frames, range = 184-729 frames). Subjects were instructed to fixate on a black crosshair presented at the center of a white background. See Power et al., 2011 for full acquisition details.

Preprocessing

The first 12 frames (30 seconds) of each functional run were discarded to account for magnetization equilibrium and an auditory evoked response at the start of the EPI sequence (Laumann et al., 2015). Slice timing correction was applied first. Then, the functional data were aligned to the first frame of the first run using rigid body transforms, motion corrected (3D-cross realigned), and whole-brain mode 1000 normalized (Miezin et al., 2000). Next, the data were resampled (3 cubic mm voxels) and registered to the T1-weighted image and then to a WashU

Talairach atlas (Ojemann et al., 1997) using affine transforms in a one-step operation (Smith et al., 2004).

Additional preprocessing of the resting-state BOLD data was applied to remove artifacts (Ciric et al., 2017; Power et al., 2014). Frame-wise displacement (FD) was calculated as in Power et al., 2012, and frames with FD greater than 0.2 mm were censored. Uncensored segments with fewer than 5 contiguous frames were censored as well (mean +/- std frames retained = 279 +/- 107). All censored frames were interpolated over using least squares spectral estimation (Hocke and Kämpfer, 2009; Power et al., 2014). Next, the data were bandpass filtered from 0.009-0.08 Hz and nuisance regression was implemented. The regression included 36 regressors: the whole-brain mean, individually defined white matter and ventricular CSF signals, the temporal derivatives of each of these regressors, and an additional 24 movement regressors derived by expansion (Friston et al., 1996; Satterthwaite et al., 2012; Yan et al., 2013). FreeSurfer 5.3 automatic segmentation was applied to the T1-weighted images to create masks of the gray matter, white matter, and ventricles for the individual-specific regressors (Fischl et al., 2002). Finally, the data were smoothed with a Gaussian smoothing kernel (FWHM = 6 mm, sigma = 2.55).

At the end of all processing, each censored/interpolated frame was removed from the time series for all further analyses.

2.2.2 Secondary dataset- HCP 80

Dataset characteristics

Due to a partial cutoff of cerebellar data in over half of the subjects in the primary dataset (outside of the field of view), an independent secondary dataset was used to supplement analyses related to the cerebellum. Since the cerebellum was not cutoff in every subject in the primary dataset, we were able to create a cerebellar portion of the group average matrix derived from just those subjects with full cerebellar coverage. We used data from 80 unrelated individuals from the Human Connectome Project (HCP) 500 Subject Release (40F, age range 22-35, mean age 28.4) who had high-quality (low-motion) data, described previously (Gordon et al., 2017a). All HCP data are available at https://db.humanconnectome.org.

Data acquisition

A custom Siemens SKYRA 3.0T MRI scanner and a custom 32 channel Head Matrix Coil were used to obtain high-resolution T1-weighted (MP-RAGE, 2.4s TR, 0.7x0.7x0.7mm voxels) and BOLD contrast sensitive (gradient echo EPI, multiband factor 8, 0.72s TR, 2x2x2mm voxels) images from each subject. The HCP used sequences with left-to-right and right-to-left phase encoding, with a single RL and LR run on each day for two consecutive days for a total of four runs (Van Essen et al., 2012). Thus, for symmetry, the BOLD time series from each subject's best (most frames retained after censoring) LR run and their best RL run were concatenated together.

Preprocessing

The preprocessing steps were the same as those detailed above, except for the following: (1) the first 41 frames (29.52 seconds) of each run were discarded, (2) no slice timing correction was applied, (3) field inhomogeneity distortion correction was applied (using the mean field map), (4) the data were not resampled (they were collected at 2 cubic mm isotropic voxels), and (5) the Gaussian smoothing kernel was smaller (FWHM = 4 mm, sigma = 1.7). The first two changes

are due to the increased temporal resolution of the HCP data acquisition (0.72s TR) and the last two changes are due to the increased spatial resolution of HCP data acquisition (Glasser et al., 2013). Distortion correction was not applied to the primary dataset because field maps were not collected in most participants. In addition, the increased temporal resolution caused respiration artifacts to alias into the FD trace (Fair et al., 2018; Siegel et al., 2017). Thus, FD values were filtered with a lowpass filter at 0.1 Hz and the filtered FD threshold was set at 0.1 mm (mean +/- std frames retained = 2236 +/- 76).

For the purpose of the winner-take-all partitioning of the secondary dataset (described in section 2.2.4), a CIFTI was created for each subject. Thus, preprocessed cortical BOLD time series data (from the secondary dataset only) were mapped to the surface, following the procedure of Gordon et al., 2016, and combined with volumetric subcortical and cerebellar data in the CIFTI format (Glasser et al., 2013; Gordon et al., 2016).

At the end of all processing, each censored/interpolated frame was removed from the time series for all further analyses.

2.2.3 Validation dataset- MSC

Dataset characteristics

Since the primary and secondary datasets were used to create the subcortical and cerebellar ROIs (described in sections 2.2.5 and 2.2.6), results for functional network community assignment (described in section 2.2.7) were validated with a third independent dataset, the Midnight Scan Club (MSC), described previously (Gordon et al., 2017b). These data are available at https://openneuro.org/datasets/ds000224/versions/00002. The MSC dataset consists of 5 hours of

resting-state BOLD data from each of 10 individuals (5 F, age range 24-34, mean age 29) over a two-week period.

Data acquisition

The same scanner, head coil, and acquisition parameters described above were used to for the MSC. However, a single resting-state run lasting 30 minutes was collected on 10 separate days. Each scan was acquired starting at midnight (Gordon et al., 2017b).

Preprocessing

For each subject, all runs were concatenated together in the order that they were collected. The initial preprocessing steps were the same as those detailed above, except for the following: (1) the functional images were registered to the average T2-weighted anatomical image (4 were collected per subject), then to the average T1-weighted anatomical image (4 were collected per subject), and finally to the Talairach atlas, (2) field inhomogeneity distortion correction was applied (using the mean field map), and (3) one subject (MSC08) was excluded due to a substantial amount of low-quality data and self-reported sleeping during acquisition, as detailed previously (Gordon et al., 2017b; Laumann et al., 2016).

Additional preprocessing followed Raut and colleagues (Raut et al., 2019). Again, FD was used to exclude high-motion frames; however, due to respiratory artifacts affecting the realignment parameters (Power et al., 2018; Siegel et al., 2017), a lowpass filter (0.1 Hz) was applied to those parameters before calculation of FD. Consequently, the threshold for frame censoring was lowered to 0.1mm. Frames with outstanding (>2.5 standard deviations above the mode computed across all runs) DVARS values (as calculated in Power et al., 2012) were also excluded. All censored frames were linearly interpolated, and then bandpass filter (0.005-0.1 Hz) was applied.

Finally, component-based nuisance regression was implemented. Individual-specific FreeSurfer 6.0 segmentation was used to define masks of the gray matter, white matter, and ventricles. A mask of extra-axial (or edge (Patriat et al., 2015)) voxels was also created by thresholding the temporal standard deviation image (>2.5%) that excluded the eyes and a dilated whole-brain mask. BOLD data was extracted from all voxels in each mask (separately), and dimensionality reduction was applied as in CompCor (Behzadi et al., 2007). The number of components retained was determined independently for each mask such that the condition number (i.e., the maximum eigenvalue divided by the minimum eigenvalue) was greater than 30. All retained components were submitted to a regressors matrix that also included the 6 realignment parameters. To avoid collinearity, singular value decomposition was applied to the regressors covariance matrix. Components of this decomposition were retained up to an upper limit (condition number >=250). Then, all of the final retained components, the whole-brain mean, and its temporal derivative were regressed from the BOLD time series (Raut et al., 2019).

At the end of all processing, each censored/interpolated frame was removed from the time series for all further analyses.

2.2.4 Winner-take-all partitioning of the subcortex and cerebellum

In order to identify functional subdivisions within subcortical structures and the cerebellum, a winner-take-all partitioning technique was applied to the basal ganglia, thalamus, and cerebellum, as previously described (Greene et al., 2014). Past applications of this winner-take-all approach have yielded results consistent with known connectivity from the animal literature (Buckner et al., 2011; Choi et al., 2012; Fair et al., 2010; Greene et al., 2014; Zhang et al., 2008).

Briefly, the mean resting-state time series were extracted from each of 11 previously defined cortical networks (Power et al., 2011): default mode, frontoparietal, cinguloopercular, salience, dorsal attention, ventral attention, visual, auditory, somatomotor dorsal, somatomotor lateral, and orbitofrontal. This subset of networks (from the original 15 described in Power et al., 2011) was selected on the basis of being previously well characterized and validated by multiple methods (see Greene et al., 2014). In order to remove the shared variance among cortical networks thereby increasing specificity of the subcortico-cortical and cerebello-cortical correlations, partial correlations were then calculated between the time series from each cortical network and the resting-state time series from each subcortical or cerebellar gray matter voxel (e.g., for each cortical network and subcortical voxel, a residual correlation was computed after partialling out the signal from the other cortical networks). Each voxel was then assigned to the network with which it correlated most in a winner-take-all fashion (Buckner et al., 2011; Choi et al., 2012; Greene et al., 2014; Zhang et al., 2010), generating a functional partition of subcortical and cerebellar structures.

2.2.5 ROI creation

Spherical ROIs (diameter = 8mm) were placed in the (volumetric) center of each of the winner-take-all partitions in the basal ganglia, thalamus, and cerebellum. Then, the ROIs were manually adjusted such that (1) all ROIs included only gray matter voxels and (2) no ROIs had any overlapping voxels. If an ROI did not fit entirely within a single winner-take-all partition, it was excluded. Two additional ROIs (one per hemisphere) were added to the center of the amygdala, since the entire structure was assigned to a single network (default mode) via the winner-take-all approach. The winner-take-all approach also assigned the entire hippocampus to a single

network (default mode). However, given previous evidence for distinct functional connectivity profiles for the anterior and posterior portions of the hippocampus (Kahn et al., 2008), we added four ROIs (two per hemisphere) to sample the anterior and posterior hippocampus. In total, 34 subcortical and 27 cerebellar ROIs were created.

These new subcortical and cerebellar ROIs were then combined with two previously described sets of cortical ROIs from our lab, as follows:

ROI Set 1 (Power264 + new): Spherical cortical ROIs were used from the 264 volumetric ROIs reported in (Power et al., 2011). Four of these ROIs in the medial temporal lobe (two per hemisphere) were removed (Talairach coordinates: (-20, -24, -18), (17, -30, -15), (-25, -41, -8), (26, -39, -11)) and replaced by the four new hippocampus ROIs, due to some overlapping voxels. In addition, the 17 subcortical and cerebellar ROIs from the original 264 were replaced by 55 new subcortical and cerebellar ROIs. Finally, the 2 new amygdala ROIs were added. Thus, ROI Set 1 is composed of 239 cortical, 34 subcortical (including the amygdala and hippocampus), and 27 cerebellar volumetric ROIs, for a total of 300 ROIs.

ROI Set 2 (Gordon333 + new): ROI set 2 was generated by combining the 333 surface-based cortical parcels (Gordon et al., 2016) with the newly generated subcortical and cerebellar ROIs. Thus, ROI Set 2 is composed of 333 surface-based cortical parcels and 34 subcortical (including the amygdala and hippocampus) and 27 cerebellar volumetric ROIs, for a total of 394 ROIs. For all analyses using this ROI set, we utilized the center of each cortical parcel projected into

volumetric atlas space (Gordon et al., 2016). The parcels in this format are publicly available at https://sites.wustl.edu/petersenschlaggarlab/parcels-19cwpgu/.

2.2.6 Seedmaps and consensus functional network communities for each ROI

Seedmaps

To validate the winner-take-all assignments of voxels used for ROI placement, we first conducted seedmap analyses to examine how each ROI was correlated with every other gray matter voxel. A seedmap represents the pattern of correlations between the mean BOLD time series from a given ROI and all other gray matter voxels in the brain. We generated group-average seedmaps for both ROI Sets and each dataset (primary, secondary, validation). The preprocessed BOLD time series for each gray matter voxel within each ROI were averaged together (after removing censored and interpolated frames). Then, the Pearson correlation between each new ROI and every other gray matter voxel in the brain was computed for each subject. The subject-specific maps were Fisher transformed, averaged together, and inverse Fisher transformed.

Correlation matrices

We generated correlation matrices to examine the community structure of the new ROIs. A correlation matrix is the set of all possible pairwise correlations between mean BOLD time series from each ROI organized into a symmetric matrix (since correlations are undirected). We computed correlation matrices for both ROI Sets and each dataset (primary, secondary, validation). The preprocessed BOLD time series for each gray matter voxel within each ROI were averaged together (after removing censored and interpolated frames). Then, the Pearson correlation between every pair of ROIs was computed to create a 300 x 300 (ROI Set 1) and 394 x 394 (ROI set 2) correlation matrix for each subject. Matrices were individually Fisher Z

transformed, all matrices were averaged together (within each ROI set and dataset; thus, six group-average matrices were created in total- one 300 x 300 and one 394 x 394 for each of the WashU 120, HCP 80, and MSC 9), and finally, inverse Fisher transformed.

Community detection

To determine the functional network membership of each ROI, an information-theoretic community detection algorithm was implemented (InfoMap (Rosvall and Bergstrom, 2008)). InfoMap requires a sparse matrix, so an edge density threshold was applied to the correlation matrices. The networks (correlation matrices) were thresholded until only the strongest X percent of edges remained. All retained edges maintained their correlation value or weight (i.e., the networks were not binarized). We ran InfoMap over a range of thresholds (X = 2-10% inclusive, with a 1% step increment, following Power et al. (2011)).

In general, the magnitude of BOLD correlations between the cortex and the subcortex, the cortex and the cerebellum, and the subcortex and the cerebellum is substantially weaker than within-structure (and particularly, cortico-cortical) correlations. The primary reasons for this are likely distance from the head matrix coil and signal dropout due to sinuses. For instance, in the primary dataset, off-diagonal (between-structure) correlations from the subcortex and cerebellum account for 40% of the weakest decile of correlations (i.e., the 10% of correlations closest to 0), even though the subcortex and cerebellum account for only 23% of all ROIs. Therefore, in order to ensure that between-structure correlations were included, structure-specific thresholding was used (Marek et al., 2018). The correlation matrix was separated into cortical, subcortical, and cerebellar components (e.g., the subcortical component is every entry in each row corresponding to any subcortical ROI) and the edge density thresholds were applied to each component

separately. Thus, if a 2% structure-specific edge density was applied to the matrix, the top 2% of cortical, top 2% of subcortical, and top 2% of cerebellar correlations (excluding diagonal entries) were extracted and all other correlations were set to 0.

Consensus network procedure

Consensus functional network communities were determined in a semi-automated, multistep process. First, a weighting procedure was applied across InfoMap thresholds. For the 2% and 3% thresholds the weight was 5, for the 4% and 5% thresholds the weight was 3, and the weight was 1 for all other thresholds. These weights were chosen to bias the consensus solution to have approximately 17 networks on the basis of work from Yeo and colleagues (Yeo et al., 2011). Since smaller networks tend to be observed at sparser thresholds, those thresholds contribute more weight than the denser thresholds. For each ROI (independently), the InfoMap-determined community at each threshold was noted, taking the weights into account, and the highest weighted community was assigned as the consensus.

After this automated consensus procedure, authors BAS, CG, and DJG reviewed the community assignment of each new subcortical and cerebellar ROI. In ambiguous cases (e.g., an even split in assignment across thresholds), we consulted literature describing the anatomy and function of that brain region. Furthermore, we visually inspected functional connectivity seedmaps for regions in which the InfoMap and the winner-take-all assignments differed (SI Figure 2.1), and assigned the region to the functional network that most closely matched the seedmap. There were 24 ROIs that required adjudication in this way.

All cortical ROIs retained their original assignment from published works (Power et al., 2011 for ROI Set 1 and from Gordon et al., 2016 for ROI Set 2) unless there was strong evidence to overturn the original. Specifically, if an ROI in the present InfoMap solution received the same assignment across all thresholds and that assignment was distinct from the original, then the ROI was assigned to the novel network community. Furthermore, 5 ROIs originally assigned to the salience network were reassigned to the cingulo-opercular network. We made this change because (1) the ROIs showed profiles intermediate between salience and cinguloopercular assignments and (2) previously published studies revealed that these brain regions demonstrate task-evoked activity consistent with the cingulo-opercular network (Dosenbach et al., 2006; Dubis et al., 2016; Gratton et al., 2018b, 2017; Neta et al., 2014).

Validation of ROIs and consensus networks

The primary and secondary datasets were used to create the subcortical and cerebellar ROIs, respectively. The validation dataset (MSC) was used to test the validity of the consensus functional network communities in both cases. The network community assignment for each ROI was compared across all datasets, and discrepancies were noted. Further, consensus networks were compared with those from previously published literature including the Morel anatomical atlas of the subcortex and the SUIT anatomical atlas of the cerebellum. Additionally, the winner-take-all assignments were compared between split-halves of the primary dataset. Finally, we measured the degree of confidence in the "winning" network for each subcortical and cerebellar voxel by calculating the difference in functional connectivity between the winning and second place network assignments, as in Marek et al., 2018. This analysis was conducted with the primary dataset (WashU 120) for the basal ganglia and thalamus, and with the validation

dataset (MSC) for the cerebellum. We examined the location of each ROI with respect to this estimation of confidence in the winner-take-all assignments (SI Figure 2.2).

2.2.7 Spring-embedded graphs and participation coefficient

To visualize the community structure of networks in an abstract graph space, spring-embedded graphs were created. The networks (correlation matrices) were thresholded in the same way as in Section 2.6.3, and the resulting matrices were submitted to a physical model of connected springs (the Kamada-Kawai algorithm, as used in Power et al., 2011). Correlations between pairs of ROIs were modeled as force constants between connected springs such that strongly correlated ROIs were "pulled" close to one another. ROIs were colored according to their consensus functional network community or their anatomical location.

To quantify the degree to which an ROI plays a hub-like role in the network, the participation coefficient of each ROI was computed across (structure-specific) edge density thresholds between 5 and 25%. Participation coefficient was calculated as defined for weighted networks in Rubinov and Sporns, 2010 using code from the Brain Connectivity Toolbox (Rubinov and Sporns, 2010).

2.3 Results

2.3.1 Subcortical and cerebellar ROIs

The final set of subcortical and cerebellar ROIs overlaid onto the winner-take-all partitions are displayed in **Figures 2.1 and 2.2**, respectively. The winner-take-all partitions were similar to previously published partitions for the basal ganglia (Choi et al., 2012; Greene et al., 2014),

thalamus (Hwang et al., 2017), and cerebellum (Buckner et al., 2011), and showed good split-half replication (dice overlap of 61.5% in the thalamus and 60.1% in the basal ganglia; SI Figure 2.3). Many ROIs outside the cortex agree with anatomical divisions from previously established subcortical (Morel, 2013) and cerebellar (Diedrichsen et al., 2009) atlases, as shown in **Figure 2.3**. ROIs that do not show perfect correspondence with anatomical parcels may reflect discrepancies between anatomical and functional division of these structures, potentially due to finer parcellations in the anatomical atlases. A majority of the ROIs were contained within high confidence winner-take-all parcels, as assessed in Marek et al., 2018 (SI Figure 2.2).

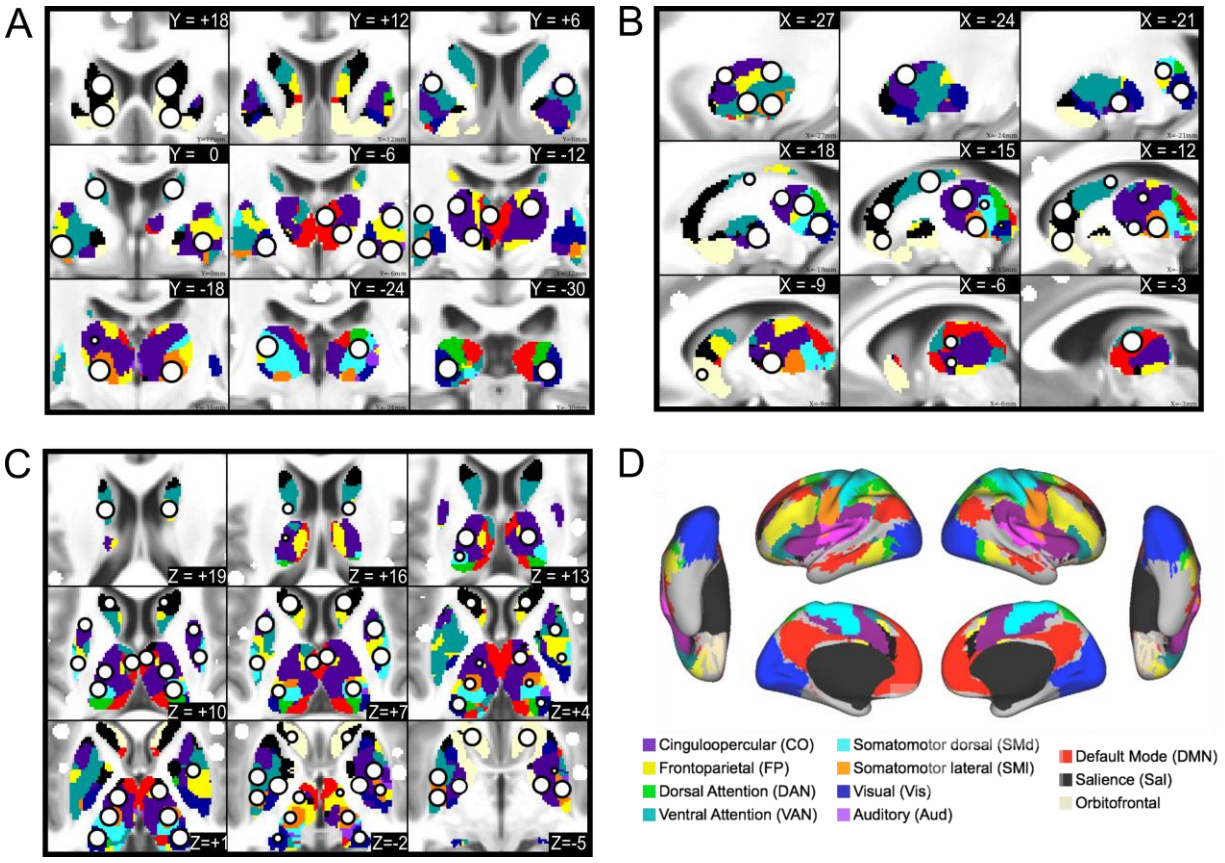

Figure 2.1: Subcortical ROIs. The new ROIs (white circle with black outline) are displayed in serial coronal (A), sagittal (B), and axial (C) sections of the thalamus and basal ganglia, with the cortical functional networks for reference (D). The ROIs are overlaid on top of the voxel-wise winner-take-all partitions.

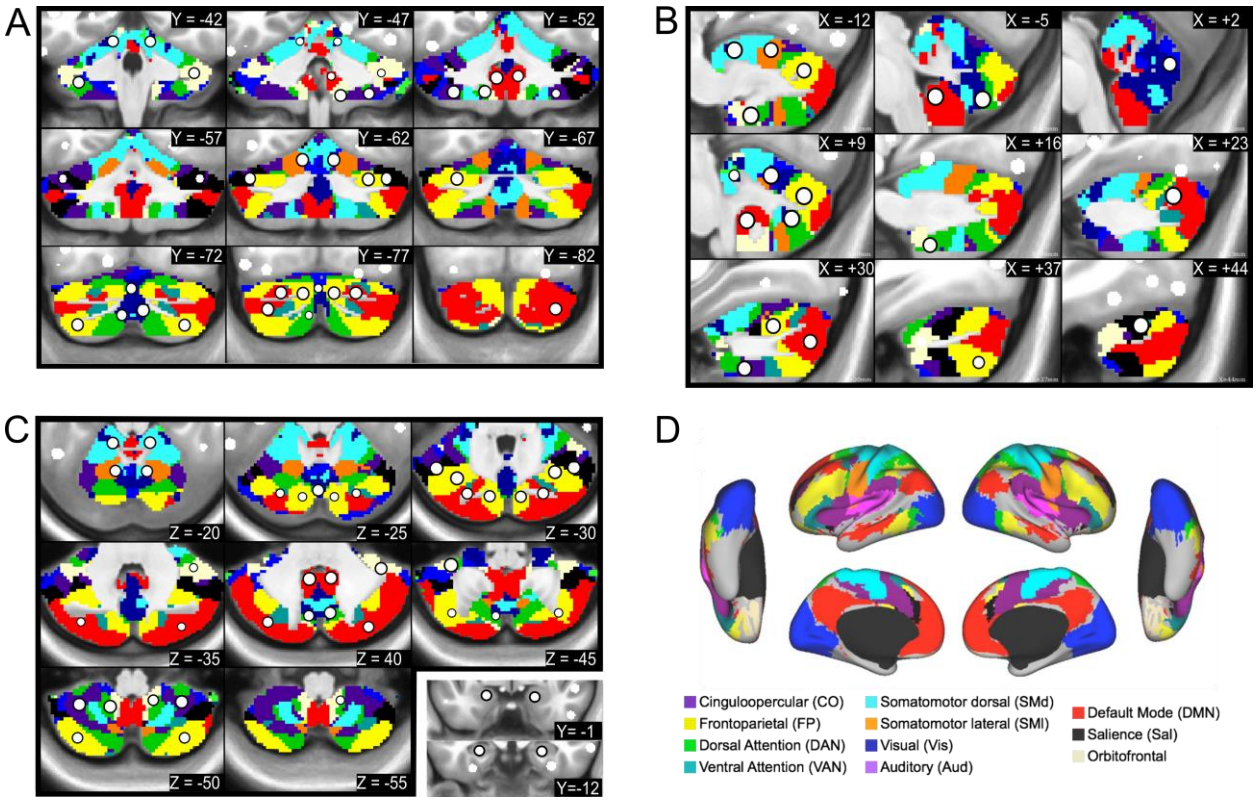

Figure 2.2: Cerebellar ROIs. The new ROIs (white circle with black outline) are displayed in serial coronal (A), sagittal (B), and axial (C) sections of the cerebellum, with the cortical functional networks for reference (D). The ROIs are overlaid on top of the voxel-wise winner-take-all partitions. ROIs in the amygdala and anterior hippocampus are overlaid on anatomical coronal sections in the bottom right panel of C.

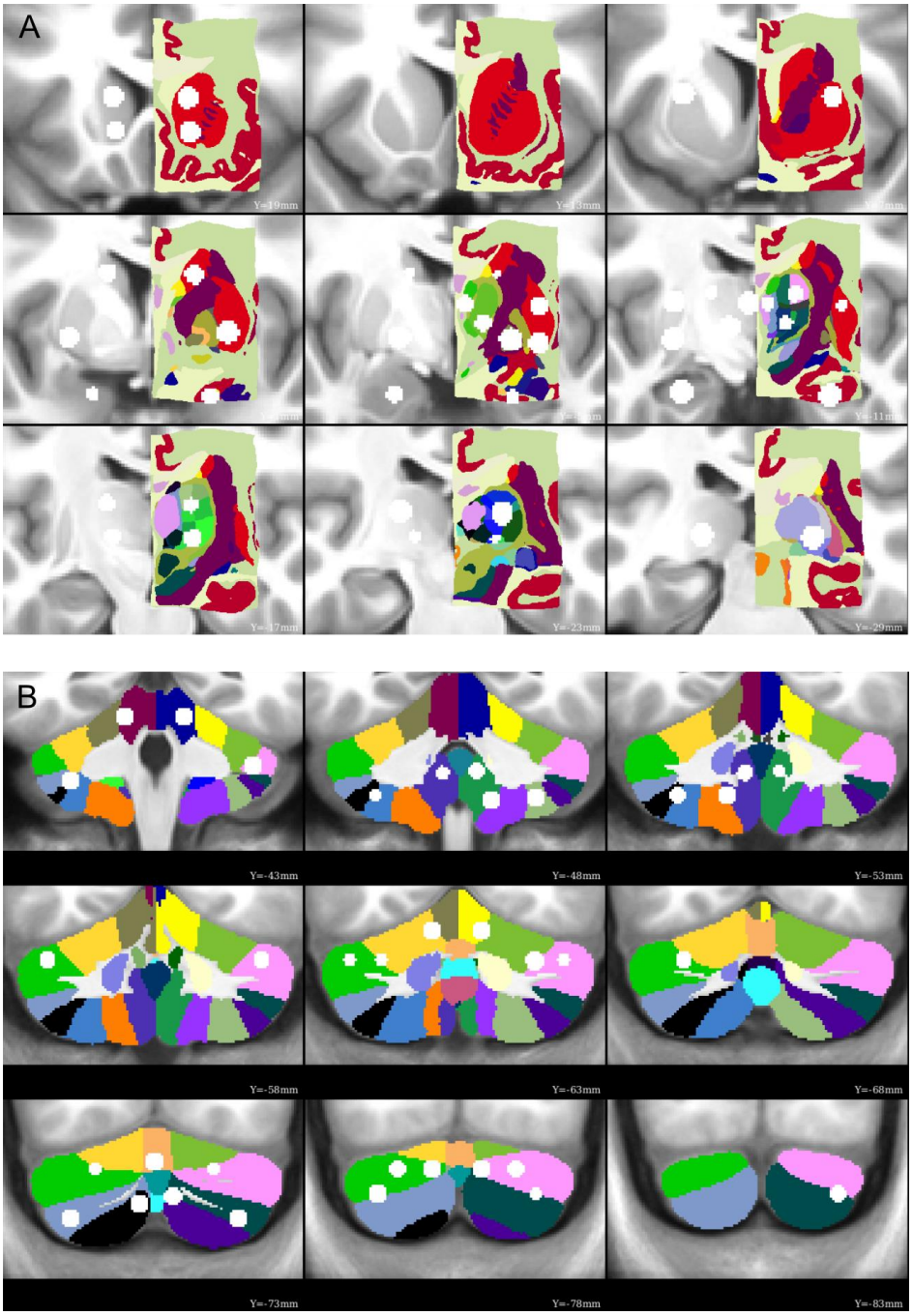

Figure 2.3: Functionally-defined ROIs overlaid onto anatomical parcellations. Many of the subcortical and cerebellar ROIs are contained within a single anatomical parcel from the Morel atlas of the subcortex (A) and the SUIT atlas of the cerebellum (B), indicating good agreement between the current functional parcellation. A few ROIs overlap multiple anatomical parcels (e.g., dorsolateral thalamus, right posterior cerebellum), which may be a consequence of a finer parcellation than is possible with the current fMRI data.

The 34 subcortical ROIs sampled the following anatomical structures (bilaterally): the head and tail of the caudate; anterior dorsal, posterior dorsal, anterior ventral, and posterior ventral putamen; the globus pallidus (internus and externus combined); the ventral striatum (i.e., nucleus accumbens); the amygdala (nuclei not distinguished); anterior and posterior hippocampus; and regions in the thalamus. The locations of the thalamic ROIs included the following nuclei and surrounding territory (the resolution of our data was not fine enough to delineate precise thalamic nuclei): medio-dorsal (MD), latero-dorsal (LD), ventro-anterior (VA), ventro-lateral (VL), ventro-postero-lateral (VPL), and lateral geniculate nucleus (LGN)-pulvinar. The 27 cerebellar ROIs sampled the vestibulo-, spino-, and cerebro-cerebellum, including the cerebellar vermis, classical motor cerebellar cortex, and cerebellar association cortex (Woolsey et al., 2008).

2.3.2 Correlation structure replicates across datasets

Exemplar seedmaps from the new ROIs for the primary dataset are displayed in **Figure 2.4** and the group-average correlation matrices for all datasets using ROI Set 1 are displayed in **Figure 2.5**. The correlation matrices using ROI Set 2 are displayed in SI Figure 2.4. The seedmaps were comparable to previously published maps (Figure 2.4). The matrices were quite similar across datasets ($r_{120,HCP} = 0.90$, $r_{120,MSC} = 0.93$, $r_{HCP,MSC} = 0.87$), with results from the primary dataset replicating best in the validation (MSC) dataset. However, in the secondary (HCP) dataset, there was approximately 0 correlation between subcortical ROIs and all other ROIs, including homotopic subcortical ROI pairs. The likely reason for this difference is due to poor temporal signal-to-noise ratio in the subcortex of HCP data (Ji et al., 2019), which we demonstrate here in SI Figure 2.5. Thus, we excluded the secondary dataset from all further analyses.

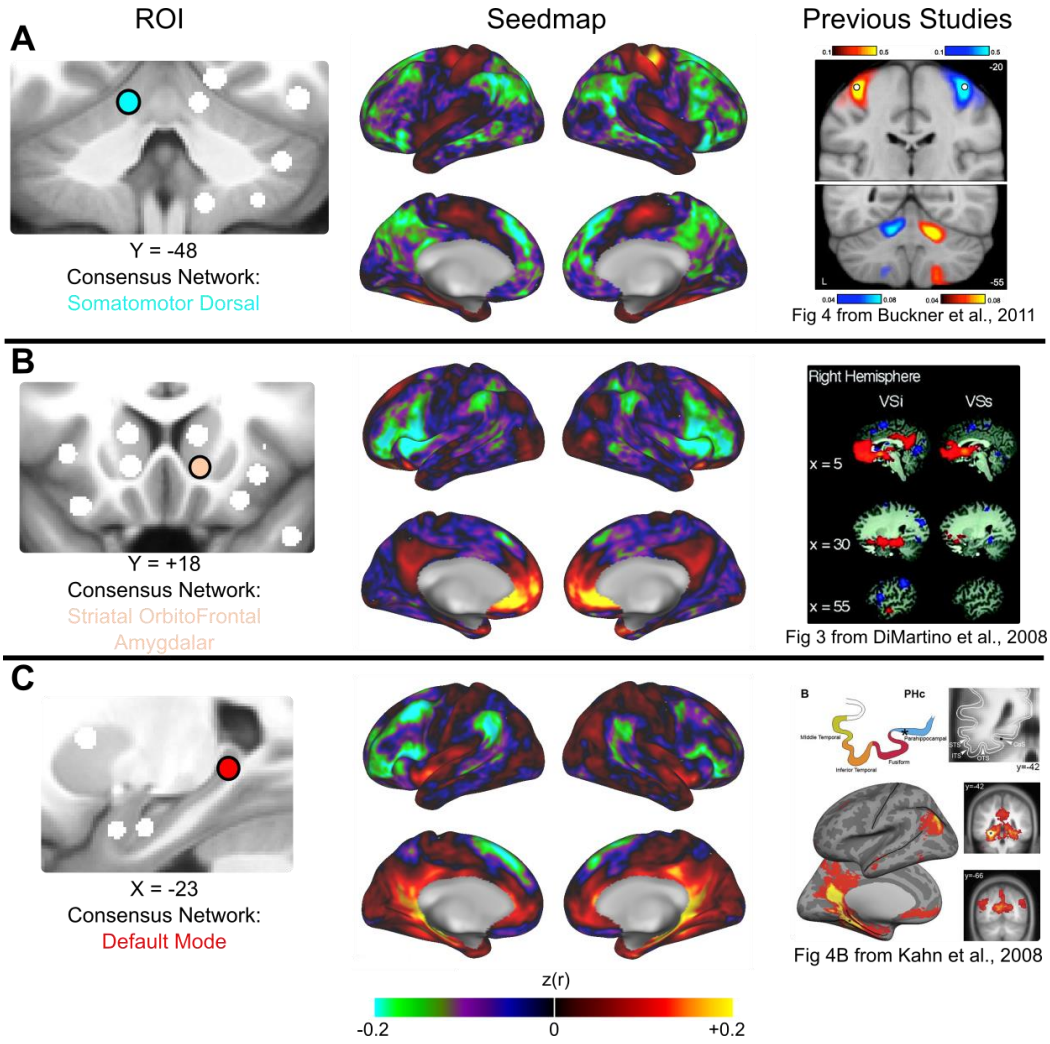

Figure 2.4: Exemplar seedmaps for the new ROIs. Functional correlation seedmaps are shown for an exemplar ROI in the cerebellum (A), ventral striatum (B), and hippocampus (C). The consensus functional network assignment of each ROI is represented by its color (left column). Seedmaps display the correlations between the mean BOLD signal from the ROI in question and the BOLD signal from every other gray matter voxel (middle column). Results were similar to comparable seedmaps from previously published studies (right column). Images from Buckner, R.L. et al., 2011. The organization of the human cerebellum estimated by intrinsic functional connectivity. *Journal of Neurophysiology* 106 (5), 2322–2345; Di Martino, A. et al., 2008. Functional Connectivity of Human Striatum: A Resting State fMRI Study. *Cerebral Cortex* 18 (12), 2735–2747; and, Kahn, I. et al., 2008. Distinct Cortical Anatomy Linked to Subregions of the Medial Temporal Lobe Revealed by Intrinsic Functional Connectivity. *Journal of Neurophysiology* 100 (1), 129–139 reproduced with permission from The American Psychological Society, Oxford University Press, and The American Psychological Society, respectively.

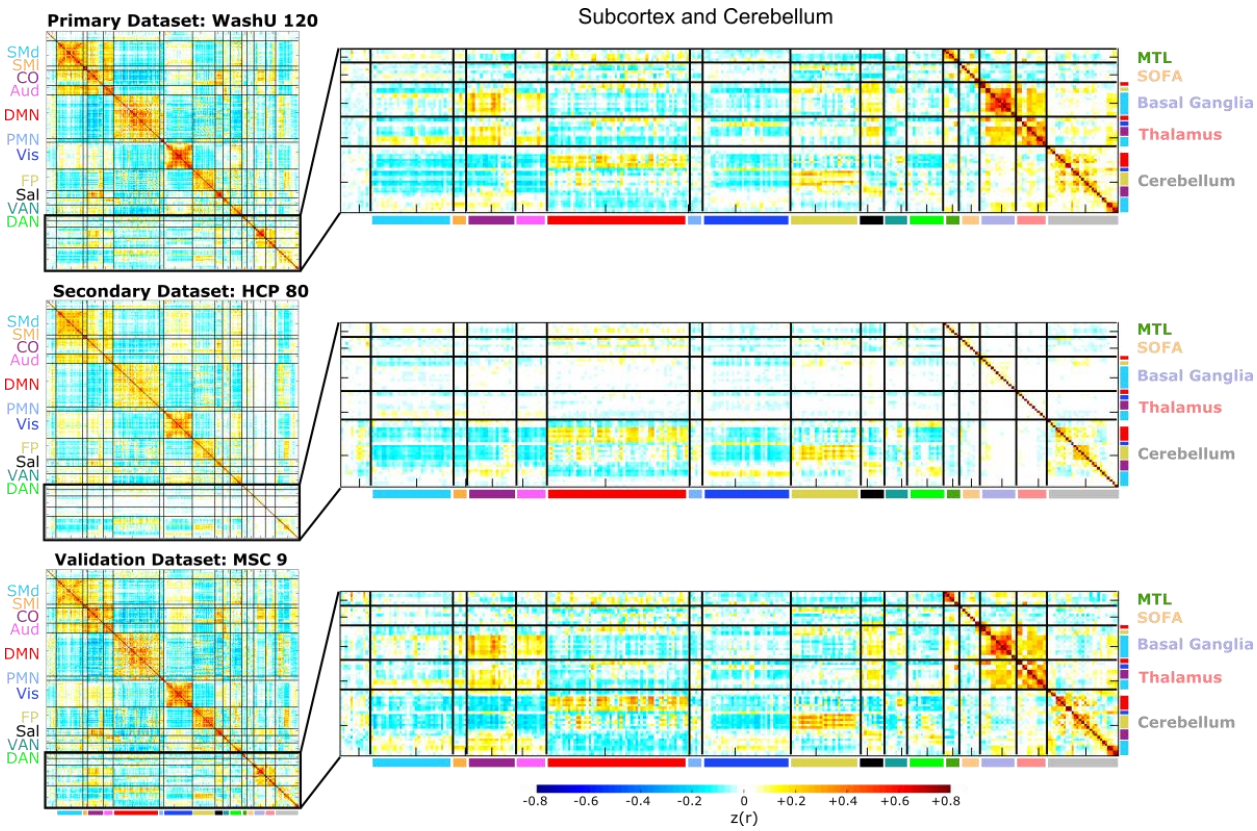

Figure 2.5: Correlation matrices are similar across datasets. The full (300 x 300) correlation matrices for ROI Set 1 are displayed for each dataset in the left column, and zoomed-in versions of the subcortical and cerebellar portions of the matrices are displayed in the right column (the corresponding images for ROI Set 2 are shown in SI Figure 2.4). The cortical portion of the correlation matrix is sorted by functional network community, whereas the subcortical and cerebellar portions are sorted first by anatomical structure (i.e., basal ganglia, thalamus, and cerebellum) and then by functional network community (within each structure). The matrices are similar to one another (e.g., the correlation between the primary and validation datasets is 0.93), except for the subcortical portion of the secondary dataset (HCP- Human Connectome Project). We observed poor temporal signal-to-noise in subcortical HCP data (SI Figure 5). The first row and column of the matrices correspond to unlabeled regions (i.e., InfoMap was unable to assign these ROIs to a network, similar to Power et al., 2011 and Gordon et al., 2016).

2.3.3 Functional network organization using the expanded ROI Set

We used a data-driven community detection algorithm (InfoMap) on weighted networks to determine the functional network community membership of the expanded set of ROIs (Rosvall and Bergstrom, 2008). The results of this analysis are displayed in **Figure 2.6**. Communities are shown for all tested edge density thresholds alongside the consensus network communities (see section 2.2.6).

In the subcortex and cerebellum, the consensus network communities were as follows: ROIs in the caudate associated with the default mode network (head) or the frontoparietal network (tail). The putamen and globus pallidus ROIs joined the somatomotor dorsal network. In the thalamus, the default mode network was assigned to mediodorsal region, the cinguloopercular network to the laterodorsal and ventral anterior regions, the somatomotor dorsal network to the ventrolateral and ventral posterolateral regions, and the visual network to the ROI that includes the lateral geniculate nucleus and the posterior portion of the pulvinar. We use the names of the thalamic nuclei for convenience here, even though the ROIs encompass more gray matter than just the nuclei themselves. Cerebellar ROIs joined various networks, including the default mode, frontoparietal, and cinguloopercular networks (lateral), the somatomotor networks (motor cerebellar cortex), and the visual network (vermis). Most of the observed network assignments agree with known brain function, such as the association between ventral posteriolateral thalamic region and the somatomotor dorsal network.

While some ROIs did not vary in network membership across thresholds (e.g., the tail of the caudate ROIs), others changed network membership after a certain threshold (e.g., the putamen

ROIs) or switched between two or more networks (e.g., some of the thalamic ROIs). This variation is similar to the variation seen with cortical ROI assignments (e.g., see Figure 1 from Power et al., 2011 and Figure 2A from Power et al., 2013) and is indicative of the loss of some finer-scale community structure at denser thresholds.

Importantly, we replicated these community assignments in the validation dataset (MSC; note that we did not use the secondary dataset for this analysis due to poor signal-to-noise in the subcortex). The consensus communities from the primary and validation datasets were broadly consistent across the two ROI Sets, with 55 out of 61 subcortical (including the amygdala and hippocampus) and cerebellar ROIs receiving the same assignment.

Most cortical ROIs retained their functional network membership from Power et al., 2011 (ROI Set 1) or Gordon et al., 2016 (ROI Set 2). Nonetheless, with to the addition of the new ROIs, we observed two functional networks not previously observed with the original ROI sets: (1) a network composed of ROIs in the amygdala, ventral striatum, and orbitofrontal cortex, which we will call the "striatal-orbitofrontal-amygdalar (SOFA)" network and (2) a network composed of ROIs in the anterior hippocampus and entorhinal cortex, which we will call the medial temporal lobe (MTL) network. In addition, in ROI Set 1, 10 previously unlabeled ROIs were now assigned to a network: 4 to the SOFA network, 3 to the MTL network, 2 to the visual network, and 1 to the dorsal attention network. Also, 12 ROIs changed network membership: 2 from the cinguloopercular network to the somatomotor dorsal network, 1 from the auditory network to cinguloopercular network, and 9 from the salience network to the frontoparietal (2), dorsal attention (1), and cinguloopercular (6) networks. For ROI Set 2, 39 previously unlabeled ROIs

were assigned to a network: 8 to the SOFA network, 10 to the MTL network, 16 to the parietooccipital network, and 5 to the default mode network (SI Figure 2.6). Again, consensus communities from the primary and validation datasets were broadly consistent.

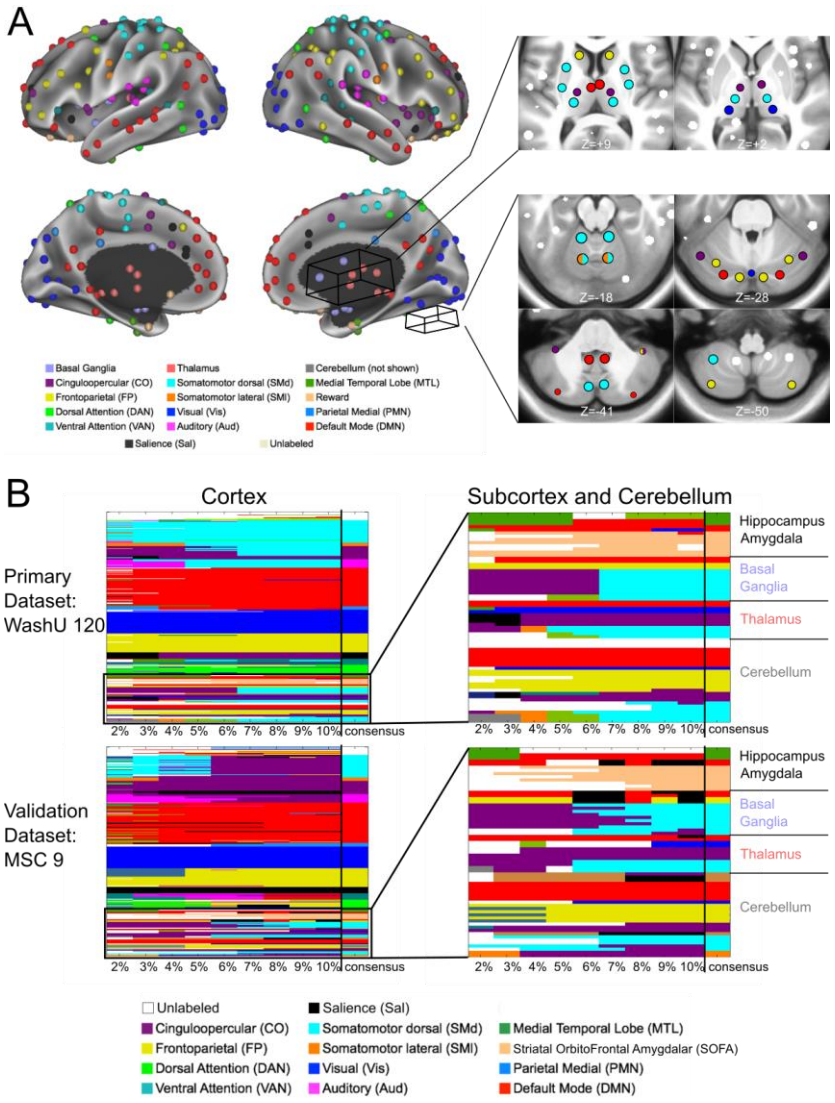

Figure 2.6: InfoMap-defined functional network communities. The InfoMap-defined functional network community of each ROI is displayed. (A) Cortical ROIs are shown projected onto the surface of the brain, and some of the non-cortical ROIs are displayed in axial slices to the right of the cortical surface. (B) The matrices represent the functional network assignment of each ROI across all tested edge densities (each column, denoted by the tick marks, represents one edge density), with the consensus functional network community displayed in the last column of each matrix (delineated by the vertical black line). Results are shown for the primary and validation datasets. The matrices on the left represent the cortical ROIs, and the colors correspond to the labels in A. The matrices on the right show zoomed-in results for all non-cortical ROIs. Results were highly consistent in the subcortex, cerebellum, amygdala, and hippocampus, with a total of 3 disagreements between datasets (in addition to 3 unlabeled ROIs at the bottom of the cerebellum forming their own "network" in the MSC dataset).

2.3.4 Subcortical and cerebellar ROIs integrate with known functional networks

To visualize the ROIs in functional network space, we created spring-embedded graphs, displayed in **Figure 2.7** (other edge densities in SI Figure 2.7). The implemented spring model aggregates nodes with strong correlations between themselves and weak correlations with other nodes. Thus, it is possible to observe which nodes segregate into separate communities and which nodes act as connector hubs, mediating interactions across different network communities (Cohen and D'Esposito, 2016; Gordon et al., 2018; Gratton et al., 2012; Hagmann et al., 2008; Mattar et al., 2015; Power et al., 2013; van den Heuvel and Sporns, 2013).

As is evident from the position of the bolded network nodes, the subcortical and cerebellar ROIs were distributed throughout the spring-embedded graph. For instance, the cerebellar ROIs (gray) were not segregated from the rest of the network communities as in previous reports (Gratton et al., 2018a; Power et al., 2011). This finding was consistent between the primary and validation datasets. However, we observed that the basal ganglia, thalamus, and cerebellum did segregate into their own network communities when the graph was created without structure-specific edge density thresholding (SI Figure 2.7; see Section 2.2.6 for the thresholding procedure). That is, the basal ganglia, thalamus, and cerebellum clustered into their own separate network communities with standard edge density thresholding (applying the threshold uniformly to the whole correlation matrix), likely because of the lower correlation magnitudes associated with these regions.

To assess the effect of including the new ROIs on network topology, we examined two graph-theoretic network measures: modularity and participation coefficient (SI Figure 2.8; Rubinov and Sporns, 2010). Addition of the non-cortical ROIs decreased modularity, with structure-specific thresholding resulting in a further decrease. Similarly, the participation coefficient of ROIs in the subcortex was significantly higher, on average, than ROIs in the other structures. Structure-specific thresholding resulted in higher average participation coefficient for all structures.

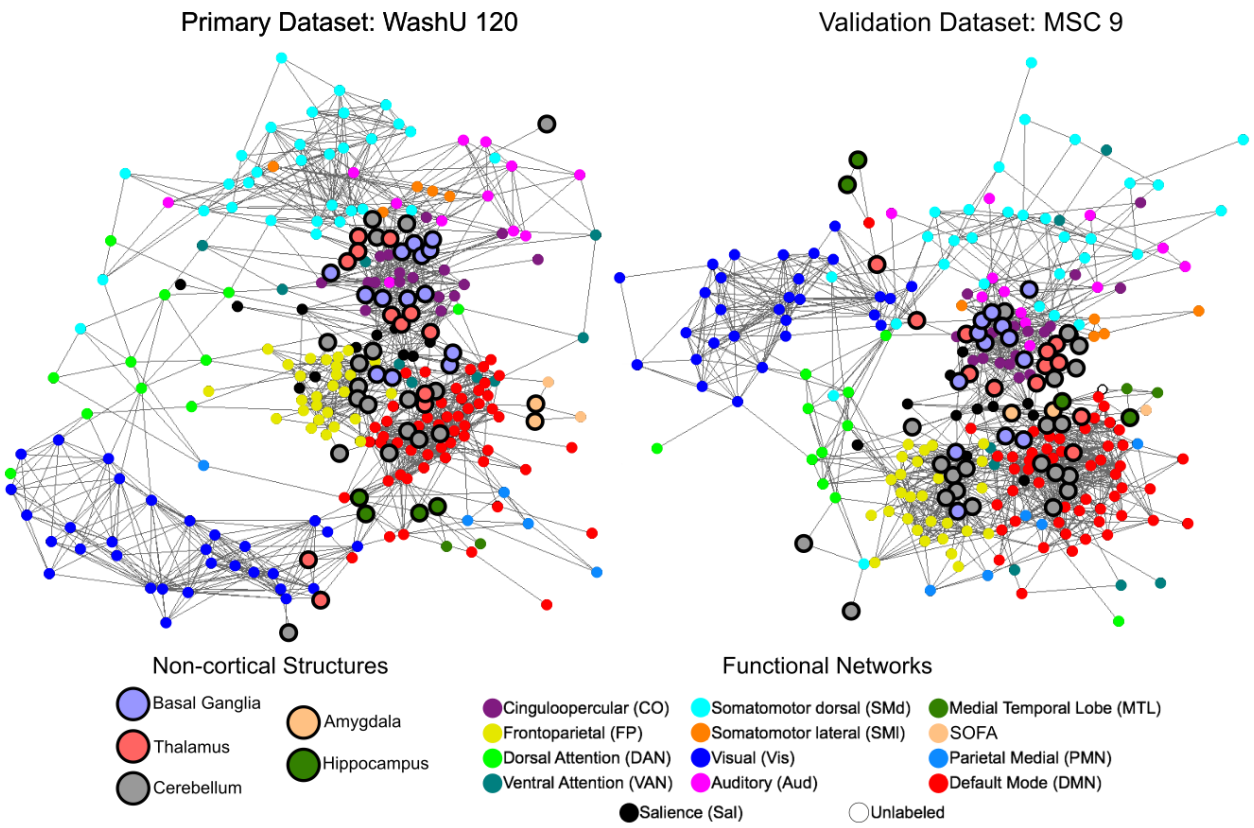

Figure 2.7: Spring-embedded graphs show that subcortical and cerebellar ROIs integrate with well-characterized network communities. Spring-embedded graphs are displayed for ROI Set 1 using the primary and validation datasets at a structure-specific edge density threshold of 3% (other edge densities shown in SI Figure 2.7; see section 2.2.6 for the thresholding procedure). Non-cortical ROIs are larger and have a bold outline. The color of each ROI represents its consensus functional network community assignment, except for the non-cortical ROIs, which are labeled by anatomical structure. The basal ganglia, thalamus, and cerebellum distribute throughout the graph, integrating with well-characterized networks rather than segregating into their own communities.

2.4 Discussion

Here we present a set of regions of interest (ROIs) that sample the basal ganglia, thalamus, cerebellum, amygdala, and hippocampus more completely than previous ROI sets in order to provide a whole-brain description of functional network organization. We found that the refined region sets recapitulate previous network organization results in the cortex and extend functional brain network characterization to the subcortex and cerebellum. Notably, these results replicated across independent datasets. In addition, with the inclusion of the new ROIs, we observe two additional functional networks that were not present in Power et al. (2011) and Gordon et al. (2016): a striatal-orbitofrontal-amygdalar (SOFA) network and a medial temporal lobe (MTL) network.

2.4.1 Improved sampling of the subcortex and cerebellum

Many recent research efforts have used the 264 ROIs from Power et al., 2011 or the 333 surface-based parcels from Gordon et al., 2016 to study brain network organization. These studies have examined both structural and functional network organization in a wide variety of samples, including healthy young adults (Power et al., 2013; Zanto and Gazzaley, 2013), developmental cohorts (Gu et al., 2015; Nielsen et al., 2018; Rudolph et al., 2017), older adults (Baniqued et al., 2018; Gallen et al., 2016), and a plethora of neurological and psychiatric populations (Gratton et al., 2018a; Greene et al., 2016; Sheffield et al., 2015; Siegel et al., 2018). We have gained a better understanding of typical and atypical human brain organization from these efforts. However, a full characterization of whole-brain network organization in these populations is incomplete due to the common unsderrepresentation of the subcortex and cerebellum. While there is recent work that has focused separately on networks in the thalamus, subcortex, and cerebellum (e.g., Bell

and Shine, 2016; Buckner et al., 2011; Choi et al., 2012; Greene et al., 2014; Hwang et al., 2017), here we offer a set of ROIs that encompass all of these structures to encourage broader adoption of a whole-brain approach.

The functionally-defined subcortical and cerebellar ROIs presented in the current work provide a better sampling of these structures. By improving their representation, we were able to delineate well-characterized and additional functional network communities (relative to our past descriptions). The ability to uncover these networks, which have been previously described using other methods, illustrates the importance of representing the entire brain in network-based analyses. Further, these improved ROI sets may allow future studies to discover previously unobserved, yet critical deviations in functional network organization in diseases and disorders in which the subcortex and cerebellum are implicated (e.g., Parkinson Disease, Tourette Syndrome, Schizophrenia).

It is worth noting that, by definition, the cortical surface parcels omit the subcortex and cerebellum. Yet, it is technically possible to parcellate the subcortex and cerebellum using an adapted gradient-based methodology (such as the one from Gordon et al., 2016). This approach would require extending the gradient technique to three dimensions. As fMRI technology and analysis strategies improve, it would be useful to compare the current results to a full subcortical and cerebellar parcellation using this or other gradient-based techniques.

A methodological issue to note is that the winner-take-all approach used to define subcortical and cerebellar parcels here may be sensitive to the number of *a priori* cortical networks used in

the analysis. Increasing the number of cortical networks included may allow for finer parcellation of certain structures. Here we used previously well-characterized cortical networks that have been consistently found using multiple methods by multiple research groups. Conversely, InfoMap does not require an *a priori* number of networks, but may be sensitive to thresholding issues (discussed below). Importantly, final network assignments for the ROIs were designated using a combination of both techniques.

2.4.2 Functional connectivity of the refined ROIs is consistent with previous studies and replicates across independent datasets

Correlation seedmaps from the refined ROIs agree with functional connectivity profiles reported in previous studies. For example, the ROIs added to the ventral striatum and the head of the caudate correspond closely to the seeds placed in the superior ventral striatum (VSs) and dorsal caudate (DC) reported in Di Martino et al., 2008, and our seedmaps are highly similar to theirs. Likewise, seedmaps from the hippocampus and amygdala agree well with those from Kahn et al., 2008 and Roy et al., 2009, respectively. The same is true for the thalamus (Hwang et al., 2017) and cerebellum (Buckner et al., 2011).

Moreover, the full correlation structure (shown in correlation matrices) was quite comparable across the diverse datasets. The one major discrepancy was that in the subcortical portion of the matrix from the secondary (HCP) dataset, we observed correlations near zero. The reason for this observation is likely poor temporal signal-to-noise ratio (tSNR) in the subcortex of HCP data (Ji et al., 2019). Several factors may contribute to this poor tSNR. (1) The HCP used a custom scanner and coil, which caused unique magnetic field inhomogeneities, possibly in part due to subjects' heads being outside of the isocenter of the field. (2) The imaging sequence used an

aggressive multiband factor and TR (MB = 8, TR = 0.72s) and (3) small voxels (2 cubic mm) were used for acquisition (Glasser et al., 2013; Van Essen et al., 2012). Each of these factors substantially increase electronic, thermal, and other physical sources of noise (Triantafyllou et al., 2005) relative to slower sequences with larger voxels. These effects may be amplified as a function of the distance of the imaged structure from the head coil, resulting in the poorest tSNR in the subcortex. Further work is needed to determine the specific contributions of each factor, as well as others heretofore unconsidered, to the observed poor tSNR.

The presented group-level descriptions converge on a very similar picture of functional network organization in the subcortex and cerebellum. However, there are individual differences in both subcortical and cerebellar functional network organization (Marek et al., 2018; Greene et al., under review), as have been found in cortical functional network organization. Future work designed for in-depth study of individuals, as in Poldrack et al., (2015), Filevich et al., 2017, Braga and Buckner (2017), and Gordon et al. (2017b), will be important for elucidating such individual differences. In fact, in-depth study of the cerebellum (Marek et al., 2018) and subcortex (Greene et al., under review) in individuals reveals both common and unique features in its functional organization. Furthermore, future work may be able to include the brainstem as well in a whole-brain functional network atlas, although there are several technical issues to overcome (e.g., CSF pulsations, small nuclei size).

2.4.3 SOFA and MTL functional networks map onto known human brain systems

Group-average functional network organization in the cerebral cortex is largely consistent across studies (Power et al., 2011; Yeo et al., 2011), and the addition of refined subcortical and

cerebellar ROIs did not change functional network organization in the cortex substantially (although we observed associations between these canonical networks and ROIs in the subcortex and cerebellum). However, the addition of these subcortical and cerebellar ROIs allowed for the identification of two additional functional networks compared to the networks reported using the original ROI sets in Power et al. (2011) and Gordon et al. (2016): (1) the "SOFA" network composed of the amygdala, orbitofrontal cortex, and ventral striatum, and (2) the "medial temporal lobe (MTL)" network composed of the anterior hippocampus and entorhinal cortex. It is worth noting that the SOFA network has been observed in studies focusing on reward and emotion processing (Camara et al., 2009) and its cortical and striatal portions are very similar to the limbic network from Yeo et al., (2011) and Choi et al., (2012). The MTL network has been observed in a study of highly-sampled individuals (Gordon et al., 2017b) as well as studies focused on the hippocampus (Greicius et al., 2009). Here, we demonstrate that these networks are measurable at the group-level when the whole brain is represented sufficiently. In addition, we found that some cortical ROIs that were previously unlabeled (i.e., they did not group with any community) received labels with the inclusion of the refined subcortical and cerebellar ROIs, with many of them joining the SOFA and MTL networks.

The SOFA and MTL functional networks map onto well-characterized brain systems. Most of the ROIs in the SOFA network are likely connected to each other anatomically in rodents, nonhuman primates, and humans (Ongur and Price, 2000; Carmichael and Price, 1995; Amaral and Price, 1984). Moreover, these brain areas are known to be functionally related, as they are important for various aspects of decision making and reward-related behavior, such as economic choice (Padoa-Schioppa and Assad, 2006), emotional regulation (Phelps, 2006), and gambling

(Bechara et al., 2000, 1997). Likewise, the ROIs in the MTL network are well-connected anatomically (Duvernoy, 1988; Woolsey et al., 2008) and support various aspects of memory formation, consolidation, and retrieval, as well as other important functions, such as spatial mapping (Burgess et al., 2002; Moser and Moser, 1998; Tulving and Markowitsch, 1998). Though our current work is agnostic to the function of these brain systems, we show that their constituent regions demonstrate coherent spontaneous fluctuations in infraslow BOLD signal.

2.4.4 Subcortical and cerebellar ROIs integrate with known functional networks

To visualize the organization of the ROIs in functional network space, we created spring-embedded graphs. We observed that the subcortical and cerebellar ROIs integrate with various well-characterized network communities composed of cortical regions instead of segregating on their own (i.e., away from cortical ROIs), particularly after structure-specific thresholding (see below). This organization fits with the known anatomy and function of the subcortex and cerebellum better than a model in which each structure is segregated into its own community. For instance, individual nuclei in the thalamus project directly to distinct brain systems (Woolsey et al., 2008) and play unique roles in behaviors associated with those systems (Guillery, 1995; Van Der Werf et al., 2000). Likewise, cortico-striatal and cerebello-cortical anatomical connections show specific projections to unique regions of cortex (Woolsey et al., 2008) and are known to be integral for the function of various large-scale, distributed systems, such as the motor system (Glickstein and Doron, 2008) and regions of higher order systems (Alexander et al., 1986; Strick et al., 2009). Investigation of network measures revealed that the subcortical ROIs have a higher participation coefficient, on average, than other structures, meaning they have modest-to-high correlations with multiple networks. This result is consistent with the idea

that subcortical structures contain integrative hubs (Hwang et al., 2017); Greene et al., under review). Likewise, the non-cortical ROIs decrease the modularity of the whole network, reflecting decreased segregation and increased integration. It should be noted, however, that several methodological factors may affect or potentially bias participation coefficient, such as structure-specific thresholding and the interaction between structure size and BOLD fMRI spatial autocorrelation.

The demonstration of integration of subcortical and cerebellar ROIs within cortical networks was revealed by the use of structure-specific edge density thresholding (i.e., thresholding the cortex, subcortex, and cerebellum separately). In most network analyses, only the strongest positive correlations are considered for network-based analyses, such as spring-embedded graphs. However, subcortical correlations are generally weaker than cortical correlations (likely due to distance from the head matrix coil and signal dropout due to sinuses). Thus, if the top 5% strongest positive correlations are selected, almost all subcortical correlations will be excluded. To avoid this exclusion, we implemented structure-specific thresholding. This choice ultimately affects the nature of the spring-embedded graph as well as the determination of functional network communities and network measures. Without structure-specific thresholding, subcortical ROIs group with one another into two separate network communities (basal ganglia and thalamus), while the entire cerebellum is lumped into one network community. In terms of human brain functional organization, this pattern of clustering seems artificially inflated due to low subcortex-to-cortex and cerebellum-to-cortex correlations. By using structure-specific thresholding, we were able to observe functional network organization that is more consistent with the known functions of the subcortex and cerebellum. However, this approach may affect

graph theoretic network measures, such as participation coefficient, in the subcortex and cerebellum, and thus, deserves future investigation.

2.4.5 "Optimal" ROI set depends on research question

There are advantages to both anatomical and functional network-based divisions of ROIs. For instance, anatomical network divisions allow for analysis of important distinctions between the cortex, subcortex, and cerebellum, whereas functional network divisions are likely to better represent putative brain function. Likewise, there are fundamental differences between anatomical and functional atlases, with anatomical atlases parsing the brain according to anatomical divisions and cytoarchitecture, and functional atlases parsing the brain according to functional criteria. For instance, the cerebellum is probabilistically divided into lobes and crura in one anatomical atlas (Diedrichsen et al., 2009). While many of these divisions align well with the ROIs presented here, some ROIs do not fit within the probabilistic boundaries. Thus, some ROIs may better reflect functional rather than anatomical divisions in the cerebellum. Similarly, many of the divisions in a commonly used subcortical anatomical atlas (Morel, 2013) agree well with the ROIs, with the exception of a few anatomical parcels that are likely beyond the resolution of the fMRI data used here. Ultimately, researchers should be cognizant of these effects when choosing how to perform network-based analyses and which atlas or ROI Set to use. We advise readers to use the analysis strategy and atlas that best suits their research questions.

2.5 Conclusions

We created new subcortical and cerebellar ROIs to improve the representation of these structures for brain network analysis. Combining these new ROIs with previously characterized cortical ROIs allowed further insight into whole-brain functional network organization. Going forward, inclusion of these ROIs will yield more comprehensive results from fMRI studies of typical and atypical brain organization and function. The ROI Sets and consensus functional network assignments described here are available for immediate download and use at https://greenelab.wustl.edu/data_software.

2.6 Acknowledgments

This work was supported by National Institutes of Health grants T32 NS073547 (BAS), F32 NS092290 (CG), T32 MH10001902 (SM), K23 NS088590 (NUFD), UL1 TR000448 (NUFD), R01 NS32979 (SEP), R01 NS06424 (SEP), and K01 MH104592 (DJG); the National Science Foundation grant DGE-1745038 (RVR); the Jacobs Foundation grant 2016121703 (NUFD); the Child Neurology Foundation (NUFD); the Mallinckrodt Institute of Radiology grant 14-011 (NUFD); the Hope Center for Neurological Disorders (NUFD, BLS, SEP); the James S. McDonnell Foundation Collaborative Activity Award (SEP); the McDonnell Center for Systems Neuroscience (NUFD, BLS, DJG); and, the Tourette Association of America (DJG).

2.7 Author Contributions

BAS, CG, and DJG designed the study. BAS, CG, SM, RVR, and DJG analyzed the data. All authors wrote the manuscript.

2.8 Competing Interests

All authors declare no competing interests.

2.9 Chapter 2 References

Alexander, G.E., DeLong, M.R., Strick, P.L., 1986. Parallel Organization of Functionally Segregated Circuits Linking Basal Ganglia and Cortex. Annu. Rev. Neurosci. 9, 357–381. doi:10.1146/annurev.neuro.9.1.357

Allman, J.M., Kaas, J.H., 1971. A representation of the visual field in the caudal third of the middle tempral gyrus of the owl monkey (Aotus trivirgatus). Brain Res. 31, 85–105. doi:10.1016/0006-8993(71)90635-4

Andreasen, N.C., Nopoulos, P., O'Leary, D.S., Miller, D.D., Wassink, T., Flaum, M., 1999. Defining the phenotype of schizophrenia: Cognitive dysmetria and its neural mechanisms. Biol. Psychiatry. doi:10.1016/S0006-3223(99)00152-3

Andreasen, N.C., O'Leary, D.S., Cizadlo, T., Arndt, S., Rezai, K., Ponto, L.L., Watkins, G.L., Hichwa, R.D., 1996. Schizophrenia and cognitive dysmetria: a positron-emission tomography study of dysfunctional prefrontal-thalamic-cerebellar circuitry. Pnas 93, 9985–9990. doi:10.1073/pnas.93.18.9985

Baniqued, P.L., Gallen, C.L., Voss, M.W., Burzynska, A.Z., Wong, C.N., Cooke, G.E., Duffy, K., Fanning, J., Ehlers, D.K., Salerno, E.A., Aguiñaga, S., McAuley, E., Kramer, A.F., D'Esposito, M., 2018. Brain network modularity predicts exercise-related executive function gains in older adults. Front. Aging Neurosci. 9. doi:10.3389/fnagi.2017.00426

Bassett, D.S., Bullmore, E., 2006. Small-world brain networks. Neuroscientist 12, 512–523. doi:10.1177/1073858406293182

Bechara, A., Damasio, H., Damasio, A.R., 2000. Emotion,Decision Making and the Orbitofrontal Cortex. Cereb. Cortex 10, 295–307. doi:10.1093/cercor/10.3.295

Bechara, A., Damasio, H., Tranel, D., Damasio, A.R., 1997. Deciding advantageously before knowing the advantageous strategy. Science (80-.). 275, 1293–1295. doi:10.1126/science.275.5304.1293

Behzadi, Y., Restom, K., Liau, J., Liu, T.T., 2007. A component based noise correction method (CompCor) for BOLD and perfusion based fMRI. Neuroimage 37, 90–101. doi:10.1016/j.neuroimage.2007.04.042

Bell, P.T., Shine, J.M., 2016. Subcortical contributions to large-scale network communication. Neurosci. Biobehav. Rev. doi:10.1016/j.neubiorev.2016.08.036

Bigelow, N.O., Turner, B.M., Andreasen, N.C., Paulsen, J.S., O'Leary, D.S., Ho, B.C., 2006. Prism adaptation in schizophrenia. Brain Cogn. 61, 235–242. doi:10.1016/j.bandc.2006.01.004

Biswal, B., Yetkin, F.Z., Haughton, V.M., Hyde, J.S., 1995. Functional connectivity in the motor cortex of resting human brain using echo-planar MRI. Magn. Reson. Med. 34, 537–541. doi:10.1002/mrm.1910340409

Bondy, J.A., Murty, U.S.R., 1976. Graph theory with applications. Graph Theory. doi:10.2307/3008805

Bostan, A.C., Strick, P.L., 2018. The basal ganglia and the cerebellum: nodes in an integrated network. Nat. Rev. Neurosci. 1–13. doi:10.1038/s41583-018-0002-7

Braga, R.M., Buckner, R.L., 2017. Parallel Interdigitated Distributed Networks within the Individual Estimated by Intrinsic Functional Connectivity. Neuron 95, 457–471.e5. doi:10.1016/j.neuron.2017.06.038

Brown, S.M., Kieffaber, P.D., Carroll, C.A., Vohs, J.L., Tracy, J.A., Shekhar, A., O'Donnell, B.F., Steinmetz, J.E., Hetrick, W.P., 2005. Eyeblink conditioning deficits indicate timing and cerebellar abnormalities in schizophrenia. Brain Cogn. 58, 94–108. doi:10.1016/j.bandc.2004.09.011

Buckner, R.L., Krienen, F.M., Castellanos, a., Diaz, J.C., Yeo, B.T.T., 2011. The organization of the human cerebellum estimated by intrinsic functional connectivity. J. Neurophysiol. 106, 2322–2345. doi:10.1152/jn.00339.2011

Bullmore, E., Sporns, O., 2009. Complex brain networks: graph theoretical analysis of structural and functional systems. Nat. Rev. Neurosci. 10, 186–98. doi:10.1038/nrn2575

Bullmore, E.T., Bassett, D.S., 2011. Brain Graphs: Graphical Models of the Human Brain Connectome. Annu. Rev. Clin. Psychol. 7, 113–140. doi:10.1146/annurev-clinpsy-040510-143934

Burgess, N., Maguire, E. a, O'Keefe, J., 2002. The human hippocampus and spatial and episodic memory 1. Neuron 35, 625–641. doi:10.1016/S0896-6273(02)00830-9

Butts, C.T., 2009. Revisiting the foundations of network analysis. Science (80-.). doi:10.1126/science.1171022

Butts, C.T., 2008. Social network analysis: A methodological introduction. Asian J. Soc. Psychol. 11, 13–41. doi:10.1111/j.1467-839X.2007.00241.x

Camara, E., Rodriguez-Fornells, A., Münte, T.F., 2009. Functional connectivity of reward processing in the brain. Front. Hum. Neurosci. 2, 19. doi:10.3389/neuro.09.019.2008

Choi, E.Y., Yeo, B.T.T., Buckner, R.L., 2012. The organization of the human striatum estimated by intrinsic functional connectivity. J. Neurophysiol. 108, 2242–63. doi:10.1152/jn.00270.2012

Ciric, R., Wolf, D.H., Power, J.D., Roalf, D.R., Baum, G., Ruparel, K., Shinohara, R.T., Elliott, M.A., Eickhoff, S.B., Davatzikos, C., Gur, R.C., Gur, R.E., Bassett, D.S., Satterthwaite, T.D., 2017. Benchmarking confound regression strategies for the control of motion artifact in studies of functional connectivity. Neuroimage 154, 174–187. doi:10.1016/j.neuroimage.2017.03.020

Cohen, A.L., Fair, D.A., Dosenbach, N.U.F., Miezin, F.M., Dierker, D., Van Essen, D.C., Schlaggar, B.L., Petersen, S.E., 2008. Defining functional areas in individual human brains using resting functional connectivity MRI. Neuroimage 41, 45–57. doi:10.1016/j.neuroimage.2008.01.066

Cohen, J.R., D'Esposito, M., 2016. The Segregation and Integration of Distinct Brain Networks and Their Relationship to Cognition. J. Neurosci. 36, 12083–12094. doi:10.1523/JNEUROSCI.2965-15.2016

Corbetta, M., Shulman, G.L., 2011. Spatial neglect and attention networks. Annu. Rev. Neurosci. 34, 569–99. doi:10.1146/annurev-neuro-061010-113731

Craddock, R.C., James, G.A., Holtzheimer, P.E., Hu, X.P., Mayberg, H.S., 2012. A whole brain fMRI atlas generated via spatially constrained spectral clustering. Hum. Brain Mapp. 33, 1914–1928. doi:10.1002/hbm.21333

Di Martino, A., Scheres, A., Margulies, D.S., Kelly, A.M.C., Uddin, L.Q., Shehzad, Z., Biswal, B., Walters, J.R., Castellanos, F.X., Milham, M.P., 2008. Functional Connectivity of Human Striatum: A Resting State fMRI Study. Cereb. Cortex 18, 2735–2747. doi:10.1093/cercor/bhn041

Diedrichsen, J., Balsters, J.H., Flavell, J., Cussans, E., Ramnani, N., 2009. A probabilistic MR atlas of the human cerebellum. Neuroimage 46, 39–46. doi:10.1016/j.neuroimage.2009.01.045

Dosenbach, N.U.F., Visscher, K.M., Palmer, E.D., Miezin, F.M., Wenger, K.K., Kang, H.C., Burgund, E.D., Grimes, A.L., Schlaggar, B.L., Petersen, S.E., 2006. A Core System for the Implementation of Task Sets. Neuron 50, 799–812. doi:10.1016/j.neuron.2006.04.031

Dubis, J.W., Siegel, J.S., Neta, M., Visscher, K.M., Petersen, S.E., 2016. Tasks Driven by Perceptual Information Do Not Recruit Sustained BOLD Activity in Cingulo-Opercular Regions. Cereb. Cortex 26, 192–201. doi:10.1093/cercor/bhu187

Duvernoy, H.M., 1988. The Human Hippocampus: An Atlas of Applied Anatomy, JF Bergmann Munich. doi:10.1007/978-3-642-54195-7

Fair, D.A., Bathula, D., Mills, K.L., Costa Dias, T.G., Blythe, M.S., Zhang, D., Snyder, A.Z., Raichle, M.E., Stevens, A.E., Nigg, J.T., Nagel, B.J., 2010. Maturing thalamocortical functional connectivity across development. Front. Syst. Neurosci. doi:10.3389/fnsys.2010.00010

Fair, D.A., Miranda-Dominguez, O., Snyder, A.Z., Perrone, A.A., Earl, E.A., Van, A.N., Koller, J.M., Feczko, E., Klein, R.L., Mirro, A.E., Hampton, J.M., Adeyemo, B., Laumann, T.O., Gratton, C., Greene, D.J., Schlaggar, B., Hagler, D., Watts, R., Garavan, H., Barch, D.M., Nigg, J.T., Petersen, S.E., Dale, A., Feldstein-Ewing, S.W., Nagel, B.J., Dosenbach, N.U.F., 2018. Correction of respiratory artifacts in MRI head motion estimates. bioRxiv.

Fatemi, S.H., Halt, A.R., Realmuto, G., Earle, J., Kist, D.A., Thuras, P., Metz, A., 2002. Purkinje cell size is reduced in cerebellum of patients with autism. Cell. Mol. Neurobiol. 22, 171–175. doi:10.1023/A:1019861721160

Felleman, D.J., Van Essen, D.C., 1991. Distributed hierarchical processing in the primate cerebral cortex. Cereb. Cortex 1, 1–47. doi:10.1093/cercor/1.1.1

Fiez, J.A., 2016. The cerebellum and language: Persistent themes and findings. Brain Lang. 161, 1–3. doi:10.1016/j.bandl.2016.09.004

Filevich, E., Lisofsky, N., Becker, M., Butler, O., Lochstet, M., Martensson, J., Wenger, E., Lindenberger, U., Kühn, S., 2017. Day2day: Investigating daily variability of magnetic resonance imaging measures over half a year. BMC Neurosci. 18. doi:10.1186/s12868-017-0383-y

Fischl, B., Salat, D.H., Busa, E., Albert, M., Dieterich, M., Haselgrove, C., Van Der Kouwe, A., Killiany, R., Kennedy, D., Klaveness, S., Montillo, A., Makris, N., Rosen, B., Dale, A.M., 2002. Whole brain segmentation: Automated labeling of neuroanatomical structures in the human brain. Neuron 33, 341–355. doi:10.1016/S0896-6273(02)00569-X

Friston, K.J., Williams, S., Howard, R., Frackowiak, R.S.J., Turner, R., 1996. Movement-related effects in fMRI time-series. Magn. Reson. Med. 35, 346–355. doi:10.1002/mrm.1910350312

Frodl, T., Meisenzahl, E., Zetzsche, T., Bottlender, R., Born, C., Groll, C., Jäger, M., Leinsinger, G., Hahn, K., Möller, H.-J., 2002. Enlargement of the amygdala in patients with a first episode of major depression. Biol. Psychiatry 51, 708–14.

Gallen, C.L., Baniqued, P.L., Chapman, S.B., Aslan, S., Keebler, M., Didehbani, N., D'Esposito, M., 2016. Modular brain network organization predicts response to cognitive training in older adults. PLoS One 11. doi:10.1371/journal.pone.0169015

Garrett, D.D., Epp, S.M., Perry, A., Lindenberger, U., 2018. Local temporal variability reflects functional integration in the human brain. Neuroimage 183, 776–787. doi:10.1016/j.neuroimage.2018.08.019

Glasser, M.F., Coalson, T.S., Robinson, E.C., Hacker, C.D., Harwell, J., Yacoub, E., Ugurbil, K., Andersson, J., Beckmann, C.F., Jenkinson, M., Smith, S.M., Van Essen, D.C., 2016. A multi-modal parcellation of human cerebral cortex. Nature 536, 171–8. doi:10.1038/nature18933

Glasser, M.F., Sotiropoulos, S.N., Wilson, J.A., Coalson, T.S., Fischl, B., Andersson, J.L., Xu, J., Jbabdi, S., Webster, M., Polimeni, J.R., Van Essen, D.C., Jenkinson, M., 2013. The minimal preprocessing pipelines for the Human Connectome Project. Neuroimage 80, 105–124. doi:10.1016/j.neuroimage.2013.04.127

Glickstein, M., Doron, K., 2008. Cerebellum: Connections and Functions. Cerebellum 7, 589–594. doi:10.1007/s12311-008-0074-4

Gordon, E.M., Laumann, T.O., Adeyemo, B., Gilmore, A.W., Nelson, S.M., Dosenbach, N.U.F., Petersen, S.E., 2017a. Individual-specific features of brain systems identified with resting state functional correlations. Neuroimage 146, 918–939. doi:10.1016/j.neuroimage.2016.08.032

Gordon, E.M., Laumann, T.O., Adeyemo, B., Huckins, J.F., Kelley, W.M., Petersen, S.E., 2016. Generation and Evaluation of a Cortical Area Parcellation from Resting-State Correlations. Cereb. Cortex 26, 288–303. doi:10.1093/cercor/bhu239

Gordon, E.M., Laumann, T.O., Gilmore, A.W., Newbold, D.J., Greene, D.J., Berg, J.J., Ortega, M., Hoyt-Drazen, C., Gratton, C., Sun, H., Hampton, J.M., Coalson, R.S., Nguyen, A.L., McDermott, K.B., Shimony, J.S., Snyder, A.Z., Schlaggar, B.L., Petersen, S.E., Nelson, S.M., Dosenbach, N.U.F., 2017b. Precision Functional Mapping of Individual Human Brains. Neuron 95, 791–807.e7. doi:10.1016/j.neuron.2017.07.011

Gordon, E.M., Lynch, C.J., Gratton, C., Laumann, T.O., Gilmore, A.W., Greene, D.J., Ortega, M., Nguyen, A.L., Schlaggar, B.L., Petersen, S.E., Dosenbach, N.U.F., Nelson, S.M., 2018. Three Distinct Sets of Connector Hubs Integrate Human Brain Function. Cell Rep. 24, 1687–1695.e4. doi:10.1016/j.celrep.2018.07.050

Gratton, C., Koller, J.M., Shannon, W., Greene, D.J., Snyder, A.Z., Petersen, S.E., Perlmutter, J.S., Campbell, M.C., 2018a. Emergent Functional Network Effects in Parkinson Disease. Cereb. Cortex 1–15. doi:10.1093/cercor/bhy121

Gratton, C., Neta, M., Sun, H., Ploran, E.J., Schlaggar, B.L., Wheeler, M.E., Petersen, S.E., Nelson, S.M., 2017. Distinct Stages of Moment-to-Moment Processing in the Cinguloopercular and Frontoparietal Networks. Cereb. Cortex 27, 2403–2417. doi:10.1093/cercor/bhw092

Gratton, C., Nomura, E.M., Pérez, F., D'Esposito, M., 2012. Focal Brain Lesions to Critical Locations Cause Widespread Disruption of the Modular Organization of the Brain. J. Cogn. Neurosci. 24, 1275–1285. doi:10.1162/jocn_a_00222

Gratton, C., Sun, H., Petersen, S.E., 2018b. Control networks and hubs. Psychophysiology. doi:10.1111/psyp.13032

Greene, D.J., Black, K.J., Schlaggar, B.L., 2013. Neurobiology and functional anatomy of tic disorders. Tourette Syndr. doi:http://dx.doi.org/10.1093/med/9780199796267.003.0012

Greene, D.J., Church, J.A., Dosenbach, N.U.F., Nielsen, A.N., Adeyemo, B., Nardos, B., Petersen, S.E., Black, K.J., Schlaggar, B.L., 2016. Multivariate pattern classification of pediatric Tourette syndrome using functional connectivity MRI. Dev. Sci. 19, 581–598. doi:10.1111/desc.12407

Greene, D.J., Laumann, T.O., Dubis, J.W., Ihnen, S.K., Neta, M., Power, J.D., Pruett, J.R., Black, K.J., Schlaggar, B.L., 2014. Developmental changes in the organization of functional connections between the basal ganglia and cerebral cortex. J. Neurosci. 34, 5842–54. doi:10.1523/JNEUROSCI.3069-13.2014

Greene, D.J., Williams, A.C., Koller, J.M., Schlaggar, B.L., Black, K.J., 2017. Brain structure in pediatric Tourette syndrome. Mol. Psychiatry 22, 972–980. doi:10.1038/mp.2016.194

Greicius, M.D., Supekar, K., Menon, V., Dougherty, R.F., 2009. Resting-state functional connectivity reflects structural connectivity in the default mode network. Cereb. Cortex 19, 72–78. doi:10.1093/cercor/bhn059

Gu, S., Satterthwaite, T.D., Medaglia, J.D., Yang, M., Gur, R.E., Gur, R.C., Bassett, D.S., 2015. Emergence of system roles in normative neurodevelopment. Proc. Natl. Acad. Sci. 112, 13681–13686. doi:10.1073/pnas.1502829112

Guell, X., Gabrieli, J.D.E., Schmahmann, J.D., 2018. Triple representation of language, working memory, social and emotion processing in the cerebellum: convergent evidence from task and seed-based resting-state fMRI analyses in a single large cohort. Neuroimage 172, 437–449. doi:10.1016/j.neuroimage.2018.01.082

Guillery, R.W., 1995. Anatomical evidence concerning the role of the thalamus in corticocortical communication: a brief review. J. Anat. 187 (Pt 3, 583–592.

Gusnard, D.A., Raichle, M.E., 2001. Searching for a baseline: functional imaging and the resting human brain. Nat. Rev. Neurosci. 2, 685–694. doi:10.1038/35094500

Hagmann, P., Cammoun, L., Gigandet, X., Meuli, R., Honey, C.J., Van Wedeen, J., Sporns, O., 2008. Mapping the structural core of human cerebral cortex. PLoS Biol. 6, 1479–1493. doi:10.1371/journal.pbio.0060159

Hardy, J., Selkoe, D.J., 2002. The amyloid hypothesis of Alzheimer's disease: Progress and problems on the road to therapeutics. Science (80-.). doi:10.1126/science.1072994

Hocke, K., Kämpfer, N., 2009. Gap filling and noise reduction of unevenly sampled data by means of the Lomb-Scargle periodogram. Atmos. Chem. Phys. 9, 4197–4206. doi:10.5194/acp-9-4197-2009

Honey, C.J., Kotter, R., Breakspear, M., Sporns, O., 2007. Network structure of cerebral cortex shapes functional connectivity on multiple time scales. Pnas 104, 10240–10245. doi:10.1073/pnas.0701519104

Hwang, K., Bertolero, M.A., Liu, W.B., D'Esposito, M., 2017. The Human Thalamus Is an Integrative Hub for Functional Brain Networks. J. Neurosci. 37, 5594–5607. doi:10.1523/JNEUROSCI.0067-17.2017

Ji, J.L., Spronk, M., Kulkarni, K., Repovš, G., Anticevic, A., Cole, M.W., 2019. Mapping the human brain's cortical-subcortical functional network organization. Neuroimage 185, 35–57. doi:10.1016/j.neuroimage.2018.10.006

Jones, E.G., 1985. The Thalamus, 1st ed. Springer.

Kaas, J.H., 2012. Evolution of columns, modules, and domains in the neocortex of primates. Proc. Natl. Acad. Sci. 109, 10655–10660. doi:10.1073/pnas.1201892109

Kahn, I., Andrews-Hanna, J.R., Vincent, J.L., Snyder, A.Z., Buckner, R.L., 2008. Distinct Cortical Anatomy Linked to Subregions of the Medial Temporal Lobe Revealed by Intrinsic Functional Connectivity. J. Neurophysiol. 100, 129–139. doi:10.1152/jn.00077.2008

Kim, D.-J., Kent, J.S., Bolbecker, A.R., Sporns, O., Cheng, H., Newman, S.D., Puce, A., O'Donnell, B.F., Hetrick, W.P., 2014. Disrupted Modular Architecture of Cerebellum in Schizophrenia: A Graph Theoretic Analysis. Schizophr. Bull. 40, 1216–1226. doi:10.1093/schbul/sbu059

Kiritani, T., Wickersham, I.R., Seung, H.S., Shepherd, G.M.G., 2012. Hierarchical Connectivity and Connection-Specific Dynamics in the Corticospinal-Corticostriatal Microcircuit in Mouse Motor Cortex. J. Neurosci. 32, 4992–5001. doi:10.1523/JNEUROSCI.4759-11.2012

Laumann, T.O., Gordon, E.M., Adeyemo, B., Snyder, A.Z., Joo, S.J., Chen, M.-Y., Gilmore, A.W., McDermott, K.B., Nelson, S.M., Dosenbach, N.U.F., Schlaggar, B.L., Mumford, J.A., Poldrack, R.A., Petersen, S.E., 2015. Functional System and Areal Organization of a Highly Sampled Individual Human Brain. Neuron 1–14. doi:10.1016/j.neuron.2015.06.037

Laumann, T.O., Snyder, A.Z., Mitra, A., Gordon, E.M., Gratton, C., Adeyemo, B., Gilmore, A.W., Nelson, S.M., Berg, J.J., Greene, D.J., McCarthy, J.E., Tagliazucchi, E., Laufs, H., Schlaggar, B.L., Dosenbach, N.U.F., Petersen, S.E., 2016. On the Stability of BOLD fMRI Correlations. Cereb. Cortex 1–14. doi:10.1093/cercor/bhw265

Marek, S., Siegel, J.S., Gordon, E.M., Raut, R. V., Gratton, C., Newbold, D.J., Ortega, M., Laumann, T.O., Adeyemo, B., Miller, D.B., Zheng, A., Lopez, K.C., Berg, J.J., Coalson, R.S., Nguyen, A.L., Dierker, D., Van, A.N., Hoyt, C.R., McDermott, K.B., Norris, S.A., Shimony, J.S., Snyder, A.Z., Nelson, S.M., Barch, D.M., Schlaggar, B.L., Raichle, M.E., Petersen, S.E., Greene, D.J., Dosenbach, N.U.F., 2018. Spatial and Temporal Organization of the Individual Human Cerebellum. Neuron.

Mattar, M.G., Cole, M.W., Thompson-Schill, S.L., Bassett, D.S., 2015. A Functional Cartography of Cognitive Systems. PLoS Comput. Biol. 11. doi:10.1371/journal.pcbi.1004533

Miezin, F.M., Maccotta, L., Ollinger, J.M., Petersen, S.E., Buckner, R.L., 2000. Characterizing the hemodynamic response: Effects of presentation rate, sampling procedure, and the possibility of ordering brain activity based on relative timing. Neuroimage 11, 735–759. doi:10.1006/nimg.2000.0568

Morel, A., 2013. Stereotactic Atlas of the Human Thalamus and Basal Ganglia, Stereotactic Atlas of the Human Thalamus and Basal Ganglia. doi:10.3109/9781420016796

Moser, M.B., Moser, E.I., 1998. Functional differentiation in the hippocampus. Hippocampus. doi:10.1002/(SICI)1098-1063(1998)8:6<608::AID-HIPO3>3.0.CO;2-7

Nelson, S.M., Cohen, A.L., Power, J.D., Wig, G.S., Miezin, F.M., Wheeler, M.E., Velanova, K., Donaldson, D.I., Phillips, J.S., Schlaggar, B.L., Petersen, S.E., 2010. A parcellation scheme for human left lateral parietal cortex. Neuron 67, 156–170. doi:10.1016/j.neuron.2010.05.025

Neta, M., Schlaggar, B.L., Petersen, S.E., 2014. Separable responses to error, ambiguity, and reaction time in cingulo-opercular task control regions. Neuroimage 99, 59–68. doi:10.1016/j.neuroimage.2014.05.053

Nielsen, A.N., Greene, D.J., Gratton, C., Dosenbach, N.U.F., Petersen, S.E., Schlaggar, B.L., 2018. Evaluating the Prediction of Brain Maturity From Functional Connectivity After Motion Artifact Denoising. Cereb. Cortex 1–15. doi:10.1093/cercor/bhy117

Ojemann, J.G., Akbudak, E., Snyder, A.Z., McKinstry, R.C., Raichle, M.E., Conturo, T.E., 1997. Anatomic localization and quantitative analysis of gradient refocused echo-planar fMRI susceptibility artifacts. Neuroimage 6, 156–167. doi:10.1006/nimg.1997.0289

Patriat, R., Molloy, E.K., Birn, R.M., 2015. Using Edge Voxel Information to Improve Motion Regression for rs-fMRI Connectivity Studies. Brain Connect. 5, 582–595. doi:10.1089/brain.2014.0321

Petersen, S.E., Sporns, O., 2015. Brain Networks and Cognitive Architectures. Neuron 88, 207–219. doi:10.1016/j.neuron.2015.09.027

Phelps, E.A., 2006. Emotion and Cognition: Insights from Studies of the Human Amygdala. Annu. Rev. Psychol. 57, 27–53. doi:10.1146/annurev.psych.56.091103.070234

Poldrack, R.A., Laumann, T.O., Koyejo, O., Gregory, B., Hover, A., Chen, M.Y., Gorgolewski, K.J., Luci, J., Joo, S.J., Boyd, R.L., Hunicke-Smith, S., Simpson, Z.B., Caven, T., Sochat, V., Shine, J.M., Gordon, E., Snyder, A.Z., Adeyemo, B., Petersen, S.E., Glahn, D.C., Mckay, D.R., Curran, J.E., Göring, H.H.H., Carless, M.A., Blangero, J., Dougherty, R., Leemans, A., Handwerker, D.A., Frick, L., Marcotte, E.M., Mumford, J.A., 2015. Long-term neural and physiological phenotyping of a single human. Nat. Commun. 6. doi:10.1038/ncomms9885

Power, J., Schlaggar, B., Lessov-Schlaggar, C., Petersen, S., 2013. Evidence for hubs in human functional brain networks. Neuron 79, 798–813. doi:10.1016/j.neuron.2013.07.035

Power, J.D., Cohen, A.L., Nelson, S.M., Wig, G.S., Barnes, K.A., Church, J.A., Vogel, A.C., Laumann, T.O., Miezin, F.M., Schlaggar, B.L., Petersen, S.E., 2011. Functional Network Organization of the Human Brain. Neuron 72, 665–678. doi:10.1016/j.neuron.2011.09.006

Power, J.D., Mitra, A., Laumann, T.O., Snyder, A.Z., Schlaggar, B.L., Petersen, S.E., 2014. Methods to detect, characterize, and remove motion artifact in resting state fMRI. Neuroimage 84, 320–341. doi:10.1016/j.neuroimage.2013.08.048

Power, J.D., Plitt, M., Gotts, S.J., Kundu, P., Voon, V., Bandettini, P.A., Martin, A., 2018. Ridding fMRI data of motion-related influences: Removal of signals with distinct spatial and physical bases in multiecho data. Proc. Natl. Acad. Sci. 201720985. doi:10.1073/pnas.1720985115

Rajput, D.R., 1993. Accuracy of clinical diagnosis of idiopathic Parkinson's disease. J. Neurol. Neurosurg. Psychiatry. doi:10.1136/jnnp.56.8.938

Raut, R. V., Mitra, A., Snyder, A.Z., Raichle, M.E., 2019. On time delay estimation and sampling error in resting-state fMRI. Neuroimage 194, 211–227. doi:10.1016/j.neuroimage.2019.03.020

Rosvall, M., Bergstrom, C.T., 2008. Maps of random walks on complex networks reveal community structure. Proc. Natl. Acad. Sci. U. S. A. 105, 1118–1123. doi:10.1073/pnas.0706851105

Roy, A.K., Shehzad, Z., Margulies, D.S., Kelly, a. M.C., Uddin, L.Q., Gotimer, K., Biswal, B.B., Castellanos, F.X., Milham, M.P., 2009. Functional connectivity of the human amygdala using resting state fMRI. Neuroimage 45, 614–626. doi:10.1016/j.neuroimage.2008.11.030

Rubinov, M., Sporns, O., 2010. Complex network measures of brain connectivity: Uses and interpretations. Neuroimage 52, 1059–1069. doi:10.1016/j.neuroimage.2009.10.003

Rudolph, M.D., Miranda-Domínguez, O., Cohen, A.O., Breiner, K., Steinberg, L., Bonnie, R.J., Scott, E.S., Taylor-Thompson, K., Chein, J., Fettich, K.C., Richeson, J.A., Dellarco, D. V., Galván, A., Casey, B.J., Fair, D.A., 2017. At risk of being risky: The relationship between "brain age" under emotional states and risk preference. Dev. Cogn. Neurosci. 24, 93–106. doi:10.1016/j.dcn.2017.01.010

Satterthwaite, T.D., Wolf, D.H., Loughead, J., Ruparel, K., Elliott, M.A., Hakonarson, H., Gur, R.C., Gur, R.E., 2012. Impact of in-scanner head motion on multiple measures of functional connectivity: Relevance for studies of neurodevelopment in youth. Neuroimage 60, 623–632. doi:10.1016/j.neuroimage.2011.12.063

Schaefer, A., Kong, R., Gordon, E.M., Laumann, T.O., Zuo, X.-N., Holmes, A.J., Eickhoff, S.B., Yeo, B.T.T., 2017. Local-Global Parcellation of the Human Cerebral Cortex from Intrinsic Functional Connectivity MRI. Cereb. Cortex 1–20. doi:10.1093/cercor/bhx179

Schmahmann, J.D., 2004. Disorders of the cerebellum: ataxia, dysmetria of thought, and the cerebellar cognitive affective syndrome. J. Neuropsychiatry Clin. Neurosci. 16, 367–378. doi:10.1176/appi.neuropsych.16.3.367

Seeley, W.W., Crawford, R.K., Zhou, J., Miller, B.L., Greicius, M.D., 2009. Neurodegenerative Diseases Target Large-Scale Human Brain Networks. Neuron 62, 42–52. doi:10.1016/j.neuron.2009.03.024

Sheffield, J.M., Repovs, G., Harms, M.P., Carter, C.S., Gold, J.M., MacDonald, A.W., Daniel Ragland, J., Silverstein, S.M., Godwin, D., Barch, D.M., 2015. Fronto-parietal and cingulo-opercular network integrity and cognition in health and schizophrenia. Neuropsychologia 73, 82–93. doi:10.1016/j.neuropsychologia.2015.05.006

Siebert, M., Markowitsch, H.J., Bartel, P., 2003. Amygdala, affect and cognition: Evidence from 10 patients with Urbach-Wiethe disease. Brain 126, 2627–2637. doi:10.1093/brain/awg271

Siegel, J.S., Mitra, A., Laumann, T.O., Seitzman, B.A., Raichle, M., Corbetta, M., Snyder, A.Z., 2017. Data quality influences observed links between functional connectivity and behavior. Cereb. Cortex 27, 4492–4502. doi:10.1093/cercor/bhw253

Siegel, J.S., Seitzman, B.A., Ramsey, L.E., Ortega, M., Gordon, E.M., Dosenbach, N.U.F., Petersen, S.E., Shulman, G.L., Corbetta, M., 2018. Re-emergence of modular brain networks in stroke recovery. Cortex 101, 44–59. doi:10.1016/j.cortex.2017.12.019

Smith, S.M., Jenkinson, M., Woolrich, M.W., Beckmann, C.F., Behrens, T.E.J., Johansen-Berg, H., Bannister, P.R., De Luca, M., Drobnjak, I., Flitney, D.E., Niazy, R.K., Saunders, J., Vickers, J., Zhang, Y., De Stefano, N., Brady, J.M., Matthews, P.M., 2004. Advances in functional and structural MR image analysis and implementation as FSL, in: NeuroImage. doi:10.1016/j.neuroimage.2004.07.051

Snyder, A.Z., Raichle, M.E., 2012. A brief history of the resting state: The Washington University perspective. Neuroimage. doi:10.1016/j.neuroimage.2012.01.044

Sorg, C., Riedl, V., Mühlau, M., Calhoun, V.D., Eichele, T., Läer, L., Drzezga, A., Förstl, H., Kurz, A., Zimmer, C., Wohlschläger, A.M., 2007. Selective changes of resting-state networks in individuals at risk for Alzheimer's disease. Proc. Natl. Acad. Sci. U. S. A. 104, 18760–18765. doi:10.1073/pnas.0708803104

Sporns, O., 2011. Networks of the Brain. MIT Press.

Sporns, O., Chialvo, D.R., Kaiser, M., Hilgetag, C.C., 2004. Organization, development and function of complex brain networks. Trends Cogn. Sci. 8, 418–425. doi:10.1016/j.tics.2004.07.008

Strick, P.L., Dum, R.P., Fiez, J.A., 2009. Cerebellum and nonmotor function. Annu. Rev. Neurosci. 32, 413–434. doi:10.1146/annurev.neuro.31.060407.125606

Triantafyllou, C., Hoge, R.D., Krueger, G., Wiggins, C.J., Potthast, A., Wiggins, G.C., Wald, L.L., 2005. Comparison of physiological noise at 1.5 T, 3 T and 7 T and optimization of fMRI acquisition parameters. Neuroimage 26, 243–250. doi:10.1016/j.neuroimage.2005.01.007

Tulving, E., Markowitsch, H.J., 1998. Episodic and declarative memory: role of the hippocampus. Hippocampus 8, 198–204. doi:10.1002/(sici)1098-1063(1998)8:3%3C198::aid-hipo2%3E3.0.co;2-g

Van den Heuvel, M.P., Sporns, O., 2013. Network hubs in the human brain. Trends Cogn. Sci. 17, 683–696. doi:10.1016/j.tics.2013.09.012

Van den Heuvel, M.P., Sporns, O., 2011. Rich-Club Organization of the Human Connectome. J. Neurosci. 31, 15775–15786. doi:10.1523/JNEUROSCI.3539-11.2011

Van Der Werf, Y.D., Witter, M.P., Uylings, H.B.M., Jolles, J., 2000. Neuropsychology of infarctions in the thalamus: A review. Neuropsychologia. doi:10.1016/S0028-3932(99)00104-9

Van Essen, D.C., Ugurbil, K., Auerbach, E., Barch, D., Behrens, T.E.J., Bucholz, R., Chang, A., Chen, L., Corbetta, M., Curtiss, S.W., Della Penna, S., Feinberg, D., Glasser, M.F., Harel, N., Heath, A.C., Larson-Prior, L., Marcus, D., Michalareas, G., Moeller, S., Oostenveld, R., Petersen, S.E., Prior, F., Schlaggar, B.L., Smith, S.M., Snyder, A.Z., Xu, J., Yacoub, E.,

2012. The Human Connectome Project: A data acquisition perspective. Neuroimage 62, 2222–2231. doi:10.1016/j.neuroimage.2012.02.018

Vonsattel, J.-P., Myers, R.H., Stevens, T.J., Ferrante, R.J., Bird, E.D., Richardson, E.P., 1985. Neuropathological Classification of Huntington's Disease. J. Neuropathol. Exp. Neurol. 44, 559–577. doi:10.1097/00005072-198511000-00003

Wig, G.S., Laumann, T.O., Petersen, S.E., 2013. An approach for parcellating human cortical areas using resting-state correlations. Neuroimage 93, 276–291. doi:10.1016/j.neuroimage.2013.07.035

Wig, G.S., Schlaggar, B.L., Petersen, S.E., 2011. Concepts and principles in the analysis of brain networks. Ann. N. Y. Acad. Sci. doi:10.1111/j.1749-6632.2010.05947.x

Wisse, L.E.M., Biessels, G.J., Geerlings, M.I., 2014. A critical appraisal of the hippocampal subfield segmentation package in FreeSurfer. Front. Aging Neurosci. 6. doi:10.3389/fnagi.2014.00261

Woolsey, T.A., Hanaway, J., Gado, M.H., 2008. The brain atlas: A visual guide to the human central nervous system (3rd ed.)., The brain atlas: A visual guide to the human central nervous system (3rd ed.).

Yan, C.-G., Craddock, R.C., He, Y., Milham, M.P., 2013. Addressing head motion dependencies for small-world topologies in functional connectomics. Front. Hum. Neurosci. 7. doi:10.3389/fnhum.2013.00910

Yeo, B.T.T., Krienen, F.M., Sepulcre, J., Sabuncu, M.R., Lashkari, D., Hollinshead, M., Roffman, Joshua L. Smoller, J.W., Zöllei, L., Polimeni, J.R., Fischl, B., Liu, H., Buckner, R.L., 2011. The organization of the human cerebral cortex estimated by intrinsic functional connectivity. J. Neurophysiol. 106, 1125–1165.

Zanto, T.P., Gazzaley, A., 2013. Fronto-parietal network: Flexible hub of cognitive control. Trends Cogn. Sci. doi:10.1016/j.tics.2013.10.001

Zhang, D., Snyder, A.Z., Fox, M.D., Sansbury, M.W., Shimony, J.S., Raichle, M.E., 2008. Intrinsic functional relations between human cerebral cortex and thalamus. J. Neurophysiol. 100, 1740–1748. doi:10.1152/jn.90463.2008

Zhang, D., Snyder, A.Z., Shimony, J.S., Fox, M.D., Raichle, M.E., 2010. Noninvasive functional and structural connectivity mapping of the human thalamocortical system. Cereb. Cortex 20, 1187–1194. doi:10.1093/cercor/bhp182

2.10 Supplemental Figures

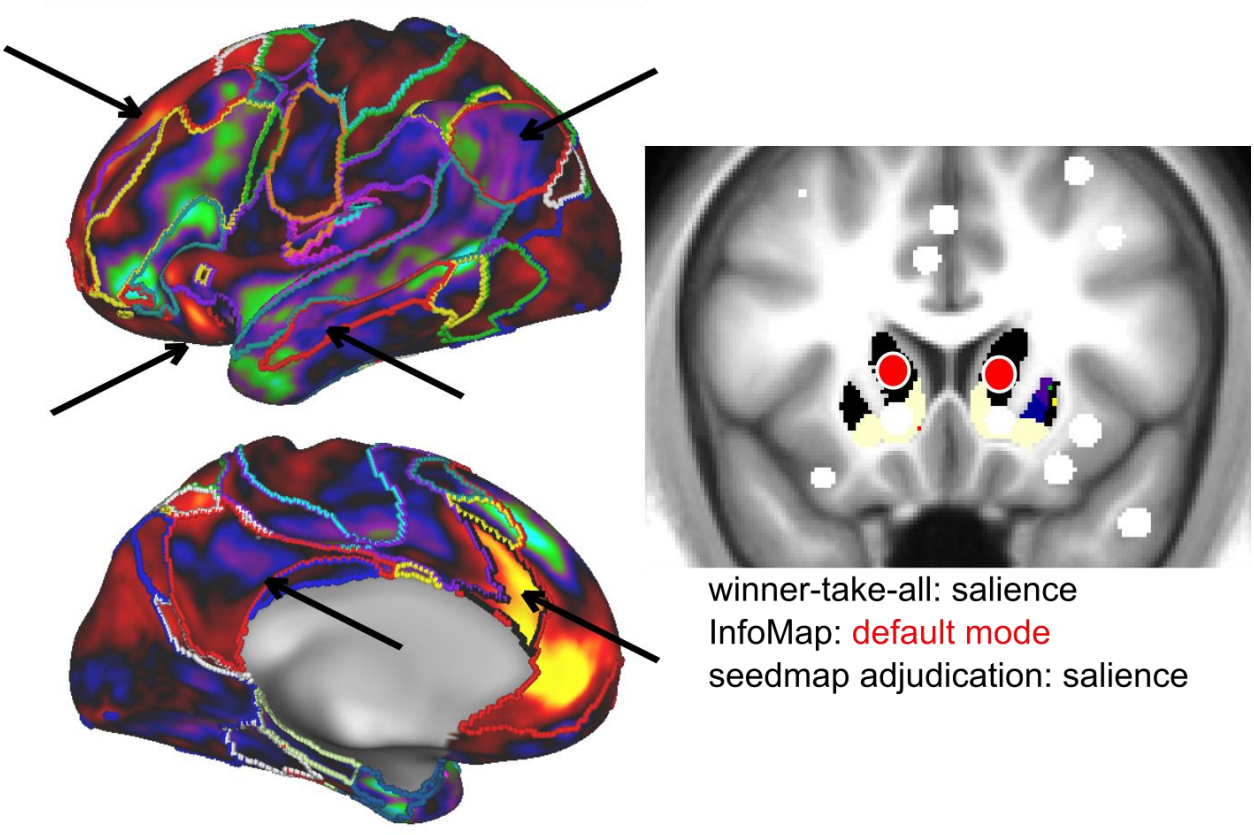

SI Figure 2.1: Disambiguation of discrepancies between assignments. In cases where the winner-take-all assignment and InfoMap solution differed, the underlying BOLD data were used to determine the consensus ROI assignment. Visual inspection of the ROI's seedmap allowed for adjudication between the two networks. This exemplar ROI (head of the caudate) was assigned to the default mode network (red) via InfoMap while the winner-take-all assignment was the salience network (black). The ROI's seedmap is more similar to the salience network (black outline) than the default mode network (red outline), especially on the lateral surface of the brain. Arrows highlight functional connectivity within salience and default mode network regions.

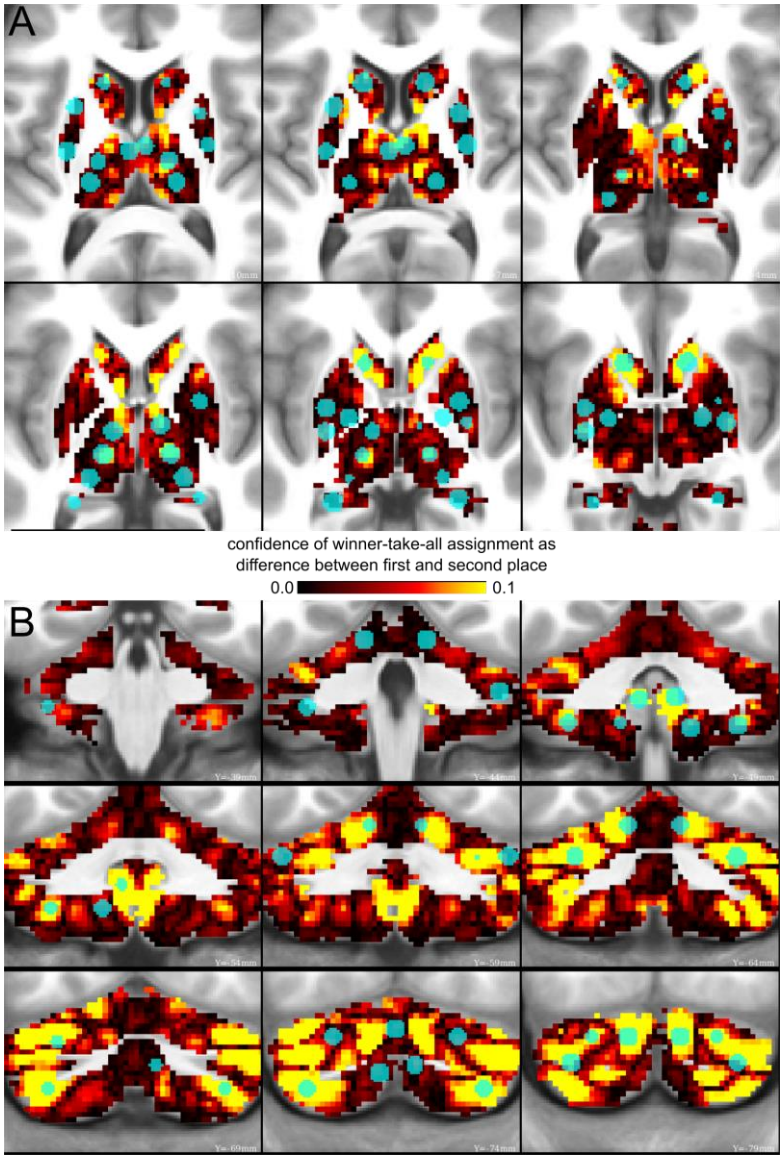

SI Figure 2.2: ROIs in high confidence winner-take-all parcels. The difference between the top two functional networks from the winner-take-all parcellation is displayed. Warmer colors indicate high confidence winner-take-all network assignments. The ROIs are overlaid in a translucent blue. We observed that 35 out of 55 (64%) ROIs in the basal ganglia and thalamus (A) and cerebellum (B) contained "clear winner" voxels (i.e., voxels with a difference in correlation strength between the first and second place networks ≥0.05). The remaining 20 ROIs contained voxels with strong functional connectivity to multiple networks, suggesting that they may act as integrative hubs (Hwang et al., 2017). An alternative interpretation is that the assignments for these 20 ROIs are low confidence (Marek et al., 2018). To allow for user flexibility, we created flags for these ROIs in the publicly available files, so users will be able to exclude them if desired.

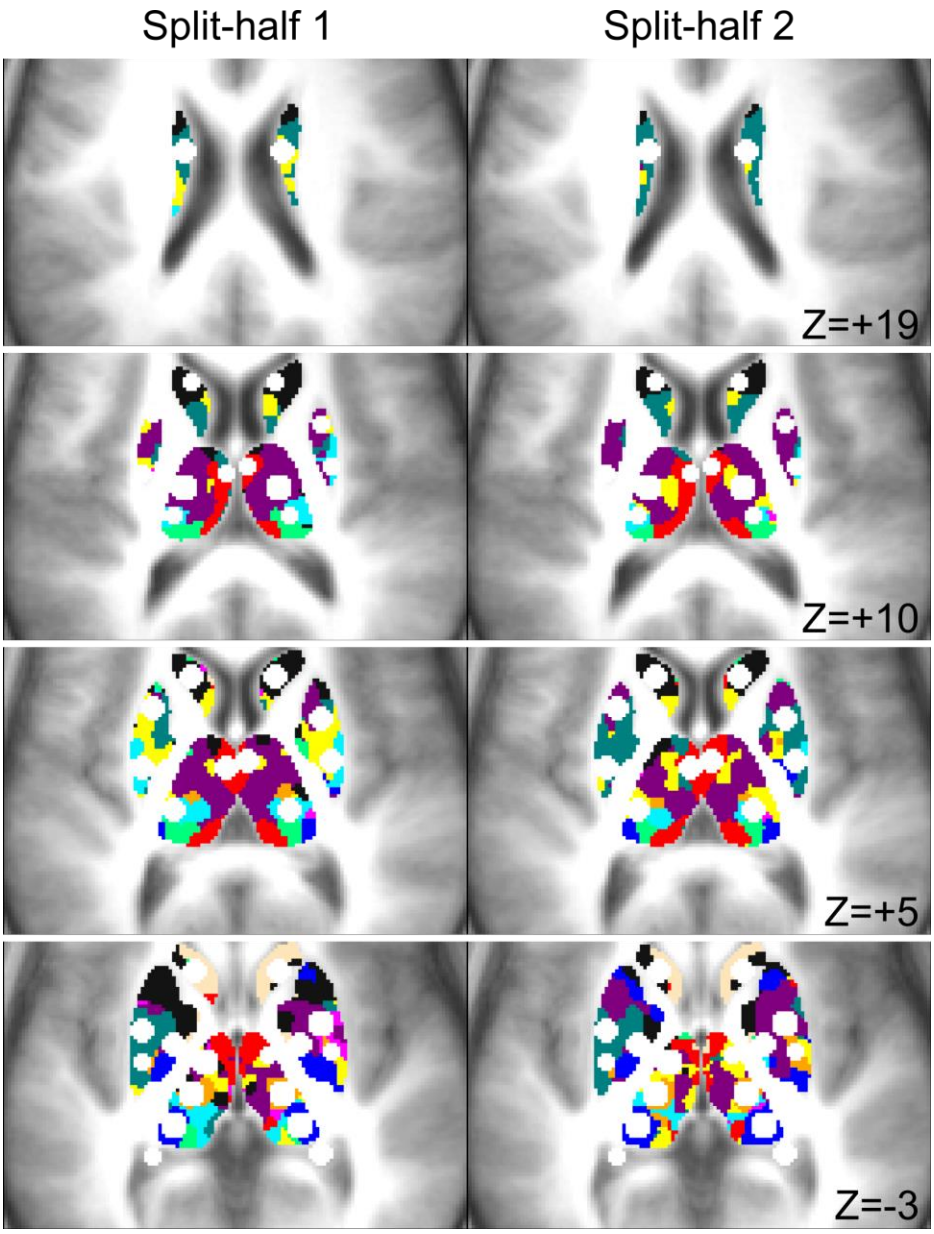

SI Figure 2.3: Consistency of winner-take-all assignment between split-halves. In locations where the ROIs are located, there is good consistency of the winner-take-all assignments in the two split-halves of the primary dataset (N=60 each).

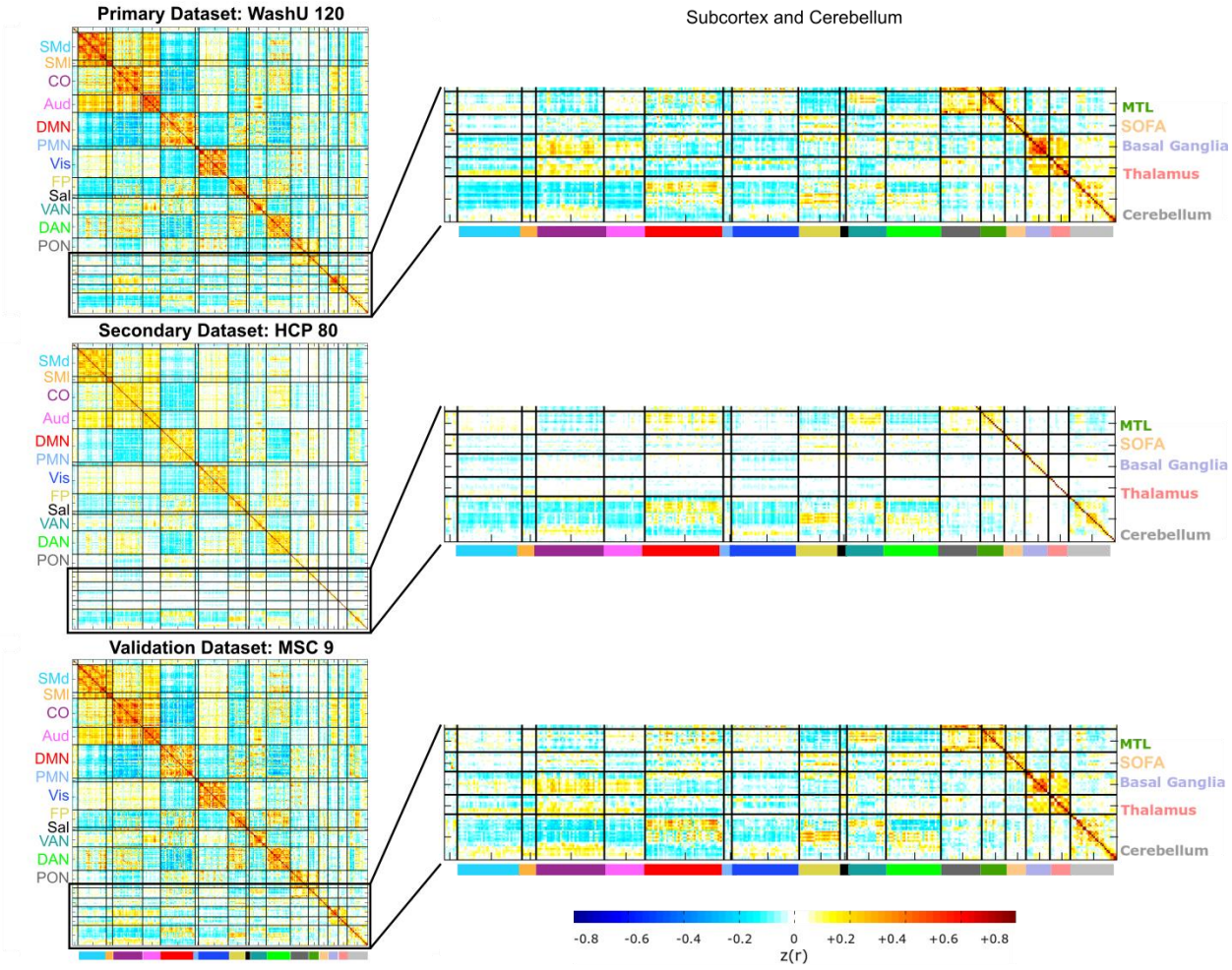

SI Figure 2.4: Correlation matrices for ROI Set 2. The center of each surface-based parcel from Gordon and Laumann et al., 2016 (*Cerebral Cortex*) was projected into volume space and combined with the new ROIs presented in this work to create ROI Set 2. The mean BOLD timeseries from all voxels within each ROI was extracted. The correlation matrices for each dataset are displayed, and zoomed-in portions of the matrix corresponding to the new ROIs are on the right.

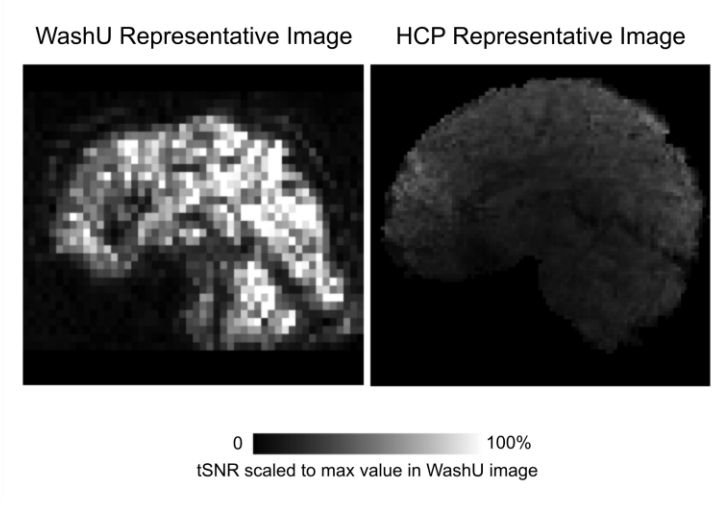

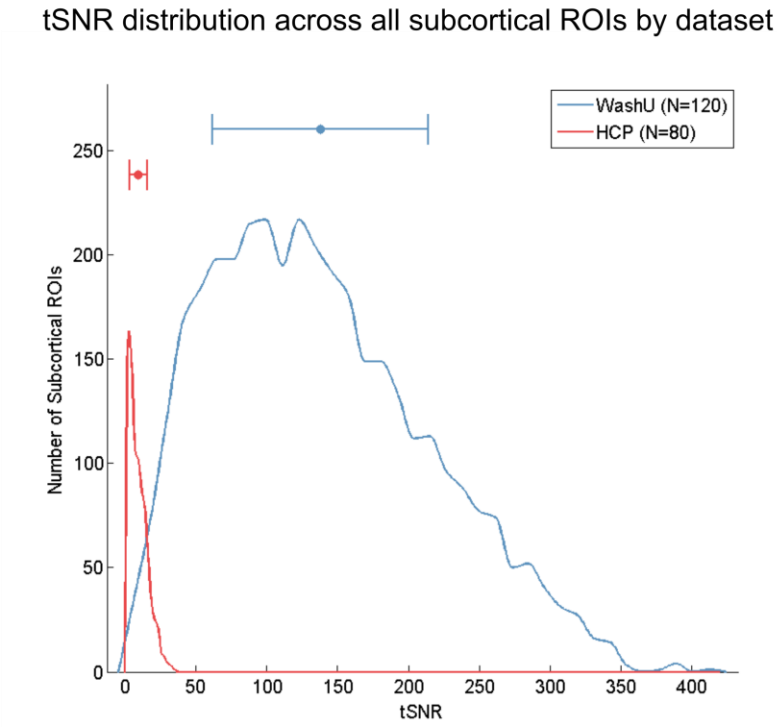

SI Figure 2.5: Poor temporal Signal-to-Noise Ratio (tSNR) in the subcortex of Human Connectome Project data. Similar to previously published studies, we found that there was poor tSNR in the subcortex of HCP data. Representative images of tSNR (mean divided by standard deviation of the BOLD timeseries at each voxel) are displayed for an individual from the primary dataset (WashU 120) and from the HCP dataset (top). The images are scaled to the maximum tSNR value in the WashU image. The distributions on the bottom represent tSNR for all subcortical ROIs across each individual in each dataset. The distribution for HCP (red) is significantly worse than the primary dataset (mean +/- std = 9.63 +/- 6.48 for HCP; 137.79 +/- 76.22 for WashU).

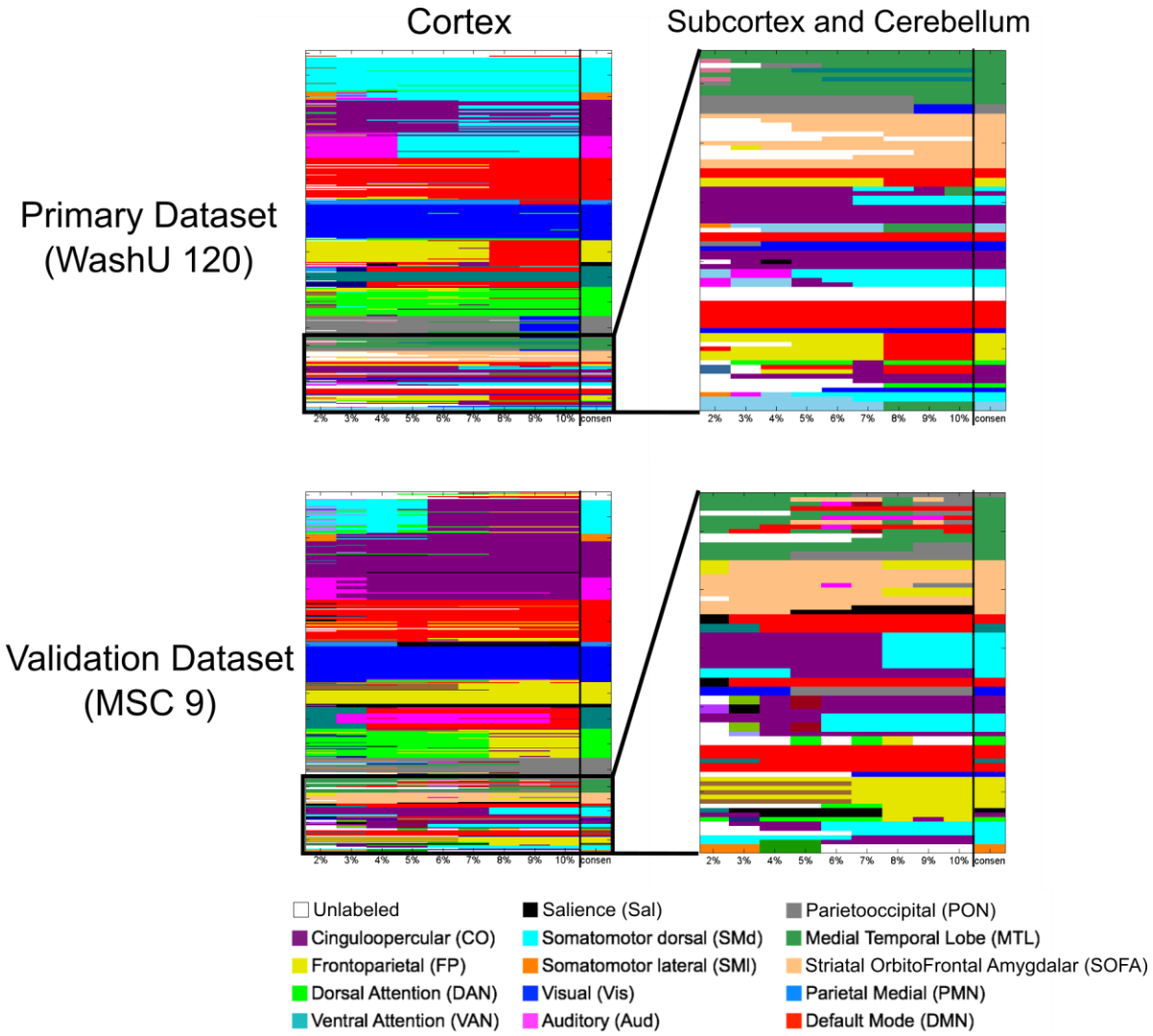

SI Figure 2.6: InfoMap-defined functional network community assignments for ROI Set 2. The functional network communities detected via InfoMap are displayed for the primary (WashU 120; top row) and validation (MSC; bottom row) datasets. The results were very similar to those shown in the main text, and there was good agreement between the two datasets. The primary difference is the presence of the Parietal Occipital Network in the cortex (gray), which was not observed with ROI Set 1.

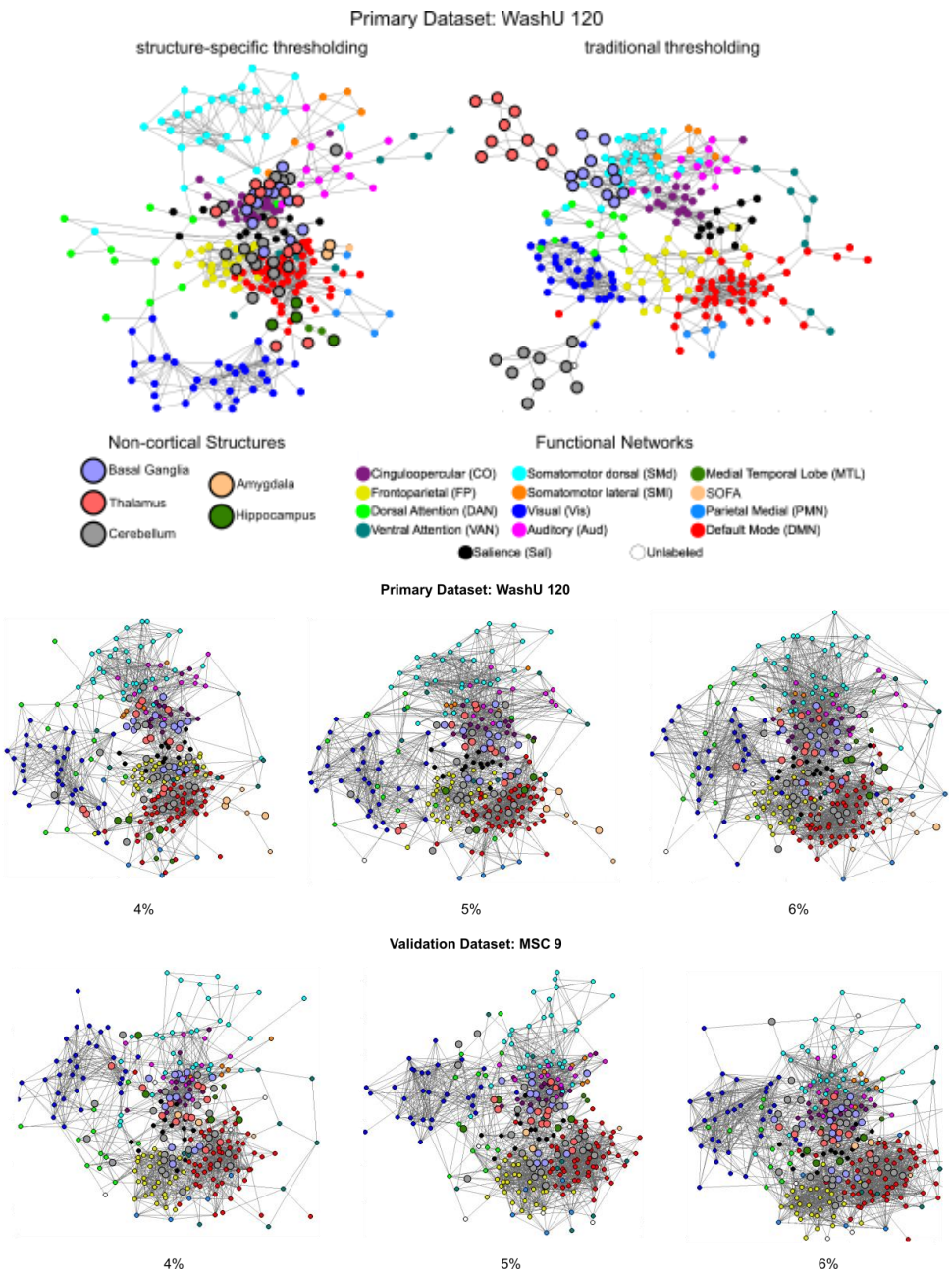

SI Figure 2.7: Spring-embedded graphs at other tested edge densities. The top portion of the figure shows the difference between structure-specific edge density thresholding and traditional thresholding (uniform across the matrix). The basal ganglia, thalamus, and cerebellum segregate into their own network communities when traditional thresholding is used (top right graph). Spring-embedded graphs for other structure-specific edge density thresholds are displayed below for the primary and validation datasets. The non-cortical ROIs (larger, bold outlines) distribute throughout each graph, integrating with known functional networks.

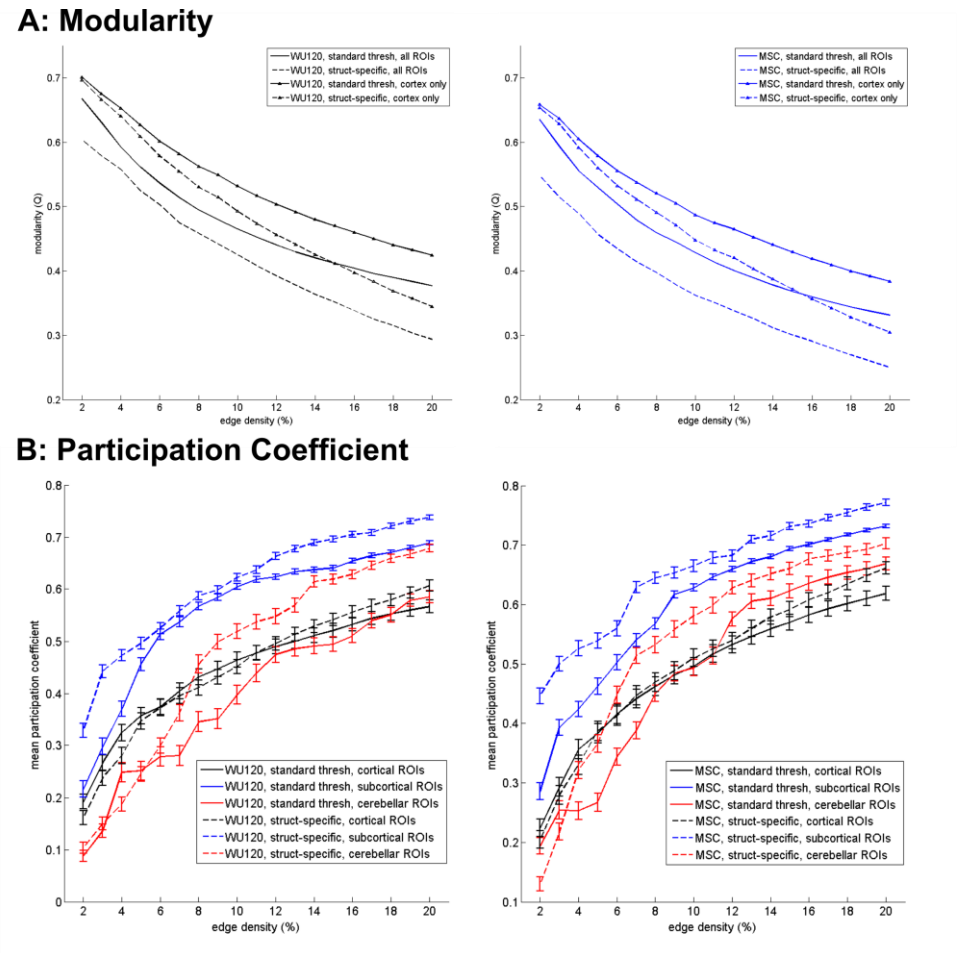

SI Figure 2.8: Graph-theoretic network measures. (A) Inclusion of non-cortical ROIs decreased modularity. Graphs display the modularity statistic for ROI Set 1 with (no marker) and without (triangle marker) the subcortical and cerebellar ROIs, as well as with (dashed lines) and without (full lines) structure-specific edge density thresholding, for the WashU 120 (black; left) and MSC (blue; right) datasets. Modularity was calculated always assuming the consensus network assignment across a variety of edge density thresholds. (B) Subcortical ROIs have higher average participation coefficient than cortical and cerebellar ROIs. Graph displays the average participation coefficient for all ROIs within a structure with (dashed lines) and without (full lines) structure-specific edge density thresholding. Participation coefficient was computed for each ROI and averaged across all ROIs in the cortex (black), subcortex (blue), and cerebellum (red) for the WashU 120 (left) and MSC (right) datasets. The result of this analysis is shown for a variety of edge densities while always assuming the consensus network assignments.

Chapter 3: Trait-like variants in human functional brain networks

Resting-state fMRI has provided converging descriptions of group-level functional brain organization. Recent work has revealed that functional networks identified in individuals contain local features that differ from the group-level description. We define these features as network variants. Building on these studies, we ask whether distributions of network variants reflect stable, trait-like differences in brain organization. Across several datasets of highly-sampled individuals we show that (1) variants are highly stable within individuals, (2) variants are found in characteristic locations and associate with characteristic functional networks across large groups, (3) task-evoked signals in variants demonstrate a link to functional variation, and (4) individuals cluster into sub-groups on the basis of variant characteristics that are related to differences in behavior. These results suggest that distributions of network variants may reflect stable, trait-like, functionally-relevant individual differences in functional brain organization.

3.1 Introduction

Identifying the nature of individual variability in human brain function is a central question in many fields of study, including psychology, psychiatry, neurology, and neuroscience. Many human neuroimaging studies have identified stable, meaningful individual differences in functional activations during task performance (Congdon et al., 2010; Miller et al., 2012, 2009; Neta and Whalen, 2011; van Horn et al., 2008) or volumetric differences (e.g., (Filipek et al., 1997; Kanai and Rees, 2011)) within specific brain regions. However, a number of recent investigations have revealed substantial individual variability while subjects are at rest not only in single regions, but also in large-scale networks throughout the brain (Braga and Buckner,

2017; Gordon et al., 2017a, 2017b, 2017c; Gratton et al., 2018; Laumann et al., 2015; Marek et al., 2018; Mueller et al., 2013; Wang et al., 2015). Here, we examine the characteristics of these individual differences in brain networks, asking if they are stable and systematic features of individual brain organization. Furthermore, we investigate if the distributions of these differences within an individual have trait-like aspects that might be linked to trait-like individual differences in behavior.

Large-scale functional brain networks are composed of distributed brain areas that demonstrate correlated fluctuations in their spontaneous (resting-state) activity measured using functional Magnetic Resonance Imaging (fMRI). Over the last decade convergent descriptions of canonical functional network organization of the human brain have emerged from fMRI studies (Power et al., 2011; Yeo et al., 2011). These efforts have revealed that functional networks map onto known large-scale brain systems, including the motor (Biswal et al., 1995), auditory (Cordes et al., 2000), and visual systems (Lowe et al., 1998), as well as higher-level systems, such as those for executive control (Dosenbach et al., 2007). Furthermore, regions within the same functional network tend to co-activate during tasks (Smith et al., 2009).

Most of the aforementioned studies have analyzed data from large groups of typical adults averaged together in order to delineate group-level descriptions of network organization (Power et al., 2011; Yeo et al., 2011). However, several recent investigations have revealed variability in functional network organization across individuals (Gordon et al., 2017a, 2017b; Mueller et al., 2013; Wang et al., 2015), including observations that highly sampled individuals show focal deviations from the group-level description (Braga and Buckner, 2017; Gordon et al., 2017c;

Laumann et al., 2015). We refer to these individual-specific deviations in functional network organization as *network variants*.

Natural questions raised by the observation of variants are whether individual differences in functional brain organization relate systematically to individual differences in function. Here, we ask specifically whether (1) network variants exhibit stability over time within an individual, (2) network variants have systematic spatial distributions and/or functional network associations, (3) individuals separate into sub-groups with different distributions of variants, and (4) aspects of network variants relate to individual differences in brain function and behavior. These questions seek to address the trait-like nature of distributions of individual differences in brain organization.

We investigate these questions using three datasets, one composed of 10 highly sampled individuals from the Midnight Scan Club (MSC) (Gordon et al., 2017c), a second of a single individual scanned over the course of a year called the MyConnectome dataset (Poldrack et al., 2015), and the third including 384 unrelated individuals with high-quality data from the Human Connectome Project (HCP; see methods for exclusion criteria) (Van Essen et al., 2012b). Furthermore, we split the HCP dataset into two matched samples for within-study replication. Together, these datasets allow us to examine both the within-individual stability of network variants as well as the distribution of network variants across larger samples.

3.2 Results

We compared individual resting-state functional correlations (rsFC) to a group-average across the entire cortex. We found that most of the brain in individuals shows moderate to high correspondence with group-average rsFC, with a few locations showing large deviations, as in (Laumann et al., 2015). We defined network variants as the locations where individuals' rsFC differs substantially from the group-average (**Fig 3.1**). Our goal was to examine the nature of these network variants and to determine if they relate to brain function.

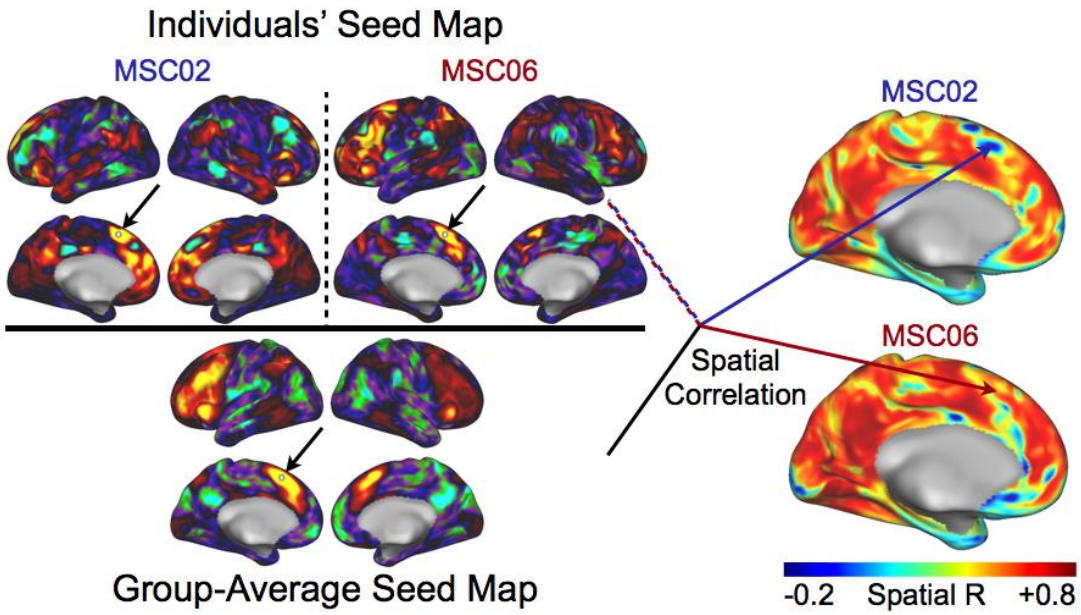

Figure 3.1: Identification of network variants. We compute a spatial correlation between an individual's seed map and the group-average seed map at every vertex on the cortical surface. An example is shown here for a seed in dorsal medial frontal cortex (white seed indicated by the black arrows). We compare the pattern of correlations for subject MSC02 with the group-average and the pattern of correlations for subject MSC06 with the group-average. Notably, MSC02's seed map differs substantially from the group-average, while MSC06's seed map agrees well. Hence, the spatial correlation at that vertex is low in MSC02 (blue arrow, top brain on the right) and high in MSC06 (red arrow, bottom brain on the right). Network variants are defined as contiguous cortical regions where this spatial correlation measure is low (dark blue areas on the brains on the right), excluding brain areas with low signal (see Methods for additional details).

3.2.1 Network variants are present and reliable in individuals

Network variants (**Fig 3.1**) were observed in all individuals included in the study, in the MSC, MyConnectome, and HCP datasets (SI Fig 3.1). All individuals have at least one brain region with low similarity to the group-average (defined as $r<0.15$ rather than lowest decile for this analysis only). Thus, network variants appear to be a common phenomenon, not just an idiosyncrasy of a few individuals. However, the location, size, and network assignments of variants differed across individuals, as will be described in more detail below.

Next, we asked if network variants were stable within an individual, rather than reflecting measurement noise, state change, or sampling variability. We examined session-to-session variability of variants in the MSC dataset. For each individual, ten separate 30-minute resting-state sessions were available (collected over 3 weeks). The spatial correlation map was robust across sessions (see example from MSC02 in **Fig 3.2A**), with high (>0.75) intraclass correlations (ICC) across sessions for 9 out of the 10 individuals, and the distribution of randomly sampled between-subject ICCs was substantially lower (**Fig 3.2B**; similar results were found with binarized network variants- SI Fig 3.2). The individual with a relatively low ICC (0.44 for MSC08) had a substantial amount of high-motion data and self-reported sleeping during extensive portions of data acquisition, as previously described (Gordon et al., 2017c; Laumann et al., 2016). Thus, this subject was excluded from all further analyses. Furthermore, we found that network variants were stable over a year in the individual from the MyConnectome dataset (SI Fig 3.3), which is a more ecologically valid timeframe. Finally, we examined the amount of data required to identify variants reliably (SI Fig 3.4), and demonstrated that roughly 40 minutes of high-quality (low-motion) data is needed (Gordon et al., 2017c; Laumann et al., 2015).

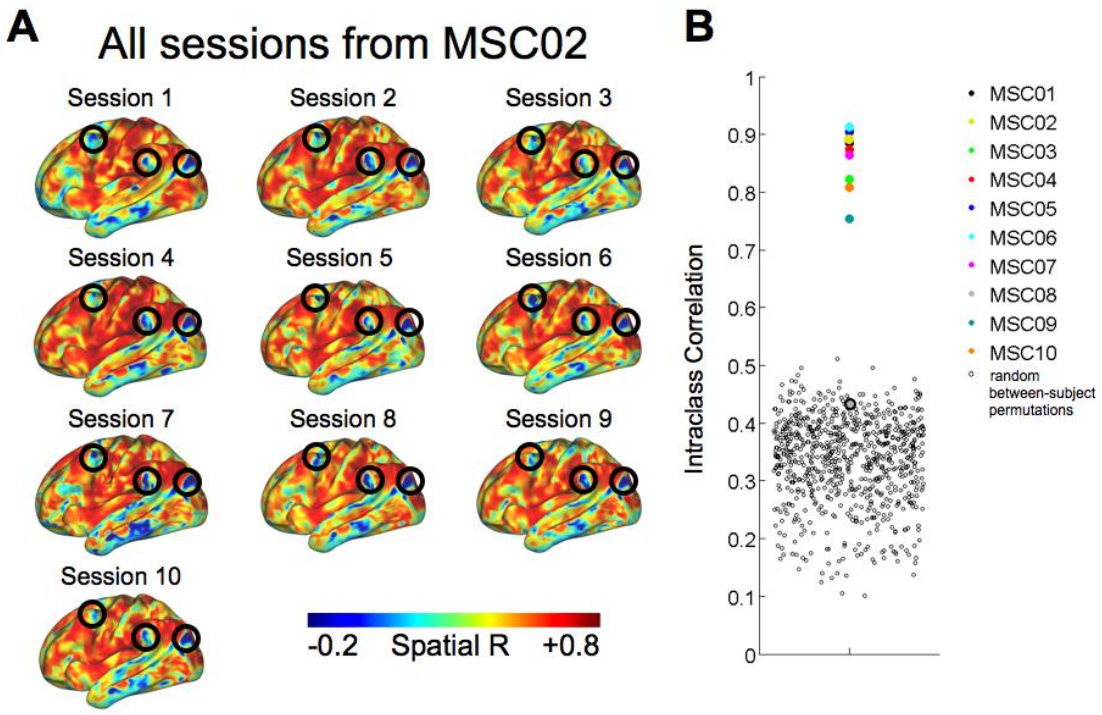

Figure 3.2: Within-subject reliability of network variants. (A) The spatial correlation values at each cortical surface vertex for all ten independent resting-state fMRI sessions from subject MSC02 are shown. Locations with low spatial correlations correspond to network variants (e.g., black circles; similar results were seen for the medial surface and right hemisphere). (B) The intraclass correlation (ICC) of the spatial correlation maps (for the entire cerebral cortex) computed across each session within each individual in the MSC dataset is shown. The ICC reflects the test-retest reliability of network variants identified via data from each session independently for an individual. The open black circles represent the correlation between two randomly selected spatial correlation maps from different subjects (one session per subject; 1000 random permutations performed). Subject MSC08 (the excluded high-motion subject) is the only individual with a relatively low ICC that overlaps the distribution of between-subject correlations.

3.2.2 Variants occur mostly in frontal and temporo-parietal cortex and often associate with higher-level functional networks

The location, size, and network associations of variants differed across individuals. If variants relate to a limited number of trait-like features, we might expect them to show characteristic patterns of variation across the population. Thus, in our next analysis we examined the characteristic spatial distribution and functional network associations of variants across individuals. We expand on previous measurements of individual variability in brain networks (Gordon et al., 2017a, 2017b; Mueller et al., 2013) by characterizing the distribution of network variants across both highly sampled (MSC) and large group (HCP) datasets.

In both datasets we find common locations for network variants near the temporo-occipito-parietal junction and in lateral frontal cortex, especially in the right hemisphere, with overlaps peaking around 33% of subjects in both datasets (3/9 highly sampled individuals, 127/384 HCP subjects). In the group-average, these regions overlap with association networks, including the frontoparietal and ventral attention networks. Conversely, network variants occur rarely in the insula, superior parietal lobe, posterior cingulate, and primary sensory and motor cortical areas, with an exception around the occipital pole (**Fig 3.3A**). Thus, there appears to be a characteristic distribution of network variants across individuals, with more network variants occurring in specific regions of association cortex. Notably, this common distribution was found using separate datasets collected from two different scanners (3T Trio vs. custom 3T HCP Skyra) with different acquisition parameters (e.g., spatial resolution of 4mm isotropic voxels vs. 2mm isotropic voxels, temporal resolution of 2.5s vs. 0.72s, AP vs. LR-RL phase encoding, and single band vs. multi-band acquisition).

To determine whether network variants are driven by individual differences in gross anatomical features, we examined the overlap between network variants and deformations that occurred during surface registration for each individual, following Gordon and colleagues (Gordon et al., 2017b). We observed extremely low overlap between network variants and deformations due to surface registration (SI Fig 3.5; mean dice overlap = 0.0001).

In addition to their location, we examined the functional network with which each variant was associated (i.e., idiosyncratically 'assigned to'). After identifying the location of the variant, we implemented a modified winner-take-all template matching approach to determine the resting state functional network to which the variant is most similar (see Methods for details) (Gordon et al., 2017a). For example, consider that the canonical (group-average) frontoparietal network is the network in which variants are most often located (e.g., dorsolateral prefrontal cortex in **Fig 3.3A**). Thus, variants in this part of the brain are non-frontoparietal by definition (e.g., the default mode variants shown in **Fig 3.4B**). We observed that variants are often assigned to the default mode, cinguloopercular, and other attention/control networks and infrequently assigned to networks related to sensorimotor and memory functions (**Fig 3.3B**). Thus, variants often "switch" from one association network to another.

Altogether, network variants' anatomical distribution and typical functional network assignments show characteristic and systematic distributions, largely related to alterations in association systems, suggesting that they may be particularly linked to individual differences in higher-level functions.

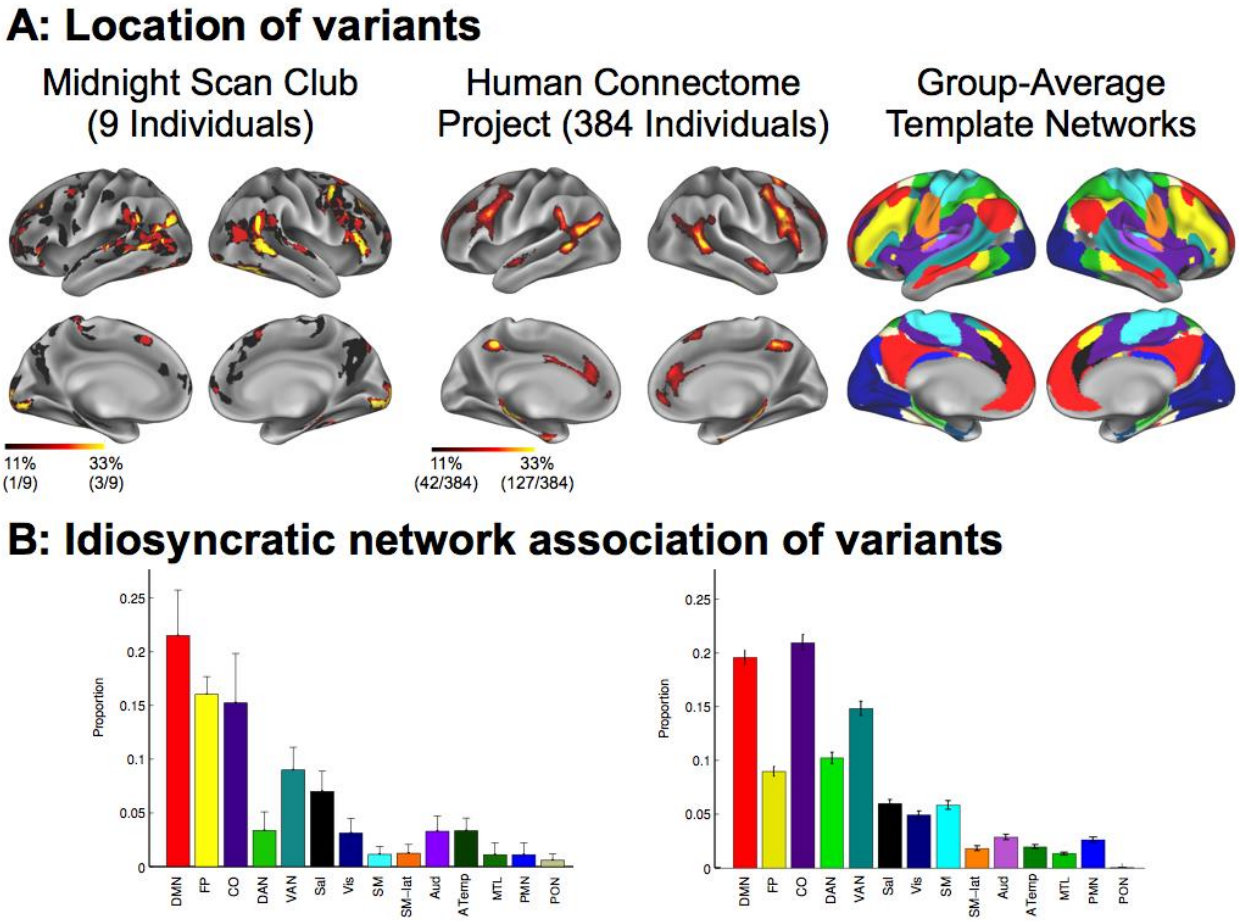

Figure 3.3: Distribution of network variants across individuals. (A) The overlap of network variant locations across individuals is displayed, with brighter colors indicating increasing levels of overlap for the MSC (left) and HCP (right) datasets. Network variants occur commonly in lateral frontal cortex and near the temporo-occipito-parietal junction, and are rarely found in primary sensorimotor areas, the insula, superior parietal lobule, or posterior cingulate cortex. (B) In addition to occurring in characteristic locations, network variants were also typically associated with a characteristic set of networks. The mean proportion of variant functional network assignments to 14 canonical networks (Gordon et al., 2017a) across individuals in the MSC (left) and HCP (right) datasets (error bars = SEM) is displayed. A plurality of variants was assigned to the default mode (DMN, red) and cinguloopercular (CO, purple) networks across individuals in both datasets.

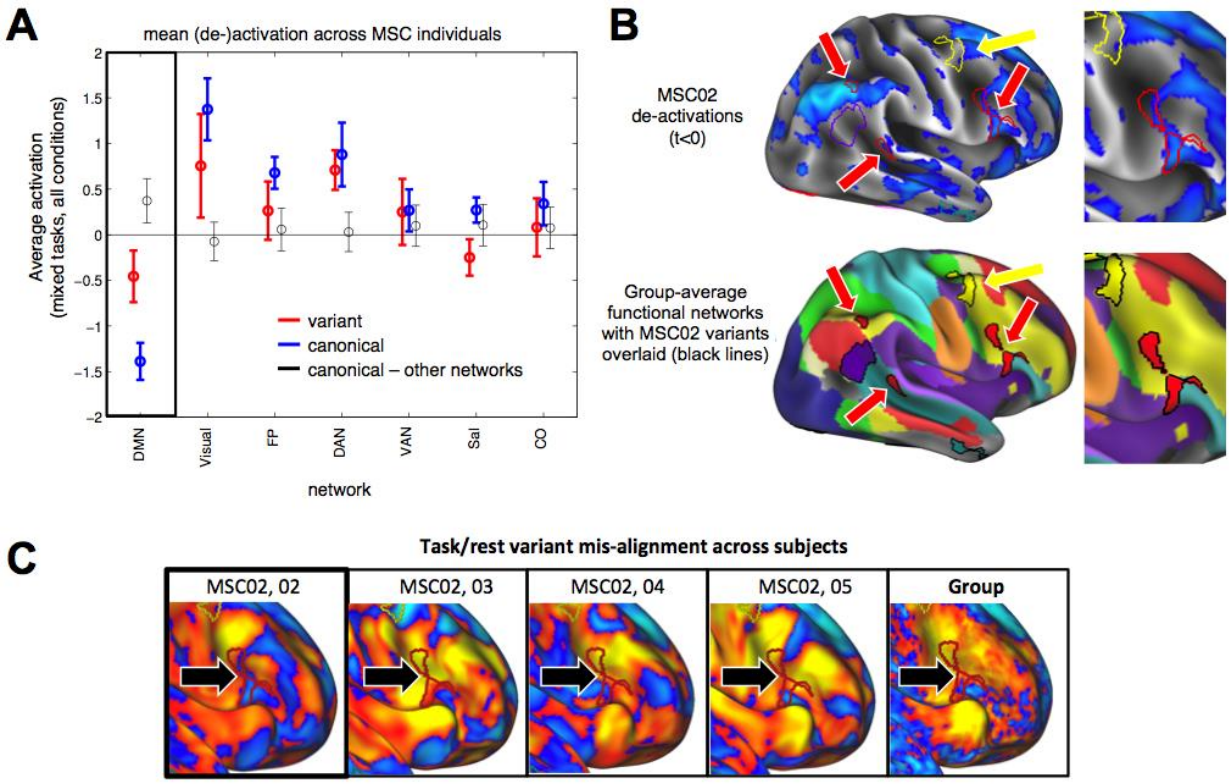

Figure 3.4: Functional activation of network variants. (A) The average task-evoked activations are displayed for variants (red) assigned to different networks (x-axis) and contrasted with the average activation for canonical regions in each network (blue) and for canonical regions in other networks (black). Mean de-activations are significantly stronger for DMN variants than in non-DMN canonical regions, and approach the levels of deactivation seen for canonical DMN locations (error bars = SEM across individuals). De-activations were not present across all variants; variants from task-activated networks, like visual, fronto-parietal (FP), and dorsal attention (DAN) show activations during the task, approaching levels for canonical regions in each network. (B) Example de-activations ($t < 0$) are displayed for subject MSC02 with outlines of the individual's network variants overlaid. Note that there is strong de-activation in DMN variants (red arrows), whereas there is no deactivation in other variants (e.g., FP variant, yellow arrow). The group-average networks with the same variants overlaid are displayed below for reference, and the righthand image shows an enlarged view of two DMN variants in right lateral frontal cortex. (C) The same variant from MSC02 (red outline) is overlaid on an activation map from MSC02 (mostly de-activated) as well as other example subjects (MSC03-05) and the group average. In other individuals, this location exhibits activations. Indeed, across DMN variants in all subjects, activations were significantly lower for DMN variants than the matched location in other subjects. See **SI Fig 3.6** for more extended examples.

3.2.3 Task-evoked signals in variants correspond to network association, not location

To further validate whether network variants are related to changes in task function, next we asked if variants exhibit task fMRI activations consistent with their novel network assignments.

To address this question, we focused on default mode (DMN) network variants as a test case because (a) all MSC subjects had examples of DMN variants and (b) the activation profile of the DMN is well described and distinct from other networks, with a robust propensity to show de-activations during most tasks (Shulman et al., 1997). Thus, we examined whether DMN variants follow the expected patterns of de-activations during task performance, despite being located in regions outside of the canonical DMN.

To this end, we measured the average BOLD activations across all task conditions in the set of mixed-design tasks (semantic, visual coherence) collected in the MSC dataset. We found that DMN variants show significantly stronger de-activations than canonical non-default regions of the brain ($t(8)=3.33$, $p=0.01$; **Fig 3.4A**, red vs. gray lines), approaching the level of de-activation shown by canonical regions of the DMN (**Fig 3.4A**, blue lines). This pattern of de-activations in variants is notable, given that variants, per our working definition, occur in locations remote from canonical DMN locations (see **Fig 3.4B** with an example of variants and task de-activations from one individual). Indeed, DMN variants in a given individual show significantly lower activations than the same location in other subjects ($t(8)=7.86$, $p<0.001$, see SI Fig 3.6C**). Fig 3.4C** and SI Fig 3.6A and 3.6B show examples of DMN variant alignments to de-activations within and across subjects, including in a region of dorsolateral prefrontal cortex that is typically associated with positive activations in these tasks.

Importantly, de-activation was not a generic characteristic of all variants, as variants associated with many other networks show activations (e.g., variants assigned to task-activated networks such as frontoparietal, dorsal attention, and visual - **Fig. 3.4A**), approaching the activations

shown by canonical regions in each network with these contrasts. To supplement this finding, we conducted a related analysis on sustained task activations in cinguloopercular network variants. Group studies have suggested that sustained activations are fairly selective to the cinguloopercular network, rather than other control-related networks, like the frontoparietal (Dosenbach et al., 2008, 2007, 2006; Dubis et al., 2016). We found a descriptive result for sustained activation in cinguloopercular network variants (SI Fig 3.7). Since only a small number of participants exhibited cinguloopercular variants in the MSC dataset (6 out of 9), we describe the result without formal statistics. These findings provide initial evidence that network variants carry task-evoked variations in their functional signals related to their idiosyncratic network identity at locations not expected from group activation maps.

3.2.4 Distinct sub-groups of individuals clustered by properties of network variants

A further hypothesis regarding the trait-like nature of network variants is that common distributions of variants may be present across individuals, much as eye color or blood type present in common clusters across individuals. To address this question, we examined whether individuals could be clustered into separate sub-groups on the basis of the distributions of network variants using a data-driven approach (InfoMap; see Methods) (Rosvall and Bergstrom, 2008). Given the exploratory nature of this analysis, we first examined different clustering possibilities in the MSC dataset, and then used two matched split-halves in the independent HCP dataset to validate the MSC results.

No clustering via anatomical location of variants

First, we examined whether individuals could be clustered according to the anatomical locations of their network variants (irrespective of functional identity). We constructed a binary map of

variant locations for each subject. Then, we computed the spatial similarity of the anatomical distribution of variants between all pairs of individuals, and applied InfoMap to this spatial similarity matrix (see Methods for details). Across InfoMap thresholds, individuals generally grouped into a single large cluster or were unassigned to a group (e.g., for the full 384 HCP subjects the average number of individuals in the large cluster was 201+/-130; SI Fig 3.8). Thus, individuals were not classified into large sub-groups of common anatomical locations of network variants.

Distinct clusters of individuals via functional network of variants

Next, we tested if individuals could be clustered according to the functional properties (network assignment) of their variants. To this end, we examined the similarity between the seed map of each variant to standard templates of canonical functional networks (14 template functional networks were derived from a separate dataset, the WashU 120 group-average; see (Gordon et al., 2017a) for more details). This procedure produced 14 correlation coefficients per network variant, conveying the extent to which a variant is default-like, visual-like, etc. The mean template similarity across variants (averaged across all variants within an individual) revealed two distinct patterns across individuals in the MSC dataset (**Fig 3.5A**). Importantly we replicated the result in two independent, matched HCP split-halves (**Fig 3.5B**). Again, this is notable given the differences in the subjects (e.g., IQs are much higher in the MSC dataset (Gordon et al., 2017c)), scanner, and acquisition parameters). Furthermore, we validated the two-group clustering solution via a modularity-based null model as well as hierarchical clustering (SI Fig 3.9). The two sub-group solution was the most robust across datasets, with some evidence for a four sub-group solution (SI Fig 3.10).

The first sub-group consisted of individuals (N_{MSC} = 3/9, $N_{HCP,1}$ = 83/192, $N_{HCP,2}$ = 80/192) whose variants exhibited stronger correlations to the cingulo-opercular (CO), dorsal attention (DAN), and sensorimotor networks (**Fig 3.5A and 3.5B**- gray), suggesting that network variants in these individuals associated more strongly with control and processing systems. The second sub-group consisted of individuals whose variants exhibited stronger correlations to the default mode (DMN) network, among others (N_{MSC}= 4/9, $N_{HCP,1}$ = 92/192, $N_{HCP,2}$ = 91/192) (**Fig 3.5A and 3.5B**- pink). The two sub-groups were strongly anti-correlated (see the matrices on the left in **Fig 3.5A and 3.5B**), indicating that functional characteristics of variants in these sub-groups differed substantially from one another. We observed a similar but weaker pattern of sub-groups when individuals were clustered based on the overall size of each functional network relative to the group-average (SI Fig 3.11).

Moreover, we observed a small but significant difference between the two HCP sub-groups in terms of neuropsychological measures of behavior (SI Fig 3.12). We found that individuals in the control and processing sub-group had a higher score ($t(344) = 2.04$, $p < 0.05$) in the positive life experience factor and a lower score ($t(344) = 2.04$, $p < 0.05$) in the history of drug abuse factor. Both differences were significant after FDR-correction (see Supplemental Information for full details).

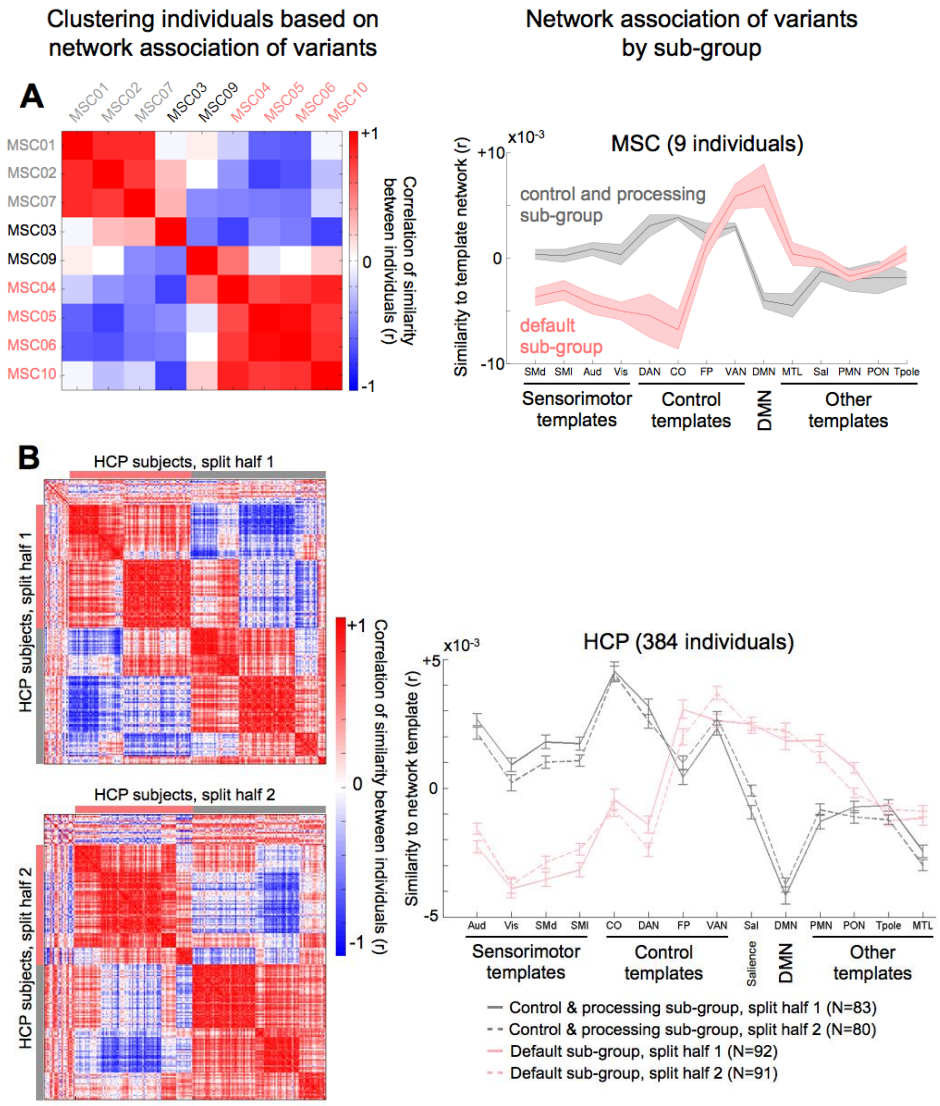

Figure 3.5: Separable groups of individuals via network associations of variants. The figure displays groups of individuals in the (A) MSC and (B) HCP datasets clustered by the network associations of their variants. Network associations were computed for each variant as their similarity to templates of 14 canonical functional networks (see Methods) (Gordon et al., 2017b). The matrices on the left show the correlation between pairs of individuals in terms of variant network associations; each row/column represents a single individual's correlation to all other individuals. The matrices were clustered in a data-driven fashion using InfoMap. The gray and pink colors or bars along the edges of the matrices denote individuals in the same sub-group. These groupings were used to create the averages (line graphs) on the right. The line graphs show the average similarity of variants to each functional network template for individuals within the control and processing sub-group (gray) and the default sub-group (pink; error bars = SEM across individuals).

Jointly, these findings suggest that individuals cluster into sub-groups based on the network assignment of each variant, with one sub-group exhibiting more control and processing-like variants and the other sub-group exhibiting more default-like variants. Importantly, these findings provide evidence for systematic variation of network variants across individuals that replicated across three independent samples, with potential implications for behavior.

As noted above, when we examined cluster solutions across alternate thresholds (see Methods and SI Fig 3.9) we observed sub-patterns within each of the two primary clusters in the large HCP samples at lower (sparser) thresholds. There was some evidence for a four sub-group solution (SI Fig 3.10), but it was less reliable than the two sub-group solution across HCP split-halves. The presence of more fine-grained sub-groups suggests that greater sample size as well as the inclusion of additional measures and data from clinical populations might yield further clusters of individuals not yet characterized, and potentially more fine-grained relationships between variants and behavior.

3.3 Discussion

The current study deepens our understanding of individual differences in the systems-level organization of the human brain by demonstrating that these differences reflect stable, trait-like features with systematic properties that cluster across individuals. Specifically, our results demonstrate that network variants (1) show high session-to-session stability in highly sampled individuals, suggesting that they are trait-like, (2) occur commonly in lateral frontal and temporoparietal regions and often associate with the default mode, cinguloopercular, and other control networks, suggesting a systematic linkage to higher-level functions, (3) are related to

functional variations during tasks, displaying brain (de-) activations consistent with their novel network re-assignment and validating their putative network function, and (4) have a systematic patterning across individuals, allowing for the clustering of individuals into sub-groups, with small differences in behavior between sub-groups. Jointly, these findings suggest that network variants are promising candidates for endo-phenotypic markers of systems-level brain variability.

3.3.1 Network variants are stable, trait-like components of individual functional brain organization

Our primary goal was to investigate properties of network variants. We hypothesized that they might show trait-like differences, including stability over time *within* individuals and systematic variation *across* individuals.

We found that all individuals across two independent datasets (with separate scanners and scan parameters, N=393) showed characteristic focal deviations from the group-level description of functional brain organization. This indicates that network variants are standard components of typical adult functional network organization, as hinted at by the strong individual variation reported in previous research (Braga and Buckner, 2017; Gordon et al., 2017a, 2017b, 2017c; Gratton et al., 2018; Laumann et al., 2015). Moreover, we expand upon these findings by showing that network variants are stable within an individual, appearing consistently across 10 independent resting-state fMRI sessions in highly sampled individuals. These findings extend previous evidence that resting-state correlations are sensitive to individual differences in brain organization, given sufficient data and adequate control for nuisance sources of variance (Birn et al., 2013; Braun et al., 2012; Chen et al., 2015; Gratton et al., 2018; Laumann et al., 2015).

Our results also indicate that group-average functional networks represent a mixture of individuals from distinct sub-groups (**Fig 3.5**). However, we demonstrate that network variants are highly localized to particular portions of cortex. In other words, individuals showed substantial similarity to the group-average networks at most cortical locations. Since the maximum spatial overlap of network variants is approximately 33%, the group-average may be a reasonable description for the majority of individuals in most brain locations. Thus, group-average functional networks provide an adequate description of the expected pattern of brain organization, but the group-average is not a good representation of any given person and is, therefore, limited in inferences that can be drawn about brain-behavior relationships.

Taken together, the presence of network variants in all individuals and their robustness over sessions provides compelling evidence that they act as stable variations in the systems-level organization of the human brain. These features may prove to be useful substrates in understanding individual differences in brain function and behavior across many domains.

3.3.2 Network variants have characteristic distributions and functional network associations across individuals

We observed that network variants are found commonly near the temporo-occipito-parietal junction and in lateral prefrontal cortex. We rarely detected network variants in primary sensorimotor cortical areas, the insula, superior parietal lobe, or posterior cingulate cortex. This finding not only replicates across independent datasets, but also converges with previous studies of individual differences in functional network organization reporting high individual differences in association networks (Chen et al., 2015; Gordon et al., 2017b; Kong et al., 2018; Mueller et al., 2013), with a few specific differences. For instance, compared to Mueller and colleagues, we

found more network variants near the inferior frontal gyrus and fewer near angular gyrus and supramarginal gyrus. Differences in data processing and registration (surface-based here) may have contributed to some of these discrepancies. This idea is supported by the similarity of the results here and those reported by Kong and colleagues (Kong et al., 2018).

Interestingly, the distribution of common locations for network variants does not appear to be symmetric between the two hemispheres, as we found generally more variants in the right hemisphere. Lateralization in the brain is a well-established phenomenon, in terms of both anatomy and function (e.g., (Broca, 1861; Sperry, 1961)), even at the level of individual resting-state functional correlations (Wang et al., 2015). The significance and implications of potential network variant lateralization is a topic for future work to explore.

Furthermore, we found that variants tend to associate with the default mode (DMN), cinguloopercular (CO), and other association networks more often than other functional networks. Networks like the CO and frontoparietal (FP) network are thought to be important for control functions and performance monitoring (Dosenbach et al., 2007; Dubis et al., 2016; Gratton et al., 2017; Neta et al., 2014; Sadaghiani and D'Esposito, 2015; Seeley et al., 2007), and the DMN has been proposed to be involved in numerous domains, including autobiographical memory, internal monitoring, and theory of mind (Buckner et al., 2008; Raichle, 2015; Spreng et al., 2009). Network variants occur most often in these "association" networks, and they tend to re-assign from one higher-level functional network to another. Together, these results suggest that flexibility in functional network organization may relate more closely to higher-level functions typically associated with these regions.

3.3.3 Network variants exhibit functional variations during tasks

We observed that network variants coincide with locations of functional variations during tasks in the MSC dataset. Specifically, we demonstrated that variants that associate with the DMN exhibit decreases in activity during task performance, as has been robustly observed for canonical DMN regions in most externally directed tasks (Shulman et al., 1997). This was the case even in DMN variants in dorsolateral prefrontal cortex, a brain region that canonically shows robust positive activity during tasks in most individuals. Moreover, this de-activation was not a general property of all variants; variants associated with task-activated systems like the visual, dorsal attention, and FP networks showed (positive) activations. Likewise, cinguloopercular (CO) network variants showed a trend toward higher levels of sustained activation, consistent with role of the CO network in the stable maintenance of task set (Dosenbach et al., 2008, 2007, 2006; Dubis et al., 2016). This finding provides initial validation that network variants shift toward the response characteristics of their functional network assignment during task performance, providing corroborating evidence that variants reflect true deviations in the functional organization of individual human brains that impact task function.

This result converges with work from Tavor and colleagues, who built a model that was able to predict individual differences in task activations on the basis of individual differences in resting-state data (Tavor et al., 2016). Their model did not specifically operate on network variants, although the presence of network variants would certainly impact the training of the model. Likewise, Gordon and colleagues demonstrated that individual specific task-related activation patterns map onto that individual's resting-state functional networks better than they map onto different individuals' networks (Gordon et al., 2017c). Here, we build on these findings by

showing that network variants specifically show improved task-rest alignment in individuals compared with canonical network assignments. Finally, seminal work from Miller and colleagues revealed stable, meaningful individual differences in brain activations during task performance (Congdon et al., 2010; Miller et al., 2012, 2009; van Horn et al., 2008). These investigations led to the idea that individual-specific activation patterns reflect, or are potentially determined by, subject-specific information processing strategies. The results presented here suggest that if these hypotheses are true, this trait-like brain activity may be localized to network variant regions, specifically.

3.3.4 Individuals cluster into discrete groups on the basis of network variant characteristics

We found evidence for sub-groups of individuals within a normative sample with similar forms of network variants, suggesting that variants demonstrate systematic variation across individuals. Intriguingly, it was the network assignment of variants, rather than their anatomical location, that appeared to be the driving force behind these distinct sub-groups. That is, it appears as though group-level variation of network variants is more related to functional assignment than location.

We observed two sub-groups across individuals that were consistent in both datasets. The two sub-groups were composed of individuals with more control and processing-like variants and individuals with more default-like variants. The strong distinction between the sub-groups may relate to the specific functional networks onto which the variants map, which generally activate and de-activate, respectively, during externally directed tasks (Fox et al., 2005; Margulies et al., 2016). A related possibility is that the distinction between the sub-groups may be due to changes in the relative size of the aforementioned networks. In other words, individuals with more

default-like variants may have an expanded DMN, which could be achieved via "trading" anatomical space canonically occupied by control and processing functional networks for DMN network variants (and vice-versa). Any of these possibilities relates to the trait-like status of the distributions of variants across individuals.

While our work provides initial evidence for groups of individuals with similar network variants across two different samples, it appears likely that additional sub-groups will be found in future studies. Some additional sub-groups may be associated with other properties of network variants (e.g., specific locations, networks, and their interactions), while others may emerge with a more behaviorally diverse range of individuals, e.g., those with neurologic or psychiatric disorders. Notably, in the larger HCP dataset we observed some evidence of further clustering, with the two initial groups dividing further into four sub-groups of individuals. The current work presents a starting point for future investigations into systematic variation in individual functional brain organization, an area that merits substantial additional exploration.

3.3.5 Network variants may relate to behavior

The trait-like nature of network variant distributions raises the question of whether or not network variants relate to individual differences in behavior. It is possible that these individual differences in brain organization reflect different manners of instantiating the same behavior, a behavioral phenocopy (Schlaggar and McCandliss, 2007), or functional degeneracy (Friston and Price, 2003; Tononi et al., 1999). In other words, network variants may reflect individual differences in processing organization that ultimately lead to similar functional outcome. Conversely, there may be systematic relationships between network variants and measures of

behaviors, either in a categorical (e.g., differences between network variant sub-groups and behavior) or continuous fashion.

We observed a small but significant relationship between network variant sub-groups and behavior. Individuals in the default mode sub-group had a lower life satisfaction and higher history of drug abuse, on average. Previous investigations revealed that individual differences in resting-state functional correlations are related to a positive and negative 'mode' of lifestyle (Bijsterbosch et al., 2018; Smith et al., 2015) as well as measures of executive function (Finn et al., 2015; Kong et al., 2018). Our finding is more consistent with the former studies.

In addition to the sub-group analysis presented here, there may be continuous relationships between network variants and measures of behavior, such as those observed by Bijsterbosch and colleagues (Bijsterbosch et al., 2018). Connections between network variants and behavior should be pursued by future studies with more specialized behavioral measures and a broader range of network variant properties and sub-groups. By extending behavioral relationships to network variants specifically, future investigations should have more precise targets, i.e. variant locations, for both basic experimentation and potential medical intervention (e.g., via stimulation-based methods). It is possible that our approach of identifying network variants may provide a rich source of targets to better understand the neurobiological sources of individual differences in behavior.

3.3.6 Neurobiological interpretations of network variants

In the present study, we demonstrate that individuals stably vary in specific elements of their functional network organization. This observation raises the question of what neural mechanisms

underlie these individual differences. Any network variant could represent (1) a regional border shift, in which a neighboring brain area is enlarged, contracted, or displaced, (2) a relative shift in the functional and connectivity properties of an existing area, leading to re-assignment to a distinct network, or (3) a *de novo* brain area unique to an individual or small group.

The appearance of completely novel cortical areas in individuals seems unlikely. Most studied cortical areas (i.e., visual areas, motor areas, attention related areas) are found reliably in essentially every individual primate (Woolsey, 1982, 1981a, 1981b). Variations in the size of brain areas have been observed previously, such as a two-fold difference in the size of some visual areas (Dougherty et al., 2003). In cases of perturbations, larger changes can be seen. For example, area V1 in congenitally blind individuals is significantly decreased in size (Jiang et al., 2009; Noppeney et al., 2005; Park et al., 2009) and genetic manipulations can affect the size and position of areas, e.g. primary sensory and motor areas are expanded and shifted rostro-laterally in mice that overexpress *Emx2* (Bishop et al., 2000; Hamasaki et al., 2004). Cortical areas may also be displaced along the cortex, as was observed for area 55b by Glasser and colleagues (Glasser et al., 2016), leading to the appearance of variant pieces in non-overlapping locations.

As a conceptual example (**Fig 3.6**), consider the Frontal Eye Fields (FEF), an area that lies close to regions where network variants are frequently found across individuals (in the right hemisphere, at least). Essentially every human likely has at least one FEF per hemisphere (Paus, 1996). If an individual has a larger (or smaller) FEF than the average, the expanded (or contracted) portion of cortex will appear as a network variant. Likewise, if FEF is displaced in an individual relative to the typical cortical location of FEF, it will be identified as a network

variant. While these more local variations likely occur (and account for some network variants), previous work has demonstrated that individually variable network assignments can occur at regions remote from network borders (Gordon et al., 2017a).

One potential explanation for remote network variants is altered functional response and connectivity properties of those areas in certain individuals. For example, individual FEF neurons code for saccades, visual stimuli, attention in space, and combinations of these three properties (Tehovnik et al., 2000). Depending on the relative proportion of these various types of FEF neurons, individuals may have different functional connectivity and task-evoked BOLD signals in this area relative to the group-average. Whereas a typical individual's FEF may have a high proportion of eye movement and attention neurons, thus producing the usual association with the dorsal attention network, another individual's FEF might contain an unusually large number of neurons coding visual stimuli (e.g., due to genetics and/or accumulated experience) and, thus, associate with the visual functional network. Therefore, one possibility is that an area may appear like a network variant *not* because it is truly a novel area, but because the distribution or function of its neurons is shifted systematically in that individual.

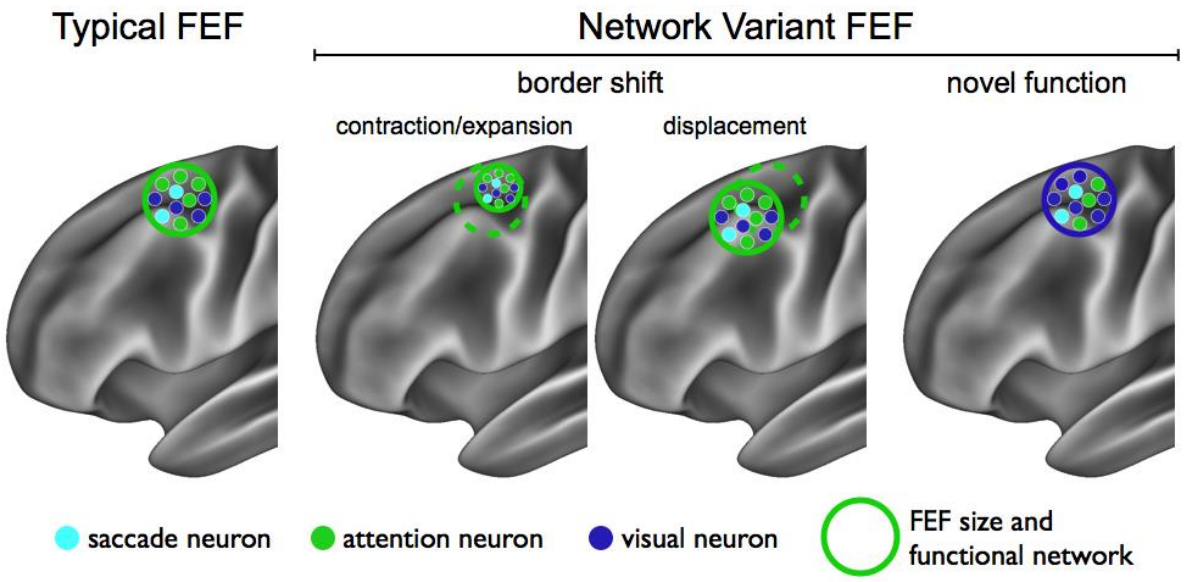

Figure 3.6: Schematic of potential neural mechanisms underlying network variants. A schematic of the typical (group-average) FEF is displayed on the left. Neurons coding for saccades, attention in space, and visual stimuli are color-coded (light blue, green, and dark blue, respectively). An individual's FEF may be identified as a network variant if its border has shifted relative to its typical location, via either contraction/expansion in size (contraction displayed middle left) or displacement along the cortex (middle right). Another possibility is that the underlying functional and connectivity properties of the individual's FEF are different from the group-average, e.g., more neurons that code for visual stimuli (right).

This last idea is supported by the observed task-related activations in network variants. For several functional networks, we showed that the level of (de-) activation in those network variants is between the level of (de-) activation seen typically for that location and what would be expected given the network variant's reassignment (**Fig 3.4A**). Moreover, a related paper by Arcaro and colleagues provided an example of functional reassignment based on lifetime experience, such that the portion of inferotemporal cortex that is typically face-selective becomes body- and hand-selective in monkeys reared without exposure to faces (Arcaro et al., 2017). The neurons in this region of cortex are innately retinotopic and biased towards the scale and curvature of visual stimuli (i.e., biased to respond to faces). However, due to the monkeys' atypical environment and experience, the response properties of the region changed (even for face stimuli), suggesting that the area may appear as a network variant compared to typical monkeys.

Each network variant may be due to one or more of the abovementioned mechanisms, and future work is necessary to determine the consequences of these different types of network variants. While the mechanisms are difficult to disambiguate precisely in humans, studies with animal models may be well equipped to examine this question and to expand our understanding of the sources of individual variability in large-scale brain networks.

3.4 Material and Methods

3.4.1 Datasets, acquisition parameters, and exclusion criteria

Three datasets are analyzed in this manuscript: the MSC (Gordon et al., 2017c), MyConnectome (Poldrack et al., 2015), and HCP (Van Essen et al., 2012b) datasets. In addition, for group-average comparisons, a previously collected dataset of 120 typical adults was used as the group-level referent (Power et al., 2011), referred to in the text as the WashU 120. All data collection was approved by the Washington University and University of Texas Internal Review Board and all procedures complied with ethical regulations for studies involving human research participants. Dataset composition, acquisition parameters, and exclusion criteria have been described in detail previously for all datasets (see Supplemental Information for a brief description).

All data and data processing code used in the manuscript are publicly available (MSC and code: https://openneuro.org/datasets/ds000224/versions/00002 MyConnectome: myconnectome.org HCP: https://db.humanconnectome.org/ WashU 120: https://legacy.openfmri.org/dataset/ds000243/). Code for network variant analyses (custom MATLAB scripts) will be made available at https://github.com/MidnightScanClub.

3.4.2 Resting-state data processing

All data processing has been described in detail previously for each dataset. For extended details see (Gordon et al., 2017c) for MSC, (Laumann et al., 2015) for MyConnectome, (Glasser et al., 2013) for HCP, and (Power et al., 2014) for WashU 120. We briefly review relevant details for each type of processing below.

Anatomical processing

First, FreeSurfer 5.3 automatic segmentation was applied to the T1-weighted images to create masks of the gray matter, white matter, and ventricles for each subject (Fischl et al., 2002). Then,

FreeSurfer's default recon-all pipeline was used to reconstruct each subject's native anatomical surface. These native surfaces were aligned to the fsaverage surface using a shape-based spherical registration (Dale and Sereno, 1993; Dale et al., 1999; Fischl et al., 1999; Ségonne et al., 2005). The two hemispheres were registered to each other using a landmark-based algorithm (Anticevic et al., 2012; Van Essen et al., 2012a). The final resolution of each subject's surface was 32,492 vertices per hemisphere.

Functional processing

For each subject, standard preprocessing procedures were applied (slice timing correction, functional realignment, mode 1000 normalization, atlas registration and resampling, and distortion correction) in addition to further preprocessing to remove motion-related artifacts (frame-wise displacement for frame censoring, regression of nuisance signals, including the whole-brain mean, interpolation over censored frames, and bandpass filtering) (Power et al., 2014). See the Supplemental Information for full details.

Volume-to-surface mapping and functional connectivity processing

After preprocessing, a CIFTI was created for each subject. Preprocessed BOLD time series data were mapped to the surface following the procedure of Gordon and Laumann et al., 2016. Before computing the correlations, all previously censored frames were discarded to account for distance-dependent motion artifacts (Power et al., 2014). Pairwise correlations between time series from every pair of cortical surface vertices from both hemispheres (59412 x 59412) were computed to construct an individual-specific vertex-to-vertex correlation matrix, which was then Fisher Transformed. For the WashU 120, the individual correlation matrices were averaged together. See the Supplemental Information for full details.

3.4.3 Task data processing

In this study, we focus on activations in the two mixed design (Petersen and Dubis, 2012) tasks from the MSC dataset: the semantic task and the coherence task. Tasks and their analyses are described in detail in (Gordon et al., 2017c). Task activations were modeled with in-house imaging analysis software (IDL) using a general linear model (GLM) approach as previously described (Gordon et al., 2017c; Gratton et al., 2018). See the Supplemental Information for a brief description.

The default mode network has been consistently linked to task-deactivations. To determine how network variants (see Section 3.4.4) associated with functional variations associated with the default mode, we examined network variant activations in all conditions (cues, trials, and sustained activations) vs. implicit baseline. We conducted this comparison for variants associated with each network, canonical (i.e., non-variant, group) regions associated with each network, and the average of canonical regions associated with all other networks. In addition, the average activation of each DMN variant in a single individual was compared with the average activation of that same location in other individuals. In all cases, statistical comparisons were carried out using paired two-sided t-tests.

In addition, we added a complementary supplementary analysis of task activations associated with the cinguloopercular system. The cinguloopercular network has been consistently linked to sustained activations, especially during resource limited tasks, unlike other control systems such as the frontoparietal (Dosenbach et al., 2008, 2007, 2006). To examine whether variants associated with the cinguloopercular network displayed sustained activations, we examined

activations associated with the sustained block regressor during a resource-limited semantic task (Dubis et al., 2016).

3.4.4 Identification of network variants

To identify network variants, individual subject correlation matrices were compared (independently) to a group-average correlation matrix generated from the WashU 120. For each individual, the spatial similarity between the individual's and the group's pattern of correlations (seed map) at each cortical surface vertex was computed. More precisely, each row of an individual's matrix was correlated with the corresponding row in the group-average matrix, resulting in one spatial correlation per vertex. Susceptibility regions were masked out using a vertex-wise measure of signal quality derived from the group-average data. All vertices with a mean BOLD signal less than 750 (as computed in (Ojemann et al., 1997)) were set to 0. Then, the spatial similarity was binarized such that all cortical vertices with a spatial correlation value in the lowest decile of the individual's distribution were considered for further analyses (these vertices were set to 1, and all others were set to 0). Network variants were defined as regions of cortex in which sets of at least 50 contiguous vertices were below the spatial correlation threshold. As an alternative to allowing the threshold for network variants to vary across individuals (lowest decile of the individual's spatial correlation distribution), the threshold was fixed at a spatial correlation value of 0.3. Results were extremely consistent between analysis procedures, given that the mean lowest decile cutoff value is 0.32 +/- 0.03.

3.4.5 Functional network assignment of network variants

A winner-take-all procedure was implemented to assign functional networks to each network variant in each individual. To do so, 14 template networks were created from the 14 group-average networks as described previously (Gordon et al., 2017a). The templates are the group-

average resting-state correlation pattern (seed map) of each canonical functional network in the WashU 120 (e.g., the group-average default mode network seed map, the group-average visual network seed map, etc.). Then, for each unique network variant the following matching procedure was applied: (1) A seed map was computed from the average BOLD time series from all vertices within the network variant. (2) The similarity between that variant seed map and each template network was computed (i.e., the spatial correlation between the template seed map and the variant seed map). (3) The template network with the highest similarity was assigned to the network variant. (4) Any network variants where the ***winning*** template system had low similarity (i.e., $r < 0.3$) were reassigned as 'unknown system.' (5) Finally, we ensured that the variant did not match the group-average network at that cortical location. In other words, we removed the variant if it overlapped (spatially) with its assigned group-average functional network by 50% or more (this occurred infrequently: 5/129 = 4% in the MSC dataset, 276/7498 = 3.7% in the HCP dataset).

3.4.6 Overlap of network variants across individuals

In order to examine the spatial overlap of network variants across individuals, binary versions of the final maps of network variants (after functional network assignment) were summed across individuals to create an overlap map within each dataset. These were divided by the number of people within each dataset, to express the frequency of network variants at each cortical vertex.

3.4.7 Within-subject reliability of network variants

To measure within-subject reliability of network variants, we compared variants across different days from the same participant. Each MSC subject had ten independent 30-minute resting-state sessions collected on separate days. We processed each session separately (as described above) in order to assess within-subject session-to-session variability of network variants. For each

session, we generated the spatial correlation map used for identifying network variants (seed maps from the session vs seed maps from the group-average). Then, we measured the intraclass correlation (ICC) of each map within an individual. In addition, this entire analysis was repeated with binarized network variant maps, but computing the mean dice coefficient instead of ICCs (since the maps are binary). The latter analysis allowed for a focused reliability measure of variant regions only. For the binarized variants analysis, we generated a null model of between-subject variant overlaps for comparison. We performed 1000 random permutations of pairs of sessions drawn from two different MSC individuals (with replacement) and computed the mean dice coefficient of the binary network variant maps from those sessions. For the MyConnectome dataset, we compared the stability of network variants from sequential 3 week blocks of data (i.e., variants identified from 6 sessions concatenated together for each 3 week block). All possible pairs of variant spatial correlation maps (from each 3 week block of time) were correlated with one another.

3.4.8 Patterns of network variants across individuals

Next, we turned our attention to whether similar types of network variants were seen across sub-groups of individuals. We tested two options: (1) whether sub-groups of individuals exhibited variants at similar anatomical locations and (2) whether sub-groups of individuals exhibited variants with similar network associations.

Anatomical: To determine whether sub-groups of individuals exhibited variants at similar anatomical locations, we compared the binary maps of (final) network variants between each pair of individuals using dice coefficients. This resulted in a symmetric dice overlap matrix with a size of N by N (9 x 9 for the MSC dataset and 192 x 192 for each HCP split-half), with each

entry representing the degree to which a given pair of individuals covaries in terms of the spatial distribution of network variants (i.e., the degree to which the pair both have variants 1, 2, and 3 and they both do not have variants 4, 5, and 6). A clustering algorithm (InfoMap) (Rosvall and Bergstrom, 2008) was applied to this dice overlap matrix. Before clustering, we applied a threshold to the matrix to create a sparse network on which to operate. We examined a wide range of density thresholds from the top 2% to 30% of correlations in increments of 1%.

Functional: To determine whether sub-groups of individuals exhibited variants with similar network associations, we compared their match to 14 standard network templates. Specifically, during functional network assignment of variants, we compute the similarity (i.e., spatial correlation) between each variant and each template functional network. This results in a 14 x 1 vector of correlations (to the 14 template networks) for each variant. This measure represents the degree to which a variant is default mode-like, visual-like, etc. Then, we computed the mean similarity for *all* variants within an individual to each template network (indicating the degree to which *all* of that individual's variants are default mode-like, visual-like, etc.). This mean measure was correlated across subjects, and the same clustering algorithm (InfoMap) was implemented to identify groups of individuals with similar patterns of network variants. We used a range of thresholds from 2% to 10% in increments of 1%.

Conceptually, the functional measure discussed above calculates the average similarity of variants to canonical networks, producing a quantitative estimate of the (e.g.) DMN-like characteristics of all variants in an individual. To complement this measure, we also clustered individuals based on the amount of the cortex (number of surface vertices) assigned to each

functional network. The WashU 120 group-average functional networks were used as a referent to compare the relative expansion or reduction of each individual's functional networks. Thus, we calculated the number of expanded or contracted surface vertices for each network (relative to the group-average) using the variants' network assignments, e.g. a given individual may have +1000 cingulo-opercular vertices, -75 default mode vertices, etc.

3.4.9 Analysis of behavior

Arguably, an important aspect of network variants is their relation to behavior. As a proof of concept, and given network variants' distributions and re-assignment to association networks, we examined relationships to the HCP behavioral measures (Barch et al., 2013). We used exploratory factor analysis (EFA) for data reduction and to identify latent constructs in the HCP data. We focused on behavior categories that included multiple instruments and/or that did not already have summary measures available, which included demographics, cognition, emotion, and substance use variables. Age, sex, and handedness were not considered in the EFA to allow flexibility to include or exclude these variables in analyses of brain-behavior relationships (e.g., as covariates). Data from all HCP subjects (N=1206) were included in the EFA. EFA factors were then compared across sub-groups using multiple linear regression. Details about the results of the EFA and the regression analysis between HCP sub-groups of individuals are in the Supplemental Information (SI Fig 12).

3.5 Conclusion

We find that network variants are stable components of typical adult functional network organization. The organization and arrangement of network variants across individuals appears

to be systematic. Specifically, they tend to occur in lateral prefrontal cortex and near the temporo-occiptio-parietal junction and are often re-assigned to association networks, suggesting a link to higher-level cognitive functions. Moreover, network variants are related to functional variations during tasks. Finally, individuals cluster into sub-groups on the basis of these variants and these sub-groups demonstrate small differences in behavior. Taken in sum, our data support the idea that network variant distributions are trait-like and their patterning across individuals is functionally-relevant.

3.6 Acknowledgments

We thank Joshua S. Siegel and Deanna M. Barch for assistance with the HCP data. This research was supported by NIH T32NS073547 (BAS), NIH F32NS092290 (CG), NSF GRFP DGE-1143954 (AWG), an APA Dissertation Research Award (AWG), NIH K01MH104592 (DJG), a Dart Neuroscience, LLC grant (KBM), a McDonnell Foundation Collaborative Activity Award (SEP), NIH R01NS32979 (SEP), and NIH R01NS06424 (SEP).

3.7 Author Contributions

BAS, CG, TOL, EMG, and SEP designed the study. AWG, JJB, MO, AN, DJG, SMN, and NUFD collected the data. BAS, CG, TOL, EMG, BA, MO, AN, and CNLS analyzed the data. All authors wrote the manuscript.

3.8 Competing Interests

All authors declare no competing interests.

3.9 Chapter 3 References

Anticevic, A., Repovs, G., Dierker, D.L., Harwell, J.W., Coalson, T.S., Barch, D.M., Van Essen, D.C., 2012. Automated landmark identification for human cortical surface-based registration. Neuroimage 59, 2539–2547. doi:10.1016/j.neuroimage.2011.08.093

Arcaro, M.J., Schade, P.F., Vincent, J.L., Ponce, C.R., Livingstone, M.S., 2017. Seeing faces is necessary for face-domain formation. Nat. Neurosci. 20, 1404–1412. doi:10.1038/nn.4635

Barch, D.M., Burgess, G.C., Harms, M.P., Petersen, S.E., Schlaggar, B.L., Corbetta, M., Glasser, M.F., Curtiss, S., Dixit, S., Feldt, C., Nolan, D., Bryant, E., Hartley, T., Footer, O., Bjork, J.M., Poldrack, R., Smith, S., Johansen-Berg, H., Snyder, A.Z., Van Essen, D.C., 2013. Function in the human connectome: Task-fMRI and individual differences in behavior. Neuroimage 80, 169–189. doi:10.1016/j.neuroimage.2013.05.033

Bijsterbosch, J.D., Woolrich, M.W., Glasser, M.F., Robinson, E.C., Beckmann, C.F., Van Essen, D.C., Harrison, S.J., Smith, S.M., 2018. The relationship between spatial configuration and functional connectivity of brain regions. Elife 7. doi:10.7554/eLife.32992

Birn, R.M., Molloy, E.K., Patriat, R., Parker, T., Meier, T.B., Kirk, G.R., Nair, V.A., Meyerand, M.E., Prabhakaran, V., 2013. The effect of scan length on the reliability of resting-state fMRI connectivity estimates. Neuroimage 83, 550–558. doi:10.1016/j.neuroimage.2013.05.099

Bishop, K.M., Goudreau, G., O'Leary, D.D.M., 2000. Regulation of area identity in the mammalian neocortex by Emx2 and Pax6. Science (80-.). 288, 344–349. doi:10.1126/science.288.5464.344

Biswal, B., Yetkin, F.Z., Haughton, V.M., Hyde, J.S., 1995. Functional connectivity in the motor cortex of resting human brain using echo-planar MRI. Magn. Reson. Med. 34, 537–541. doi:10.1002/mrm.1910340409

Braga, R.M., Buckner, R.L., 2017. Parallel Interdigitated Distributed Networks within the Individual Estimated by Intrinsic Functional Connectivity. Neuron 95, 457–471.e5. doi:10.1016/j.neuron.2017.06.038

Braun, U., Plichta, M.M., Esslinger, C., Sauer, C., Haddad, L., Grimm, O., Mier, D., Mohnke, S., Heinz, A., Erk, S., Walter, H., Seiferth, N., Kirsch, P., Meyer-Lindenberg, A., 2012. Test-retest reliability of resting-state connectivity network characteristics using fMRI and graph theoretical measures. Neuroimage 59, 1404–1412. doi:10.1016/j.neuroimage.2011.08.044

Broca, P., 1861. Remarques sur le siège de la faculté du langage articulé, suivies d'une observation d'aphémie (perte de la parole). Bull. la Société Anat. 6, 330–357.

Buckner, R.L., Andrews-Hanna, J.R., Schacter, D.L., 2008. The brain's default network: Anatomy, function, and relevance to disease. Ann. N. Y. Acad. Sci. 1124, 1–38. doi:10.1196/annals.1440.011

Chen, B., Xu, T., Zhou, C., Wang, L., Yang, N., Wang, Z., Dong, H.M., Yang, Z., Zang, Y.F., Zuo, X.N., Weng, X.C., 2015. Individual variability and test-retest reliability revealed by ten repeated resting-state brain scans over one month. PLoS One 10. doi:10.1371/journal.pone.0144963

Congdon, E., Mumford, J.A., Cohen, J.R., Galvan, A., Aron, A.R., Xue, G., Miller, E., Poldrack, R.A., 2010. Engagement of large-scale networks is related to individual differences in inhibitory control. Neuroimage 53, 653–663. doi:10.1016/j.neuroimage.2010.06.062

Cordes, D., Haughton, V.M., Arfanakis, K., Wendt, G.J., Turski, P.A., Moritz, C.H., Quigley, M.A., Meyerand, M.E., 2000. Mapping functionally related regions of brain with functional connectivity MR imaging. Am. J. Neuroradiol. 21, 1636–1644. doi:10.1016/j.amepre.2011.10.016

Dale, A.M., Fischl, B., Sereno, M.I., 1999. Cortical surface-based analysis: I. Segmentation and surface reconstruction. Neuroimage 9, 179–194. doi:10.1006/nimg.1998.0395

Dale, A.M., Sereno, M.I., 1993. Improved Localizadon of Cortical Activity by Combining EEG and MEG with MRI Cortical Surface Reconstruction: A Linear Approach. J. Cogn. Neurosci. 5, 162–176. doi:10.1162/jocn.1993.5.2.162

Dosenbach, N.U.F., Fair, D.A., Cohen, A.L., Schlaggar, B.L., Petersen, S.E., 2008. A dual-networks architecture of top-down control. Trends Cogn. Sci. 12, 99–105. doi:10.1016/j.tics.2008.01.001

Dosenbach, N.U.F., Fair, D.A., Miezin, F.M., Cohen, A.L., Wenger, K.K., Dosenbach, R. a T., Fox, M.D., Snyder, A.Z., Vincent, J.L., Raichle, M.E., Schlaggar, B.L., Petersen, S.E., 2007. Distinct brain networks for adaptive and stable task control in humans. Proc. Natl. Acad. Sci. U. S. A. 104, 11073–8. doi:10.1073/pnas.0704320104

Dosenbach, N.U.F., Visscher, K.M., Palmer, E.D., Miezin, F.M., Wenger, K.K., Kang, H.C., Burgund, E.D., Grimes, A.L., Schlaggar, B.L., Petersen, S.E., 2006. A Core System for the Implementation of Task Sets. Neuron 50, 799–812. doi:10.1016/j.neuron.2006.04.031

Dougherty, R.F., Koch, V.M., Brewer, A.A., Fischer, B., Modersitzki, J., Wandell, B.A., 2003. Visual field representations and locations of visual areas V1/2/3 in human visual cortex. J. Vis. 3, 1. doi:10.1167/3.10.1

Dubis, J.W., Siegel, J.S., Neta, M., Visscher, K.M., Petersen, S.E., 2016. Tasks Driven by Perceptual Information Do Not Recruit Sustained BOLD Activity in Cingulo-Opercular Regions. Cereb. Cortex 26, 192–201. doi:10.1093/cercor/bhu187

Filipek, P.A., Semrud-Clikeman, M., Steingard, R.J., Renshaw, P.F., Kennedy, D.N., Biederman, J., 1997. Volumetric MRI analysis comparing subjects having attention-deficit hyperactivity disorder with normal controls. Neurology 48, 589–601. doi:10.1212/WNL.48.3.589

Finn, E.S., Shen, X., Scheinost, D., Rosenberg, M.D., Huang, J., Chun, M.M., Papademetris, X., Constable, R.T., 2015. Functional connectome fingerprinting: Identifying individuals using patterns of brain connectivity. Nat. Neurosci. 18, 1664–1671. doi:10.1038/nn.4135

Fischl, B., Salat, D.H., Busa, E., Albert, M., Dieterich, M., Haselgrove, C., Van Der Kouwe, A., Killiany, R., Kennedy, D., Klaveness, S., Montillo, A., Makris, N., Rosen, B., Dale, A.M., 2002. Whole brain segmentation: Automated labeling of neuroanatomical structures in the human brain. Neuron 33, 341–355. doi:10.1016/S0896-6273(02)00569-X

Fischl, B., Sereno, M.I., Dale, A.M., 1999. Cortical surface-based analysis: II. Inflation, flattening, and a surface-based coordinate system. Neuroimage. doi:10.1006/nimg.1998.0396

Fox, M.D., Snyder, A.Z., Vincent, J.L., Corbetta, M., Van Essen, D.C., Raichle, M.E., 2005. The human brain is intrinsically organized into dynamic, anticorrelated functional networks. Proc. Natl. Acad. Sci. 102, 9673–9678. doi:10.1073/pnas.0504136102

Friston, K.J., Price, C.J., 2003. Degeneracy and redundancy in cognitive anatomy. Trends Cogn. Sci. doi:10.1016/S1364-6613(03)00054-8

Glasser, M.F., Coalson, T.S., Robinson, E.C., Hacker, C.D., Harwell, J., Yacoub, E., Ugurbil, K., Andersson, J., Beckmann, C.F., Jenkinson, M., Smith, S.M., Van Essen, D.C., 2016. A multi-modal parcellation of human cerebral cortex. Nature 536, 171–8. doi:10.1038/nature18933

Glasser, M.F., Sotiropoulos, S.N., Wilson, J.A., Coalson, T.S., Fischl, B., Andersson, J.L., Xu, J., Jbabdi, S., Webster, M., Polimeni, J.R., Van Essen, D.C., Jenkinson, M., 2013. The minimal preprocessing pipelines for the Human Connectome Project. Neuroimage 80, 105–124. doi:10.1016/j.neuroimage.2013.04.127

Gordon, E.M., Laumann, T.O., Adeyemo, B., Gilmore, A.W., Nelson, S.M., Dosenbach, N.U.F., Petersen, S.E., 2017a. Individual-specific features of brain systems identified with resting state functional correlations. Neuroimage 146, 918–939. doi:10.1016/j.neuroimage.2016.08.032

Gordon, E.M., Laumann, T.O., Adeyemo, B., Petersen, S.E., 2017b. Individual Variability of the System-Level Organization of the Human Brain. Cereb. Cortex 27, 386–399. doi:10.1093/cercor/bhv239

Gordon, E.M., Laumann, T.O., Gilmore, A.W., Newbold, D.J., Greene, D.J., Berg, J.J., Ortega, M., Hoyt-Drazen, C., Gratton, C., Sun, H., Hampton, J.M., Coalson, R.S., Nguyen, A.L., McDermott, K.B., Shimony, J.S., Snyder, A.Z., Schlaggar, B.L., Petersen, S.E., Nelson, S.M., Dosenbach, N.U.F., 2017c. Precision Functional Mapping of Individual Human Brains. Neuron 95, 791–807.e7. doi:10.1016/j.neuron.2017.07.011

Gratton, C., Laumann, T.O., Nielsen, A.N., Greene, D.J., Gordon, E.M., Gilmore, A.W., Nelson, S.M., Coalson, R.S., Snyder, A.Z., Schlaggar, B.L., Dosenbach, N.U.F., Petersen, S.E., 2018. Functional Brain Networks Are Dominated by Stable Group and Individual Factors, Not Cognitive or Daily Variation. Neuron. doi:10.1016/j.neuron.2018.03.035

Gratton, C., Neta, M., Sun, H., Ploran, E.J., Schlaggar, B.L., Wheeler, M.E., Petersen, S.E., Nelson, S.M., 2017. Distinct Stages of Moment-to-Moment Processing in the Cinguloopercular and Frontoparietal Networks. Cereb. Cortex 27, 2403–2417. doi:10.1093/cercor/bhw092

Hamasaki, T., Leingärtner, A., Ringstedt, T., O'Leary, D.D.M., 2004. EMX2 regulates sizes and positioning of the primary sensory and motor areas in neocortex by direct specification of cortical progenitors. Neuron 43, 359–372. doi:10.1016/j.neuron.2004.07.016

Jiang, J., Zhu, W., Shi, F., Liu, Y., Li, J., Qin, W., Li, K., Yu, C., Jiang, T., 2009. Thick Visual Cortex in the Early Blind. J. Neurosci. 29, 2205–2211. doi:10.1523/JNEUROSCI.5451-08.2009

Kanai, R., Rees, G., 2011. The structural basis of inter-individual differences in human behaviour and cognition. Nat Rev Neurosci 12, 231–242. doi:10.1038/nrn3000

Kong, R., Li, J., Orban, C., Sabuncu, M.R., Liu, H., Schaefer, A., Sun, N., Zuo, X.-N., Holmes, A.J., Eickhoff, S.B., Yeo, B.T.T., 2018. Spatial Topography of Individual-Specific Cortical Networks Predicts Human Cognition, Personality, and Emotion. Cereb. Cortex. doi:10.1093/cercor/bhy123

Laumann, T.O., Gordon, E.M., Adeyemo, B., Snyder, A.Z., Joo, S.J., Chen, M.-Y., Gilmore, A.W., McDermott, K.B., Nelson, S.M., Dosenbach, N.U.F., Schlaggar, B.L., Mumford, J.A., Poldrack, R.A., Petersen, S.E., 2015. Functional System and Areal Organization of a Highly Sampled Individual Human Brain. Neuron 1–14. doi:10.1016/j.neuron.2015.06.037

Laumann, T.O., Snyder, A.Z., Mitra, A., Gordon, E.M., Gratton, C., Adeyemo, B., Gilmore, A.W., Nelson, S.M., Berg, J.J., Greene, D.J., McCarthy, J.E., Tagliazucchi, E., Laufs, H., Schlaggar, B.L., Dosenbach, N.U.F., Petersen, S.E., 2016. On the Stability of BOLD fMRI Correlations. Cereb. Cortex 1–14. doi:10.1093/cercor/bhw265

Lowe, M.J., Mock, B.J., Sorenson, J.A., 1998. Functional connectivity in single and multislice echoplanar imaging using resting-state fluctuations. Neuroimage 7, 119–132. doi:10.1006/nimg.1997.0315

Marek, S., Siegel, J.S., Gordon, E.M., Raut, R. V., Gratton, C., Newbold, D.J., Ortega, M., Laumann, T.O., Adeyemo, B., Miller, D.B., Zheng, A., Lopez, K.C., Berg, J.J., Coalson, R.S., Nguyen, A.L., Dierker, D., Van, A.N., Hoyt, C.R., McDermott, K.B., Norris, S.A., Shimony, J.S., Snyder, A.Z., Nelson, S.M., Barch, D.M., Schlaggar, B.L., Raichle, M.E., Petersen, S.E., Greene, D.J., Dosenbach, N.U.F., 2018. Spatial and Temporal Organization of the Individual Human Cerebellum. Neuron.

Margulies, D.S., Ghosh, S.S., Goulas, A., Falkiewicz, M., Huntenburg, J.M., Langs, G., Bezgin, G., Eickhoff, S.B., Castellanos, F.X., Petrides, M., Jefferies, E., Smallwood, J., 2016. Situating the default-mode network along a principal gradient of macroscale cortical organization. Proc. Natl. Acad. Sci. 113, 12574–12579. doi:10.1073/pnas.1608282113

Miller, M.B., Donovan, C.L., Bennett, C.M., Aminoff, E.M., Mayer, R.E., 2012. Individual differences in cognitive style and strategy predict similarities in the patterns of brain activity between individuals. Neuroimage. doi:10.1016/j.neuroimage.2011.05.060

Miller, M.B., Donovan, C.L., Van Horn, J.D., German, E., Sokol-Hessner, P., Wolford, G.L., 2009. Unique and persistent individual patterns of brain activity across different memory retrieval tasks. Neuroimage 48, 625–635. doi:10.1016/j.neuroimage.2009.06.033

Mueller, S., Wang, D., Fox, M.D., Yeo, B.T.T., Sepulcre, J., Sabuncu, M.R., Shafee, R., Lu, J., Liu, H., 2013. Individual Variability in Functional Connectivity Architecture of the Human Brain. Neuron 77, 586–595. doi:10.1016/j.neuron.2012.12.028

Neta, M., Schlaggar, B.L., Petersen, S.E., 2014. Separable responses to error, ambiguity, and reaction time in cingulo-opercular task control regions. Neuroimage 99, 59–68. doi:10.1016/j.neuroimage.2014.05.053

Neta, M., Whalen, P.J., 2011. Individual differences in neural activity during a facial expression vs. identity working memory task. Neuroimage 56, 1685–1692. doi:10.1016/j.neuroimage.2011.02.051

Noppeney, U., Friston, K.J., Ashburner, J., Frackowiak, R., Price, C.J., 2005. Early visual deprivation induces structural plasticity in gray and white matter [1]. Curr. Biol. doi:10.1016/j.cub.2005.06.053

Ojemann, J.G., Akbudak, E., Snyder, A.Z., McKinstry, R.C., Raichle, M.E., Conturo, T.E., 1997. Anatomic localization and quantitative analysis of gradient refocused echo-planar fMRI susceptibility artifacts. Neuroimage 6, 156–167. doi:10.1006/nimg.1997.0289

Park, H.J., Lee, J.D., Kim, E.Y., Park, B., Oh, M.K., Lee, S.C., Kim, J.J., 2009. Morphological alterations in the congenital blind based on the analysis of cortical thickness and surface area. Neuroimage 47, 98–106. doi:10.1016/j.neuroimage.2009.03.076

Paus, T., 1996. Location and function of the human frontal eye-field: A selective review. Neuropsychologia. doi:10.1016/0028-3932(95)00134-4

Petersen, S.E., Dubis, J.W., 2012. The mixed block/event-related design. Neuroimage. doi:10.1016/j.neuroimage.2011.09.084

Poldrack, R.A., Laumann, T.O., Koyejo, O., Gregory, B., Hover, A., Chen, M.Y., Gorgolewski, K.J., Luci, J., Joo, S.J., Boyd, R.L., Hunicke-Smith, S., Simpson, Z.B., Caven, T., Sochat, V., Shine, J.M., Gordon, E., Snyder, A.Z., Adeyemo, B., Petersen, S.E., Glahn, D.C., Mckay, D.R., Curran, J.E., Göring, H.H.H., Carless, M.A., Blangero, J., Dougherty, R., Leemans, A., Handwerker, D.A., Frick, L., Marcotte, E.M., Mumford, J.A., 2015. Long-term neural and physiological phenotyping of a single human. Nat. Commun. 6. doi:10.1038/ncomms9885

Power, J.D., Cohen, A.L., Nelson, S.M., Wig, G.S., Barnes, K.A., Church, J.A., Vogel, A.C., Laumann, T.O., Miezin, F.M., Schlaggar, B.L., Petersen, S.E., 2011. Functional Network Organization of the Human Brain. Neuron 72, 665–678. doi:10.1016/j.neuron.2011.09.006

Power, J.D., Mitra, A., Laumann, T.O., Snyder, A.Z., Schlaggar, B.L., Petersen, S.E., 2014. Methods to detect, characterize, and remove motion artifact in resting state fMRI. Neuroimage 84, 320–341. doi:10.1016/j.neuroimage.2013.08.048

Raichle, M.E., 2015. The Brain's Default Mode Network. Annu. Rev. Neurosci. 413–427. doi:10.1146/annurev-neuro-071013-014030

Rosvall, M., Bergstrom, C.T., 2008. Maps of random walks on complex networks reveal community structure. Proc. Natl. Acad. Sci. U. S. A. 105, 1118–1123. doi:10.1073/pnas.0706851105

Sadaghiani, S., D'Esposito, M., 2015. Functional characterization of the cingulo-opercular network in the maintenance of tonic alertness. Cereb. Cortex 25, 2763–2773. doi:10.1093/cercor/bhu072

Schlaggar, B.L., McCandliss, B.D., 2007. Development of Neural Systems for Reading. Annu. Rev. Neurosci. 30, 475–503. doi:10.1146/annurev.neuro.28.061604.135645

Seeley, W.W., Menon, V., Schatzberg, A.F., Keller, J., Glover, G.H., Kenna, H., Reiss, A.L., Greicius, M.D., 2007. Dissociable intrinsic connectivity networks for salience processing and executive control. J. Neurosci. 27, 2349–2356. doi:10.1523/JNEUROSCI.5587-06.2007

Ségonne, F., Grimson, E., Fischl, B., 2005. A genetic algorithm for the topology correction of cortical surfaces. Inf. Process. Med. Imaging 19, 393–405. doi:10.1007/11505730_33

Shulman, G.L., Fiez, J.A., Corbetta, M., Buckner, R.L., Miezin, F.M., Raichle, M.E., Petersen, S.E., 1997. Common Blood Flow Changes across Visual Tasks: II. Decreases in Cerebral Cortex. J. Cogn. Neurosci. 9, 648–663. doi:10.1162/jocn.1997.9.5.648

Smith, S.M., Fox, P.T., Miller, K.L., Glahn, D.C., Fox, P.M., Mackay, C.E., Filippini, N., Watkins, K.E., Toro, R., Laird, A.R., Beckmann, C.F., 2009. Correspondence of the brain's functional architecture during activation and rest. Proc. Natl. Acad. Sci. U. S. A. 106, 13040–5. doi:10.1073/pnas.0905267106

Smith, S.M., Nichols, T.E., Vidaurre, D., Winkler, A.M., J Behrens, T.E., Glasser, M.F., Ugurbil, K., Barch, D.M., Van Essen, D.C., Miller, K.L., 2015. A positive-negative mode of population covariation links brain connectivity, demographics and behavior. Nat. Neurosci. 18, 1–7. doi:10.1038/nn.4125

Sperry, R.W., 1961. Cerebral Organization and Behavior: The split brain behaves in many respects like two separate brains, providing new research possibilities. Science (80-.). 133, 1749–1757. doi:10.1126/science.133.3466.1749

Spreng, R.N., Mar, R.A., Kim, A.S.N., 2009. The Common Neural Basis of Autobiographical Memory, Prospection, Navigation, Theory of Mind, and the Default Mode: A Quantitative Meta-analysis. J. Cogn. Neurosci. 21, 489–510. doi:10.1162/jocn.2008.21029

Tavor, I., Parker Jones, O., Mars, R.B., Smith, S.M., Behrens, T.E., Jbabdi, S., 2016. Task-free MRI predicts individual differences in brain activity during task performance. Science (80-.). 352, 216–220. doi:10.1126/science.aad8127

Tehovnik, E.J., Sommer, M.A., Chou, I.H., Slocum, W.M., Schiller, P.H., 2000. Eye fields in the frontal lobes of primates. Brain Res. Rev. doi:10.1016/S0165-0173(99)00092-2

Tononi, G., Sporns, O., Edelman, G.M., 1999. Measures of degeneracy and redundancy in biological networks. Proc. Natl. Acad. Sci. 96, 3257–3262. doi:10.1073/pnas.96.6.3257

Van Essen, D.C., Glasser, M.F., Dierker, D.L., Harwell, J., Coalson, T., 2012a. Parcellations and hemispheric asymmetries of human cerebral cortex analyzed on surface-based atlases. Cereb. Cortex 22, 2241–2262. doi:10.1093/cercor/bhr291

Van Essen, D.C., Ugurbil, K., Auerbach, E., Barch, D., Behrens, T.E.J., Bucholz, R., Chang, A., Chen, L., Corbetta, M., Curtiss, S.W., Della Penna, S., Feinberg, D., Glasser, M.F., Harel, N., Heath, A.C., Larson-Prior, L., Marcus, D., Michalareas, G., Moeller, S., Oostenveld, R., Petersen, S.E., Prior, F., Schlaggar, B.L., Smith, S.M., Snyder, A.Z., Xu, J., Yacoub, E., 2012b. The Human Connectome Project: A data acquisition perspective. Neuroimage 62, 2222–2231. doi:10.1016/j.neuroimage.2012.02.018

Van Horn, J.D., Grafton, S.T., Miller, M.B., 2008. Individual variability in brain activity: A nuisance or an opportunity? Brain Imaging Behav. 2, 327–334. doi:10.1007/s11682-008-9049-9

Wang, D., Buckner, R.L., Fox, M.D., Holt, D.J., Holmes, A.J., Stoecklein, S., Langs, G., Pan, R., Qian, T., Li, K., Baker, J.T., Stufflebeam, S.M., Wang, K., Wang, X., Hong, B., Liu, H., 2015. Parcellating cortical functional networks in individuals. Nat. Neurosci. 18, 1853–1860. doi:10.1038/nn.4164

Woolsey, C.N., 1982. Cortical Sensory Organization- Volume 3: Multiple Auditory Areas. Humana Press. doi:10.1007/978-1-4612-5811-7

Woolsey, C.N., 1981a. Cortical Sensory Organization- Volume 2: Multiple Visual Areas. Humana Press. doi:10.1007/978-1-4612-5811-7

Woolsey, C.N., 1981b. Cortical Sensory Organization- Volume 1: Multiple Somatic Areas. Humana Press. doi:10.1007/978-1-4612-5811-7

Yeo, B.T.T., Krienen, F.M., Sepulcre, J., Sabuncu, M.R., Lashkari, D., Hollinshead, M., Roffman, Joshua L. Smoller, J.W., Zöllei, L., Polimeni, J.R., Fischl, B., Liu, H., Buckner, R.L., 2011. The organization of the human cerebral cortex estimated by intrinsic functional connectivity. J. Neurophysiol. 106, 1125–1165.

3.10 Supplemental Information

3.10.1 Supplemental Figures

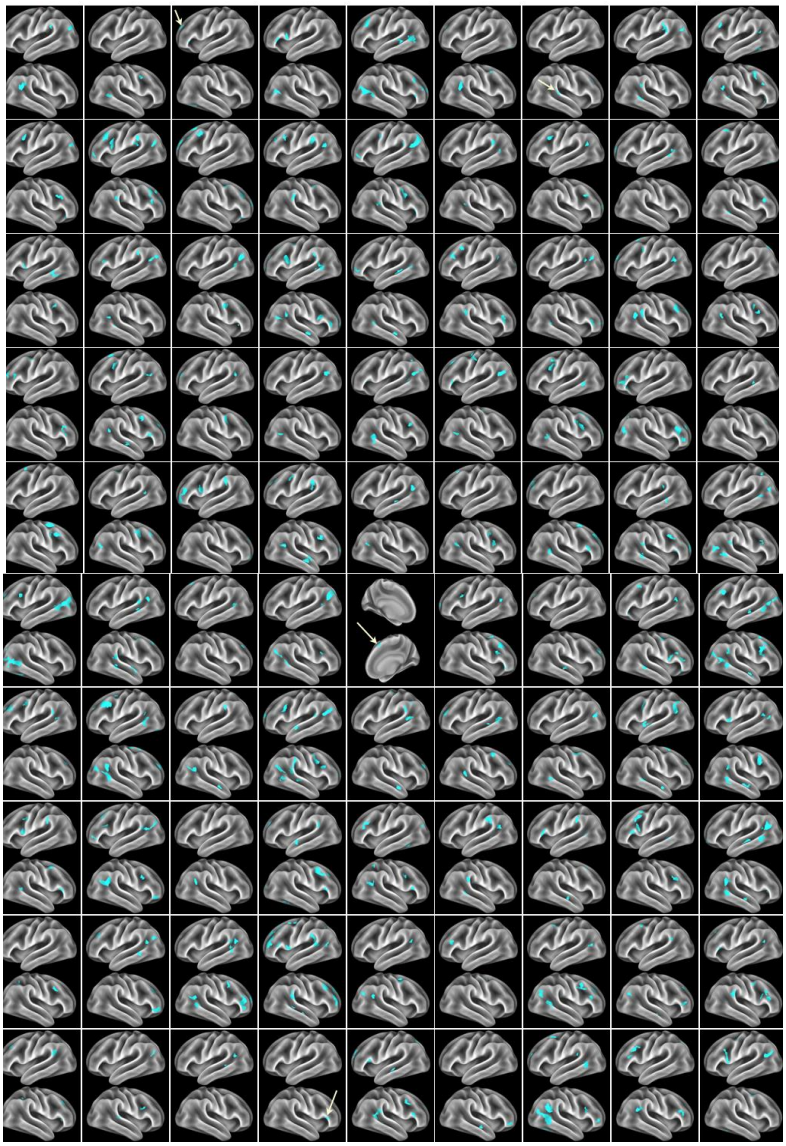

SI Figure 3.1: Network variants are present in all individuals. Network variants are present in each individual included in the study. The figure displays binarized variants (light blue) for all MSC individuals and 81 randomly selected HCP subjects. Variants were created by use of a conservative fixed threshold of spatial correlations less than 0.15 (rather than lowest decile as used in the main text, to determine if low similarity locations were present in all individuals). Size and SNR exclusion criteria were also applied, as described in the methods.

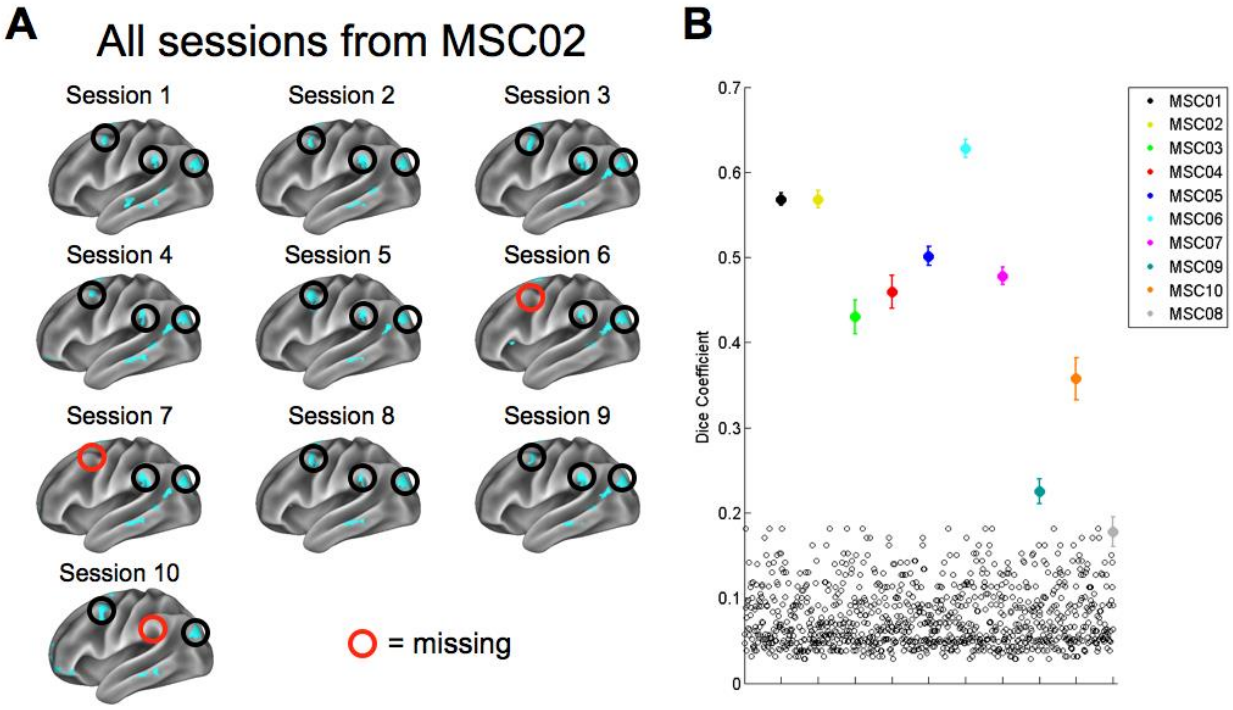

SI Figure 3.2: Reliability of binarized network variants. The figure shows the session-to-session reliability of binarized network variants within each MSC individual. (A) Binary variants for all 10 sessions from MSC02 are displayed. Most variants are consistent across sessions, with a few missing variants highlighted (red circle; note that these often still showed relatively low spatial correlations, as in Fig. 3.2, but did not pass the threshold to be in the lowest decile for that session). (B) We quantified the reliability of variant locations across sessions within an individual using the dice coefficient instead of the intraclass correlation (ICC), since the data are binary. The mean and standard error of within-subject variant reliability (i.e., mean +/- SE across all 10 sessions) is shown for each individual. The open black circles represent the null distribution of variant reliability. To create the null, we performed 1000 random permutations of pairs of sessions drawn from two different MSC individuals (with replacement). Only MSC08 shows a dice coefficient in the range of between subject variant dice.

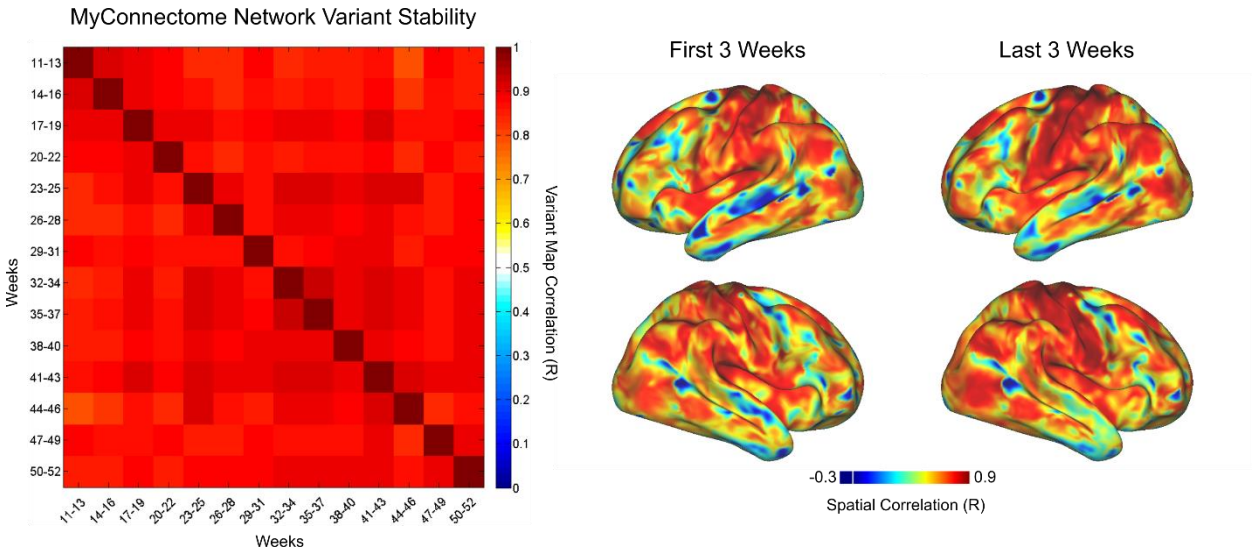

SI Fig 3.3: Stability of network variants over a year. Using data from MyConnectome, we tested the stability of network variants over a year in a single individual. The correlation matrix on the left demonstrates that the individual's network variants (i.e., the spatial correlation maps) are quite stable from month-to-month (data from all sessions within a 3 week block are concatenated together). The brains on the right show that the individual's network variants are extremely similar (r = 0.85) at the beginning and end of the year.

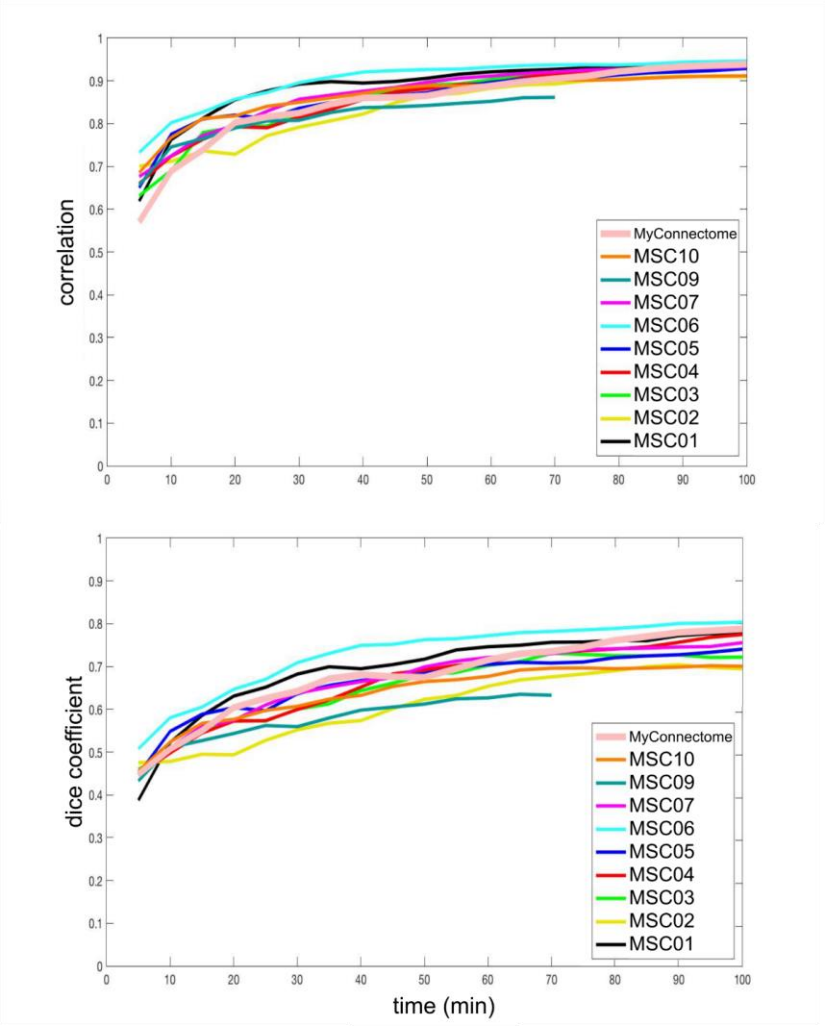

SI Figure 3.4: Sampling variability affects identification of network variants. To quantify the effects of sampling variability on network variants, data from both the MSC and MyConnectome individuals were used. Split-halves of the data were generated, and the BOLD time series in one of the split-halves was sampled consecutively in 5-minute increments. Network variants were identified via a spatial correlation between the individual and the group-average data (as in Figure 3.1). Then, at each 5-minute increment, both the spatial correlation map (top) and the map of binarized network variants (bottom; lowest decile of spatial correlation map, SNR and size exclusion applied) were compared to the corresponding map generated from the remaining "true" half of the data (as in (Evan M. Gordon et al., 2017; Laumann et al., 2015)). Spatial correlation maps were compared via Pearson correlation and binarized maps were compared via dice overlap. To prevent an artificial inflation of the dice coefficient due to the large number of vertices that did not contain variants, only vertices that were classified as variants in at least one of the split-halves were considered.

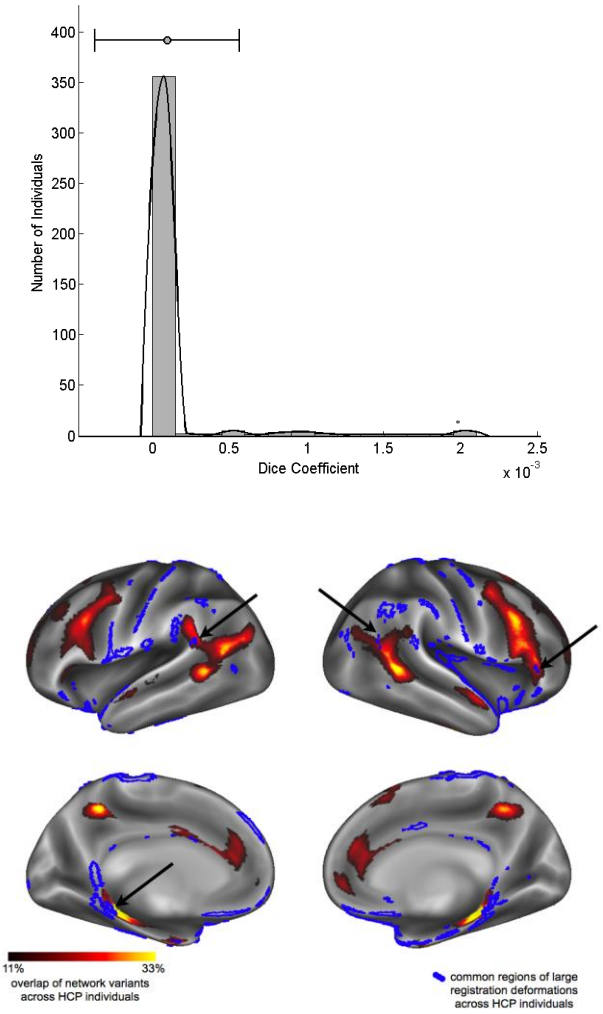

SI Figure 3.5: Overlap of network variants and surface registration deformations. The distribution (top) displays the dice coefficient overlap between an individual's network variants and large deformations (both contractions and expansions) that occurred during surface registration, a proxy measure of anatomical variability, across the HCP dataset. Large deformations are defined as the top decile of the absolute value of the areal distortion map, an output from the HCP registration procedure (registering the individual's FreeSurfer defined-surface to the Conte69 atlas; (Glasser et al., 2013)). There is little to no overlap between network variants and registration deformations within individuals. Common regions of registration deformations across HCP individuals (>30% of individuals) are displayed as blue borders on the brains (bottom), with the scale bar showing the overlap of network variants across HCP subjects (reproduced from Figure 3.3A). There is minimal overlap between common locations for network variants and common locations for large deformations across individuals (black arrows).

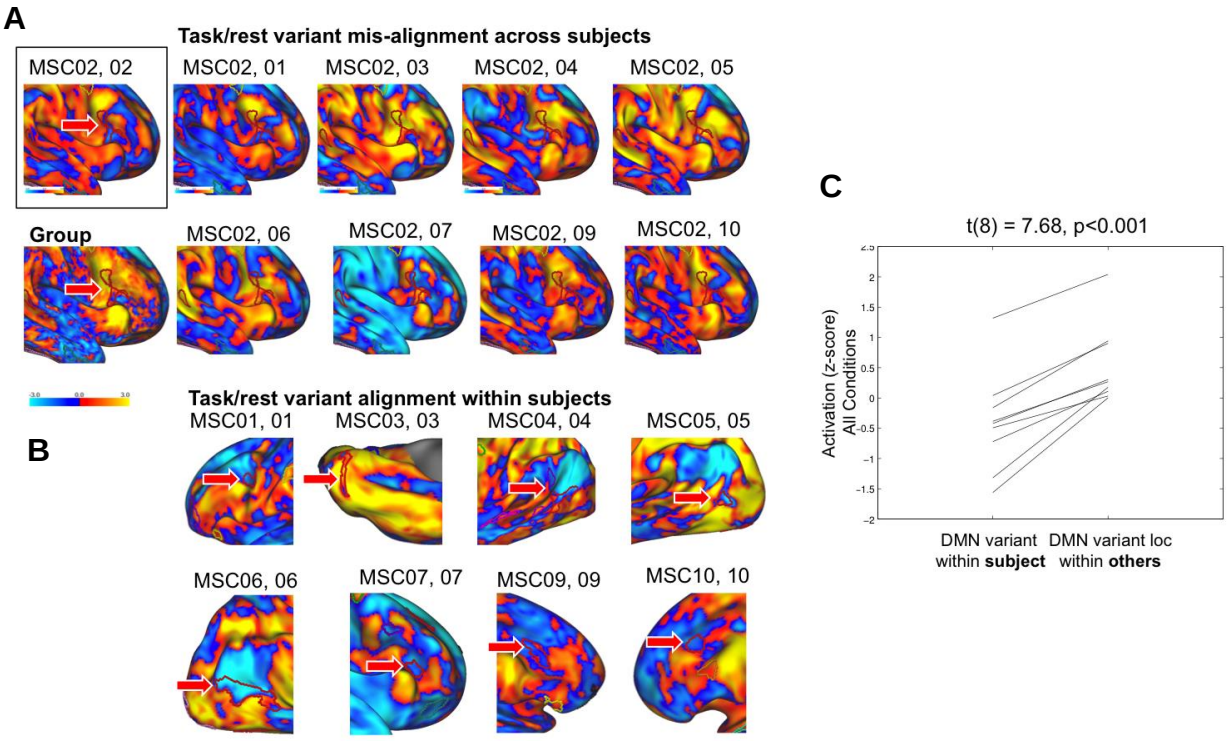

SI Figure 3.6: Task-rest alignment of DMN variants. (A) Alignment of a DMN variant from MSC02 to task activations from all other subjects. Note that while MSC02 shows deactivations in this variant, other participants and the group show primarily activations. (B) DMN variants in other participants also align with deactivations during mixed design tasks. (C) DMN variants from a given subject show significantly lower activations than the same location from other subjects (each line represents a single subject).

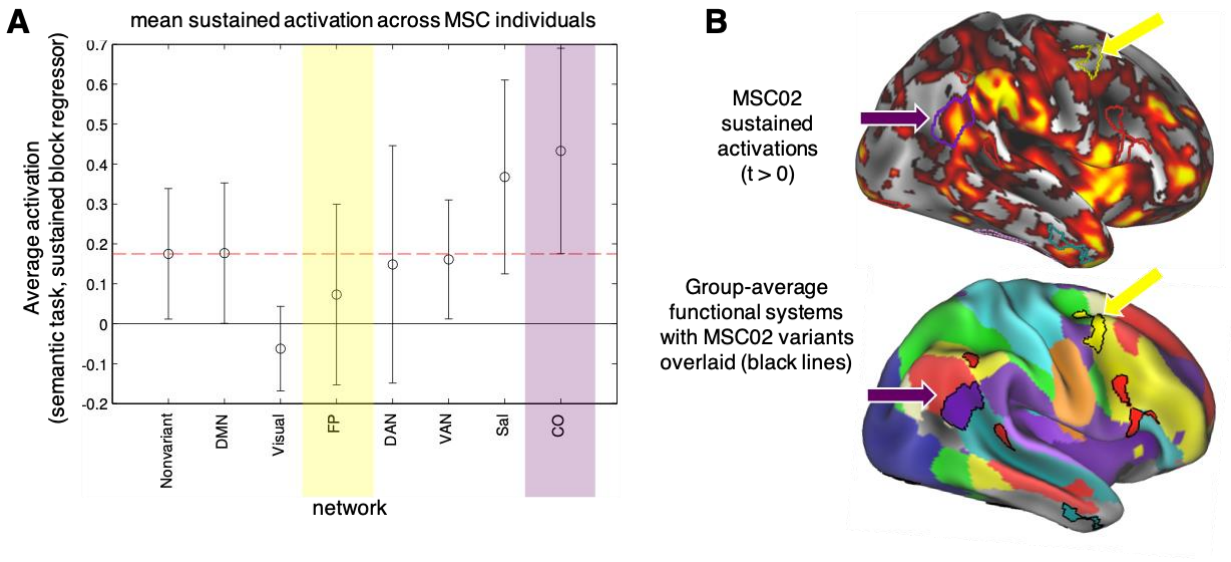

SI Figure 3.7: Sustained activation in cinguloopercular variants. Task-evoked activations during a mixed design task are displayed for network variants. The mean and standard error across the 9 included highly sampled subjects reveals that sustained activations (all conditions – baseline) are stronger in cinguloopercular variants specifically. Example sustained activations ($t > 0$) are displayed for subject MSC02 with outlines of the subject's variants overlaid (as in Figure 3.4). Note that there is strong activation in the cinguloopercular variant near the angular gyrus (purple arrow), whereas there is no activation in the frontoparietal variant near the superior frontal gyrus (yellow arrow). The group-average functional networks with the same variants overlaid are displayed below for reference (variants shown with black outlines).

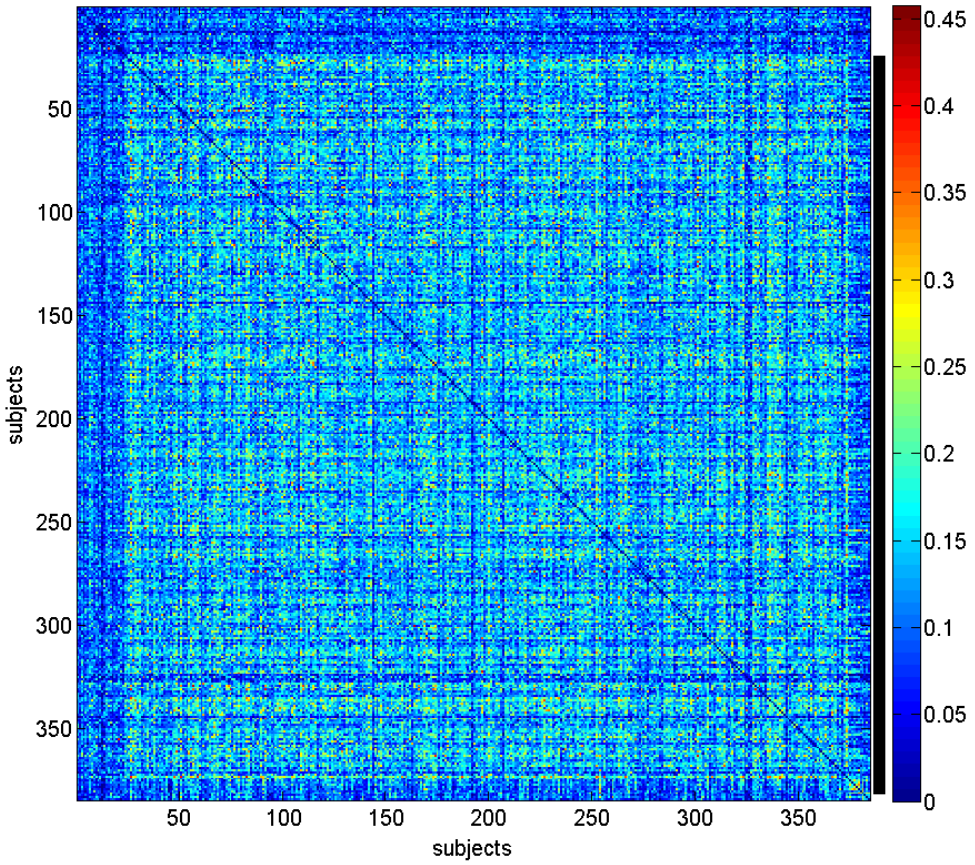

SI Figure 3.8: Clustering via anatomical location of network variants. The matrix displays the dice coefficient overlap between the locations of network variants in all pairs of individuals (i.e., the degree to which two individuals both have variants 1, 2, and 3 and both do not have variants 4, 5, and 6). The matrix is sorted by clusters, with unlabeled subjects in the first portion of the matrix. Across InfoMap thresholds (see Methods), individuals cluster into one large group (solid black line). Thus, we did not find evidence for sub-groups of individuals with similar anatomical distributions of network variants.

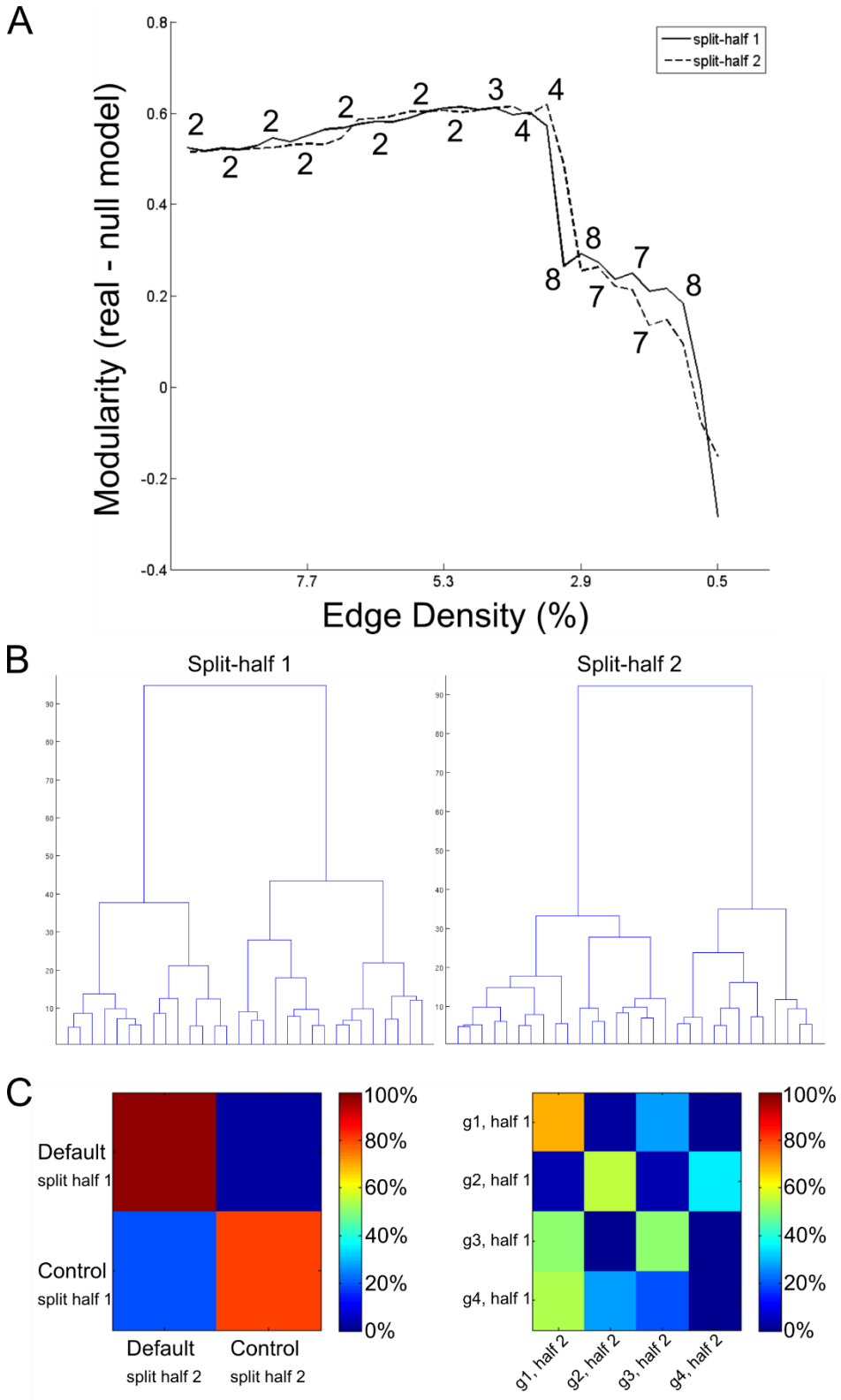

SI Figure 3.9: Validation of the sub-group clustering. We validated the clustering of individuals in two sub-groups (**Fig 3.5** in the main text) via two methods: (1) modularity versus a null model that preserves the degree

distribution and (2) hierarchical clustering. **(A)** The number of clusters found by InfoMap (see Methods in the main text) varies as a function of edge density. Thus, for each edge density we tested the modularity of the real solution against a null model. The null model is a random network (at that specific edge density) with the same degree distribution as the real network (generated via the Brain Connectivity Toolbox function null_model_und_sign.m; (Rubinov and Sporns, 2010)). The two sub-group solution was the most robust across edge density thresholds and split-halves, as indicated by the numbers near the lines. **(B)** The dendrograms produced by hierarchical clustering (created via MATLAB functions dendrogram and linkage, Ward's minimum variance method) are displayed for each split-half. The cophentic correlation coefficient was greater than 0.8 for each split-half. **(C)** A confusion matrix was generated for the two- and four-group hierarchical clustering solutions to test their reliability across each split-half. If split-half 1 is the 'true answer,' then the confusion matrix represents the degree to which split-half 2 matches the true answer (in terms of sub-group labeling). In order to align sub-group labels across each split-half (e.g., to ensure that individuals in the default sub-group are labeled with a 1 in each split-half), the average network template match was used (i.e., the line graphs in Figure 3.5 in the main text). The two sub-group solution had a much higher percentage of true positives and a much lower percentage of false positives and false negatives than the four sub-group solution.

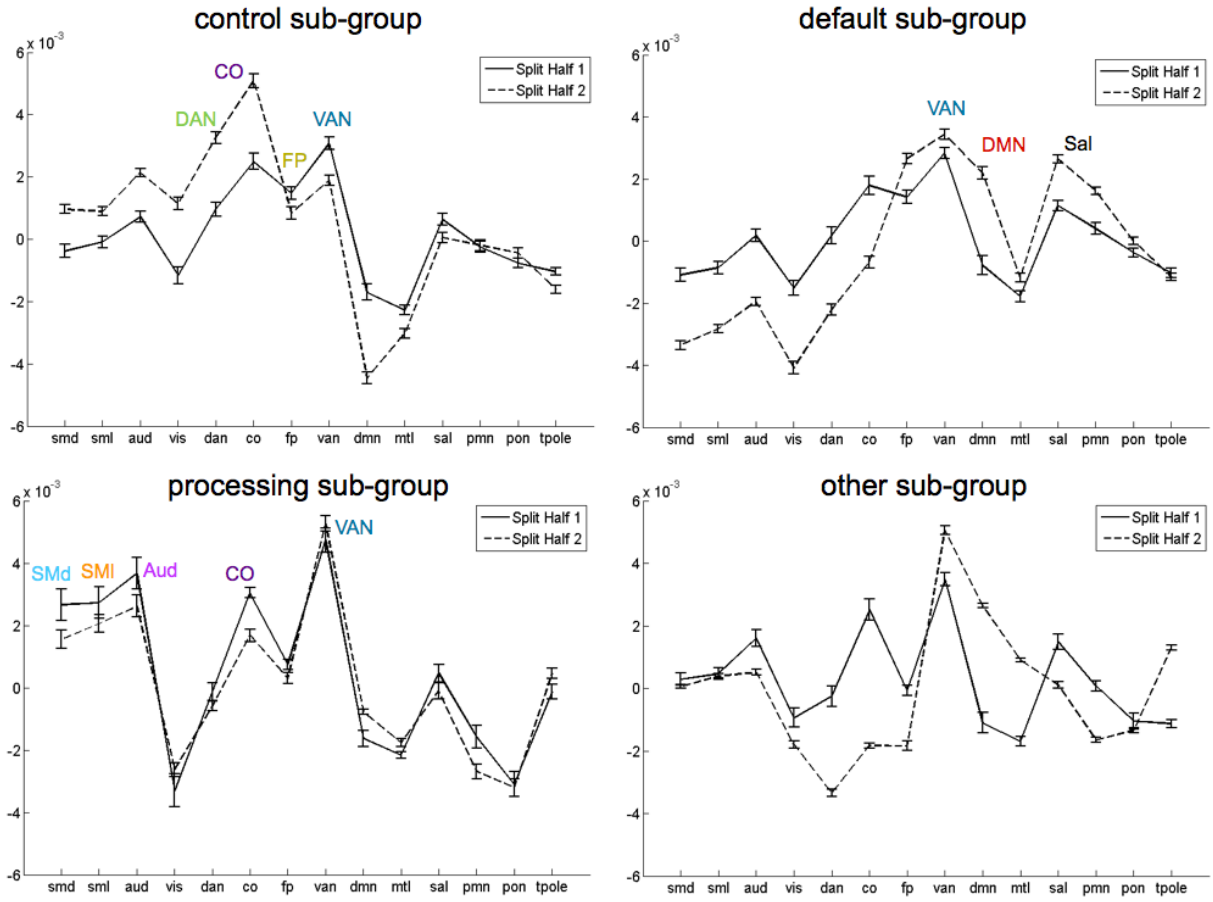

SI Figure 3.10: The four sub-group solution. The four sub-groups of individuals from the HCP dataset, identified via patterns of network variants, are displayed. Individuals in these sub-groups have variants that are more like the frontoparietal, dorsal attention, and cinguloopercular networks (top left), the default mode, frontoparietal, and ventral attention networks (top right), the motor, auditory, ventral attention, and cinguloopercular networks (bottom left), or a mixed pattern (bottom right).

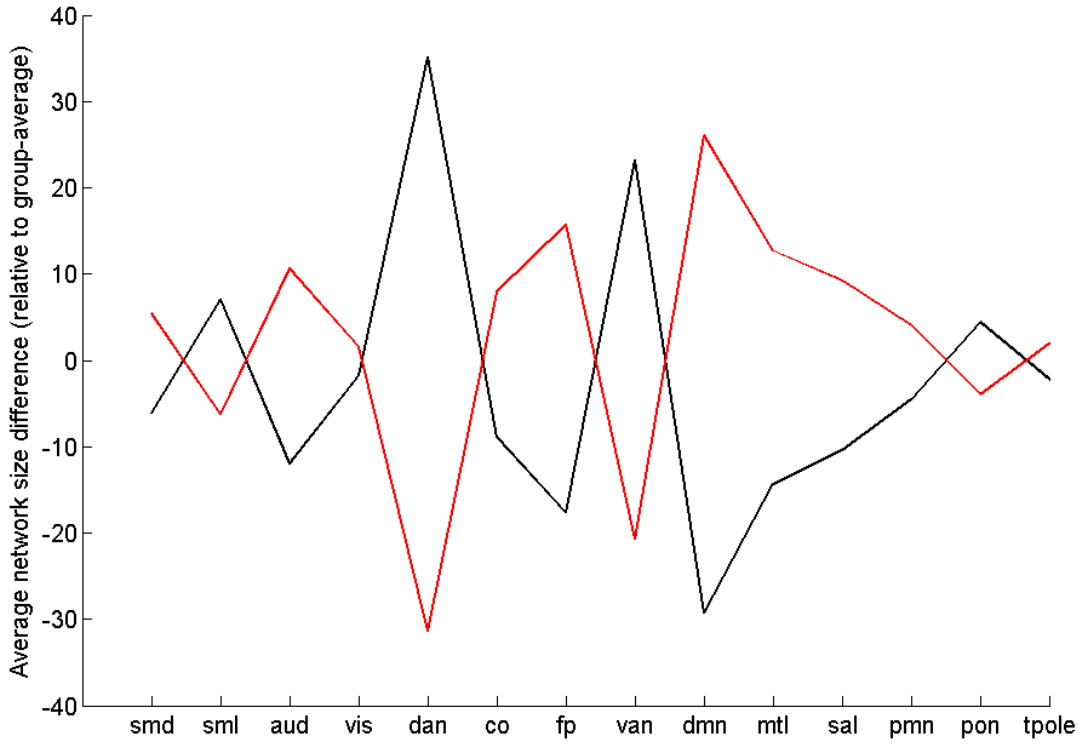

SI Figure 3.11: Group-wise differences in the size of each network. The solid line represents the mean expansion or contraction of each functional network in individuals in the two sub-groups identified in the main results (black = control and processing, red = default). The specific measure is the number of surface vertices assigned to each network in the individual minus the same number for the group-average. A positive number means more vertices assigned to that network than the group-average (an expansion), a negative number means fewer vertices assigned to that network than the group-average (a contraction), and zero means an identical number of vertices assigned to that network as the group-average. The pattern is partially consistent with that observed in **Fig 3.5B**, but sub-group differences are driven by the dorsal and ventral attention networks versus the default mode, salience, and frontoparietal networks.

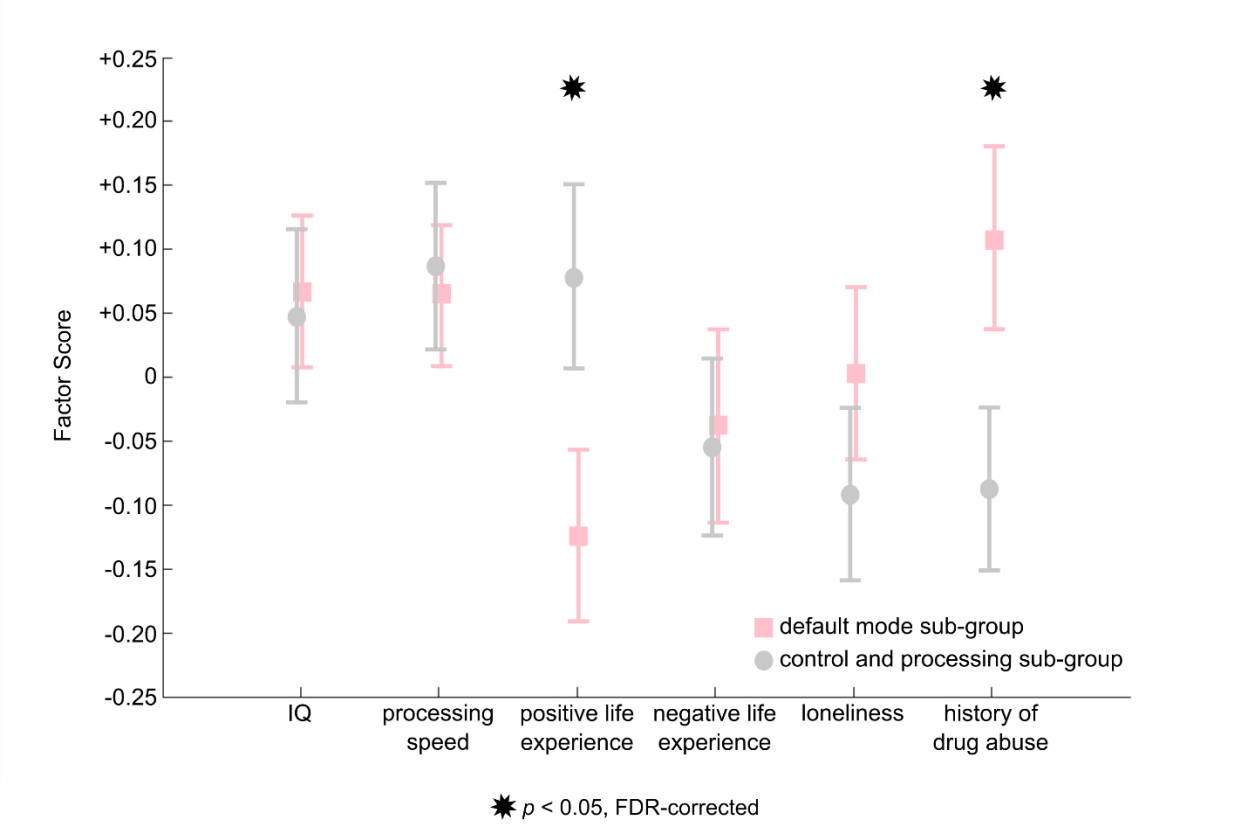

SI Figure 3.12: Group-wise differences in neuropsychological measures. Factor scores derived from the HCP behavioral measures are displayed (mean and standard error) for the two larger sub-groups from the HCP dataset (**Fig 3.5B**). Factor scores for the control and processing sub-group were significantly higher in the Positive Life Experience factor ($t(344) = 2.038$) and significantly lower in the History of Drug Abuse factor ($t(344) = -2.039$) than scores for the default sub-group. Two-sample *t*-tests were performed with subjects from both split-halves grouped together.

3.10.2 Supplemental Methods

Acquisition details

Three datasets are included in this manuscript: the first contains five hours of resting-state data from each of 10 highly-sampled individual subjects, referred to as the Midnight Scan Club or MSC dataset; the second includes 14 hours of resting-state data from a single individual collected over the course of a year, referred to as the MyConnectome dataset; and, the third includes one hour of resting-state data from 384 unrelated individuals from the Human Connectome Project 1200 subject release, referred to as the HCP dataset.

Briefly, for the MSC and WashU 120, high-resolution T1-weighted, T2-weighted, and resting-state BOLD data were collected on a Siemens 3T Magnetom Tim Trio with a 12-channel head coil (gradient-echo EPI sequence, isotropic 4 mm^3 voxels, TE of 27ms, and TR of 2.2s and 2.5s, respectively; (Evan M Gordon et al., 2017; Power et al., 2013)). The MyConnectome dataset was acquired on a Siemens 3T Skyra with a 32-channel head coil (multi-band sequence with MB factor 4, isotropic 2.4 mm^3 voxels, TE of 30ms, and TR of 1.16s; (Laumann et al., 2015; Poldrack et al., 2015)). The HCP was collected on a custom Siemens 3T Skyra with a custom 32-channel head coil (multi-band sequence with MB factor 8, isotropic 2 mm^3 voxels, TE of 33ms, and TR of 0.72s (Van Essen et al., 2012)).

We excluded all subjects whose resting-state BOLD runs contained large to moderate amounts of head motion in order to ensure reliable identification of network variants. Thus, we excluded data from one MSC individual with a substantial amount of head motion and drowsiness (Evan M. Gordon et al., 2017; Laumann et al., 2016). We included all high-quality (low-motion)

MyConnectome sessions after the schedule shift to Tuesday and Thursday acquisitions, following Laumann and colleagues (Laumann et al., 2015). A total of 84 sessions were included. Exclusion criteria for individuals from the full HCP 1200-subject HCP release were as follows: (1) we removed duplicates and subjects who did not complete the study; (2) we required subjects to have >75% of their data, i.e. 45 minutes, retained post motion censoring (see description of censoring procedures below); (3) we required that all subjects be unrelated (if more than one family member passed the previous criteria, the subject with the most data was selected). Thus, 384 HCP subjects were included. From these 384 individuals, two split-halves were created for within-dataset replication of our findings. Split-halves were balanced on the factors of age, sex, handedness, race, mean frames retained post motion censoring, and years of education. See **SI Table 3.1** for full details.

SI Table 3.1: HCP exclusion criteria and split-halves. The flow diagram at the top shows the exclusion criteria applied to obtain the final set of 384 HCP subjects. The table shows demographic variables on which the split-halves were balanced, as well as t-tests for each variable.

HCP subject exclusion criteria

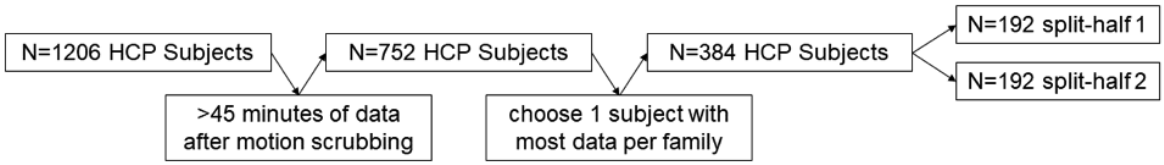

Split-half demographics

Group	N (N male)	N Right Handed	N Caucasian	N African American	N Asian	N Mixed or Unknown	N Hispanic	Mean (+/- std) Age in Years	Mean (+/- std) Frames Retained post-scrubbing	Mean (+/- std) Years of Education
Split Half 1	192 (87M)	120	129	24	13	4	22	28.4 +/- 3.7	4324 +/- 322	15.0 +/- 1.7
Split Half 2	192 (87M)	120	129	25	12	5	21	28.4 +/- 3.6	4332 +/- 324	15.0 +/- 1.8
t-test (382 degrees of freedom)	p = 1 t = 0	p = 1 t = 0	p = 0.951 t = 0.062					p = 0.945 t = 0.070	p = 0.815 t = -0.234	p = 0.815 t = 0.235

Functional preprocessing

For each subject, the volumetric BOLD time series from each run were concatenated together. Slice timing correction was applied first (but not in the HCP dataset, per recommendation from Glasser et al., 2013). Then, all functional data were aligned to the first frame of the first run using rigid body transforms, after which they were normalized to a whole-brain mode of 1000 (Miezin et al., 2000). For the WashU 120 and HCP, the functional data were registered to the high-resolution T1 image. Following this, a one-step operation (Smith et al., 2004) was applied to resample (3 cubic mm) and register the data to the 711-2B atlas (Ojemann et al., 1997). For the MSC, the functional data were first registered to the T2 image and then to the T1 image, which separately registered to the template space. Finally, field inhomogeneity distortion correction was applied using the mean field map applied to all sessions (Evan M. Gordon et al., 2017; Laumann et al., 2015). Distortion correction was not applied to the WashU 120 because field maps were not collected.

In order to remove further artifacts additional preprocessing was applied (Power et al., 2014). Frame-wise displacement (FD) was calculated (Power et al., 2012), and frames with FD greater than 0.2 mm were flagged for censoring for the MSC and WashU 120 datasets. However, the increased temporal resolution of the HCP acquisition (0.72s TR) caused respiration artifacts to alias into the FD trace (Siegel et al., 2017). Thus, the 6 realignment (motion) parameters were filtered with a lowpass filter at 0.1 Hz before calculating FD values. The filtered FD threshold for frame censoring was 0.1 mm. Uncensored segments with fewer than 5 contiguous frames were also flagged for censoring as well. First, the aligned and registered BOLD data were demeaned and detrended. Multi-linear nuisance regression was implemented with 36 regressors:

the whole-brain mean, individually defined white matter and ventricular CSF signals, the temporal derivatives of each of these regressors, and an additional 24 movement regressors derived by expansion (Friston et al., 1996; Satterthwaite et al., 2013). Then, the previously flagged frames were removed and interpolated over using least squares spectral estimation (Power et al., 2014). Finally, the data were bandpass filtered from 0.009-0.08 Hz. The MyConnectome data were processed identically to the MSC data, except the FD threshold was 0.25 mm.

Volume-to-surface mapping and functional connectivity processing

Unsmoothed (but otherwise completely processed) BOLD data were mapped to each individual's native midthickness surface via the ribbon-constrained sampling procedure (Connectome Workbench v1.0) (Marcus et al., 2013). Then, the mapped data were registered to the fsaverage surface in one step using the deformation map generated from the aforementioned shape-based spherical registration. Afterwards, a geodesic Gaussian smoothing kernel was applied (FWHM = 6 mm, sigma = 2.55) to the surface registered data (Gordon et al., 2016). Subcortical and cerebellar data were not considered in any further analyses due to substantial signal-to-noise issues in HCP data.

Before computing correlations (functional connectivity), the first 30 seconds of each functional run (14, 41, and 12 frames, for the MSC, HCP, and WashU-120, respectively) were discarded to account for magnetization equilibrium and an auditory evoked response to the start of the EPI sequence in addition to frame censoring (Laumann et al., 2015). For the MyConnectome data, the 60 seconds of each run (52 frames) were discarded due to an amplified evoked response as a function of noise cancelling headphones.

Task data processing

In this study, we focus on activations in the two mixed design (Petersen and Dubis, 2012) tasks from the MSC dataset: the semantic task and the coherence task. Briefly, the semantic task required a noun or verb judgment on a series of presented words, while the coherence task required a yes/no judgment regarding whether an array of dots was arranged concentrically on the screen (Glass, 1969). Blocks of each task consisted of start cues signaling the beginning of the block, followed by a series of randomly intermixed trials in each condition (nouns and verbs in the semantic task, 0% and 50% coherence arrays in the coherence task).

Task activations were modeled with in-house imaging analysis software (IDL) using a general linear model (GLM) approach as previously described (Evan M. Gordon et al., 2017; Gratton et al., 2018). Eight time-points were modeled for cues and each trial type in each condition. In addition, block regressors for sustained activations were included across the full task block. MSC individuals completed two runs of each task in each of their 10 sessions; each individual was analyzed separately.

Behavioral measures

Demographic variables included education recoded into fewer categories to avoid small cell sizes (≤high school graduate, some college, ≥4-year college graduate), employment (not working, part time, full time), family income, also recoded into fewer categories (bottom quartile ≤$29,999, median $30,000-49,999, 3rd quartile $50,000-74,999, 4th quartile >$75,000), and whether the respondent was still in school or taking courses for a degree (Yes/No), was married or in a live-in relationship (Yes/No), and was born in Missouri (Yes/No). Race/ethnicity was recoded per NIH guidelines – not Hispanic White (n=814, 67.5%), Black/African American (n=191, 15.84%),

Asian (n=68, 5.64%), American Indian/mixed/unknown (n=28, 2.32%; there were only n=2 American Indian individuals), and Hispanic/Latino (n=105, 8.71%) – and dummy coded (not Hispanic White vs all others, Black/African American vs all others, etc).

Cognitive variables included all measures from the NIH Toolbox Cognition Battery (Picture Vocabulary, Oral Reading Recognition, the Flanker Task, Dimensional Change Card Sort, List Sorting, Picture Sequence Memory, and Pattern Completion Processing Speed; (Weintraub et al., 2013)) in addition to the number of correct responses from the Penn Progressive Matrices (Bilker et al., 2012), the Variable Short Penn Line Orientation, the Penn Word Memory Test, true positives from the Short Penn Continuous Performance Test (Gur et al., 2010), and Delay Discounting Area Under the Curve for $200 and $40,000 (Estle et al., 2006; Myerson et al., 2001). Cognitive variables were Z-score normalized across all HCP subjects and were not adjusted for age or sex to allow flexibility in covariate adjustment in other analyses.

Emotion variables included all NIH Toolbox surveys (Anger-Affect, Anger-Hostility, Anger-Physical Aggression, Fear-Affect, Fear-Somatic Arousal, Sadness, General Life Satisfaction, Meaning and Purpose, Positive Affect, Friendship, Loneliness, Perceived Hostility, Perceived Rejection, Emotional Support, Instrumental Support, Perceived Stress, and Self-Efficacy). They were Z-score normalized and also not adjusted for age or sex. Drug use variables were derived from SSAGA interviews on lifetime use and captured lifetime quantity/severity of use: history of alcohol abuse or dependence (Yes/No); number of cigarettes smoked: never smoked (0 cigarettes), experimented (1-19 cigarettes), occasional use (20-99 cigarettes), regular use (≥100

cigarettes); number of times used cannabis (never, 1, ≥2); and number of times used each of cocaine, hallucinogens, opiates, sedatives, or stimulants (never, ≥1).

For each behavior category, relationships between variables were examined using Pearson or polychoric/tetrachoric correlations for continuous and categorical variables, respectively. If a variable did not have a correlation of ≥0.32 with at least one other variable, which would suggest ~10% shared variance, that variable was excluded from consideration. Oblique rotation was always tested first and was retained if inter-factor correlations were significantly different from zero at $p<0.05$ (uncorrected). Final EFA structure was determined based on a combination of indicators including: (1) factor eigenvalues and scree plot; (2) variables had high loadings (≥0.32, accounting for approximately 10% of factor variance) on at least one factor; (3) variables had high loadings on one factor and relatively low loadings on all other factors, i.e., cross-loading was minimal; (4) at least two variables had high loadings on a factor; and (5) interpretability (Tabachnick and Fidell, 2007). Factor scores were output for use in subsequent analyses. Internal consistency of the factors was assessed using estimates of the squared multiple correlations (SMCs) of variables with each factor, where factor scores are predicted from the observed variables. SMCs vary from 0 to 1 and high SMCs (≥0.7) indicate that observed variables account for significant factor score variance. All data manipulation and EFA analysis was conducted in SAS 9.2 (SAS Institute Inc., 2008, Cary, NC, USA).

EFA results

Demographic variables (final n=1199): Whether a respondent was born in Missouri did not correlate with other variables and was not further considered. Being Black/African American was related to three other demographic variables and this dummy variable was retained for

analysis. EFA resulted in a single factor. Being in school or employed had low factor loadings and these variables were dropped from analysis. The four remaining variables (income, education, relationship status, and Black/African American) had inadequate internal consistency (SMC=0.59) suggesting that as a group, these variables are poor indicators of an underlying construct. We suggest that these variables be considered separately.

Cognitive variables (final n=1193): The two delay discounting variables correlated only with each other (r=0.675) and not with any other variables. In addition, the partial correlation remained high (r=0.65) after controlling for all other variables suggesting that delay discounting does not share variance with the other cognitive measures and was therefore not considered further. Likewise, Penn continuous performance and word memory tests did not correlate with any other variables and were not considered further. The picture sequence task had low loadings on all factors and was excluded. The final EFA consisted of two factors (**SI Table 3.2**). Variables that loaded highly on the first factor reflected fluid intelligence, reading and comprehension, spatial orientation and working memory; we named this factor General IQ. Processing speed variables loaded highly on the second factor which we named Processing Speed. The inter-factor correlation was 0.40 suggesting that higher general IQ is related to higher processing speed. The General IQ and Processing Speed factors had good to fair internal consistency (SMCs=0.80 and 0.65, respectively).

SI Table 3.2. Exploratory factor analysis of HCP behavioral variables. Factor loadings for the cognition, emotion, and substance use variables are displayed. Loadings of at least 0.32 (accounting for approximately 10% of factor variance) are bolded. Internal consistency of the factors is shown at the bottom of each factor loading vector, and inter-factor correlations are shown where applicable.

Cognition (n=1193)	**General IQ**	**Processing Speed**	
Card sort based on color or shape	0.06	**0.66**	
Flanker inhibitory control	0.00	**0.64**	
Progressive matrices	**0.63**	0.03	
Oral reading recognition	**0.79**	-0.03	
Picture vocabulary	**0.78**	-0.06	
Processing speed - pattern comparison	0.01	**0.54**	
Variable short line orientation	**0.50**	0.13	
List sorting working memory	**0.45**	0.08	
Internal consistency	0.80	0.65	
Inter-factor correlation	*0.40*		
Emotion (n=1204)	**Negative**	**Positive**	**Loneliness**
Anger - affect	**0.73**	-0.02	0.09
Fear - affect	**0.82**	-0.08	-0.08
Fear - somatic arousal	**0.59**	0.14	0.01
Sadness	**0.65**	**-0.32**	-0.02
Life satisfaction	-0.02	**0.71**	-0.02
Meaning and purpose	0.04	**0.69**	-0.05
Positive affect	-0.09	**0.64**	-0.03
Friendship	0.09	0.29	**-0.53**
Loneliness	0.18	-0.28	**0.46**
Perceived hostility	**0.34**	0.21	**0.56**
Perceived rejection	0.22	0.04	**0.70**
Emotional social support	0.16	**0.34**	**-0.60**
Instrumental social support	0.15	**0.33**	**-0.38**
Perceived stress	**0.49**	**-0.33**	0.10
Self-efficacy	-0.12	**0.43**	-0.08
Internal consistency	0.87	0.83	0.82
Inter-factor correlations			
Positive	*-0.53*		
Loneliness	*0.49*	*-0.57*	
Lifetime Drug Use (n=1204)	**Quantity/Frequency**		
Alcohol abuse or dependence	**0.50**		
Number of cigarettes (0, 1-19, 20-99, ≥100)	**0.50**		
Cocaine (0, ≥1)	**0.65**		
Hallucinogens (0, ≥1)	**0.67**		
Opiates (0, ≥1)	**0.66**		
Sedatives (0, ≥1)	**0.60**		
Stimulants (0, ≥1)	**0.66**		
Marijuana (0, 1, ≥2)	**0.60**		
Internal consistency	0.82		

Emotion variables (final n=1204): The variables anger-hostility and anger-physical aggression had low factor loadings and were excluded. The final EFA solution consisted of three factors (**SI Table 3.2**). Fear, anger, sadness, perceived social hostility and stress loaded on the first factor which we call Negative. Life satisfaction, meaning and purpose, social support, and self-efficacy loaded on the second factor which we call Positive. The third factor was characterized by positive loadings of loneliness and perceived social hostility and rejection, and negative loadings of social support and social relationship and we call this factor Loneliness. Higher score on the Negative factor was related to higher score on the Loneliness factor and higher score on the Positive factor was related to lower scores on both Negative and Loneliness factors. All three factors had good internal consistency (SMCs=0.87, 0.83, and 0.82, respectively).

Drug use variables (final n=1204): Drug use variables comprised a single factor that captured overall quantity and heaviness of use. This factor had good internal consistency (SMC=0.82).

Statistical analysis of behavior

Analysis of the variance of behavioral factor scores explained by network variant group assignment was conducted in MATLAB R2012a using the Statistics and Machine Learning Toolbox multi-linear regression (MathWorks Inc., 2012, Natick, MA, USA). Factor scores were modeled as dependent variables and variant group as the independent variable of interest. Regressions were performed both including and excluding other covariates, which included age, sex, handedness, and number of frames retained post-scrubbing. Further, *t*-tests were used to compare differences in factor scores between sub-groups, with an FDR correction for multiple comparisons.

3.10.3 Supplemental References

Bilker, W.B., Hansen, J.A., Brensinger, C.M., Richard, J., Gur, R.E., Gur, R.C., 2012. Development of Abbreviated Nine-Item Forms of the Raven's Standard Progressive Matrices Test. Assessment 19, 354–369. doi:10.1177/1073191112446655

Estle, S.J., Green, L., Myerson, J., Holt, D.D., 2006. Differential effects of amount on temporal and probability discounting of gains and losses. Mem. Cogn. 34, 914–928. doi:10.3758/BF03193437

Friston, K.J., Williams, S., Howard, R., Frackowiak, R.S.J., Turner, R., 1996. Movement-related effects in fMRI time-series. Magn. Reson. Med. 35, 346–355. doi:10.1002/mrm.1910350312

Glass, L., 1969. Moiré effect from random dots. Nature 223, 578–580. doi:10.1038/223578a0

Glasser, M.F., Sotiropoulos, S.N., Wilson, J.A., Coalson, T.S., Fischl, B., Andersson, J.L., Xu, J., Jbabdi, S., Webster, M., Polimeni, J.R., Van Essen, D.C., Jenkinson, M., 2013. The minimal preprocessing pipelines for the Human Connectome Project. Neuroimage 80, 105–124. doi:10.1016/j.neuroimage.2013.04.127

Gordon, E.M., Laumann, T.O., Adeyemo, B., Huckins, J.F., Kelley, W.M., Petersen, S.E., 2016. Generation and Evaluation of a Cortical Area Parcellation from Resting-State Correlations. Cereb. Cortex 26, 288–303. doi:10.1093/cercor/bhu239

Gordon, E.M., Laumann, T.O., Gilmore, A.W., Newbold, D.J., Greene, D.J., Berg, J.J., Ortega, M., Hoyt-Drazen, C., Gratton, C., Sun, H., Hampton, J.M., Coalson, R.S., Nguyen, A.L., McDermott, K.B., Shimony, J.S., Snyder, A.Z., Schlaggar, B.L., Petersen, S.E., Nelson, S.M., Dosenbach, N.U.F., 2017. Precision Functional Mapping of Individual Human Brains. Neuron 95, 791–807.e7. doi:10.1016/j.neuron.2017.07.011

Gordon, E.M., Laumann, T.O., Gilmore, A.W., Petersen, S.E., Nelson, S.M., Dosenbach, N.U.F., Gordon, E.M., Laumann, T.O., Gilmore, A.W., Newbold, D.J., Greene, D.J., 2017. Precision Functional Mapping of Individual Human NeuroResource Precision Functional Mapping of Individual Human Brains. Neuron 95, 1–17. doi:10.1016/j.neuron.2017.07.011

Gratton, C., Laumann, T.O., Nielsen, A.N., Greene, D.J., Gordon, E.M., Gilmore, A.W., Nelson, S.M., Coalson, R.S., Snyder, A.Z., Schlaggar, B.L., Dosenbach, N.U.F., Petersen, S.E., 2018. Functional Brain Networks Are Dominated by Stable Group and Individual Factors, Not Cognitive or Daily Variation. Neuron. doi:10.1016/j.neuron.2018.03.035

Gur, R.C., Richard, J., Hughett, P., Calkins, M.E., Macy, L., Bilker, W.B., Brensinger, C., Gur, R.E., 2010. A cognitive neuroscience-based computerized battery for efficient measurement of individual differences: Standardization and initial construct validation. J. Neurosci. Methods 187, 254–262. doi:10.1016/j.jneumeth.2009.11.017

Laumann, T.O., Gordon, E.M., Adeyemo, B., Snyder, A.Z., Joo, S.J., Chen, M.-Y., Gilmore, A.W., McDermott, K.B., Nelson, S.M., Dosenbach, N.U.F., Schlaggar, B.L., Mumford, J.A., Poldrack, R.A., Petersen, S.E., 2015. Functional System and Areal Organization of a Highly Sampled Individual Human Brain. Neuron 1–14. doi:10.1016/j.neuron.2015.06.037

Laumann, T.O., Snyder, A.Z., Mitra, A., Gordon, E.M., Gratton, C., Adeyemo, B., Gilmore, A.W., Nelson, S.M., Berg, J.J., Greene, D.J., McCarthy, J.E., Tagliazucchi, E., Laufs, H., Schlaggar, B.L., Dosenbach, N.U.F., Petersen, S.E., 2016. On the Stability of BOLD fMRI Correlations. Cereb. Cortex 1–14. doi:10.1093/cercor/bhw265

Marcus, D.S., Harms, M.P., Snyder, A.Z., Jenkinson, M., Wilson, J.A., Glasser, M.F., Barch, D.M., Archie, K.A., Burgess, G.C., Ramaratnam, M., Hodge, M., Horton, W., Herrick, R., Olsen, T., McKay, M., House, M., Hileman, M., Reid, E., Harwell, J., Coalson, T., Schindler, J., Elam, J.S., Curtiss, S.W., Van Essen, D.C., 2013. Human Connectome Project informatics: Quality control, database services, and data visualization. Neuroimage 80, 202–219. doi:10.1016/j.neuroimage.2013.05.077

Miezin, F.M., Maccotta, L., Ollinger, J.M., Petersen, S.E., Buckner, R.L., 2000. Characterizing the hemodynamic response: Effects of presentation rate, sampling procedure, and the possibility of ordering brain activity based on relative timing. Neuroimage 11, 735–759. doi:10.1006/nimg.2000.0568

Myerson, J., Green, L., Warusawitharana, M., 2001. Area under the curve as a measure of discounting. J. Exp. Anal. Behav. 76, 235–243. doi:10.1901/jeab.2001.76-235

Ojemann, J.G., Akbudak, E., Snyder, A.Z., McKinstry, R.C., Raichle, M.E., Conturo, T.E., 1997. Anatomic localization and quantitative analysis of gradient refocused echo-planar fMRI susceptibility artifacts. Neuroimage 6, 156–167. doi:10.1006/nimg.1997.0289

Petersen, S.E., Dubis, J.W., 2012. The mixed block/event-related design. Neuroimage. doi:10.1016/j.neuroimage.2011.09.084

Poldrack, R.A., Laumann, T.O., Koyejo, O., Gregory, B., Hover, A., Chen, M.Y., Gorgolewski, K.J., Luci, J., Joo, S.J., Boyd, R.L., Hunicke-Smith, S., Simpson, Z.B., Caven, T., Sochat, V., Shine, J.M., Gordon, E., Snyder, A.Z., Adeyemo, B., Petersen, S.E., Glahn, D.C., Mckay, D.R., Curran, J.E., Göring, H.H.H., Carless, M.A., Blangero, J., Dougherty, R., Leemans, A., Handwerker, D.A., Frick, L., Marcotte, E.M., Mumford, J.A., 2015. Long-term neural and physiological phenotyping of a single human. Nat. Commun. 6. doi:10.1038/ncomms9885

Power, J., Schlaggar, B., Lessov-Schlaggar, C., Petersen, S., 2013. Evidence for hubs in human functional brain networks. Neuron 79, 798–813. doi:10.1016/j.neuron.2013.07.035

Power, J.D., Barnes, K.A., Snyder, A.Z., Schlaggar, B.L., Petersen, S.E., 2012. Spurious but systematic correlations in functional connectivity MRI networks arise from subject motion. Neuroimage 59, 2142–2154. doi:10.1016/j.neuroimage.2011.10.018

Power, J.D., Mitra, A., Laumann, T.O., Snyder, A.Z., Schlaggar, B.L., Petersen, S.E., 2014. Methods to detect, characterize, and remove motion artifact in resting state fMRI. Neuroimage 84, 320–341. doi:10.1016/j.neuroimage.2013.08.048

Rubinov, M., Sporns, O., 2010. Complex network measures of brain connectivity: Uses and interpretations. Neuroimage 52, 1059–1069. doi:10.1016/j.neuroimage.2009.10.003

Satterthwaite, T.D., Elliott, M.A., Gerraty, R.T., Ruparel, K., Loughead, J., Calkins, M.E., Eickhoff, S.B., Hakonarson, H., Gur, R.C., Gur, R.E., Wolf, D.H., 2013. An improved framework for confound regression and filtering for control of motion artifact in the preprocessing of resting-state functional connectivity data. Neuroimage 64, 240–256. doi:10.1016/j.neuroimage.2012.08.052

Siegel, J.S., Mitra, A., Laumann, T.O., Seitzman, B.A., Raichle, M., Corbetta, M., Snyder, A.Z., 2017. Data quality influences observed links between functional connectivity and behavior. Cereb. Cortex 27, 4492–4502. doi:10.1093/cercor/bhw253

Smith, S.M., Jenkinson, M., Woolrich, M.W., Beckmann, C.F., Behrens, T.E.J., Johansen-Berg, H., Bannister, P.R., De Luca, M., Drobnjak, I., Flitney, D.E., Niazy, R.K., Saunders, J., Vickers, J., Zhang, Y., De Stefano, N., Brady, J.M., Matthews, P.M., 2004. Advances in functional and structural MR image analysis and implementation as FSL, in: NeuroImage. doi:10.1016/j.neuroimage.2004.07.051

Tabachnick, B.G., Fidell, L.S., 2007. Using Multivariate Statistics, 5th ed. Allyn and Bacon, Boston, MA.

Van Essen, D.C., Ugurbil, K., Auerbach, E., Barch, D., Behrens, T.E.J., Bucholz, R., Chang, A., Chen, L., Corbetta, M., Curtiss, S.W., Della Penna, S., Feinberg, D., Glasser, M.F., Harel, N., Heath, A.C., Larson-Prior, L., Marcus, D., Michalareas, G., Moeller, S., Oostenveld, R., Petersen, S.E., Prior, F., Schlaggar, B.L., Smith, S.M., Snyder, A.Z., Xu, J., Yacoub, E., 2012. The Human Connectome Project: A data acquisition perspective. Neuroimage 62, 2222–2231. doi:10.1016/j.neuroimage.2012.02.018

Weintraub, S., Dikmen, S.S., Heaton, R.K., Tulsky, D.S., Zelazo, P.D., Bauer, P.J., Carlozzi, N.E., Slotkin, J., Blitz, D., Wallner-Allen, K., Fox, N.A., Beaumont, J.L., Mungas, D., Nowinski, C.J., Richler, J., Deocampo, J.A., Anderson, J.E., Manly, J.J., Borosh, B., Havlik, R., Conway, K., Edwards, E., Freund, L., King, J.W., Moy, C., Witt, E., Gershon, R.C., 2013. Cognition assessment using the NIH Toolbox. Neurology 80, S54–S64. doi:10.1212/WNL.0b013e3182872ded

Chapter 4: Heritability of individual variant sub-groups in functional brain networks

Many recent research efforts have focused on uncovering individual differences in functional brain networks measured with fMRI data. We have recently demonstrated the presence of stable localized regions of the brain where individuals differ from the typical group-average network organization – regions we call network variants. Evidence suggests that network variants are systematically organized; they appear in characteristic regions of the brain and tend to associate with particular functional networks. Moreover, the distribution of network variants across individuals clusters into at least two distinct sub-groups in multiple datasets. Given these trait-like properties, here we investigated the heritability of network variants. We exploited the familial design of the Human Connectome Project, analyzing resting-state fMRI data from monozygotic (85 pairs) and dizygotic twins (46 pairs), non-twin siblings (64 pairs), and unrelated individuals (N = 362). As has been described previously, overall network structure showed significant heritability. Interestingly, network variant sub-groups also showed significant heritability (h^2 = 47%): monozygotic twin pairs were significantly more likely to be in the same sub-group (determined via network variant distributions) than any other relationship pairing. This may suggest that some network structure heritability derives from common patterns of individual differences. Overall, our results suggest that network variant sub-types may be partially affected by genetic influences. In addition, the results point to unique environmental contributions to distributions of network variants.

4.1 Introduction

The study of the relationship between genes and behavior is known as the field of Behavior Genetics. Insights from Behavior Genetics have resulted in the proposal of three laws (Turkheimer, 2000): (1) all human behavioral traits are heritable; (2) the effect of being raised in the same family is smaller than the effect of genes; and, (3) a substantial portion of the variation in complex human behavioral traits is not accounted for by the effects of genes or families. More recently, a fourth law was proposed (Chabris et al., 2015): (4) a typical human behavioral trait is associated with very many genetic variants, each of which accounts for a very small percentage of the behavioral variability.

To illustrate these laws, consider the example of head motion inside of an MRI scanner. Some have argued that there is a "head motion phenotype" (Couvy-Duchesne et al., 2014; Zeng et al., 2014). If so, then the four laws suggest that we should observe that: (1) head motion inside of an MRI scanner is heritable; (2) individuals in the same family have similar head motion; (3) a substantial amount of variance in head motion is unexplained by (1) and (2); and, (4) head motion is related to a large number of genes, with each explaining a small amount of variance.

In support of the "head motion phenotype," previous work has shown that head motion is heritable (Couvy-Duchesne et al., 2014; Engelhardt et al., 2017). This conclusion is impactful because head motion has been revealed to be a major issue for functional connectivity analyses (studying correlations in spontaneous resting-state fMRI signals between brain regions) (Power et al., 2012; Satterthwaite et al., 2012; van Dijk et al., 2012). Since head motion causes systematic changes in functional connectivity patterns (Burgess et al., 2016; Power et al., 2018,

2017, 2014, 2012), two groups of individuals will appear to differ in functional connectivity if they differ systematically in head motion (e.g., children versus adults, patients versus controls).

The prevailing argument is that head motion-related changes in functional connectivity are artifactual, and, thus, head motion must be addressed by preprocessing fMRI data adequately (Ciric et al., 2017; Power et al., 2014). However, if there is a true "head motion phenotype," then removing head motion-related patterns from functional connectivity may be incorrectly distorting true differences (e.g., between groups of children and adults) (Couvy-Duchesne et al., 2016). Alternatively, head motion may appear heritable for other reasons (e.g., factors known to affect head motion estimates may be heritable, rather than head motion itself) (Hodgson et al., 2017; Siegel et al., 2017). It is important to resolve this issue for those interested in functional connectivity analyses, especially with regards to estimating the heritability of functional connectivity.

Previous studies have observed that functional connectivity is heritable (Adhikari et al., 2018; Colclough et al., 2017; Elliott et al., 2019; Fornito et al., 2011; Fu et al., 2015; Ge et al., 2017; Glahn et al., 2010; Yang et al., 2016). The extent to which these heritability estimates are affected by head motion is unknown. It is reasonable to hypothesize that artifactual head-motion related patterns of functional connectivity would inflate estimates of functional connectivity heritability. Moreover, the heritability of individual differences in functional connectivity is another open question of interest. There have been recent advances in our understanding of individual differences in functional connectivity (Bijsterbosch et al., 2018; Braga and Buckner,

2017; Finn et al., 2015; Evan M Gordon et al., 2017; Evan M. Gordon et al., 2017a, 2017b; Kong et al., 2018; Laumann et al., 2015; Mueller et al., 2013; Wang et al., 2015).

Work from Seitzman and colleagues has demonstrated that punctate regions of individual difference, called network variants, have intriguing properties, including stability over time within individuals, characteristic locations of occurrence and idiosyncratic network assignment to higher-level association networks, task activations consistent with the function of their idiosyncratic network, and systematic organization across individuals. The systematicity of network variants allows for the identification of sub-groups of individuals (with similar distributions of network variants) who differ on neuropsychological measures of behavior (see Chapter 3). The authors conclude that distributions of network variants seem to be trait-like, with functionally relevant patterning across individuals. If network variant properties prove to be heritable, then their trait-like status will be supported further.

The present study investigated the heritability of functional connectivity and network variant properties, including locations of occurrence in cortex and their patterning across individuals. Additionally, motion-related functional connectivity differences were compared within the same individuals and between groups of individuals with differing amounts of head motion in order to examine the possibility of a head motion phenotype. Data from 752 individuals from the Human Connectome Project were used to address these questions.

4.2 Material and Methods

Data from the Human Connectome Project (HCP) 1200 Subject release were analyzed in this manuscript (Van Essen et al., 2012b). The HCP dataset is appropriate for the study of network variant heritability because of its extended twin-family design (Posthuma et al., 2000) and the relatively large amount of resting-state fMRI data collected from each subject (i.e., a sufficient amount for network variant analyses) (see Chapter 3). However, there are previously described issues with the resting-state fMRI data that prevent investigation of certain questions (e.g., network variants in the subcortex- see SI Figure 2.5 in Chapter 2).

4.2.1 Data acquisition and subjects

Data acquisition parameters have been described in detail previously (Van Essen et al., 2012b). Briefly, high-resolution T1-weighted (MP-RAGE) and BOLD contrast sensitive images (multiband gradient-echo planar imaging) were acquired on a custom 3T Siemens Skyra with a custom 32-channel head matrix coil. Novel scanning sequences were designed to enhance the spatial and temporal resolution of the data. Thus, the T1-weighted and BOLD images were sampled at 0.7 and 2.0 mm^3 isotropic voxels, respectively. A multiband factor of 8 was implemented to reduce the TR of the BOLD data to 0.72s (TE=33ms). A total of 1 hour of eyes-open resting-state BOLD data was collected from each subject. Four separate 15-minute runs were acquired per subject over two consecutive days. On each day, there was one left-to-right (LR) phase encoding scan and one right-to-left (RL) phase encoding scan. This LR-RL phase encoding scheme was implemented (instead of tradition anterior-to-posterior phase encoding) in order to enhance signal-to-noise in ventromedial prefrontal cortex, a typical susceptibility region (Glasser et al., 2013).

The HCP dataset is composed of monozygotic and dizygotic twin-pairs and their non-twin siblings. Reliable identification of network variants requires more than 40 minutes of resting-state data; therefore, individuals with less than 45 minutes of high-quality (low-motion) resting-state data were excluded. Thus, data from 752 individuals were analyzed: 85 pairs of monozygotic twins (N=170), 46 pairs of dizygotic twins (N=92), 64 pairs of non-twin siblings (N=128), and a sample of unrelated individuals (N=362).

4.2.2 Anatomical processing and surface creation

Anatomical processing and surface creation were performed by Glasser and colleagues (Glasser et al., 2013). Briefly, for each subject the T1-weighted image was segmented into a gray matter ribbon enclosed between the pial and white matter surfaces by use of FreeSurfer (Fischl et al., 2002). These delineations were used to create a native cortical surface to which the processed BOLD data are projected.

4.2.3 Functional processing

The HCP provides fully processed resting-state BOLD data, which includes FIX ICA correction for motion-related artifacts (Salimi-Khorshidi et al., 2014) and a multimodal surface matching registration algorithm (Robinson et al., 2014), as an open resource (Glasser et al., 2013). However, Burgess and colleagues (Burgess et al., 2016), Siegel and colleagues (Siegel et al., 2017), as well as Power and colleagues (Power et al., 2018) demonstrated that this pipeline provides insufficient correction for head motion. Thus, the minimally preprocessed BOLD data were further processed following the methodology of Power and colleagues (Power et al., 2014).

These details are described fully in Chapter 3. However, data from both processing pipelines were used for the between-subject functional connectivity analysis (see below).

Briefly, all functional data were concatenated, aligned to the reference image (first frame of the first run), and then normalized to a whole-brain mode of 1000 (Miezin et al., 2000). Slice timing correction was not applied to HCP BOLD data due to the fast TR (Glasser et al., 2013). A one-step spline interpolation was used to align the functional data to the T1-weighted image and to resample to 2 mm^3 isotropic voxels (Smith et al., 2004). Finally, distortion correction was applied using a bias field map. The data were processed further as follows: the data were demeaned and detrended. Then, multi-linear nuisance regression (whole-brain mean, individually defined white matter and CSF signals, the temporal derivatives of each, and 24 movement regressors derived by expansion (Friston et al., 1996), frame censoring (filtered FD threshold of 0.1mm, minimum of 5 contiguous frames, as described in Chapter 3 and Siegel et al., 2017, interpolation over censored frames via least-squares spectral estimation, and a bandpass filter (0.009-0.08Hz) were applied.

Fully processed (but unsmoothed) data were mapped to the native surface (created above) for each individual (Gordon et al., 2016), smoothed via a geodesic Gaussian kernel (FWHM = 4mm, sigma = 1.7), and registered to the Conte69 atlas surface (deformation field computed by a spherical, landmark-based registration of the individual's native surface and the Conte69 atlas surface) (Van Essen et al., 2012a). The resolution of the cortical surface is 32492 vertices per hemisphere. Previously censored frames were removed from the timeseries for all further

analyses. All subcortical and cerebellar data were excluded from all analyses due to the aforementioned issues with SNR (Ji et al., 2019).

4.2.4 Network variant analysis

Network variant locations and functional 're-assignments' were identified as in Chapter 3 for each individual. Briefly, a seedmap was computed at each cortical surface vertex for a given individual, and all individual-specific seedmaps were correlated with the corresponding seedmap from a group-average of healthy adults. Sufficiently large patches of contiguous vertices (more than 50 vertices) located outside of susceptibility regions (mean BOLD signal < 750 (Ojemann et al., 1997)) with sufficiently low correlation to the group-average (lowest decile) were identified as network variants.

The average BOLD timeseries from each variant was correlated with the BOLD timeseries from every cortical surface vertex within an individual. This 'whole variant seedmap' was compared against 14 canonical network templates (Evan M. Gordon et al., 2017a) via Pearson correlation. The full pattern of variant-to-network-template correlations (the mean across all network variants within an individual) was used to classify each individual into *a priori* defined network variant sub-groups. The two large sub-groups described in Chapter 3, i.e. the "default mode" sub-group and the "control and processing" sub-group, were used. Each individual was assigned to the sub-group to which their pattern of variant-to-network-template correlations best matched.

4.2.5 Between-subject functional connectivity comparison

To determine the heritability of functional connectivity between pairs of individuals, a vertex-wise correlation matrix was computed for each individual. The Pearson correlation between

BOLD timeseries from every pair of cortical vertices was calculated, resulting in a 59412x59412 symmetric correlation matrix (vertices from the medial wall were discarded). The matrix for each subject was Fisher-Z transformed, and then matrices from monozygotic twin-pairs (MZ), dizygotic twin-pairs (DZ), non-twin sibling pairs (Sibs), and randomly selected pairs of unrelated individuals were correlated against one another. The mean correlation and standard error within each group (MZ, DZ, Sibs, and unrelated) was calculated.

4.2.6 Within-subject functional connectivity comparison

Some studies have criticized techniques that remove head motion-related artifacts from resting-state fMRI because head motion is heritable. They argue that this explains or is the neurobiological basis for the differences in functional connectivity between low- and high-motion groups. To address these critiques, several groups of HCP subjects were created. Between subject high and low motion groups, paralleling that found in Power et al., 2014 were created. Two within-subject groups were also created. Individuals in the low-low motion group had two consecutive days of low-motion BOLD runs. Individuals in the low-high motion group had one of low-motion BOLD runs and one day of high-motion BOLD runs. This between-, within-subject design allows for direct comparison of the effects of head motion within the same individuals, as compared to differing individuals, directly addressing the heritability of head motion argument. For all comparisons, two sample *t*-tests were used to determine the number of functional connectivity edges that were different between runs ($p < 0.05$ uncorrected) (Power et al., 2014).

4.2.7 Between-subject network variant comparison

To determine the heritability of network variant properties, the maps of network variant locations (binarized as in Chapter 3) were compared between monozygotic twin-pairs (MZ), dizygotic twin-pairs (DZ), non-twin sibling pairs (Sibs), and the same randomly selected pairs of unrelated individuals as above. The dice coefficient was used for this comparison, and the mean and standard error within each group was calculated. Similarly, the proportion of pairs assigned to the same network variant sub-group was compared between MZs, DZs, Sibs, and unrelated individuals.

4.2.8 Statistical analyses

In order to test for significant differences between groups (e.g., MZs versus DZs) for both functional connectivity and network variant locations, two-sample t-tests were computed. To determine the significance of the proportion of pairs assigned to the same sub-group, a permutation test was used. Subject labels within each group (within MZs, within DZs, etc.) were randomly permuted 1000 times, and the proportion of pairs assigned to the same network variant sub-group was assessed. To test for significant between group differences, a tetrachoric correlation was computed by use of the polycor package in R version 3.5.2 (Drasgow, 1986; Olsson, 1979; R Foundation for Statistical Computing., 2018).

4.2.9 Heritability analysis

Formal testing of heritability was performed using Falconer's formula [DS Falconer, 1960] for the functional connectivity and network variant location results. A categorical unbounded ACE model was used to estimate the heritability of network variant sub-groups. The ACE model was implemented in OpenMx (Boker et al., 2011) using R version 3.5.2 (R Foundation for Statistical

Computing., 2018). Model specifics were described previously by Reineberg and colleagues (Reineberg et al., 2018). Falconer's formula estimates heritability as $2*(r_{MZ} - r_{DZ})$, where r_{MZ} is the twin-pair correlation for monozygotic twins and r_{DZ} is the twin-pair correlation for dizygotic twins. Generally, an ACE model estimates narrow-sense heritability (h^2), i.e. heritability due to additive genetics only, whereas Falconer's formula estimates broad-sense heritability (H^2), i.e. heritability due to total genetic variance (Falconer, 1960; Weber, 2008).

4.3 Results

We examined the heritability of network variant properties in order to understand the effects of genetics and shared environmental factors on individual differences in human brain functional organization.

4.3.1 Functional connectivity is weakly heritable

Previous investigations have demonstrated that functional connectivity is moderately heritable, on average, with estimates ranging between 10-80% (**Table 4.1**). Here, we found that resting-state functional connectivity was weakly heritable (H^2 = 15.0 +/- 0.2%) in the included sample of individuals. Similarity of functional connectivity (cortex only) between monozygotic twin-pairs was higher than dizygotic twin-pairs and non-twin siblings, both of which were higher than pairs of unrelated individuals (**Fig 4.1**). While significant, the observed result is smaller than most previously published effects. Furthermore, this finding was affected by differences in processing pipelines, with functional connectivity heritability substantially reduced by the standard HCP processing pipeline in this sample of subjects (H^2 = 10.3 +/- 0.3%). Moreover, the overall correlation between the same pairs of subjects processed with the HCP pipeline was decidedly

lower than when their data were processed with direct motion-related artifact elimination procedures.

Table 4.1: Previous estimates of the heritability of functional connectivity. The table lists a number of previously published studies of the heritability of functional connectivity. Heritability is estimated for a wide variety of measures (e.g., within default mode network connectivity, global efficiency, voxel-wise correlations) and with a diverse range of processing schemes. Estimates range from low (10-15%) to strong (75-80%).

Previous studies of the heritability of functional connectivity					
Journal	**Year**	**First Author**	**Dataset**	**N subjects**	**Heritability Estimate**
NeuroImage	2019	M. L. Elliot	HCP & Dunedin	144 MZ, 85 DZ twin-pairs	20-25%
Human Brain Mapping	2018	B. M. Adhikari	GOBS & HCP	128 MZ, 89 DZ twin-pairs	20-40%
eLife	2017	G. L. Colclough	HCP	103 MZ, 54 DZ twin-pairs	15-18%
PNAS	2017	T. Ge	HCP & GSP	92 MZ, 46 DZ twin-pairs	45-75%
Cerebral Cortex	2016	Z. Yang	5.25min/person	78 MZ, 58 DZ twin-pairs	23-65%
Human Brain Mapping	2015	Y. Fu	12min/person	32 MZ, 24 DZ twin-pairs	10-60%
J Neuroscience	2011	A. Fornito	20min/person	16 MZ, 13 DZ twin-pairs	30-80%
PNAS	2010	D.C. Glahn	GOBS	333 individuals, 29 pedigrees	10-42%

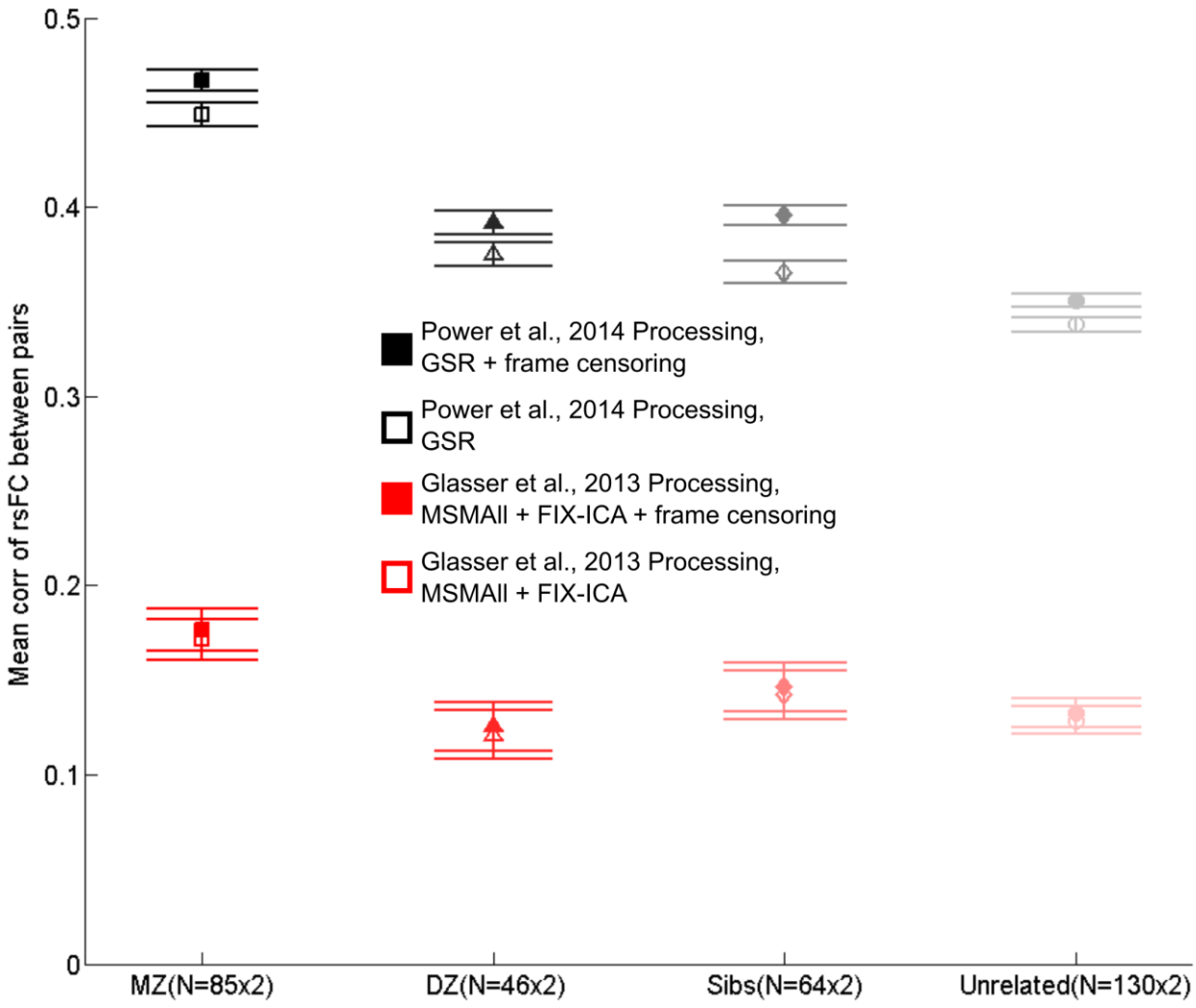

Figure 4.1: Heritability of functional connectivity in the present dataset. The average correlation of cortical functional connectivity between pairs of monozygotic twins was higher than dizygotic twin-pairs, non-twin sibling, and unrelated individuals. The processing pipeline that includes global signal (whole-brain mean) regression and frame censoring resulted in the highest correlations between pairs of individuals, and a heritability estimate of 15%. Exclusion of frame censoring slightly reduced between-subject correlations, and the HCP processing pipeline (MSMAll surface registration and FIX-ICA artifact correction) resulted in extremely small between-subject correlations for all groups, and a substantially reduced estimate of heritability (10%).

The processing pipeline implemented here has been criticized for removing motion-related artifacts because head motion may be heritable and, thus, phenotypically related to specific functional connectivity patterns (Couvy-Duchesne et al., 2014; Zeng et al., 2014). To address this critique, we assessed the similarity of functional connectivity within, as well as between, HCP subjects. Two separate groups of individuals were created on the basis of within-subject head motion during resting-state runs acquired over two consecutive days: individuals with two days of low-motion runs (the low-low group) and individuals with one day of low-motion and one day of high-motion runs (the low-high group).

First, we replicated a result from Power et al., 2014 (**Fig 4.2A**). We observed that between-subject, motion-related functional connectivity differences (i.e., differences between separate groups of individuals with low or high amounts of head motion in their data) were eliminated by the processing pipeline implemented here. Then, we found that within-subject, motion-related functional connectivity differences (i.e., between low-motion and high-motion runs from the same individuals) were more numerous than the between-subject number of differences (**Fig 4.2B**). As a control, we showed that there were minimal within-subject differences for individuals with two low-motion runs.

Both within- and between-subject motion-related differences in functional connectivity were substantially and similarly ameliorated by the processing pipeline implemented here (i.e., inclusion of global signal regression and frame censoring). It appears that the application of these techniques addressed differences in motion between scans, rather than an underlying phenotypic difference between groups.

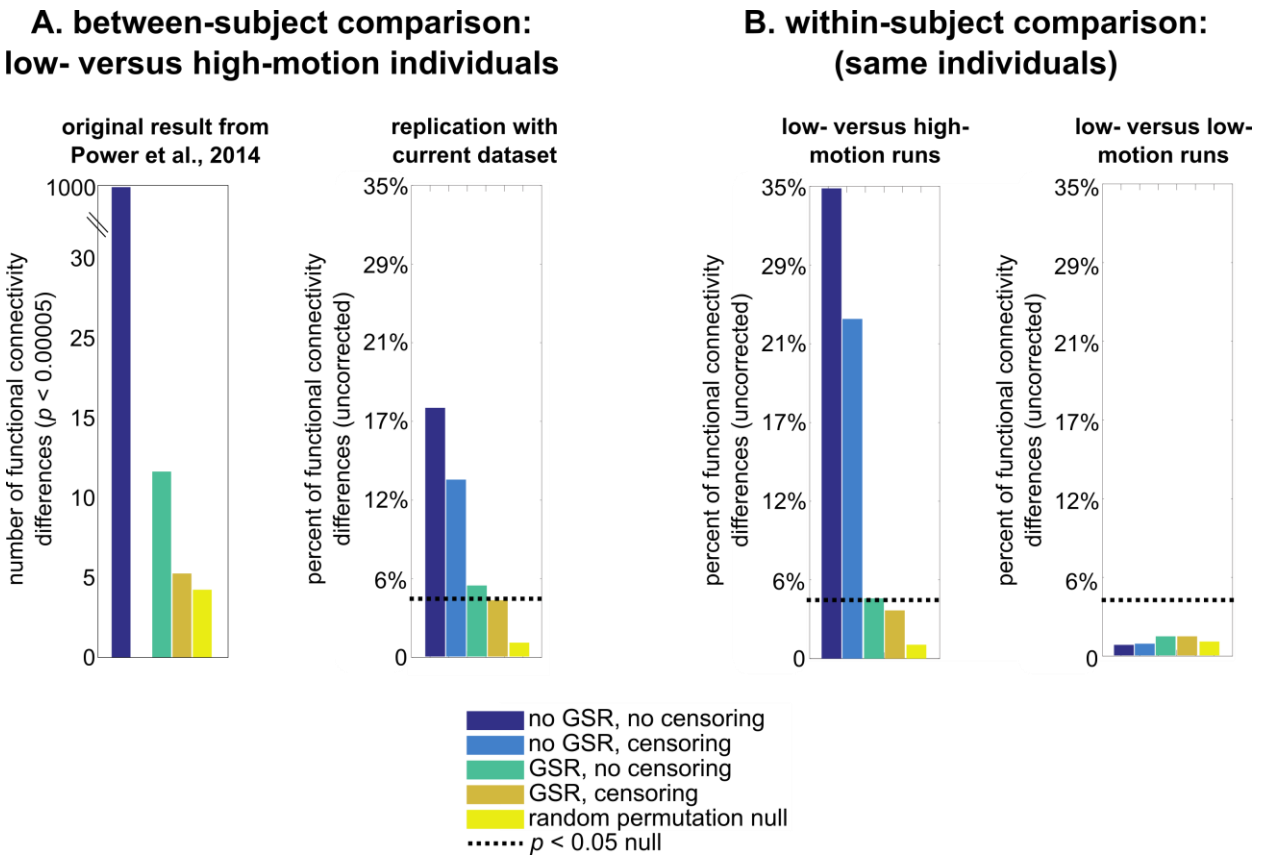

Figure 4.2: Within- and between-subject motion-related functional connectivity differences. Within- and between-subject differences in functional connectivity were assessed via *t*-test between every edge in the correlation matrix. The between-subject comparisons **(A)** include a result previously published by Power et al., 2014 in which a set of low-motion runs are compared against a set of high-motion runs from different individuals. A replication using data from individuals in the HCP dataset is also included. The within-subject comparisons **(B)** use data from the same individuals. The first test compared a set of low-motion runs against a set of high-motion runs from the same individuals (in the low-high motion group). The other within-subject test compared two sets of low-motion runs against one another from the same individuals in the low-low motion group. There were numerous within- and between-subject differences. The use of global signal regression and scrubbing reduced all such differences to chance levels.

4.3.2 Network variant sub-group is heritable, but not location

We observed that the distribution of network variant locations is not heritable (H^2 = 4.2 +/- 0.8%) while network variant sub-group is moderately heritable (h^2 = 47.1 +/- 1.0%; **Fig 4.3 and Table 4.2**). Further, we found that only the true proportion of monozygotic twins in the same sub-group was significantly higher than chance (Z = 2.82, p = 0.002), and the tetrachoric MZ twin-pair correlation (R_{MZ} = 0.51) was more than double that of dizygotic twins (R_{DZ} = 0.10) or non-twin siblings (R_{Sibs} = 0.25). These findings suggest that network variant sub-group heritability is due to additive genetic variance without the influence of environmental factors shared by co-twins.

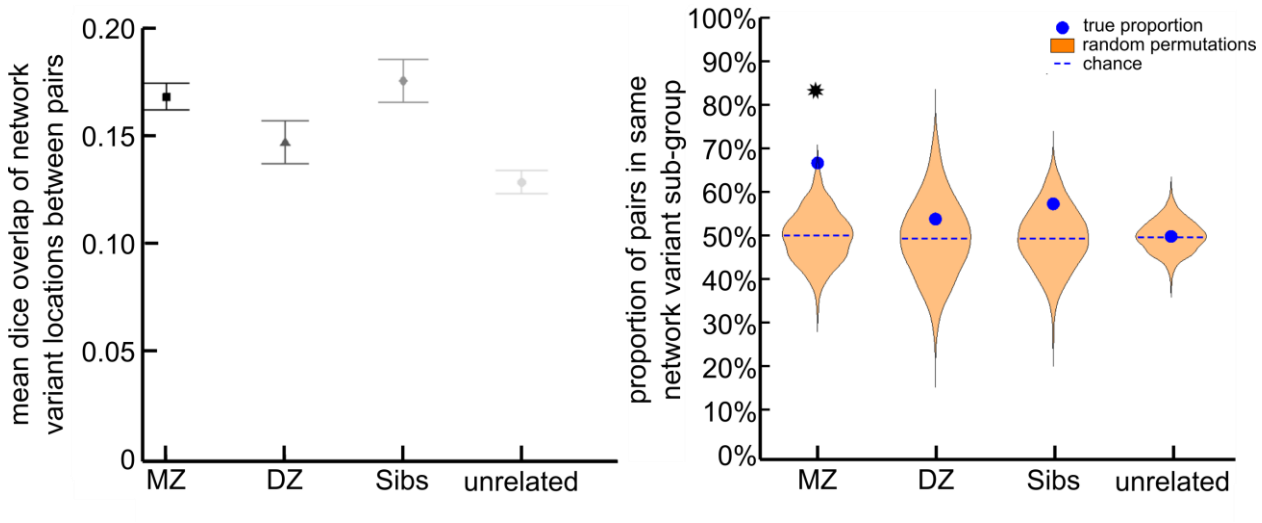

Figure 4.3: Network variant sub-groups are heritable. The similarity of the distribution of network variant locations between pairs of individuals is displayed on the left. The plot on the right shows the proportion of pairs of individuals in the same network variant sub-group. Monozygotic (MZ) twin-pairs are the only group with a significantly higher proportion than expected by chance. To generate a null distribution, 1000 random permutations of subject labels were performed within each group (MZs, DZs, etc.).

Table 4.2: ACE model results. Estimates of variance for additive genetics (A), common/shared environment (C), and unique environment (E) are displayed. Network variant sub-group was estimated to be 47% heritable. The full ACE model was contrasted against AE, CE, and E models. Since results for the AE model are nearly identical to the full ACE model, there appears to be no contribution of common/shared environmental variance to variant sub-groups.

variant sub-group	A	C	E		versus AE model		versus CE model		versus E model	
					df	*p*	df	*p*	df	*p*
ACE model	0.4711	0.0000	0.5289		260	1.0000	260	0.1809	261	**0.0099**
AE model	0.4711		0.5289						261	**0.0024**
CE model		0.3667	0.6333						261	**0.0064**
E model			1.0000							

4.4 Discussion

The present study examined the heritability of functional connectivity and network variant properties, as well as investigated the possibility of a head motion phenotype. Both functional connectivity and network variant sub-group were observed to be heritable, but network variant location was not. The heritability of network variant sub-group appears to be a consequence of additive genetic and unique environmental variance, with little or no influence of shared environmental variance. Furthermore, we observed that the implemented processing pipeline, which includes global signal regression and frame censoring, effectively eliminated both within- and between-subject motion-related differences in functional connectivity. This result suggests that motion-related functional connectivity differences are primarily noise (rather than signal), and thus, there is no evidence to support a head motion phenotype in functional connectivity data.

4.4.1 Heritability estimates depend on processing pipeline

We observed that functional connectivity is weakly heritable (15%), with our estimate substantially reduced (10%) when data from the HCP processing pipeline were used. Both estimates are on the low end of previously published results (which range from 10% to 80% with an average near 40% (Adhikari et al., 2018; Colclough et al., 2017; Elliott et al., 2019; Fornito et al., 2011; Fu et al., 2015; Ge et al., 2017; Glahn et al., 2010; Yang et al., 2016)). There is a clear effect of processing pipeline on heritability estimates, since many of the previously published studies used the same dataset. However, sample size is a confounding variable, as each study included a different number of monozygotic and dizygotic twin-pairs. Here, we tested four different processing strategies on the exact same set of subjects (85 monozygotic and 46

dizygotic twin-pairs). The processing pipeline that included both global signal regression and scrubbing resulted in the highest heritability estimate.

This pipeline has been shown to be extremely effective at dealing with the effects of head motion in resting-state fMRI data (Ciric et al., 2017; Power et al., 2014). It is critically important to remove motion-related effects from the data when estimating heritability because two recent investigations demonstrated that head motion itself (e.g., framewise displacement) is moderately heritable (~40%) (Couvy-Duchesne et al., 2014; Hodgson et al., 2017). Since various pipelines deal with head motion effects to varying degrees (Ciric et al., 2017), it is reasonable to expect that any residual head motion remaining in the data will affect heritability estimates. The wide range of heritability estimates in the literature is likely due to the varied effectiveness of different processing pipelines addressing head motion.

Furthermore, most previous investigations implemented processing strategies that do not fully remove motion-related effects from the data (Ciric et al., 2017), which may explain why our heritability estimate is much smaller than most. However, this does not explain why the HCP processing pipeline results in a reduced estimate, since this pipeline has been shown to be ineffective at removing motion-related effects (Burgess et al., 2016; Ciric et al., 2017; Power et al., 2018). One possibility is that the HCP pipeline introduces additional noise into the functional connectivity data. This additional noise may mask the effect of head motion on heritability and also explain why the average correlation of functional connectivity between pairs of individuals is substantially reduced. Alternative reasons for the reduction in the correlation of functional

connectivity and heritability estimates include the lack of a bandpass filter and smoothing. Disambiguation between these possibilities requires further investigation by future work.

4.4.2 Network variant location is not heritable

We found that the location of network variants is not heritable. In other words, the chance that one twin's distribution of network variant locations matches their co-twin is approximately the same for monozygotic and dizygotic twins.

This result interacts with previous findings from Seitzman and colleagues, who demonstrated that network variant sub-groups could not be found by use of network variant locations (see Chapter 3). One interpretation of these two results is that there is no systematicity to network variant locations in cortex. However, across individuals, network variants tend to occur in association cortex and almost never occur in primary sensorimotor areas. Thus, the specific location of network variants within association cortex may be purely a consequence of an individual's unique experience, with no influences of additive genetics or shared environment. Alternatively, network variants may be randomly distributed within association cortex. Regardless, neither option precludes the possibility that network variants rarely occur in sensorimotor cortex as a consequence of additive genetics and/or shared environment. Future work (likely using animal models) is required to substantiate this latter idea.

If network variant location is not random, but rather a consequence of unique environmental variance, then network variant location may be due to experience-dependent plasticity (Hebb, 1949; Nithianantharajah and Hannan, 2006). In other words, variant locations may arise as a response to environmental demands as an individual navigates life and/or unique biological

experiences that occur during development. However, if this were the case, one would expect to observe an effect of shared environment on variant locations, given that co-twins often share a womb and experience similar environmental demands in the same place at the same time. Therefore, of the options discussed, the most likely is that network variant locations are randomly distributed within association cortex (with a potential genetic and/or developmental restriction keeping network variant away from sensorimotor cortex).

4.4.3 Network variant sub-group is due to additive genetic and unique environmental variance

We observed that monozygotic twins are more likely to be in the same sub-group than dizygotic twins, non-twin siblings, and unrelated individuals. Further, we found these sub-groups to be moderately heritable, with approximately half of the variance in sub-groups explained by additive genetics. Since the remaining variance in sub-group heritability is explained by unique environment (and model error), there appears to be no effect of common/shared environment on network variant sub-groups.

Seitzman and colleagues demonstrated previously that these sub-groups are found via associations between an individual's network variants and canonical functional networks (see Chapter 3). That is, some individuals tend to have variants more strongly associated with the default mode network, primarily, whereas other individuals tend to have variants more strongly associated with control and processing networks (e.g., the frontoparietal, motor, and visual networks). The heritability results presented here suggest that there may be a genetic predisposition for the sub-group phenomenon. Furthermore, since the twin-pair correlation for monozygotic twins is more than double the dizygotic twin-pair correlation, non-additive genetic

variance (e.g., gene-gene interaction effects) may also be a contributor to sub-group heritability. Taken together, it is possible that there is a genetic template for individual differences in functional connectivity such that a specific amount of association cortex is pre-determined to be related to either the default mode network or various control and processing systems.

Since approximately half of the variance in sub-groups is explained by unique environment, it is likely that there is a substantial effect of development on variant functional network associations. Even if some network variants are pre-allocated for associations with either the default mode network or control and processing networks, those relationships may be altered as an individual develops and navigates their environment. Likewise, novel network variants may arise during the course of development and/or in response to environmental challenges. Future studies of the development of network variants with specific attention towards the sub-group phenomenon are crucial.

4.4.4 No evidence for a head motion phenotype

We found that there were substantial motion-related functional connectivity differences when comparing data acquired from low-motion and high-motion runs. It did not matter whether these runs were acquired from the same individuals (within-subject) or from different groups of individuals (between-subject), as there were sizable differences in both cases. However, we observed that the processing pipeline implemented here reduced both within- and between-subject differences to chance levels.

Head motion has a systematic effect on functional connectivity, whereby local correlations are increased and long-range correlations are decreased (Power et al., 2012; Satterthwaite et al.,

2012; van Dijk et al., 2012). Because the effect is systematic, differences in head motion between two groups (e.g., control and patient populations) will lead to spurious differences in functional connectivity. Many have argued that this effect is artifactual and must be removed from the data via appropriate processing strategies (Ciric et al., 2017; Power et al., 2014). However, more recent investigations have suggested that head motion inside of an MRI scanner is heritable, and thus, head motion effects on MRI data is a phenotype (Couvy-Duchesne et al., 2014; Zeng et al., 2014). If so, then motion-related functional connectivity differences should be considered true signal (rather than artifact or noise) and perhaps should not be removed from the data (Couvy-Duchesne et al., 2016).

An alternative explanation for the observed heritability of head motion is that there are heritable factors that causally affect head motion. Body Mass Index (BMI), the ratio of an individual's height and weight, has been shown to be (1) strongly heritable (Allison et al., 1996; Schousboe et al., 2003) and (2) substantially correlated with head motion (Siegel et al., 2017). A recent investigation demonstrated that there are shared genetic factors influencing both BMI and head motion inside of an MRI scanner (Hodgson et al., 2017). If BMI, a bonafide phenotype, is the reason for the apparent heritability of head motion, then it is reasonable to argue that head motion itself is not true signal and, consequently, must be removed from functional connectivity data. Our findings suggest that there is not a strong head motion phenotype, since both within- and between-subject differences in functional connectivity were eliminated by the implemented processing pipeline, which has been shown to address head motion adequately(Ciric et al., 2017; Power et al., 2014).

4.5 Conclusion

We investigated the heritability of functional connectivity broadly and of properties related to network variants (e.g., location). Further, we examined within- and between-subject differences in functional connectivity attributable to motion-related artifacts in order to assess the possibility of a head motion phenotype that affects fcMRI signals. We observed that functional connectivity is weakly heritable, network variant location is not heritable, and network variant sub-group is moderately heritable. Network variant sub-group appeared to be due to additive genetic variance and unique environmental variance, with no influence of shared environment. Finally, we found that heritability estimates were affected by differences in processing pipelines, and we observed no evidence for a head motion phenotype.

4.6 Chapter 4 References

Adhikari, B.M., Jahanshad, N., Shukla, D., Glahn, D.C., Blangero, J., Fox, P.T., Reynolds, R.C., Cox, R.W., Fieremans, E., Veraart, J., Novikov, D.S., Nichols, T.E., Hong, L.E., Thompson, P.M., Kochunov, P., 2018. Comparison of heritability estimates on resting state fMRI connectivity phenotypes using the ENIGMA analysis pipeline. Hum. Brain Mapp. 39, 4893–4902. doi:10.1002/hbm.24331

Allison, D.B., Kaprio, J., Korkeila, M., Koskenvuo, M., Neale, M.C., Hayakawa, K., 1996. The heritability of body mass index among an international sample of monozygotic twins reared apart. Int. J. Obes. Relat. Metab. Disord. 20, 501–6.

Bijsterbosch, J.D., Woolrich, M.W., Glasser, M.F., Robinson, E.C., Beckmann, C.F., Van Essen, D.C., Harrison, S.J., Smith, S.M., 2018. The relationship between spatial configuration and functional connectivity of brain regions. Elife 7. doi:10.7554/eLife.32992

Boker, S., Neale, M., Maes, H., Wilde, M., Spiegel, M., Brick, T., Spies, J., Estabrook, R., Kenny, S., Bates, T., Mehta, P., Fox, J., 2011. OpenMx: An Open Source Extended Structural Equation Modeling Framework. Psychometrika 76, 306–317. doi:10.1007/s11336-010-9200-6

Braga, R.M., Buckner, R.L., 2017. Parallel Interdigitated Distributed Networks within the Individual Estimated by Intrinsic Functional Connectivity. Neuron 95, 457–471.e5. doi:10.1016/j.neuron.2017.06.038

Burgess, G.C., Kandala, S., Nolan, D., Laumann, T.O., Power, J.D., Adeyemo, B., Harms, M.P., Petersen, S.E., Barch, D.M., 2016. Evaluation of Denoising Strategies to Address Motion-Correlated Artifacts in Resting-State Functional Magnetic Resonance Imaging Data from the Human Connectome Project. Brain Connect. 6, 669–680. doi:10.1089/brain.2016.0435

Chabris, C.F., Lee, J.J., Cesarini, D., Benjamin, D.J., Laibson, D.I., 2015. The Fourth Law of Behavior Genetics. Curr. Dir. Psychol. Sci. 24, 304–312. doi:10.1177/0963721415580430

Ciric, R., Wolf, D.H., Power, J.D., Roalf, D.R., Baum, G., Ruparel, K., Shinohara, R.T., Elliott, M.A., Eickhoff, S.B., Davatzikos, C., Gur, R.C., Gur, R.E., Bassett, D.S., Satterthwaite, T.D., 2017. Benchmarking confound regression strategies for the control of motion artifact in studies of functional connectivity. Neuroimage 154, 174–187. doi:10.1016/j.neuroimage.2017.03.020

Colclough, G.L., Smith, S.M., Nichols, T.E., Winkler, A.M., Sotiropoulos, S.N., Glasser, M.F., Van Essen, D.C., Woolrich, M.W., 2017. The heritability of multi-modal connectivity in human brain activity. Elife 6. doi:10.7554/eLife.20178

Couvy-Duchesne, B., Blokland, G.A.M., Hickie, I.B., Thompson, P.M., Martin, N.G., de Zubicaray, G.I., McMahon, K.L., Wright, M.J., 2014. Heritability of head motion during resting state functional MRI in 462 healthy twins. Neuroimage 102, 424–434. doi:10.1016/j.neuroimage.2014.08.010

Couvy-Duchesne, B., Ebejer, J.L., Gillespie, N.A., Duffy, D.L., Hickie, I.B., Thompson, P.M., Martin, N.G., De Zubicaray, G.I., McMahon, K.L., Medland, S.E., Wright, M.J., 2016. Head motion and Inattention/Hyperactivity share common genetic influences: Implications for fMRI studies of ADHD. PLoS One 11. doi:10.1371/journal.pone.0146271

Drasgow, F., 1986. Polychoric and polyserial correlations. Encycl. Stat. Vol. 7.

Elliott, M.L., Knodt, A.R., Cooke, M., Kim, M.J., Melzer, T.R., Keenan, R., Ireland, D., Ramrakha, S., Poulton, R., Caspi, A., Moffitt, T.E., Hariri, A.R., 2019. General functional connectivity: Shared features of resting-state and task fMRI drive reliable and heritable individual differences in functional brain networks. Neuroimage 189, 516–532. doi:10.1016/j.neuroimage.2019.01.068

Engelhardt, L.E., Roe, M.A., Juranek, J., DeMaster, D., Harden, K.P., Tucker-Drob, E.M., Church, J.A., 2017. Children's head motion during fMRI tasks is heritable and stable over time. Dev. Cogn. Neurosci. 25, 58–68. doi:10.1016/j.dcn.2017.01.011

Falconer, D.S., 1960. Introduction to Quantitative Genetics. Oliver and Boyd, Edinburgh and London. Biom. Z. doi:10.1002/bimj.19620040211

Finn, E.S., Shen, X., Scheinost, D., Rosenberg, M.D., Huang, J., Chun, M.M., Papademetris, X., Constable, R.T., 2015. Functional connectome fingerprinting: Identifying individuals using patterns of brain connectivity. Nat. Neurosci. 18, 1664–1671. doi:10.1038/nn.4135

Fischl, B., Salat, D.H., Busa, E., Albert, M., Dieterich, M., Haselgrove, C., Van Der Kouwe, A., Killiany, R., Kennedy, D., Klaveness, S., Montillo, A., Makris, N., Rosen, B., Dale, A.M., 2002. Whole brain segmentation: Automated labeling of neuroanatomical structures in the human brain. Neuron 33, 341–355. doi:10.1016/S0896-6273(02)00569-X

Fornito, A., Zalesky, A., Bassett, D.S., Meunier, D., Ellison-Wright, I., Yucel, M., Wood, S.J., Shaw, K., O'Connor, J., Nertney, D., Mowry, B.J., Pantelis, C., Bullmore, E.T., 2011. Genetic Influences on Cost-Efficient Organization of Human Cortical Functional Networks. J. Neurosci. 31, 3261–3270. doi:10.1523/jneurosci.4858-10.2011

Friston, K.J., Williams, S., Howard, R., Frackowiak, R.S.J., Turner, R., 1996. Movement-related effects in fMRI time-series. Magn. Reson. Med. 35, 346–355. doi:10.1002/mrm.1910350312

Fu, Y., Ma, Z., Hamilton, C., Liang, Z., Hou, X., Ma, X., Hu, X., He, Q., Deng, W., Wang, Y., Zhao, L., Meng, H., Li, T., Zhang, N., 2015. Genetic influences on resting-state functional networks: A twin study. Hum. Brain Mapp. 36, 3959–3972. doi:10.1002/hbm.22890

Ge, T., Holmes, A.J., Buckner, R.L., Smoller, J.W., Sabuncu, M.R., 2017. Heritability analysis with repeat measurements and its application to resting-state functional connectivity. Proc. Natl. Acad. Sci. 114, 5521–5526. doi:10.1073/pnas.1700765114

Glahn, D.C., Winkler, A.M., Kochunov, P., Almasy, L., Duggirala, R., Carless, M.A., Curran, J.C., Olvera, R.L., Laird, A.R., Smith, S.M., Beckmann, C.F., Fox, P.T., Blangero, J., 2010. Genetic control over the resting brain. Proc. Natl. Acad. Sci. 107, 1223–1228. doi:10.1073/pnas.0909969107

Glasser, M.F., Sotiropoulos, S.N., Wilson, J.A., Coalson, T.S., Fischl, B., Andersson, J.L., Xu, J., Jbabdi, S., Webster, M., Polimeni, J.R., Van Essen, D.C., Jenkinson, M., 2013. The minimal preprocessing pipelines for the Human Connectome Project. Neuroimage 80, 105–124. doi:10.1016/j.neuroimage.2013.04.127

Gordon, E.M., Laumann, T.O., Adeyemo, B., Gilmore, A.W., Nelson, S.M., Dosenbach, N.U.F., Petersen, S.E., 2017a. Individual-specific features of brain systems identified with resting state functional correlations. Neuroimage 146, 918–939. doi:10.1016/j.neuroimage.2016.08.032

Gordon, E.M., Laumann, T.O., Adeyemo, B., Huckins, J.F., Kelley, W.M., Petersen, S.E., 2016. Generation and Evaluation of a Cortical Area Parcellation from Resting-State Correlations. Cereb. Cortex 26, 288–303. doi:10.1093/cercor/bhu239

Gordon, E.M., Laumann, T.O., Adeyemo, B., Petersen, S.E., 2017b. Individual Variability of the System-Level Organization of the Human Brain. Cereb. Cortex 27, 386–399. doi:10.1093/cercor/bhv239

Gordon, E.M., Laumann, T.O., Gilmore, A.W., Petersen, S.E., Nelson, S.M., Dosenbach, N.U.F., Gordon, E.M., Laumann, T.O., Gilmore, A.W., Newbold, D.J., Greene, D.J., 2017. Precision Functional Mapping of Individual Human NeuroResource Precision Functional Mapping of Individual Human Brains. Neuron 95, 1–17. doi:10.1016/j.neuron.2017.07.011

Hebb, D.O., 1949. The Organization of Behavior: A Neuropsychological Theory, The Organization of Behavior. doi:10.2307/1418888

Hodgson, K., Poldrack, R.A., Curran, J.E., Knowles, E.E., Mathias, S., Göring, H.H.H., Yao, N., Olvera, R.L., Fox, P.T., Almasy, L., Duggirala, R., Barch, D.M., Blangero, J., Glahn, D.C., 2017. Shared Genetic Factors Influence Head Motion During MRI and Body Mass Index. Cereb. Cortex 27, 5539–5546. doi:10.1093/cercor/bhw321

Ji, J.L., Spronk, M., Kulkarni, K., Repovš, G., Anticevic, A., Cole, M.W., 2019. Mapping the human brain's cortical-subcortical functional network organization. Neuroimage 185, 35–57. doi:10.1016/j.neuroimage.2018.10.006

Kong, R., Li, J., Orban, C., Sabuncu, M.R., Liu, H., Schaefer, A., Sun, N., Zuo, X.-N., Holmes, A.J., Eickhoff, S.B., Yeo, B.T.T., 2018. Spatial Topography of Individual-Specific Cortical Networks Predicts Human Cognition, Personality, and Emotion. Cereb. Cortex. doi:10.1093/cercor/bhy123

Laumann, T.O., Gordon, E.M., Adeyemo, B., Snyder, A.Z., Joo, S.J., Chen, M.-Y., Gilmore, A.W., McDermott, K.B., Nelson, S.M., Dosenbach, N.U.F., Schlaggar, B.L., Mumford, J.A., Poldrack, R.A., Petersen, S.E., 2015. Functional System and Areal Organization of a Highly Sampled Individual Human Brain. Neuron 1–14. doi:10.1016/j.neuron.2015.06.037

Miezin, F.M., Maccotta, L., Ollinger, J.M., Petersen, S.E., Buckner, R.L., 2000. Characterizing the hemodynamic response: Effects of presentation rate, sampling procedure, and the possibility of ordering brain activity based on relative timing. Neuroimage 11, 735–759. doi:10.1006/nimg.2000.0568

Mueller, S., Wang, D., Fox, M.D., Yeo, B.T.T., Sepulcre, J., Sabuncu, M.R., Shafee, R., Lu, J., Liu, H., 2013. Individual Variability in Functional Connectivity Architecture of the Human Brain. Neuron 77, 586–595. doi:10.1016/j.neuron.2012.12.028

Nithianantharajah, J., Hannan, A.J., 2006. Enriched environments, experience-dependent plasticity and disorders of the nervous system. Nat. Rev. Neurosci. doi:10.1038/nrn1970

Ojemann, J.G., Akbudak, E., Snyder, A.Z., McKinstry, R.C., Raichle, M.E., Conturo, T.E., 1997. Anatomic localization and quantitative analysis of gradient refocused echo-planar fMRI susceptibility artifacts. Neuroimage 6, 156–167. doi:10.1006/nimg.1997.0289

Olsson, U., 1979. Maximum likelihood estimation of the polychoric correlation coefficient. Psychometrika 44, 443–460. doi:10.1007/BF02296207

Posthuma, D., De Geus, E.J.C., Neale, M.C., Hulshoff Pol, H.E., Baaré, W.E.C., Kahn, R.S., Boomsma, D., 2000. Multivariate genetic analysis of brain structure in an extended twin design. Behav. Genet. 30, 311–319. doi:10.1023/A:1026501501434

Power, J.D., Barnes, K.A., Snyder, A.Z., Schlaggar, B.L., Petersen, S.E., 2012. Spurious but systematic correlations in functional connectivity MRI networks arise from subject motion. Neuroimage 59, 2142–2154. doi:10.1016/j.neuroimage.2011.10.018

Power, J.D., Mitra, A., Laumann, T.O., Snyder, A.Z., Schlaggar, B.L., Petersen, S.E., 2014. Methods to detect, characterize, and remove motion artifact in resting state fMRI. Neuroimage 84, 320–341. doi:10.1016/j.neuroimage.2013.08.048

Power, J.D., Plitt, M., Gotts, S.J., Kundu, P., Voon, V., Bandettini, P.A., Martin, A., 2018. Ridding fMRI data of motion-related influences: Removal of signals with distinct spatial and physical bases in multiecho data. Proc. Natl. Acad. Sci. 201720985. doi:10.1073/pnas.1720985115

Power, J.D., Plitt, M., Laumann, T.O., Martin, A., 2017. Sources and implications of whole-brain fMRI signals in humans. Neuroimage 146, 609–625. doi:10.1016/j.neuroimage.2016.09.038

R Foundation for Statistical Computing., 2018. R: a Language and Environment for Statistical Computing., http://www.R-project.org/.

Reineberg, A.E., Hatoum, A.S., Hewitt, J.K., Banich, M.T., Friedman, N.P., 2018. Genetic and environmental influence on the human functional connectome. bioRxiv 277996. doi:10.1101/277996

Robinson, E.C., Jbabdi, S., Glasser, M.F., Andersson, J., Burgess, G.C., Harms, M.P., Smith, S.M., Van Essen, D.C., Jenkinson, M., 2014. MSM: A new flexible framework for multimodal surface matching. Neuroimage 100, 414–426. doi:10.1016/j.neuroimage.2014.05.069

Salimi-Khorshidi, G., Douaud, G., Beckmann, C.F., Glasser, M.F., Griffanti, L., Smith, S.M., 2014. Automatic denoising of functional MRI data: Combining independent component analysis and hierarchical fusion of classifiers. Neuroimage 90, 449–468. doi:10.1016/j.neuroimage.2013.11.046

Satterthwaite, T.D., Wolf, D.H., Loughead, J., Ruparel, K., Elliott, M.A., Hakonarson, H., Gur, R.C., Gur, R.E., 2012. Impact of in-scanner head motion on multiple measures of functional connectivity: Relevance for studies of neurodevelopment in youth. Neuroimage 60, 623–632. doi:10.1016/j.neuroimage.2011.12.063

Schousboe, K., Willemsen, G., Kyvik, K.O., Mortensen, J., Boomsma, D.I., Cornes, B.K., Davis, C.J., Fagnani, C., Hjelmborg, J., Kaprio, J., De Lange, M., Luciano, M., Martin, N.G., Pedersen, N., Pietiläinen, K.H., Rissanen, A., Saarni, S., Sørensen, T.I.A., Van Baal, G.C.M., Harris, J.R., 2003. Sex Differences in Heritability of BMI: A Comparative Study of Results from Twin Studies in Eight Countries. Twin Res. 6, 409–421. doi:10.1375/136905203770326411

Siegel, J.S., Mitra, A., Laumann, T.O., Seitzman, B.A., Raichle, M., Corbetta, M., Snyder, A.Z., 2017. Data quality influences observed links between functional connectivity and behavior. Cereb. Cortex 27, 4492–4502. doi:10.1093/cercor/bhw253

Smith, S.M., Jenkinson, M., Woolrich, M.W., Beckmann, C.F., Behrens, T.E.J., Johansen-Berg, H., Bannister, P.R., De Luca, M., Drobnjak, I., Flitney, D.E., Niazy, R.K., Saunders, J., Vickers, J., Zhang, Y., De Stefano, N., Brady, J.M., Matthews, P.M., 2004. Advances in functional and structural MR image analysis and implementation as FSL, in: NeuroImage. doi:10.1016/j.neuroimage.2004.07.051

Turkheimer, E., 2000. Three laws of behavior genetics and what they mean. Curr. Dir. Psychol. Sci. 9, 160–164. doi:10.1111/1467-8721.00084

Van Dijk, K.R.A., Sabuncu, M.R., Buckner, R.L., 2012. The influence of head motion on intrinsic functional connectivity MRI. Neuroimage 59, 431–438. doi:10.1016/j.neuroimage.2011.07.044

Van Essen, D.C., Glasser, M.F., Dierker, D.L., Harwell, J., Coalson, T., 2012a. Parcellations and hemispheric asymmetries of human cerebral cortex analyzed on surface-based atlases. Cereb. Cortex 22, 2241–2262. doi:10.1093/cercor/bhr291

Van Essen, D.C., Ugurbil, K., Auerbach, E., Barch, D., Behrens, T.E.J., Bucholz, R., Chang, A., Chen, L., Corbetta, M., Curtiss, S.W., Della Penna, S., Feinberg, D., Glasser, M.F., Harel, N., Heath, A.C., Larson-Prior, L., Marcus, D., Michalareas, G., Moeller, S., Oostenveld, R., Petersen, S.E., Prior, F., Schlaggar, B.L., Smith, S.M., Snyder, A.Z., Xu, J., Yacoub, E., 2012b. The Human Connectome Project: A data acquisition perspective. Neuroimage 62, 2222–2231. doi:10.1016/j.neuroimage.2012.02.018

Wang, D., Buckner, R.L., Fox, M.D., Holt, D.J., Holmes, A.J., Stoecklein, S., Langs, G., Pan, R., Qian, T., Li, K., Baker, J.T., Stufflebeam, S.M., Wang, K., Wang, X., Hong, B., Liu, H., 2015. Parcellating cortical functional networks in individuals. Nat. Neurosci. 18, 1853–1860. doi:10.1038/nn.4164

Weber, W.W., 2008. Genetics in Pharmacology: Twin Studies, in: Pharmacogenetics. Oxford University Press, Oxford, pp. 107–108.

Yang, Z., Zuo, X.N., McMahon, K.L., Craddock, R.C., Kelly, C., De Zubicaray, G.I., Hickie, I., Bandettini, P.A., Castellanos, F.X., Milham, M.P., Wright, M.J., 2016. Genetic and

Environmental Contributions to Functional Connectivity Architecture of the Human Brain. Cereb. Cortex 26, 2341–2352. doi:10.1093/cercor/bhw027

Zeng, L.-L., Wang, D., Fox, M.D., Sabuncu, M., Hu, D., Ge, M., Buckner, R.L., Liu, H., 2014. Neurobiological basis of head motion in brain imaging. Proc. Natl. Acad. Sci. 111, 6058–6062. doi:10.1073/pnas.1317424111

Chapter 5: Conclusion

5.1 Summary

Individual differences in human brain functional network organization are signal, not noise (van Horn et al., 2008). Seminal fMRI investigations of areal- and systems-level brain organization hypothesized that individual differences were background noise (Biswal et al., 1995; Greicius et al., 2003). In order to overcome the noise, these studies averaged together data from distinct individuals. Averaging was necessary at the time, since small amounts of data were collected per individual and MRI hardware (e.g., head matrix coils) and software (e.g., pulse sequences, image reconstruction algorithms) were in their infancies. Thus, individual differences could not be measured reliably, and therefore, seemed to be noise (Evan M Gordon et al., 2017; Laumann et al., 2015). As the field matured and technology improved, the importance of individual differences was slowly recognized (Finn et al., 2015; Miller et al., 2012, 2009; Mueller et al., 2013; Wang et al., 2015). Now that many of these technical issues have been resolved and there has been a focus on individual-specific experimental designs and analyses, a converging picture of individual-specific functional network organization has emerged (Bijsterbosch et al., 2018; Braga and Buckner, 2017; Evan M Gordon et al., 2017; Evan M. Gordon et al., 2017a, 2017b; Kong et al., 2018).

Recent experimenters have acquired substantial amounts of resting-state fMRI data from individual healthy adults (Braga and Buckner, 2017; Evan M Gordon et al., 2017; Kong et al., 2018; Poldrack et al., 2015). As such, these investigators have been able to identify a comparable set of brain regions in which individual differences in brain network organization may be found, i.e. parts of association cortex, and a separate set of brain regions in which network organization

is highly consistent, e.g. primary sensory areas (Evan M. Gordon et al., 2017a, 2017b; Kong et al., 2018; Mueller et al., 2013). Likewise, regions of individual difference have been shown to be remarkably stable over days (Kong et al., 2018), weeks (Gratton et al., 2018a), months (Chen et al., 2015; Filevich et al., 2017), and even a year (Laumann et al., 2017, 2015) within individuals. Several advances in our understanding of these individual differences are presented in this dissertation, including: (1) a neurobiologically-grounded framework for the terminology and interpretation of regions of individual difference, i.e. network variants; (2) the systematic nature of the idiosyncratic networks to which variants are re-assigned; (3) the observation that task-induced brain activations in network variants match those expected to occur in their idiosyncratic network; (4) the identification of discrete sub-groups of individuals with similar network variant properties; and, (5) the trait-like nature of an individual's distribution of network variants, including the heritability of this distribution.

5.2 Interpretation

In my opinion, two of the aforementioned findings are most important, and thus, warrant the primary focus of the discussion and interpretation: the task-induced brain activation result and the identification of sub-groups of individuals. To recap, (1) we observed that network variants re-assigned to the default mode network (DMN) tended to de-activate, as expected for canonical DMN regions (Raichle et al., 2001; Shulman et al., 1997), even though many of these network variants were located in regions that canonically activate during goal-directed tasks (Dosenbach et al., 2006; Klingberg et al., 1997); and, (2) we identified two main sub-groups of individuals who differed in network variant properties.

The fact that network variants show the pattern of brain (de-) activations expected to occur in their idiosyncratic network (during goal-directed tasks) helps validate their neurobiological function. For instance, dorsolateral prefrontal cortex (dlPFC) has been shown to be an important region of control for task performance, which is consistent with the fact that dlPFC is part of the frontoparietal network, a functional system of the brain thought to be important for systems-level control processes (Dosenbach et al., 2007, 2006; Gratton et al., 2017; He et al., 2007; Woolgar et al., 2011; Zanto and Gazzaley, 2013). Yet, this evidence comes from group-level studies, and therefore, such results and interpretations are valid only at the group-level. Here, we demonstrated that in some individuals, certain regions within dlPFC are not affiliated with the frontoparietal network, but rather are aligned with the DMN, which decreases its activity level (relative to its baseline state) during goal-directed tasks. It is difficult to argue that a brain region expected to activate (because of its physical location) that instead de-activates during task performance has the same function as a brain region in the same physical location (in a different individual) that shows the expected activation. If the expected activation is necessary for some aspect of performing the task, then one must conclude that the network variant region (which deactivated) is performing a different process during this task. Thus, network variants appear to play a role in task processing that is consistent with their novel, idiosyncratic network, even if it's the opposite of what would be predicted from the group-average.

The two distinct sub-groups of individuals identified via network variant properties are equally intriguing, as the same two sub-groups were identified in three separate groups of individuals. We observed that one sub-group was composed of individuals whose network variants tend to align, primarily, with the DMN, whereas individuals in the other sub-group have network

variants that tend to align with control (e.g., cinguloopercular) and processing (e.g., visual, auditory) networks. An alternative way to think about this result is in terms of the size of these networks (e.g., the DMN is expanded in one sub-group of individuals), but this idea is not a perfect representation of the true result (see Chapter 3 for technical details). Moreover, we found that these two sub-groups are moderately heritable, with 47% of the variance apparently explained by additive genetics. There is substantial evidence supporting the idea that the sub-group phenomenon is a fundamental aspect of healthy adult functional network organization.

The meaning behind this phenomenon is less clear. Previous work has shown that the control and processing networks are activated during goal-directed tasks (Gratton et al., 2018b, 2017, 2016). Thus, they are thought to be important for controlling and executing aspects of the tasks (Dosenbach et al., 2008; Nelson et al., 2010). Conversely, the DMN, which tends to de-activate during such tasks, is thought to be involved in more internal processes, such as introspection (Raichle, 2015). Thus, individuals in the so-called control and processing sub-group appear to have more association cortex aligned with brain functional networks important for accomplishing goal-directed tasks (among other processes). Therefore, a reasonable hypothesis is that individuals in the control and processing sub-group will perform such tasks more efficiently or accurately. Further, individuals in the control and processing sub-group may have higher scores on behavioral measures of relevant for goal-directed tasks, e.g. executive function.

We did not find direct evidence to support either of these hypotheses. However, we did observe a weak but significant difference between the sub-groups in terms of some neuropsychological measures of behavior. Specifically, individuals in the control and processing sub-group tended to

have a more positive outlook on life and were less likely to have a history of drug abuse than individuals in the DMN sub-group. Previous studies have shown significant relationships between individual differences in functional network organization and behavior (Bijsterbosch et al., 2018; Kong et al., 2018; Smith et al., 2015), some of which are consistent with our results. However, there is not yet a consensus as to the nature and extent of the relationship between network variants (individual differences in functional network organization) and behavior.

Additionally, we found that the two sub-groups were anticorrelated with one another. This observation poses an issue for group-level studies that average individuals together. When two anticorrelated signals (of approximately equal magnitude) are averaged together, the resultant signal is near zero, even though neither original signal was near zero. This means that group-level studies comparing two populations of individuals (e.g., patients versus controls) may have obscured a bonafide difference between the populations as a direct consequence of averaging individuals together. As a hypothetical example, consider a patient population in which there are three clear sub-groups: the two main sub-groups observed in the control population, and a smaller but distinct third sub-group. Such a result would almost certainly be missed at the group-level, since the two main sub-groups are anticorrelated, and thus, will cancel each other out at the group-level (since the third sub-group is smaller than the main two). The third sub-group may reveal an insight into the neurobiology of the disease, but until a network variant approach is taken, this insight will remain hidden.

However, such obfuscation would not occur if, for a given disease, there is a systematic shift in sub-groups. Moving away from the hypothetical, previous investigations have revealed both

decreased activation during a working memory task (Meyer-Lindenberg et al., 2005) and aberrant functional connectivity (Lawrie et al., 2002; Lynall et al., 2010) in dorsolateral prefrontal cortex (dlPFC) in patients with Schizophrenia relative to controls. Since network variants commonly occur in dlPFC, it is reasonable to expect that individuals with Schizophrenia (1) will have more network variants aligned with the DMN in dlPFC and (2) will have a higher proportion of individuals in the DMN sub-group relative to healthy controls. This example is one of many possible re-interpretations of well-known findings from earlier fMRI studies of psychiatric disease.

The lens through which prior neuroimaging literature is viewed, as well as future experimental designs, should be informed by the discovery of network variants and their systematic patterning across individuals.

5.3 Future Experiments

5.3.1 Basic Neuroscience

There are several interesting questions for future research to address concerning network variants and their many features described in this thesis. As discussed in Chapter 3, understanding the neurobiological source(s) of network variants may require non-human research. If this line of inquiry is pursued, the presence of network variants must first be established in the animal model in question. Consider a popular non-human primate research model- the rhesus macaque. Confirmation of the presence of network variants will require a large amount of resting-state

fMRI data from a reasonable amount of individual macaques, as well as a macaque group-average for comparison.

The most straightforward experiment will use either extant fMRI data from lightly anesthetized macaques (Vincent et al., 2007) or require training a reasonable number of macaques to perform eyes-open resting-state fMRI. Once the data are in hand and processed appropriately (e.g., for motion artifacts (Power et al., 2014)), all individual data must be registered to a common atlas space. Pipelines for surface-based registration of macaque fMRI data have been developed by the Van Essen lab and colleagues, and there is a well-constructed surface atlas from the Yerkes National Primate Research Center (similar to the Conte69 surface atlas used for all of the human data included in this thesis) (Donahue et al., 2018). After such technical details are resolved, network variants can be identified in individual macaques by comparing their resting-state correlation matrices against the group-average correlation matrix.

I hypothesize that network variants: (1) will be found in non-human primates (macaque or otherwise) in proportional numbers to humans (after normalizing for differences in cortical size), (2) will be located in association cortex and rarely in sensorimotor cortex, and (3) will be reassigned to higher-level systems (e.g., Frontoparietal and Default Mode Networks) more often than to sensorimotor systems. Furthermore, I would not be surprised to observe that network variants are distributed systematically across individual macaques, allowing for identification of sub-groups of individuals. In sum, I expect the results of this first experiment to reveal very similar characteristics to human network variants. However, this study is necessary because all

other experiments require identification, localization, and validation of network variants in the macaque.

Subsequent studies could involve in-depth electrophysiological studies of macaque network variants. In the discussion section of Chapter 3, we speculated about the neurobiological source of network variants near Frontal Eye Fields (FEF). To recap, an FEF network variant may occur in an individual because that individual's FEF is displaced/enlarged/contracted relative to the average FEF or the function of FEF neurons is systematically shifted away from the typical distribution of FEF neuronal function (e.g., more attention neurons than average). Electrophysiology will allow for disambiguation between these possibilities, assuming a macaque with an FEF network variant is discovered. Since FEF is a common location for human network variants, it is reasonable to expect to find macaques with FEF network variants.

Single- or multi-unit recordings will allow for precise localization and characterization of all FEF neurons in an individual macaque. However, many such recordings will need to be acquired across a fairly large number of macaques in order to delineate the central tendency of macaque FEF location and the typical distribution of FEF neuronal functions. Fortunately, FEF has been studied for many years in the macaque (Petit and Pouget, 2019), so there may exist an adequate database of FEF neuronal recordings from which the group-average location and distribution of FEF neuronal functions may be derived. I expect that network variants will be explained by a systematic shift in the distribution of neuronal functions most often. I base this hypothesis on the observation that network variants appear to shift their task processing profile to the profile of their idiosyncratic network assignment.

Additional basic neuroscience experiments include extending network variant investigations to non-cortical structures. There is evidence to suggest that the expansion of association cortex in humans is mirrored in the cerebellum (Buckner, 2013; Buckner et al., 2011). Furthermore, a recent study demonstrated that there is individual variability in the size of cerebellar Frontoparietal Network (FP), with many individuals having an overrepresentation relative to cortical FP (Marek et al., 2018). These findings, in addition to well-established evidence that cognitive processing occurs in the cerebellum (Fiez, 2016; Fiez et al., 1992; Petersen et al., 1988; Strick et al., 2009), suggest that network variants are likely present in cerebellar association cortex. Speculatively, a Default Mode Network (DMN) network variant located in *right* dorsolateral prefrontal cortex may predict the presence of a DMN network variant in *left* cerebellar association cortex (that is typically assigned to FP at the group-level).

Contralateral mirroring of cortical and cerebellar network variants is forecasted by the known anatomy of cortico-cerebellar projections (which decussate in the pons) (Woolsey et al., 2008). Such a finding would reveal a whole-brain, systems-level network variant effect, as opposed to single areal-level changes. Further questions concerning anatomical projections to/from network variant regions may be addressed by use of diffusion tensor imaging in humans and tracer studies in non-human primates. For example, an individual with a DMN network variant in right dorsolateral prefrontal cortex may have a different pattern of anatomical wiring to/from that region compared to an individual with the typical FP network representation in that same cortical location. This would indicate that network variants involve a change in both function and anatomy.

A final set of basic experiments to consider involves the origin of network variants. The moderate heritability of network variants discussed in Chapter 4 suggests that approximately half of the variance in network variants is due to unique environmental/experiential factors. Thus, developmental studies of network variants are required to understand when, and potentially why, they occur. Developmental studies are complicated by technical issues of network variant identification, since identification of network variants requires a group-level referent. In my opinion, it is incorrect to compare individuals to a group-average from a different developmental window. This complication is compounded by individual differences in rate of development. The ideal study of network variants across development will involve a longitudinal design, similar to the ABCD study (Jernigan et al., 2018), but begin near post-natal day one and continue through puberty. Capturing critical periods (e.g., the various stages of language acquisition) may prove to be quite revealing in terms of network variant development.

5.3.2 Translational Neuroscience

There are many extant datasets of fMRI data acquired from a variety of patient populations. Network variant analysis of these datasets is low hanging fruit. One interesting possibility follows from the work of Eve Marder and colleagues, who demonstrated that there is a range of 'acceptable' temperatures (subject to neuromodulatory tone) for the maintenance of a healthy pyloric rhythm in the crab stomatogastic ganglion (Kushinsky et al., 2019). A similar principle may be at play with respect to network variants. There could be a range of 'acceptable' variant location and network re-assignment distributions, with deviations outside of the range coinciding with disease. For example, network variants located in primary sensorimotor cortex may coincide with related diseases (e.g., blind or vision-impaired individuals may have network

variants in V1). Since network variants rarely occur in these regions, such an observation would be considered a deviation outside of the network variant location distribution. Likewise, idiosyncratic re-assignment of network variants that includes an unusual distribution of networks (e.g., a large amount of parietal memory and parietal occipital network) may be associated with a particular disorder.

The result of distinct sub-groups of individuals provides the most leverage for translational neuroscience questions, in my opinion. In Chapter 3, we described two distinct sub-groups of individuals (with some evidence for four sub-groups) identified via differences in network variants. These findings replicated across three independent datasets of unrelated individuals, and the percent of individuals in each sub-group was approximately 50%. It may be the case that individuals with a given neurologic or psychiatric disease are systematically shifted towards one sub-group. Alternatively, a novel sub-group, present in patients only, may be identified. It is possible that either of these results may already be evident at the group-average level. However, such differences may be hidden at the group-average level, as described at the end of the Summary and Interpretation section.

For instance, previous investigations have shown that there are functional connectivity differences in right dorsolateral prefrontal cortex in individuals with Schizophrenia compared to healthy controls (Lawrie et al., 2002; Lynall et al., 2010). Given that these differences were observed at the group-average level, it is almost certain that there will be differences in network variants in these same regions (and preliminary evidence suggests that this is the case). The more interesting question is if network variants in individuals with Schizophrenia are systematically

shifted towards one sub-group (or individuals with Schizophrenia are in their own sub-group), are there further sub-types in terms of network variants. If so, what are the characteristics of those sub-types. For a disease like Schizophrenia, with large individual differences in behavioral manifestations (e.g., positive versus negative symptoms), such a result may map onto distinct disease sub-types. Moreover, differences in network variants between individuals with Schizophrenia may provide novel insight for individual-specific, personalized treatment protocols and neurobiological targets for intervention (e.g., transcranial magnetic stimulation).

5.4 Chapter 5 References

Bijsterbosch, J.D., Woolrich, M.W., Glasser, M.F., Robinson, E.C., Beckmann, C.F., Van Essen, D.C., Harrison, S.J., Smith, S.M., 2018. The relationship between spatial configuration and functional connectivity of brain regions. Elife 7. doi:10.7554/eLife.32992

Biswal, B., Yetkin, F.Z., Haughton, V.M., Hyde, J.S., 1995. Functional connectivity in the motor cortex of resting human brain using echo-planar MRI. Magn. Reson. Med. 34, 537–541. doi:10.1002/mrm.1910340409

Braga, R.M., Buckner, R.L., 2017. Parallel Interdigitated Distributed Networks within the Individual Estimated by Intrinsic Functional Connectivity. Neuron 95, 457–471.e5. doi:10.1016/j.neuron.2017.06.038

Buckner, R.L., 2013. The cerebellum and cognitive function: 25 years of insight from anatomy and neuroimaging. Neuron 80, 807–15. doi:10.1016/j.neuron.2013.10.044

Buckner, R.L., Krienen, F.M., Castellanos, a., Diaz, J.C., Yeo, B.T.T., 2011. The organization of the human cerebellum estimated by intrinsic functional connectivity. J. Neurophysiol. 106, 2322–2345. doi:10.1152/jn.00339.2011

Chen, B., Xu, T., Zhou, C., Wang, L., Yang, N., Wang, Z., Dong, H.M., Yang, Z., Zang, Y.F., Zuo, X.N., Weng, X.C., 2015. Individual variability and test-retest reliability revealed by ten repeated resting-state brain scans over one month. PLoS One 10. doi:10.1371/journal.pone.0144963

Donahue, C.J., Glasser, M.F., Preuss, T.M., Rilling, J.K., Van Essen, D.C., 2018. Quantitative assessment of prefrontal cortex in humans relative to nonhuman primates. Proc. Natl. Acad. Sci. 115, E5183–E5192. doi:10.1073/pnas.1721653115

Dosenbach, N.U.F., Fair, D.A., Cohen, A.L., Schlaggar, B.L., Petersen, S.E., 2008. A dual-networks architecture of top-down control. Trends Cogn. Sci. 12, 99–105. doi:10.1016/j.tics.2008.01.001

Dosenbach, N.U.F., Fair, D.A., Miezin, F.M., Cohen, A.L., Wenger, K.K., Dosenbach, R. a T., Fox, M.D., Snyder, A.Z., Vincent, J.L., Raichle, M.E., Schlaggar, B.L., Petersen, S.E., 2007. Distinct brain networks for adaptive and stable task control in humans. Proc. Natl. Acad. Sci. U. S. A. 104, 11073–8. doi:10.1073/pnas.0704320104

Dosenbach, N.U.F., Visscher, K.M., Palmer, E.D., Miezin, F.M., Wenger, K.K., Kang, H.C., Burgund, E.D., Grimes, A.L., Schlaggar, B.L., Petersen, S.E., 2006. A Core System for the Implementation of Task Sets. Neuron 50, 799–812. doi:10.1016/j.neuron.2006.04.031

Fiez, J.A., 2016. The cerebellum and language: Persistent themes and findings. Brain Lang. 161, 1–3. doi:10.1016/j.bandl.2016.09.004

Fiez, J.A., Petersen, S.E., Cheney, M.K., Raichle, M.E., 1992. Impaired non-motor learning and error detection associated with cerebellar damage: A single case study. Brain 115, 155–178. doi:10.1093/brain/115.1.155

Filevich, E., Lisofsky, N., Becker, M., Butler, O., Lochstet, M., Martensson, J., Wenger, E., Lindenberger, U., Kühn, S., 2017. Day2day: Investigating daily variability of magnetic resonance imaging measures over half a year. BMC Neurosci. 18. doi:10.1186/s12868-017-0383-y

Finn, E.S., Shen, X., Scheinost, D., Rosenberg, M.D., Huang, J., Chun, M.M., Papademetris, X., Constable, R.T., 2015. Functional connectome fingerprinting: Identifying individuals using patterns of brain connectivity. Nat. Neurosci. 18, 1664–1671. doi:10.1038/nn.4135

Gordon, E.M., Laumann, T.O., Adeyemo, B., Gilmore, A.W., Nelson, S.M., Dosenbach, N.U.F., Petersen, S.E., 2017a. Individual-specific features of brain systems identified with resting state functional correlations. Neuroimage 146, 918–939. doi:10.1016/j.neuroimage.2016.08.032

Gordon, E.M., Laumann, T.O., Adeyemo, B., Petersen, S.E., 2017b. Individual Variability of the System-Level Organization of the Human Brain. Cereb. Cortex 27, 386–399. doi:10.1093/cercor/bhv239

Gordon, E.M., Laumann, T.O., Gilmore, A.W., Petersen, S.E., Nelson, S.M., Dosenbach, N.U.F., Gordon, E.M., Laumann, T.O., Gilmore, A.W., Newbold, D.J., Greene, D.J., 2017. Precision Functional Mapping of Individual Human NeuroResource Precision Functional Mapping of Individual Human Brains. Neuron 95, 1–17. doi:10.1016/j.neuron.2017.07.011

Gratton, C., Laumann, T.O., Gordon, E.M., Adeyemo, B., Petersen, S.E., 2016. Evidence for Two Independent Factors that Modify Brain Networks to Meet Task Goals. Cell Rep. 17, 1276–1288. doi:10.1016/j.celrep.2016.10.002

Gratton, C., Laumann, T.O., Nielsen, A.N., Greene, D.J., Gordon, E.M., Gilmore, A.W., Nelson, S.M., Coalson, R.S., Snyder, A.Z., Schlaggar, B.L., Dosenbach, N.U.F., Petersen, S.E., 2018a. Functional Brain Networks Are Dominated by Stable Group and Individual Factors, Not Cognitive or Daily Variation. Neuron. doi:10.1016/j.neuron.2018.03.035

Gratton, C., Neta, M., Sun, H., Ploran, E.J., Schlaggar, B.L., Wheeler, M.E., Petersen, S.E., Nelson, S.M., 2017. Distinct Stages of Moment-to-Moment Processing in the Cinguloopercular and Frontoparietal Networks. Cereb. Cortex 27, 2403–2417. doi:10.1093/cercor/bhw092

Gratton, C., Sun, H., Petersen, S.E., 2018b. Control networks and hubs. Psychophysiology. doi:10.1111/psyp.13032

Greicius, M.D., Krasnow, B., Reiss, a. L., Menon, V., 2003. Functional connectivity in the resting brain: A network analysis of the default mode hypothesis. Proc. Natl. Acad. Sci. 100, 253–258. doi:10.1073/pnas.0135058100

He, B.J., Snyder, A.Z., Vincent, J.L., Epstein, A., Shulman, G.L., Corbetta, M., 2007. Breakdown of Functional Connectivity in Frontoparietal Networks Underlies Behavioral Deficits in Spatial Neglect. Neuron 53, 905–918. doi:10.1016/j.neuron.2007.02.013

Jernigan, T.L., Brown, S.A., Dowling, G.J., 2018. The Adolescent Brain Cognitive Development Study. J. Res. Adolesc. doi:10.1111/jora.12374

Klingberg, T., O'Sullivan, B.T., Roland, P.E., 1997. Bilateral activation of fronto-parietal networks by incrementing demand in a working memory task. Cereb. Cortex 7, 465–471. doi:10.1093/cercor/7.5.465

Kong, R., Li, J., Orban, C., Sabuncu, M.R., Liu, H., Schaefer, A., Sun, N., Zuo, X.-N., Holmes, A.J., Eickhoff, S.B., Yeo, B.T.T., 2018. Spatial Topography of Individual-Specific Cortical Networks Predicts Human Cognition, Personality, and Emotion. Cereb. Cortex. doi:10.1093/cercor/bhy123

Kushinsky, D., Morozova, E.O., Marder, E., 2019. In vivo effects of temperature on the heart and pyloric rhythms in the crab Cancer borealis . J. Exp. Biol. 222, jeb199190. doi:10.1242/jeb.199190

Laumann, T.O., Gordon, E.M., Adeyemo, B., Snyder, A.Z., Joo, S.J., Chen, M.-Y., Gilmore, A.W., McDermott, K.B., Nelson, S.M., Dosenbach, N.U.F., Schlaggar, B.L., Mumford, J.A., Poldrack, R.A., Petersen, S.E., 2015. Functional System and Areal Organization of a Highly Sampled Individual Human Brain. Neuron 1–14. doi:10.1016/j.neuron.2015.06.037

Laumann, T.O., Snyder, A.Z., Mitra, A., Gordon, E.M., Gratton, C., Adeyemo, B., Gilmore, A.W., Nelson, S.M., Berg, J.J., Greene, D.J., McCarthy, J.E., Tagliazucchi, E., Laufs, H., Schlaggar, B.L., Dosenbach, N.U.F., Petersen, S.E., 2017. On the Stability of BOLD fMRI Correlations. Cereb. Cortex 27, 4719–4732. doi:10.1093/cercor/bhw265

Lawrie, S.M., Buechel, C., Whalley, H.C., Frith, C.D., Friston, K.J., Johnstone, E.C., 2002. Reduced frontotemporal functional connectivity in schizophrenia associated with auditory hallucinations. Biol. Psychiatry 51, 1008–1011. doi:10.1016/S0006-3223(02)01316-1

Lynall, M.-E., Bassett, D.S., Kerwin, R., McKenna, P.J., Kitzbichler, M., Muller, U., Bullmore, E., 2010. Functional connectivity and brain networks in schizophrenia. J. Neurosci. 30, 9477–9487. doi:10.1523/JNEUROSCI.0333-10.2010

Marek, S., Siegel, J.S., Gordon, E.M., Raut, R. V., Gratton, C., Newbold, D.J., Ortega, M., Laumann, T.O., Adeyemo, B., Miller, D.B., Zheng, A., Lopez, K.C., Berg, J.J., Coalson, R.S., Nguyen, A.L., Dierker, D., Van, A.N., Hoyt, C.R., McDermott, K.B., Norris, S.A., Shimony, J.S., Snyder, A.Z., Nelson, S.M., Barch, D.M., Schlaggar, B.L., Raichle, M.E., Petersen, S.E., Greene, D.J., Dosenbach, N.U.F., 2018. Spatial and Temporal Organization of the Individual Human Cerebellum. Neuron.

Meyer-Lindenberg, A.S., Olsen, R.K., Kohn, P.D., Brown, T., Egan, M.F., Weinberger, D.R., Berman, K.F., 2005. Regionally specific disturbance of dorsolateral prefrontal-hippocampal functional connectivity in schizophrenia. Arch. Gen. Psychiatry 62, 379–386. doi:10.1001/archpsyc.62.4.379

Miller, M.B., Donovan, C.L., Bennett, C.M., Aminoff, E.M., Mayer, R.E., 2012. Individual differences in cognitive style and strategy predict similarities in the patterns of brain activity between individuals. Neuroimage. doi:10.1016/j.neuroimage.2011.05.060

Miller, M.B., Donovan, C.L., Van Horn, J.D., German, E., Sokol-Hessner, P., Wolford, G.L., 2009. Unique and persistent individual patterns of brain activity across different memory retrieval tasks. Neuroimage 48, 625–635. doi:10.1016/j.neuroimage.2009.06.033

Mueller, S., Wang, D., Fox, M.D., Yeo, B.T.T., Sepulcre, J., Sabuncu, M.R., Shafee, R., Lu, J., Liu, H., 2013. Individual Variability in Functional Connectivity Architecture of the Human Brain. Neuron 77, 586–595. doi:10.1016/j.neuron.2012.12.028

Nelson, S.M., Dosenbach, N.U.F., Cohen, A.L., Wheeler, M.E., Schlaggar, B.L., Petersen, S.E., 2010. Role of the anterior insula in task-level control and focal attention. Brain Struct. Funct. 1–12. doi:10.1007/s00429-010-0260-2

Petersen, S.E., Fox, P.T., Posner, M.I., Mintun, M., Raichle, M.E., 1988. Positron emission tomographic studies of the cortical anatomy of single-word processing. Nature 331, 585–589. doi:10.1038/331585a0

Petit, L., Pouget, P., 2019. The comparative anatomy of frontal eye fields in primates. Cortex. doi:10.1016/j.cortex.2019.02.023

Poldrack, R.A., Laumann, T.O., Koyejo, O., Gregory, B., Hover, A., Chen, M.Y., Gorgolewski, K.J., Luci, J., Joo, S.J., Boyd, R.L., Hunicke-Smith, S., Simpson, Z.B., Caven, T., Sochat, V., Shine, J.M., Gordon, E., Snyder, A.Z., Adeyemo, B., Petersen, S.E., Glahn, D.C., Mckay, D.R., Curran, J.E., Göring, H.H.H., Carless, M.A., Blangero, J., Dougherty, R., Leemans, A., Handwerker, D.A., Frick, L., Marcotte, E.M., Mumford, J.A., 2015. Long-term neural and physiological phenotyping of a single human. Nat. Commun. 6. doi:10.1038/ncomms9885

Power, J.D., Mitra, A., Laumann, T.O., Snyder, A.Z., Schlaggar, B.L., Petersen, S.E., 2014. Methods to detect, characterize, and remove motion artifact in resting state fMRI. Neuroimage 84, 320–341. doi:10.1016/j.neuroimage.2013.08.048

Raichle, M.E., 2015. The Brain's Default Mode Network. Annu. Rev. Neurosci. 413–427. doi:10.1146/annurev-neuro-071013-014030

Raichle, M.E., MacLeod, A.M., Snyder, A.Z., Powers, W.J., Gusnard, D.A., Shulman, G.L., 2001. A default mode of brain function. Proc. Natl. Acad. Sci. U. S. A. 98, 676–682. doi:10.1073/pnas.98.2.676

Shulman, G.L., Fiez, J.A., Corbetta, M., Buckner, R.L., Miezin, F.M., Raichle, M.E., Petersen, S.E., 1997. Common Blood Flow Changes across Visual Tasks: II. Decreases in Cerebral Cortex. J. Cogn. Neurosci. 9, 648–663. doi:10.1162/jocn.1997.9.5.648

Smith, S.M., Nichols, T.E., Vidaurre, D., Winkler, A.M., J Behrens, T.E., Glasser, M.F., Ugurbil, K., Barch, D.M., Van Essen, D.C., Miller, K.L., 2015. A positive-negative mode of population covariation links brain connectivity, demographics and behavior. Nat. Neurosci. 18, 1–7. doi:10.1038/nn.4125

Strick, P.L., Dum, R.P., Fiez, J.A., 2009. Cerebellum and nonmotor function. Annu. Rev. Neurosci. 32, 413–434. doi:10.1146/annurev.neuro.31.060407.125606

Van Horn, J.D., Grafton, S.T., Miller, M.B., 2008. Individual variability in brain activity: A nuisance or an opportunity? Brain Imaging Behav. 2, 327–334. doi:10.1007/s11682-008-9049-9

Vincent, J.L., Patel, G.H., Fox, M.D., Snyder, A.Z., Baker, J.T., Van Essen, D.C., Zempel, J.M., Snyder, L.H., Corbetta, M., Raichle, M.E., 2007. Intrinsic functional architecture in the anaesthetized monkey brain. Nature 447, 83–6. doi:10.1038/nature05758

Wang, D., Buckner, R.L., Fox, M.D., Holt, D.J., Holmes, A.J., Stoecklein, S., Langs, G., Pan, R., Qian, T., Li, K., Baker, J.T., Stufflebeam, S.M., Wang, K., Wang, X., Hong, B., Liu, H., 2015. Parcellating cortical functional networks in individuals. Nat. Neurosci. 18, 1853–1860. doi:10.1038/nn.4164

Woolgar, A., Hampshire, A., Thompson, R., Duncan, J., 2011. Adaptive Coding of Task-Relevant Information in Human Frontoparietal Cortex. J. Neurosci. 31, 14592–14599. doi:10.1523/JNEUROSCI.2616-11.2011

Woolsey, T.A., Hanaway, J., Gado, M.H., 2008. The brain atlas: A visual guide to the human central nervous system (3rd ed.)., The brain atlas: A visual guide to the human central nervous system (3rd ed.).

Zanto, T.P., Gazzaley, A., 2013. Fronto-parietal network: Flexible hub of cognitive control. Trends Cogn. Sci. doi:10.1016/j.tics.2013.10.001